THE UNIVERSITY OF TEXAS AT AUSTIN
CENTER FOR TRANSPORTATION RESEARCH

TECHNICAL REPORT 0-6858-1
TxDOT PROJECT NUMBER 0-6858

Laboratory and Outdoor Exposure Site Evaluations of Portland Limestone Cements

Dr. Jose E. Garcia
Dr. Nicolas N. Tiburzi
Dr. Kevin J. Folliard
Dr. Thano Drimalas
Dr. Michael D.A. Thomas

August 2018; Published October 2019

http://library.ctr.utexas.edu/ctr-publications/0-6858-1.pdf

Technical Report Documentation Page

1. Report No. FHWA/TX-18/0-6858-1	2. Government Accession No.	3. Recipient's Catalog No.
4. Title and Subtitle Laboratory and Outdoor Exposure Site Evaluations of Portland Limestone Cements		5. Report Date August 2018; October 2019 6. Performing Organization Code
7. Author(s) Dr. Jose E. Garcia, Dr. Nicolas B. Tuburzi, Dr. Kevin J. Folliard, Dr. Thano Drimalas, Dr. Michael D.A. Thomas		8. Performing Organization Report No. 0-6858-1
9. Performing Organization Name and Address Center for Transportation Research The University of Texas at Austin 3925 W. Braker Lane, 4th Floor Austin, TX 78759		10. Work Unit No. (TRAIS) 11. Contract or Grant No. 0-6858
12. Sponsoring Agency Name and Address Texas Department of Transportation Research and Technology Implementation Division P.O. Box 5080 Austin, TX 78763-5080		13. Type of Report and Period Covered Technical Report January 2015–August 2018 14. Sponsoring Agency Code
15. Supplementary Notes Project performed in cooperation with the Texas Department of Transportation.		

16. Abstract

The research described in this report was funded by the Texas Department of Transportation (TxDOT), with an emphasis on portland limestone cements (PLCs) with higher limestone contents (e.g., greater than 15%), particularly in paving applications. The project was quite comprehensive and included the full-scale production of seven different cements at two Texas cement plants, with limestone contents as high as 30 percent. These cements were then evaluated in the laboratory and at outdoor exposure sites, studying a wide range of fresh, hardened, and durability properties of PLC concrete, including select mixtures in combination with supplementary cementing materials (SCMs) with limestone contents of up to 30% limestone, in selected combinations with supplementary cementitious materials (SCMs). The results show that PLCs can be produced that are constructible, durable, and sustainable, but a thorough understanding of PLCs and SCMs is needed to optimize the overall performance. More research and, particularly, more well-monitored, real-world applications of PLCs with higher limestone contents are needed to better correlate the results of laboratory tests to actual pavements or structures.

17. Key Words Portland Limestone Cement, PLC, Sulfate Attack, Carbonation, Ettringite, ASR, Mechanical Properties, Durability	18. Distribution Statement No restrictions. This document is available to the public through the National Technical Information Service, Springfield, Virginia 22161; www.ntis.gov.

19. Security Classif. (of report) Unclassified	20. Security Classif. (of this page) Unclassified	21. No. of pages 316	22. Price

Form DOT F 1700.7 (8-72) Reproduction of completed page authorized

THE UNIVERSITY OF TEXAS AT AUSTIN
CENTER FOR TRANSPORTATION RESEARCH

Laboratory and Outdoor Exposure Site Evaluations of Portland Limestone Cements

Dr. Jose E. Garcia
Dr. Nicolas N. Tiburzi
Dr. Kevin J. Folliard
Dr. Thano Drimalas
Dr. Michael D.A. Thomas

CTR Technical Report:	0-6858-1
Report Date:	August 2018; Published October 2019
Project:	0-6858
Project Title:	Evaluating Limestone Cements Containing >15% Limestone
Sponsoring Agency:	Texas Department of Transportation
Performing Agency:	Center for Transportation Research at The University of Texas at Austin

Project performed in cooperation with the Texas Department of Transportation and the Federal Highway Administration.

Center for Transportation Research
The University of Texas at Austin
3925 W. Braker Lane, 4th floor
Austin, TX 78759

http://ctr.utexas.edu/

Disclaimers

Author's Disclaimer: The contents of this report reflect the views of the authors, who are responsible for the facts and the accuracy of the data presented herein. The contents do not necessarily reflect the official view or policies of the Federal Highway Administration or the Texas Department of Transportation (TxDOT). This report does not constitute a standard, specification, or regulation.

Patent Disclaimer: There was no invention or discovery conceived or first actually reduced to practice in the course of or under this contract, including any art, method, process, machine manufacture, design or composition of matter, or any new useful improvement thereof, or any variety of plant, which is or may be patentable under the patent laws of the United States of America or any foreign country.

Engineering Disclaimer

NOT INTENDED FOR CONSTRUCTION, BIDDING, OR PERMIT PURPOSES.

Research Supervisor: Kevin J. Folliard

Acknowledgments

The authors express appreciation to the TxDOT Project Director, members of the PMC Committee and to the TxDOT district offices who helped with the field site investigations.

Table of Contents

List of Tables

List of Figures

Chapter 1. Introduction and Scope

In a 2014 survey, it was estimated that portland cement production was responsible for approximately 5.8% (626 million tons) of annual global carbon dioxide emissions (Boden et al., 2017). The emissions from a typical cement plant are derived from two sources: the burning of fossil fuels (about 40 to 50% of CO_2 emissions) required to attain high temperature clinkering and the calcination of limestone (about 50 to 60% of CO_2 emissions), which extracts CaO from the limestone but drives off CO_2 as part of the process (NRMCA, 2008). For every ton of ordinary portland cement that is produced, there is approximately 0. 9 to one ton of carbon dioxide that is produced (Marceau, et al., 2006). There have been significant efforts worldwide to curb CO_2 emissions from cement plants and to reduce the overall carbon footprint of concrete products, including the use of alternate fuels in cement plants and the use of supplementary cementing materials (SCMs) as a partial replacement for cement in concrete.

Another effective approach to reduce the carbon footprint of cement and concrete, which has only recently been introduced in the United States, is the production of portland limestone cements (PLCs), which include the intergrinding of limestone powder with clinker and gypsum. Using uncalcined limestone has the direct effect of reducing CO_2 in proportion with the percent replacement of clinker, and for cement producers, limestone powder is readily available at the plant, assuming the native limestone source has a calcium carbonate content above the prescribed limit. The production of PLCs requires less energy and decreases the amount of CO_2 emissions, when compared to ordinary portland cement (OPC) (Cost et al., 2013).

The research described in this report was funded by the Texas Department of Transportation (TxDOT), with an emphasis on PLCs with higher limestone contents (e.g., greater than 15%), particularly in paving applications. The project was quite comprehensive and included the full-scale production of seven different cements at two Texas cement plants, with limestone contents as high as 30 percent. These cements were then evaluated in the laboratory and at outdoor exposure sites, studying a wide range of fresh, hardened, and durability properties of PLC concrete, including select mixtures in combination with supplementary cementing materials (SCMs) with limestone contents of up to 30% limestone, in selected combinations with supplementary cementitious materials (SCMs).

This introductory chapter first provides some brief background information on PLCs, then presents a breakdown of the chapter-by-chapter organization of this report. The Ph.D. dissertations of Jose Garcia (Garcia, 2018) and Nicolas Tiburzi (Tiburzi, 2018) serve as the basis for this final project report, which covers research performed over a 44 month period.

1.1. Portland Limestone Cements—Brief Background

Before briefly describing portland limestone cements, it is prudent to first consider the case for the standard production of ordinary portland cement. There are four basic ingredients required to produce a Type I ordinary portland cement clinker: lime, silica, alumina, and iron oxide. The approximate chemical composition (Bohan, 2004) of each ingredient for typical cement clinker can be seen in Table 1.1.

Table 1.1: Typical Clinker Composition

Ingredient	Chemical Formula	Approximate Composition by Mass (%)
Lime	CaO	65 +/- 3
Silica	SiO_2	21 +/- 2
Alumina	Al_2O_3	5 +/- 1.5
Iron oxide	Fe_2O_3	3 +/- 1

As shown in Equation 1.1, limestone, or calcium carbonate, can be heated to obtain the desirable lime, but carbon dioxide is a consequence of this process; this process is known as calcination.

$$CaCO_3 + Heat \rightarrow CaO + CO_2 \qquad \text{(Eq. 1.1)}$$

In summary, to produce cement clinker, limestone is combined with sources of silica, alumina, and iron oxide in a rotary kiln, which must reach an approximate temperature of 1450 ^{o}C (2640 ^{o}F) to achieve the desired chemical reactions to produce clinker. The clinker is then ground with gypsum to control setting time. PLCs are produced in a similar manner as ordinary portland cements, with the exception that limestone powder (typically from same quarry) is interblended with ground portland cement or interground with clinker and gypsum, with the latter being the most common.

1.1.1. Types of PLCs

Before cement producers were allowed to incorporate a small amount of limestone into the cement, the producers were only introducing gypsum into the steel ball mills during the clinker grinding process to create OPC. Therefore, the most common way to obtain a PLC at the time would be to pulverize crushed limestone separately and combine it with OPC, creating blended portland limestone cements. Although producing PLCs in this manner achieves the desired sustainability benefits and lowers the cost of concrete by replacing the most expensive ingredient (cement) with inexpensive limestone, there are some significant drawbacks:

- The limestone must be ground separately and then combined with OPC in a way such that homogeneity is achieved

- Unless the limestone is ground as fine as the average cement particle or finer (about 45 μm) there is significant evidence that the limestone is only present as inert filler, leading to decreased compressive strength due to a cement dilution effect (Hooton, 1990; Hawkins et al., 2003; Cam, & Neithalath, 2010).

Instead of pulverizing limestone and combining it with cement after the clinker has been ground in the steel ball mills at the cement plant, the limestone can be added to the mill at the same time as the clinker and gypsum. In other words, the key distinction between blended PLCs and interground PLCs is whether the limestone is interground with the clinker or blended afterwards. Figure 1.1 is a schematic that summarizes the process for both types of PLCs.

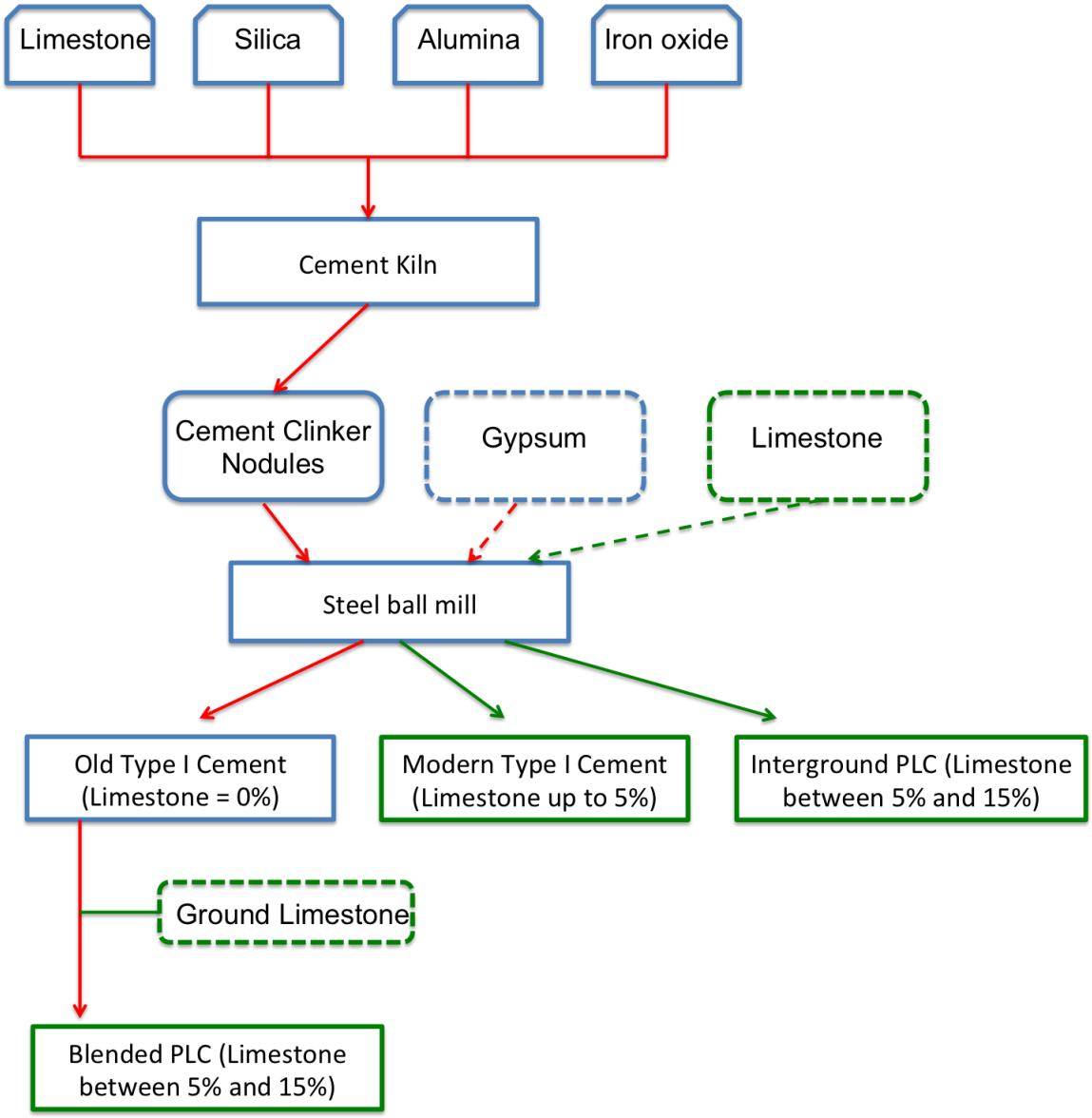

Figure 1.1: Schematic of OPC and PLC Production Processes

The benefits of intergrinding limestone with the clinker and gypsum are well established. Because limestone is softer than clinker, when portland limestone cement is interground, the end product will typically be a PLC that is finer than OPC (Tennis et al. 2011). Finer cement leads to a higher specific surface area, which increases the cement reactivity. In addition to increasing the reactivity of the cement, intergrinding limestone with the clinker also results in finer limestone particles, which has two additional benefits: the fine limestone particles increase the particle-packing effect and they also act as nucleation sites for hydration products (Tennis et al. 2011).

It should not come as a surprise then that, due to the increased reactivity, increased particle-packing effect, and increased nucleation and growth sites, many researchers have reported approximately equivalent compressive strength as OPC in cases where the limestone content in the tested PLCs is up to 15% (Tsivilis et al., 2000; Voglis et al., 2005; Ramezanianpour & Hooton, 2014).

1.1.2. History of PLCs

The practice of adding limestone to cement in Europe dates back to the 1960s and 1970s (Schmidt, 1992), and up to 35% limestone is currently permitted in the European standard, EN 197-1, for portland-limestone cements. As shown in Figure 1.2, OPC accounted for over 35% of cement use in Europe in 1999, compared to PLC, which was used approximately 15% of the time. The use of OPC in Europe decreased to about 27% in 2007, and the use of PLC increased by a factor of two in 2004 before decreasing to approximately 21%. The probable reason for the "decrease" of PLC use from 2004 to 2007 is that PLCs were combined with other SCMs, such as slag and fly ash, becoming "portland-composite" cements instead of pure portland limestone cements.

Canada has allowed the addition of limestone, up to 5%, to OPC since 1983 (Hooton et al., 2007), and the current Canadian standard, CSA A3001, allows up to 15% limestone for type GUL (general use limestone) cements. Over the years, the use of PLCs has extended across continents and there are several countries that allow a high limestone replacement of cement in their PLCs: Argentina (up to 20%), Mexico (up to 35% limestone, cement may include other ingredients as long as clinker and gypsum combined are more than 50% by mass), New Zealand (up to 15%) and Peru (up to 15%), to name a few (Tennis et al., 2011).

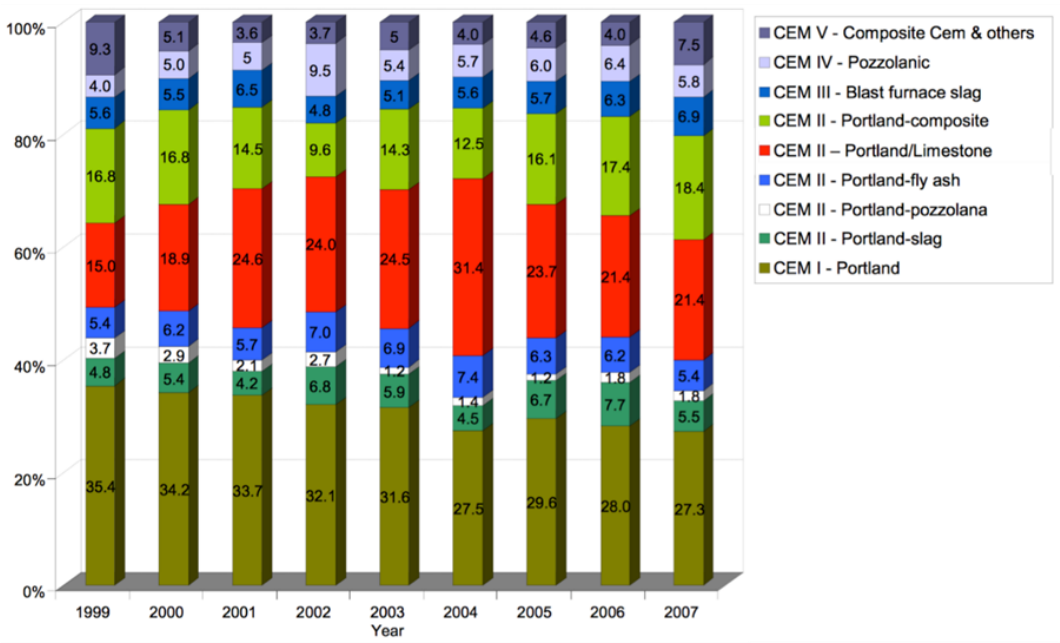

Figure 1.2: Percentage of Cement Types in Europe Conforming to EN 197-1 (Adapted from Innis, 2014, quoting Cembureau data)

In the United States, cement producers were allowed to add up to 5% limestone to OPC, per ASTM C150, in 2004 (Hooton et al., 2007). In 2012, ASTM C595 introduced Type IL cement, a portland limestone cement with a limestone content between 5% and 15%, and it specified that the added limestone must have a minimum calcium carbonate content of 70% by mass. The requirements for Type IL cement remain the same in the current version of ASTM C595. Although most Type I cements produced in the U.S. will now include a small amount of limestone, the use of Type IL cements is still fairly limited. As of 2014, only 18 states had adopted using limestone cements, and only seven had used PLCs for paving applications (Innis, 2014).

1.1.3. Environmental Benefits

There is a general consensus in the scientific community that global-warming is a major threat primarily caused by human activities (IPCC, 2013). Carbon dioxide, a heat-trapping gas directly linked to global-warming, is the most abundant of the greenhouse gases and the concentration levels of CO2 are projected to keep increasing (IPCC, 2013). As mentioned in section 1.1, cement production is a major contributor to carbon dioxide emissions worldwide; although meaningful progress has been made by the cement industry to reduce its CO2 footprint, it can and must do a better job to increase sustainability.

Fortunately, there are substantial environmental benefits that portland limestone cements offer in comparison to ordinary portland cements, and if PLCs are used properly, the disadvantages are insignificant, if not inexistent. A number of researchers have performed in-depth studies on

environmental benefits of PLCs in detail; a good summary of these studies is provided by Tennis et al. (Tennis et al., 2011).

As shown in Table 1.2, PLC containing 15% limestone results in an approximate CO2 emissions reduction of 141,000 tons for every 1 million tons of cement produced, when compared to OPC. Since there is approximately 0.9 tons of CO2 emissions for every ton of OPC that is produced, the CO2 emissions would be reduced by approximately 14%. Additionally, PLCs offer a reduction of around 10% in the consumption of raw materials (Tennis et al., 2011).

Table 1.2: Estimated Annual Reduction in Emissions from use of PLC (Adapted from Tennis et al., 2011) Note: 1 metric ton = 1.1 U.S tons, 1 metric ton = 1000 kg, 1 U.S. ton = 2000 lbs

Emissions Reduction	10% limestone (per million metric tons of cement)	15% limestone (per million metric tons of cement)
SO_2 (lbs)	527,070	789,250
NO_X (lbs)	526,170	789,250
CO (lbs)	94,350	140,610
CO_2 (tons)	85,280	127,910
Total Hydrocarbon, THC (lbs)	12,970	19,410

1.1.4. Advantages and Disadvantages over OPC

As can be seen in Table 1.3, there are significant advantages to using portland limestone cement over ordinary portland cement, while at the same time there are some drawbacks that need to be mentioned.

In addition to the substantial environmental benefits provided by PLC over OPC, it is also worth mentioning that portland limestone cement concrete is similar enough to ordinary portland cement concrete that contractors will not need special training, nor special equipment, to incorporate PLC concrete into daily operations.

Additional environmental benefits can be achieved by incorporating supplementary cementitious materials (SCMs) into the concrete mix, which not only further reduces concrete cost, but also, as some researchers have shown, there is an increase in compressive strength and a decrease in porosity, when PLCs with up to 11% limestone were combined with 15% slag (Ramezanianpour & Hooton, 2014).

Thomas et al. (2013) were able to achieve equivalent durability performance for PLCs with 12% limestone content in terms of alkali-silica reaction (def), sulfate attack, carbonation, freeze-thaw damage, and salt scaling. It is worth noting that they incorporated 40% slag in combination with

the PLC for some mixes, meaning that the clinker and gypsum fraction of the total cementitious material was less than 50%.

There are some challenges associated with using PLC concrete that need to be mentioned. One of the challenges is due to the resistance by some state Departments of Transportation (DOTs) to specify use of portland limestone cement, more than likely due to the fact that it is still a fairly new product in the United States. The other challenge with PLC concrete is that special attention must be paid to a couple of durability issues, namely thaumasite form of sulfate attack (TSA) and carbonation.

Ramezanianpour & Hooton have reported thaumasite form of sulfate attack, a special form of sulfate attack that requires calcium carbonate, to occur in PLC concrete exposed to sulfates and it usually, but not necessarily, occurs at lower temperatures; a range of 0 ^{o}C to 5 ^{o}C has been reported as optimal (Ramezanianpour & Hooton, 2013).

There is a lot of evidence which supports that concrete designed to have equivalent compressive strength will have very similar carbonation resistance, regardless of whether SCMs or limestone is incorporated into the concrete (Thomas & Matthews, 1992; Thomas et al., 2013) Therefore, unless the PLC concrete mix is designed to achieve equivalent compressive strength as OPC concrete, a faster rate of carbonation should be expected for PLC concrete, especially at higher limestone contents. Equivalent strength can be achieved by grinding the PLC finer or by lowering the water-to-cementitious ratio (w/cm), however, both of these methods will likely result in a decrease in environmental benefits.

Table 1.3: Summary of Advantages and Disadvantages of PLC over OPC

Advantages	Disadvantages
Reduced CO_2 emissions	Some resistance from DOTs and project specifications
Lower raw material requirements	Possibly susceptible to thaumasite form of sulfate attack
Other environmental benefits	Special attention must be paid in terms of carbonation
Combination with SCMs possible for additional environmental benefits	
Reduced cost of cement	
No specialty equipment required	
Contractor does not need specialty training	
Equivalent mechanical performance possible (up to 15% limestone)	
Equivalent durability performance possible (up to 15% limestone)	

1.2. Organization of Final Report

This remainder of this report is presented in the following chapters:

- **Chapter 2** describes the materials used throughout the study, including PLCs, SCMs, aggregates, and chemical admixtures.
- **Chapter 3** presents the findings of hydration and microstructural evaluations of PLCs.
- **Chapter 4** presents the results of isothermal calorimetry tests of various PLCs, in combination with SCMs.
- **Chapter 5** describes the results of strength (compressive and tensile) and elastic modulus tests on concrete mixtures containing PLCs.

- **Chapter 6** presents the results of drying shrinkage tests performed on PLC concrete mixtures.
- **Chapter 7** presents the findings from studies on the effects of PLCs on the corrosion resistance and chloride diffusion of concrete mixtures.
- **Chapter 8** describes the impact of PLCs on the depth of carbonation of mortar and concrete mixtures.
- **Chapter 9** describes the sulfate resistance of *mortar* mixtures containing PLCs, with and without SCMS, and across a range of test temperatures.
- **Chapter 10** describes the sulfate resistance of *concrete* mixtures containing PLCs, with and without SCMS, and across a range of test temperatures.
- **Chapter 11** describes the impact of PLCs on the susceptibility to alkali-silica reaction (ASR) and delayed ettringite formation (DEF).
- **Chapter 12** outlines the main findings from this study and discusses potential areas for future research.

Chapter 2. Materials

The materials used throughout this study are summarized in this section. The materials fall into one of the following categories: cements, supplementary cementitious materials, aggregate, and water.

The following characterization techniques were used for the powder materials (cements and SCMs):

- X-ray fluorescence (XRF): XRF analysis was performed by TxDOT at the Cedar Park Campus to obtain the chemical composition of each powder.
- X-ray diffraction (XRD): Quantitative XRD analysis was performed to identify the phases present in each powder using a Siemens D500 Diffractometer using the following parameters: 2θ range of 5-70o, 2θ step size of 0.02o, and a 6-second dwell time for each step.

2.1. Cements

Two cement plants in the state of Texas with the capability to produce interground PLCs were asked to produce cements with varying limestone contents in the range of 0 to 30%. Each plant agreed to produce cement with the following approximate limestone contents:

- 0-5% limestone: Type I or Type I/II (Control)
- ~10% limestone: Type IL
- ~20% limestone
- ~30% limestone

Figure 2.1 shows a schematic of the cements produced by each cement plant, the nomenclature that was used for the cements, and the actual limestone content as obtained by loss-on-ignition (LOI) and verified by quantitative x-ray diffraction analysis. Table 2.1 shows the chemical composition of each cement given by XRF analysis, and Table 2.2 shows the complete phase composition of each cement given by XRD analysis. Please note the following observations:

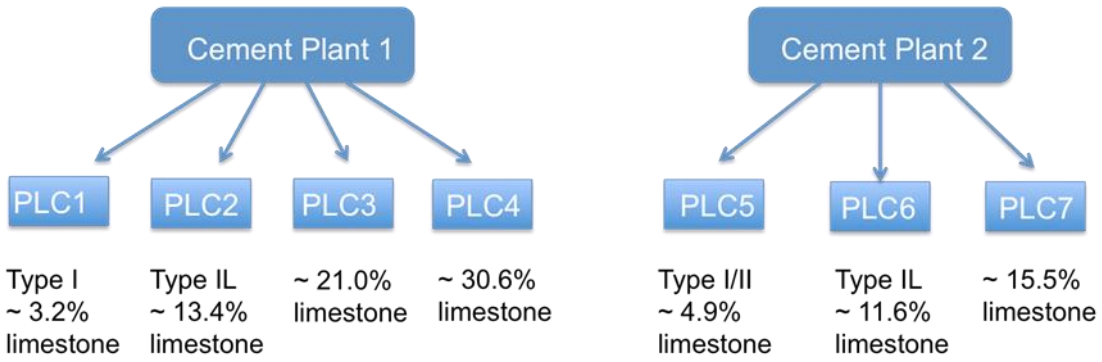

Figure 2.1: Cement ID and Approximate Limestone Content in Cement Produced by Each Cement Plant

- All cements were interground
- Cement Plant 1 was able to use the same limestone available on site to produce cements PLC2 trough PLC4
- Cement Plant 2 was not able to use the same limestone that is used for their Type I/II cement because the limestone available on site does not meet the requirements specified for Type IL cement in ASTM C595. Thus, a different source of limestone was added during the grinding process
- Cement Plant 2 optimized PLC7 (ground finer) in an attempt to achieve equivalent strength to PLC5, which was the control cement for Cement Plant 2 (Type I/II)
- Cement Plant 2 was unable to produce PLC8, which would have had a target limestone content of approximately 30%. This was due to the high moisture content of the limestone.

Table 2.1: Chemical Composition of Cements (% of Mass)

Cement ID	SiO_2	Al_2O_3	Fe_2O_3	CaO	MgO	Na_2O	K_2O	SO_3	LOI
PLC1	19.84	5.50	1.97	64.76	1.07	0.11	0.63	4.10	1.42
PLC2	18.63	5.22	1.84	66.39	1.05	0.11	0.54	4.21	5.90
PLC3	18.10	4.73	1.68	67.11	1.02	0.09	0.58	4.60	9.22
PLC4	16.93	4.66	1.47	68.11	1.21	0.09	0.38	4.70	13.45
PLC5	19.93	4.70	3.25	64.79	0.77	0.11	0.59	3.75	2.15
PLC6	19.03	4.63	3.26	65.73	0.80	0.12	0.67	3.78	5.09
PLC7	19.46	5.02	3.32	64.80	0.83	0.14	0.61	3.90	6.84

Table 2.2: Phase Composition of Cements (% by Mass)

Cement ID	C_3S	C_2S	C_3A	C_4AF	$CaCO_3$
PLC1	47.8	20.9	9.17	3.5	5.2
PLC2	44.9	16.8	7.62	3.1	13.9
PLC3	41.1	17.8	6.51	2.0	24.8
PLC4	34.2	13.6	6.03	3.0	30.3
PLC5	47.9	22.4	4.19	7.3	1.8
PLC6	46.5	28.7	2.94	8.1	12.0
PLC7	35.1	24.6	3.78	4.6	14.1

The particle size distribution (PSD) for each different cement was analyzed using a Malvern Mastersizer 2000 Laser Diffraction Particle Size Distribution Analyzer. Extra pure isopropanol was used as a dispersing agent. The particle diameters, in micrometers, corresponding to the 10%, 50%, and 90% values of the cumulative particle size distribution curve are shown in Table 2.3. These values are denoted as d_{10}, d_{50}, and d_{90}.

Table 2.3: Particle Diameters Given by Laser PSD Analysis

Cement ID	d_{10} (µm)	d_{50} (µm)	d_{90} (µm)
PLC1	4.3	17.3	47.1
PLC2	3.2	15.8	43.0
PLC3	2.8	14.6	44.1
PLC4	2.1	12.6	42.0
PLC5	3.8	15.7	43.4
PLC6	3.1	14.8	43.7
PLC7	2.0	13.9	44.8

The particle size distribution curves for the cements produced by Cement Plant 1, PLC1-PLC4, can be seen in Figure 2.2. The particle size distribution curves for the cements produced by Cement Plant 2, PLC5-PLC7, can be seen in Figure 2.3. Figure 2.4 shows the particle size distribution curves for all cements plotted on the same graph, for comparison.

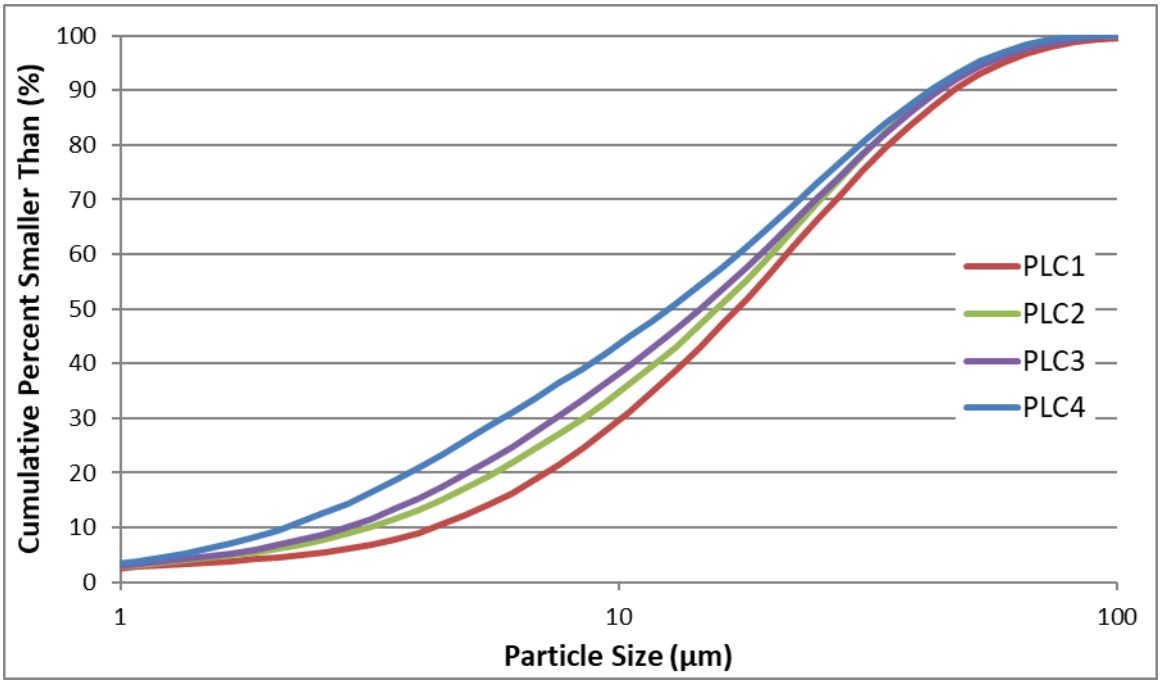

Figure 2.2: Particle Size Distribution Curves for Cements Produced by Cement Plant 1

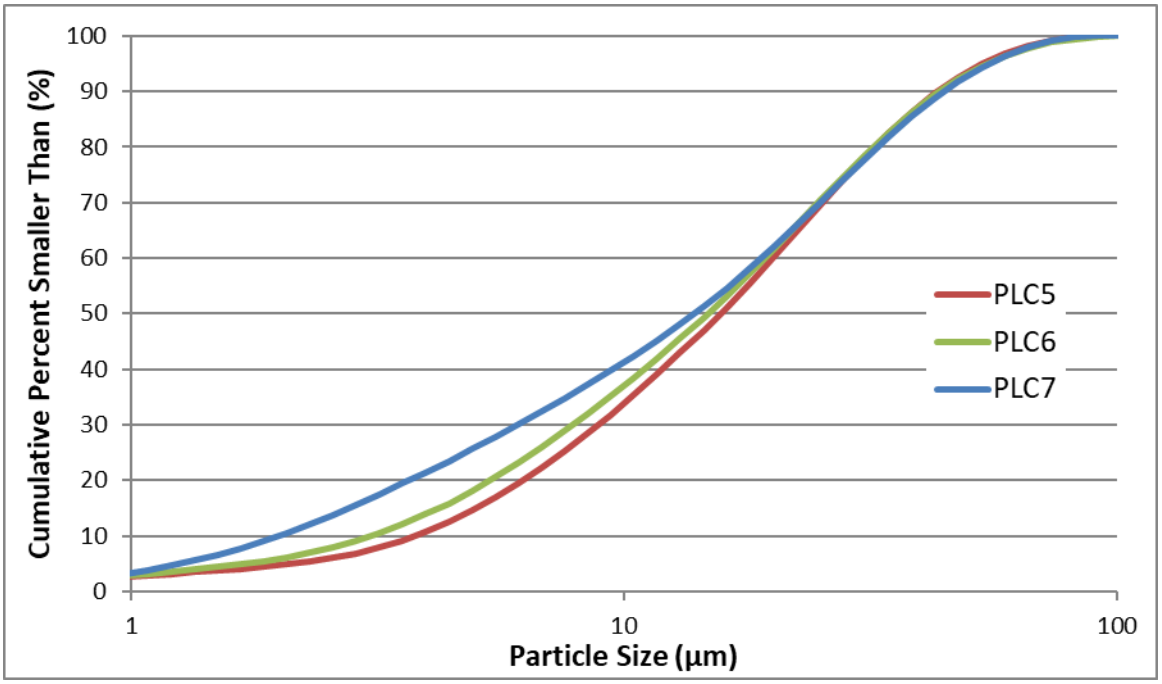

Figure 2.3: Particle Size Distribution Curves for Cements Produced by Cement Plant 2

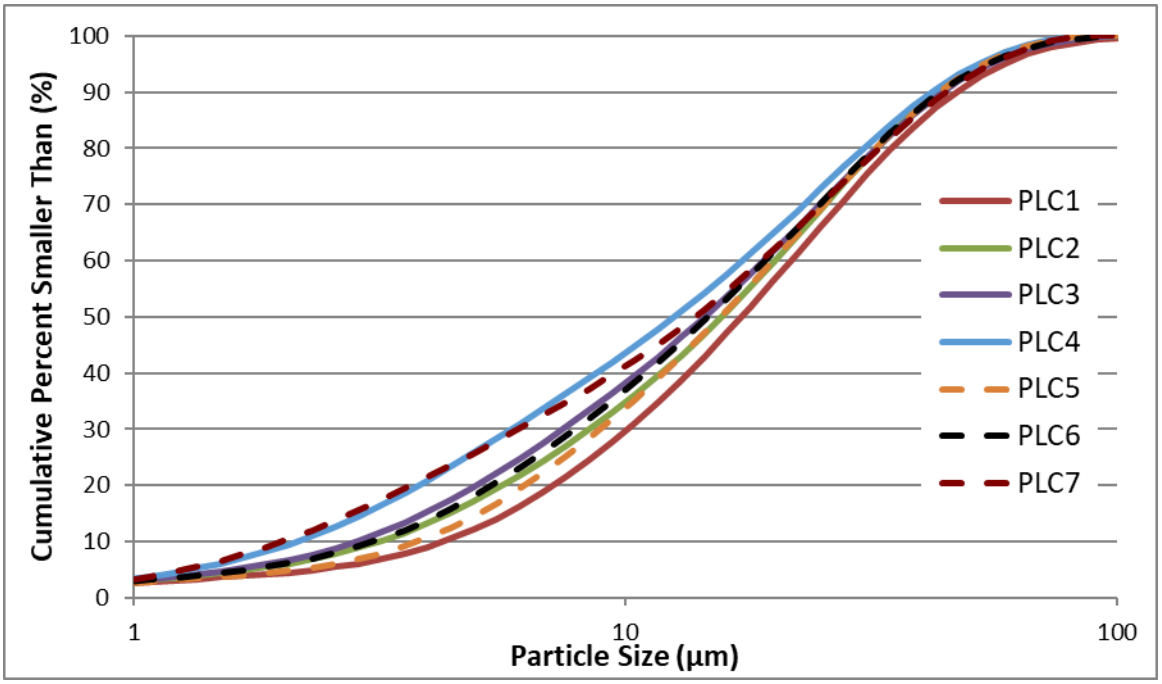

Figure 2.4: Particle Size Distribution Curves for All Cements

As expected, as the limestone content of the cement increases, the fineness of the cement also increases when comparing the cements produced by each plant separately. Additionally, it is important to note that the cements produced by Cement Plant 2 are finer than the cements produced by Cement Plant 1, at approximately equivalent limestone contents. It is also important to note that even though PLC7 has about half the interground limestone content of PLC4, the particle size distribution curves are very similar. Thus, it is safe to conclude that Cement Plant 2 ground their cements for a longer period of time than Cement Plant 1.

2.2. Limestone Powder

The limestone that was used at Cement Plant 1 to produce ordinary portland cement and also to intergrind the portland limestone cements was analyzed using quantitative XRD analysis. The plot of relative intensity vs. 2-Theta angle for the limestone powder is shown in Figure 2.5. Please note that, when normalized to account for the presence of rutile as an internal standard, the calcium carbonate content of the sample is 98.3%, indicating the high purity of the limestone. Loss-on ignition was also done on pulverized limestone powder and the results are shown in Table 2.4. Based on loss-on-ignition, the estimated calcium carbonate content is 98.9%, confirming the results of the quantitative XRD analysis. Unfortunately, a limestone sample from Cement Plant 2 could not be procured and the chemical and mineralogical compositions were not determined.

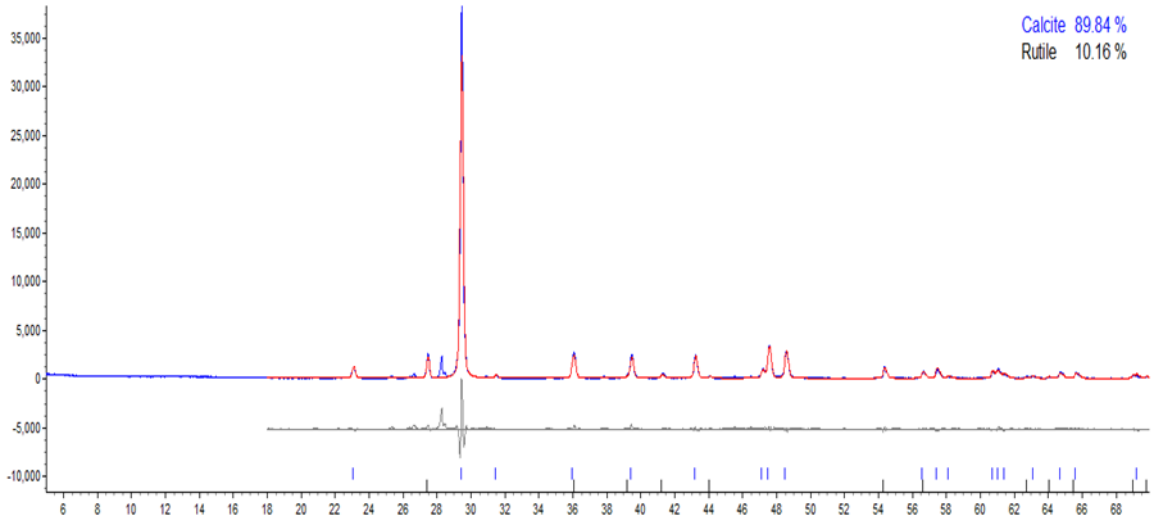

Figure 2.5: XRD Scan of Limestone Filler for Cement Plant 1

Table 2.4: Loss-on-Ignition of Limestone Filler for Cement Plant 1 (% by Mass)

Powder ID	LOI
Limestone	43.50

2.3. Supplementary Cementitious Materials (SCMs)

Five SCMs were used during the research project including: one Class F fly ash, and two Class C fly ashes, conforming to the requirements set forth in ASTM C618; ASTM C989 compliant Grade 100 ground-granulated blast furnace slag, commonly referred to as slag cement or GGBFS; and densified silica fume meeting ASTM C1240 requirements. Table 2.5 shows the nomenclature assigned to each SCM, and Table 2.6 shows the chemical composition for each SCM.

Table 2.5: SCM Nomenclature

SCM	SCM ID
Class F Fly Ash	FAF1
Class C Fly Ash 1	FAC1
Class C Fly Ash 2	FAC2
Slag	S
Densified Silica Fume	SF

Table 2.6: Chemical Composition of SCMs (% by Mass)

SCM ID	SiO_2	Al_2O_3	Fe_2O_3	CaO	MgO	Na_2O	K_2O	SO_3
FAF1	53.17	17.98	8.10	10.81	2.36	0.29	1.13	0.46
FAC1	38.55	18.34	5.37	22.62	4.83	1.19	0.67	1.78
FAC2	32.39	17.3	6.06	27.72	5.29	1.64	0.30	2.46
S	36.09	8.03	0.57	39.83	10.68	0.32	0.48	2.59
SF	97.16	0.31	0.12	0.92	0.28	0.06	0.65	0.20

2.4. Aggregates

Different types of fine and coarse aggregate were used to complete the research described in this Final Report. The selection of aggregate was dependent upon the specific test and/or intended research objective. All aggregates met the requirements specified in ASTM C33.

2.4.1. Fine Aggregate

There were two types of fine aggregate used to mix concrete. The first type of fine aggregate is classified as natural river sand obtained from a local source on the Colorado River, a river running through Central Texas. The second fine aggregate is classified as manufactured limestone sand obtained by the crushing of limestone rock from a local limestone source. The river sand is known to be ASR reactive, whereas the manufactured sand is non-reactive. The natural river sand was used to mix concrete for the purpose of mechanical properties testing, and the manufactured limestone sand was used for drying shrinkage and durability testing. The bulk specific gravity and absorption capacity of each aggregate are found in Table 2.7.

Table 2.7: Fine Aggregate Properties

Fine Aggregate	Bulk Specific Gravity	Absorption Capacity (%)
Natural River Sand	2.59	0.56
Manufactured Limestone Sand	2.42	3.77

2.4.2. Coarse Aggregate

Local limestone gravel conforming to size 56 grading requirements established in ASTM C33 was used for all concrete testing that is reported in this Final Report. The bulk specific gravity of the gravel is 2.47 and the absorption capacity is 3.12%.

2.5. Water

Potable tap water was used as mix water to mix all concrete that is presented in this report.

2.6. Nomenclature, Cement Chemistry Notation, and Abbreviations

A nomenclature system was developed to facilitate the identification of the different concrete mixes tested under the experimental investigation described in this Final Report. Unless otherwise noted in a specific section or chapter, this nomenclature system is used. Each concrete mix label consists of three parts separated by hyphens. The first part indicates the cement that was used in the concrete mix. The second part indicates the supplementary cementitious material(s), if any, which were incorporated into the concrete mix and the percent replacement of cement of each SCM. Please note that the second part of the label is only present if any supplementary cementitious materials were incorporated into the mixture. The third and final part of the label indicates the water to cementitious materials ratio. A schematic showing the nomenclature system can be found in Figure 2.6.

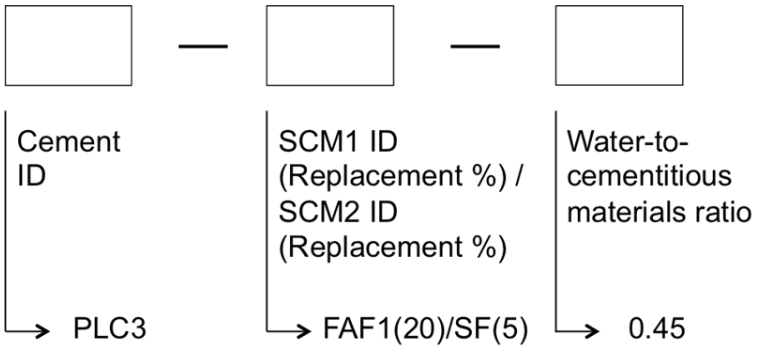

Figure 2.6: Graphical Representation of Nomenclature System

For example, the mix label of PLC2-FAF1(20)-0.45 explains that the concrete was made with cement PLC2 and 20% class F fly ash (as a replacement of cement) at a water to cementitious materials ratio of 0.45.

The following mix label would be used for a ternary blend: PLC3-FAC2(25)/SF(5)-0.50. In this case, the concrete was made with cement PLC3, 25% class C fly ash 2, and 5% silica fume with a water to cementitious materials ratio of 0.50.

Also, please note that throughout this report, cement chemistry notation and other common abbreviations typically used in cement and concrete research will be used. Please refer to the glossary for a list of the abbreviations used and to learn more about cement chemistry notation.

Chapter 3. Hydration of Portland Limestone Cement Systems

3.1. Introduction

Chapter 3 presents a brief overview of the hydration of ordinary portland cement and the research to date on the hydration of portland limestone cement. The hydration of portland limestone cement with significant limestone content, and in combination with supplementary cementitious materials, at a water to cementitious materials ratio of 0.45 is detailed in this chapter. The main objective of the study was to characterize the hydration of the portland limestone cement systems, which helped to better understand the development of mechanical and durability properties of these systems, the results of which are presented in other chapters of this Final Report.

The hydration of the system was monitored using x-ray diffraction (XRD) at three different temperatures: 5 ºC (41 ºF), 23 ºC (73 ºF), and 38 ºC (100 ºF). Hydration was stopped at 1, 7, and 56 days for all mixtures cured at 23 ºC, and at 7 and 56 days for mixtures cured at 5 ºC and 38 ºC. The experimental results are compared to theoretical results obtained with the use of thermodynamic modeling software.

3.2. Review of Hydration

3.2.1. Review of Hydration of Ordinary Portland Cement

When water is added to cement, the cement is said to undergo hydration. The reactants: cement and water, combine to form hydration products, which give concrete its strength, permeability, and durability properties. The most important hydration reactions are shown in Equations 3.1 to 3.6 (Mindess et al., 2003).

$$2C_3S + 11H \rightarrow C_3S_2H_8 + 3CH \quad \text{(Eq. 3.1)}$$

$$2C_2S + 9H \rightarrow C_3S_2H_8 + CH \quad \text{(Eq. 3.2)}$$

$$C_3A + 26H + 3C\$H_2 \rightarrow C_6A\$_3H_{32} \quad \text{(Eq. 3.3)}$$

$$2C_3A + 4H + C_6A\$_3H_{32} \rightarrow 3C_4A\$H_{12} \quad \text{(Eq. 3.4)}$$

$$2C_3A + 21H \rightarrow C_4AH_{13} + C_2AH_8 \quad \text{(Eq. 3.5)}$$

$$C_4AF + 3C\$H_2 + 21H \rightarrow C_6A\$_3H_{32} + AH_3 \quad \text{(Eq. 3.6)}$$

To summarize, the combination of calcium silicates and water results in calcium silicate hydrate (C-S-H) and calcium hydroxide (CH), also known as portlandite, and the addition of water to the calcium aluminate phases in OPC results in calcium aluminate hydrates. The most important hydration product is C-S-H, since it is the hydration product that is mainly responsible for binding all of the components in concrete and providing strength. The most common calcium aluminate

hydrates are ettringite ($C_6A\$_3H_{32}$), which is also commonly referred to as AFt, and monosulfate hydrate ($3C_4A\$H_{12}$), which can also be referred to as AFm. Table 3.1 shows the approximate volume percentage of each component for a typical Type I OPC hardened cement paste at a water-to-cement ratio of 0.5.

Table 3.1: Composition of Hardened Cement Paste Made from Type I OPC (w/c = 0.5) (Adapted from Bensted & Barnes, 2002)

Component	Approximate Volume (%)
C-S-H	50
CH	12
AFt and AFm combined	13
Unreacted cement	5
Capillary pores	20

3.2.2. Review of Hydration of Portland Limestone Cement—Research To Date

The hydration of portland limestone cement is similar to that of ordinary portland cement, but there are a few differences that should be mentioned. The limestone component of PLC is not an inert filler, as was previously believed, as it has been reported to participate in the hydration process to form carboaluminate phases (Hooton et al., 2007). The addition of limestone also was found to increase the reactivity of the cement because of the limestone powder particles acting as nucleation and growth sites for hydration products (Tennis et al., 2011).

Matschei et al. (2007) reported that, for cements with up to 5% limestone, all of the limestone participated in hydration to form monocarboaluminate, or monocarbonate, and hemicarboaluminate, or hemicarbonate. Table 3.2 shows the chemical formulas for monocarboaluminate and hemicarboaluminate. Whether hemicarboaluminate or monocarboaluminate form depends on a number of factors including the amount of carbonate, alumina, and sulfate (from gypsum) present in the cement (Matschei et al., 2007). Voglis et al. (2005) reported the formation of monocarboaluminate at 1-day and its presence at 2, 7, and 28 days. Zajac et al. (2014) reported that the addition of limestone leads to the formation of hemicarbonate at the expense of monosulfoaluminate and the conversion of hemicarbonate to monocarboaluminate at later ages.

Table 3.2: Common Hydration Products in PLC

Name	Chemical Formula
Monocarboaluminate	$Ca_4Al_2(CO_3)(OH)_{12}\cdot 5H_2O$
Hemicarboaluminate	$Ca_4Al_2(CO_3)_{0.5}(OH)_{13}\cdot 5.5H_2O$

3.3. Materials

Paste samples were cast using a water-to-cementitious materials ratio of 0.45. The cementitious materials include cements and supplementary cementitious materials (SCMs).

3.3.1. Cements

Cements PLC1 through PLC7, which have varying limestone contents, were used for this experimental investigation. For more information on the chemical composition and phase composition of all cements, please refer to section 2.1.

3.3.2. Supplementary Cementitious Materials

For this experimental investigation, the following supplementary cementitious materials were used: Class F fly ash, Class C fly ash 2, and Grade 100 slag. Please refer to section 2.3 for information on the chemical composition of each SCM.

3.3.3. Water

De-ionized water was used to mix paste specimens for this study.

3.4. Experimental Procedures

The paste samples were cured at different temperatures and the hydration products that were formed were obtained by using XRD at different ages to assess how the following factors affect the hydration of portland limestone cement systems:

- Limestone content in the cement
- Interaction between limestone and SCMs
- Curing temperature
- Curing time

3.4.1. Test Matrices, Casting, and Curing

Table 3.3 shows the test matrix for the paste mixtures cured at a temperature of 23 ^{o}C, and powder samples were obtained at 1, 7, and 56 days for XRD analysis. Table 3.4 shows the test matrix for the paste mixtures cured at temperatures of 5 ^{o}C and 38 ^{o}C, and powder samples were obtained at the ages of 7 and 56 days. Each sample was obtained by combining the cement, SCM, and water for each mixture in a plastic cup, covering the cup with a plastic lid, and shaking the cup at high

speed using an ultrasonic shaker for 60 seconds. The sample was then cured in a temperature-controlled chamber until the desired curing age was reached.

Table 3.3: Test Matrix for Temperature of 23 ºC

Cement ID	Straight Cement	20% Class F Fly Ash	20% Class C Fly Ash	35% Grade 100 Slag
PLC1	□	□	□	□
PLC2	□	□	□	□
PLC3	□	□	□	□
PLC4	□	□	□	□
PLC5	□	□	□	□
PLC6	□	□	□	□
PLC7	□	□	□	□

Table 3.4: Test Matrix for Temperatures of 5 ºC and 38 ºC

Cement ID	Straight Cement	20% Class F Fly Ash	20% Class C Fly Ash	35% Grade 100 Slag
PLC1	□			
PLC2	□			
PLC3	□	□	□	□
PLC4	□			
PLC5	□			
PLC6	□			
PLC7	□			

3.4.2. Procedure to Stop Hydration

Once the sample reached the proper curing age, a solvent exchange method was used to stop hydration. The solvent exchange method is a modified version of the method described by Lute (2016):

1. Remove the exterior surface of the sample.
2. Break down remaining interior sample into multiple small chunks of approximately 3–4 mm (0.12–0.16 in) in diameter.
3. Place 3–4 mm diameter samples in 99.5% isopropanol (100–125 mL) for 7 days.
4. Remove samples from isopropanol and place in a vacuum desiccator for 3 days.

3.4.3. XRD Procedure

After removing the sample from the vacuum desiccator, the samples were crushed into a fine powder passing the No. 140 sieve. The powder was then placed in a sample holder, the sample

holder was placed in a Siemens D500 Diffractometer, and the sample was tested using the following parameters: 2θ range of 5-70°, 2θ step size of 0.02°, and a 4-second dwell time for each step.

3.4.4. Nomenclature

A similar nomenclature system as described in section 2.6 was developed for use in this chapter. Each paste mixture label consists of four parts separated by hyphens. The first part indicates the cement that was used in the mixture. The second part indicates the supplementary cementitious material(s), if any, which were incorporated into the mixture and the percent replacement of cement of each SCM. Please note that the second part of the label is only present if any supplementary cementitious materials were incorporated into the mixture. The third part of the label indicates the temperature, in degrees Celsius, at which the mixture was cured. The fourth and final part of the label specifies the curing age, in days, before hydration was stopped and the sample was pulverized and scanned. A schematic showing the nomenclature system can be found in Figure 3.1.

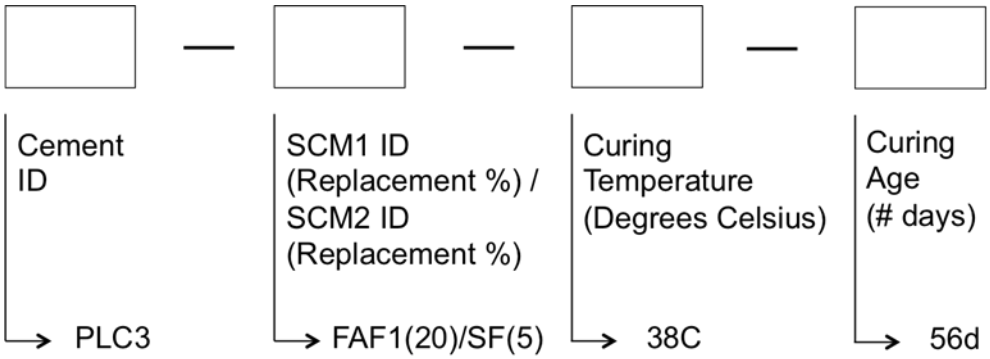

Figure 3.1: Graphical Representation of Nomenclature

3.5. Results and Discussion

3.5.1. X-Ray Diffraction Analysis

Qualitative x-ray diffraction analysis was used to study the phase assemblage of portland limestone cement systems and how it changes with time and temperature. Although each powder sample was tested using a 2θ range of 5-70°, the range of 5-35° is shown in the figures in this section as the most relevant characteristic x-ray diffraction peaks for cementitious materials occur in this range.

To facilitate the labeling of the characteristic peaks in each figure, a unique symbol, consisting of one or two letters, has been assigned to each mineral. The nomenclature can be seen in Table 3.5.

Table 3.5: Nomenclature Used for XRD Peak Identification

Symbol	Mineral
P	Portlandite
E	Ettringite
MS	Monosulfoaluminate
C	Calcite
A	Anhydrous cement (Includes alite, belite, C_3A)
H	Hemicarboaluminate
cH	Carbonated Hemicarboaluminate
MC	Monocarboaluminate
Q	Quartz
Gi	Gismondine
S	Srebrodol'skite

3.5.1.1. Straight Cement Mixtures at 23 ºC

The plots of relative intensity vs. 2θ angle after 1, 7, and 56 days for the straight cement mixtures cured at a constant temperature of 23 ºC can be seen in the following figures. For the control cement of Cement Plant 1, PLC1, XRD analysis shows that PLC1 behaves exactly as expected (Figure 3.2). Following is a short analysis at each day for this cement. This analysis will be useful to differentiate between the hydration products as increasing limestone is introduced into system for PLC2, PLC3, and PLC4.

- ***Day 1:*** there is anhydrous (unreacted) cement, denoted by symbol "A" in the 2θ range of about 31–35 degrees. There is also unreacted calcite, denoted by the symbol "C", which shows up at about 29 degrees. As expected, the anhydrous cement and the limestone react to form hydration products, and thus their respective peaks decrease progressively with age. Portlandite and ettringite have also formed, as shown by their characteristic peaks.

- ***Day 7:*** There is less anhydrous cement and an increased amount of portlandite due to the chemical reactions shown in Equations 3.1 and 3.2 continuing to take place. Please note that the amount of calcite is less and also note that a very small amount of ettringite is present at 7 days, due to dissolution of ettringite.

- ***Day 56:*** There is even less anhydrous cement present after 56 days of curing. As suggested by Equation 3.4, some of the dissolved ettringite has reacted with C_3A to form a relatively small amount of monosulfoaluminate.

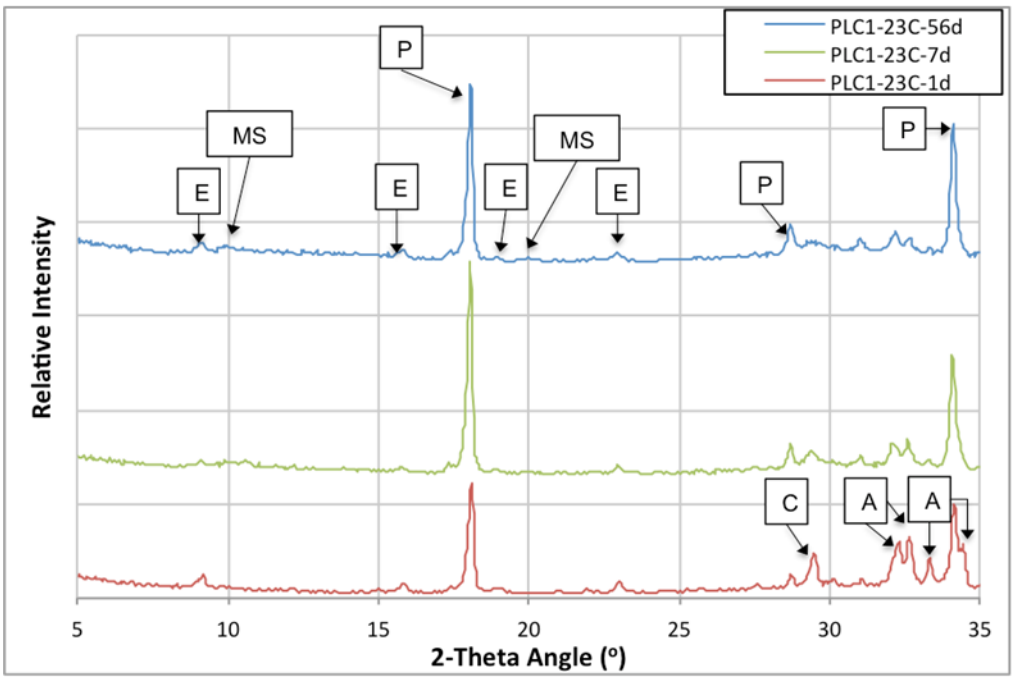

Figure 3.2: XRD Scans for PLC1 at 23 °C after 1, 7, and 56 Days

The scans for PLC2, PLC3, and PLC4 are shown in Figures 3.5 through 3.5. The formation of hydration products of the cements with higher limestone contents is very similar to PLC1, with three very important differences:

- Hemicarboaluminate is present after 7 days of hydration
- Monosulfoaluminate is not present after 56 days of hydration
- Monocarboaluminate is present after 56 days of hydration

These results are consistent with what other researchers have reported in the past (Lothenbach et. al, 2008; De Weerdt et al., 2011; Zajac et al., 2014). Zajac et al. showed that these trends held for cements containing up to 15% limestone and they performed XRD analysis after 1, 2, 7, 28, 90, and 180 days. The absence of monosulfoaluminate is attributed to the stabilization of ettringite by the limestone powder (Lothenbach et al., 2008).

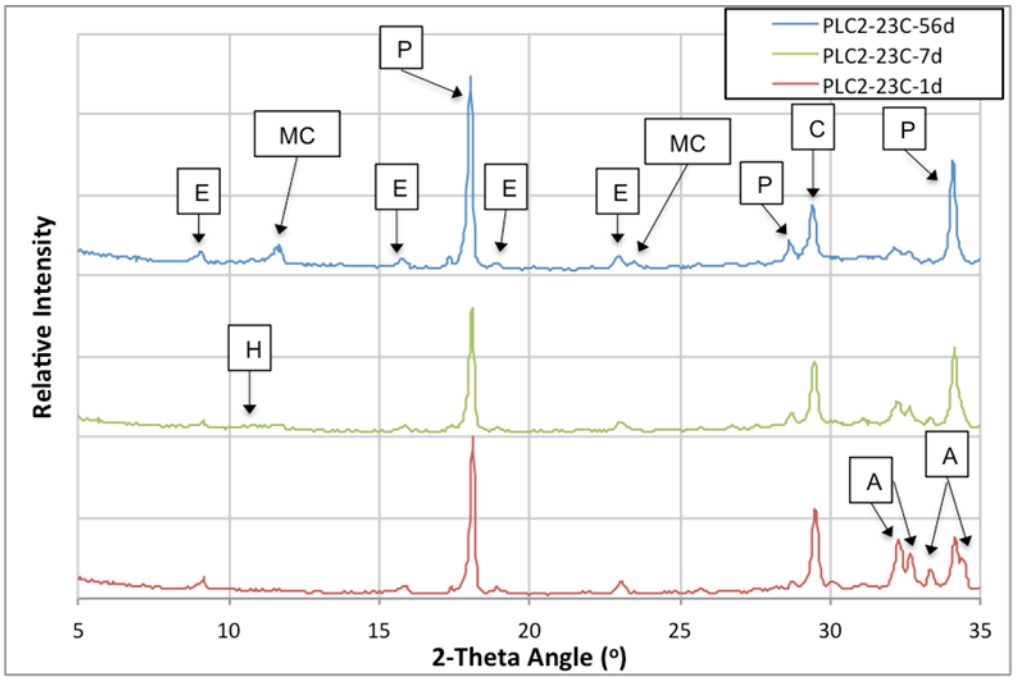

Figure 3.3: XRD Scans for PLC2 at 23 °C after 1, 7, and 56 Days

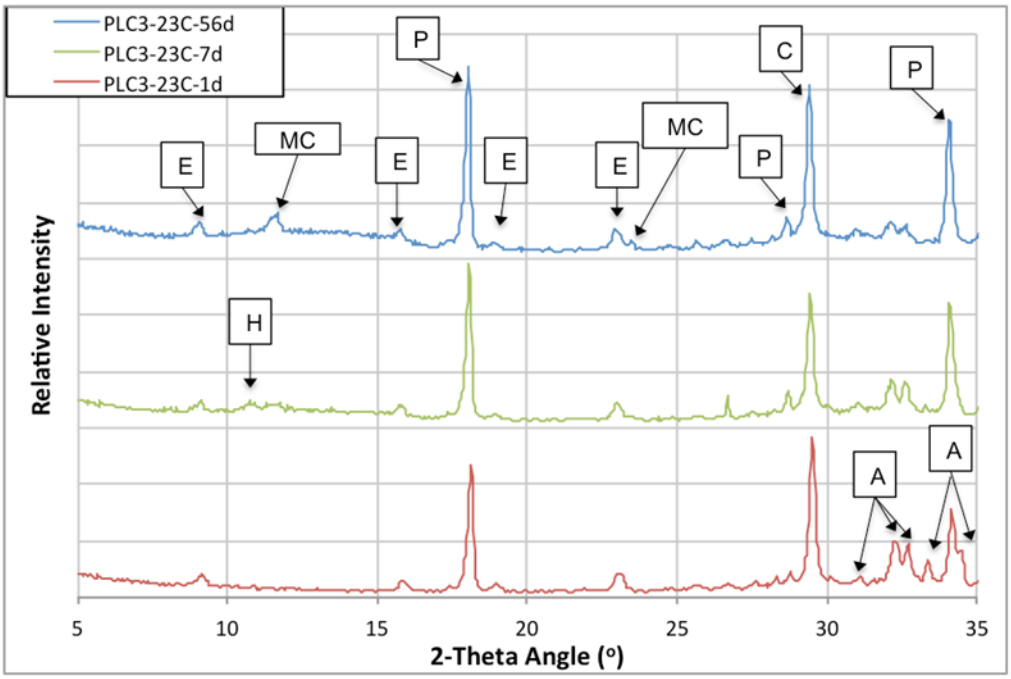

Figure 3.4: XRD Scans for PLC3 at 23 °C after 1, 7, and 56 Days

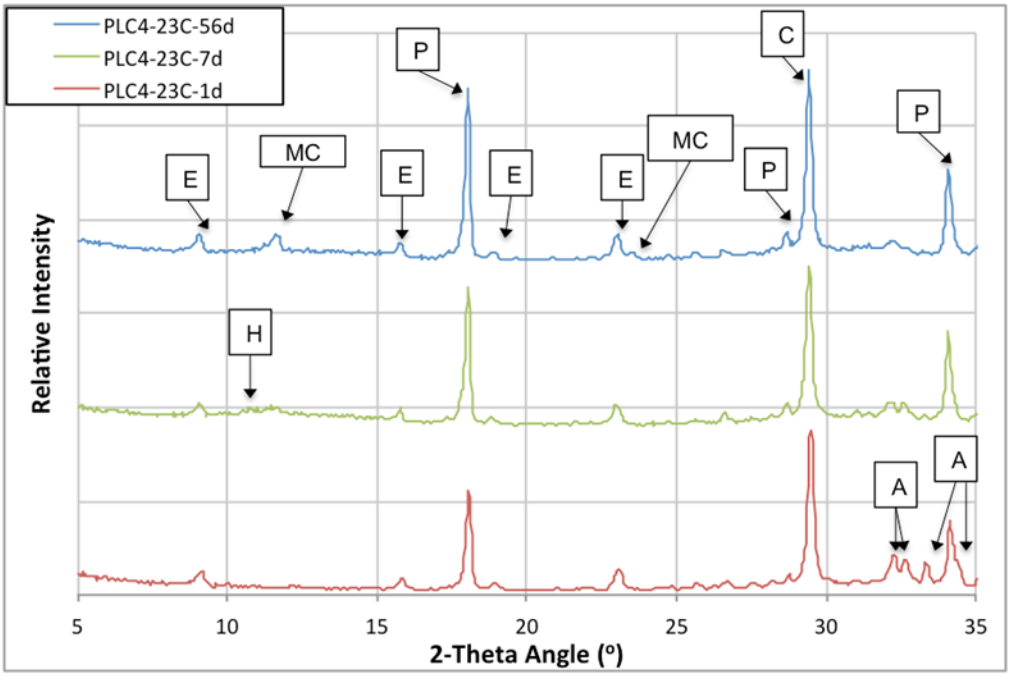

Figure 3.5: XRD Scans for PLC4 at 23 °C after 1, 7, and 56 Days

The XRD scans for PLC5 are shown in Figure 3.6. PLC5, which is the control cement from Cement Plant 2, shows similar hydration products to PLC1, except that PLC5 does not form monosulfoaluminate. Instead, hemicarboaluminate and monocarboaluminate are present after 7 and 56 days respectively. A possible explanation could be the low C_3A content in PLC5.

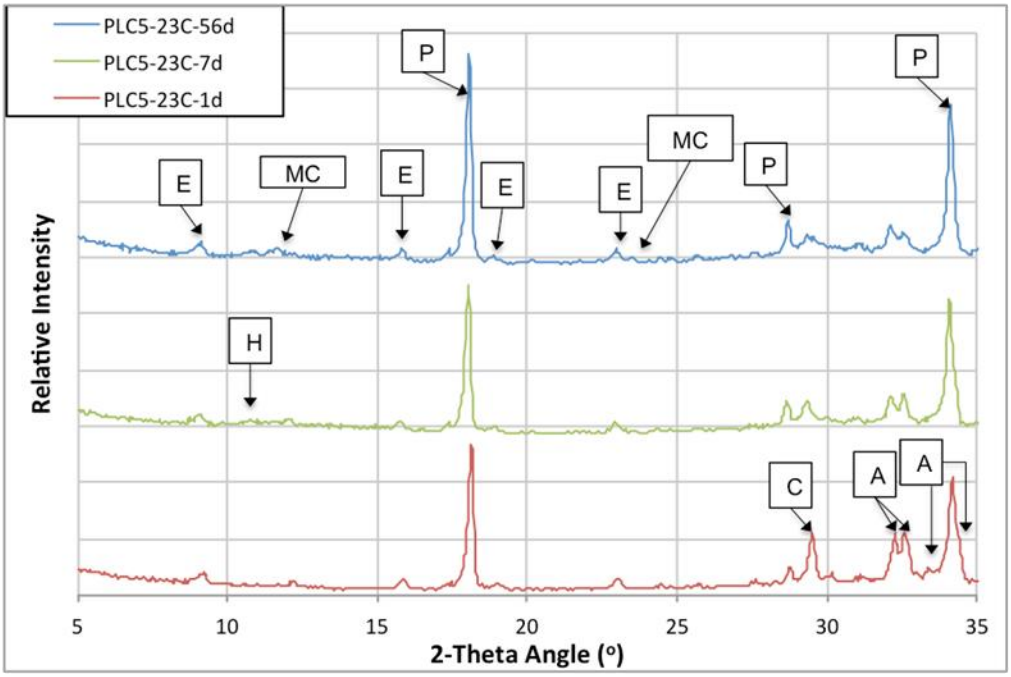

Figure 3.6: XRD Scans for PLC5 at 23 °C after 1, 7, and 56 Days

PLC6 and PLC7, which have approximate limestone contents of 11.6% and 15.5%, respectively, also formed hemicarboaluminate and monocarboaluminate at later ages, as shown in Figures 3.7 and 3.8. It is worth noting that a small amount of hemicarbonate is still present at 56 days for PLC5 through PLC7, which was not observed for PLC1 through PLC4. Based on the work of Zajac et al. (2014), it is expected that conversion of hemicarboaluminate to monocarboaluminate would progress to completion, had the reaction been given enough time.

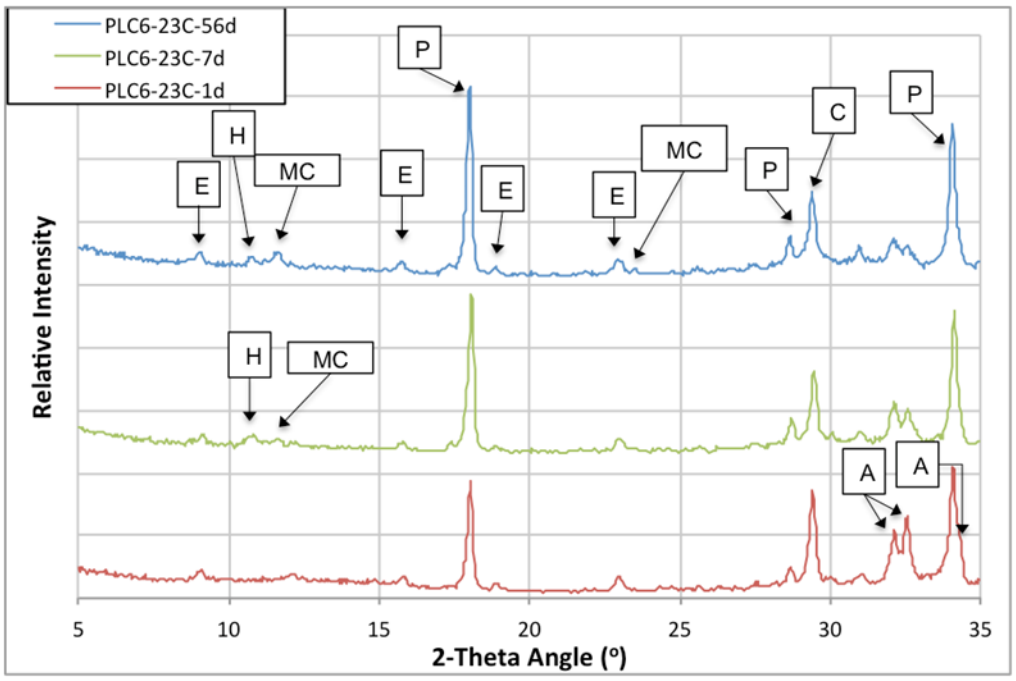

Figure 3.7: XRD Scans for PLC6 at 23 °C after 1, 7, and 56 Days

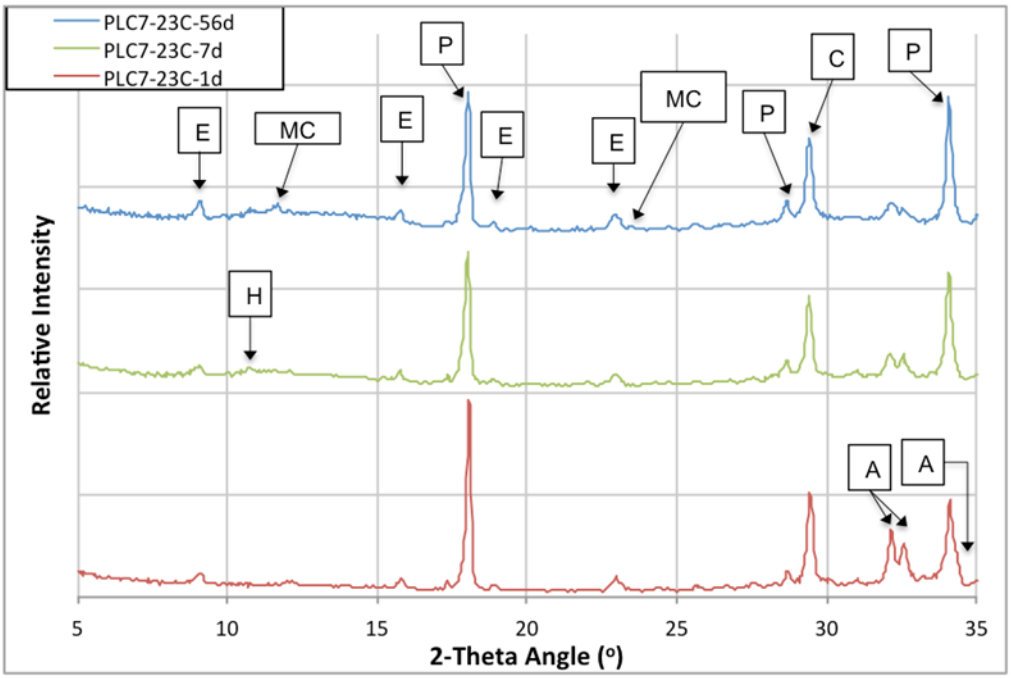

Figure 3.8: XRD Scans for PLC7 at 23 °C after 1, 7, and 56 Days

The effect of increased limestone content on phase assemblage after 56 days can be seen in Figures 3.9 and 3.10. The approximate limestone content for each mixture is provided for convenience in red bold font next to the beginning of each curve. Please note that the content of the anhydrous

cement appears to decrease as the limestone content of the cement increases. This could be further evidence that limestone powder accelerates hydration by providing nucleation and growth sites for hydration products, however, further research is needed to verify this is the reason for a decrease in unreacted cement with an increasing limestone content.

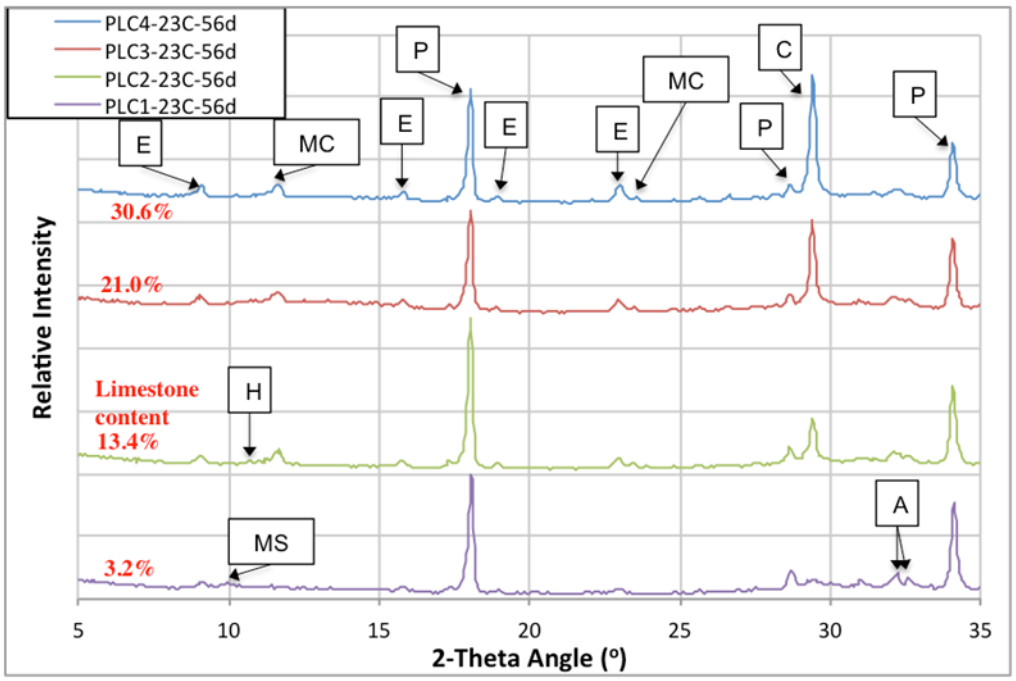

Figure 3.9: XRD Scans of PLC1-PLC4 at 23 °C after 56 Days

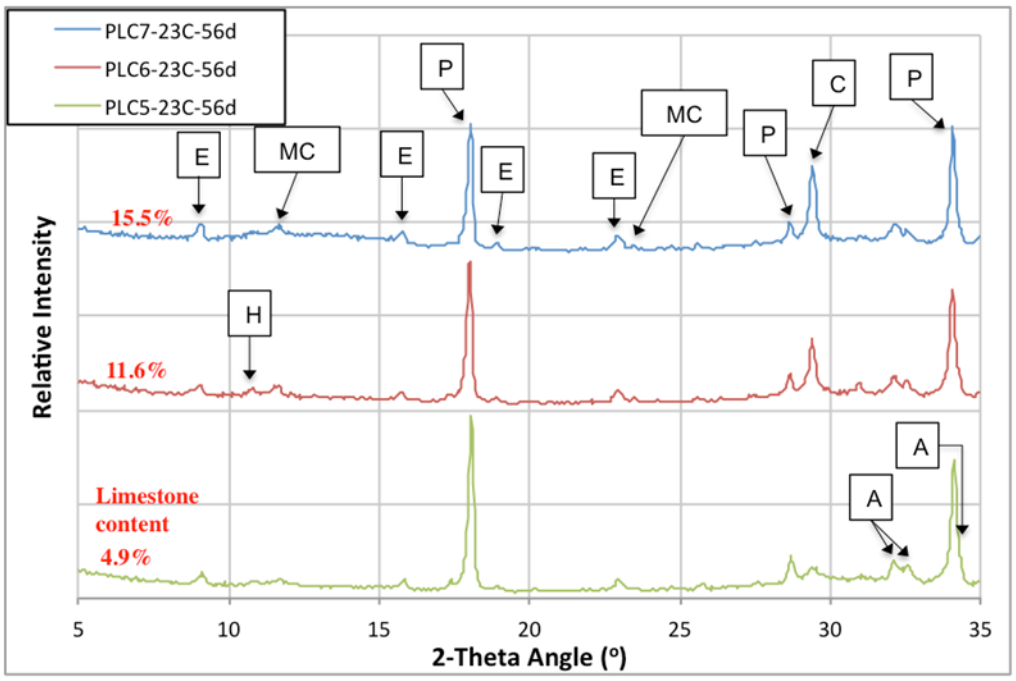

Figure 3.10: XRD Scans of PLC5-PLC7 at 23 °C after 56 Days

3.5.1.2. Effect of SCMs at 23 °C

To investigate the effect of the interaction between cements with high limestone content and supplementary cementitious materials on the formation of hydration products, PLC3 was combined with 20% class F fly ash (10.8% CaO), 20% Class C fly ash (27.7% CaO), or 35% grade 100 slag. The results of replacing the cement with fly ash can be seen in Figures 3.11 through 3.14.

The XRD scans for the mixtures with PLC3 and SCMs are similar to the scan of the PLC3 mixture. For the mixtures with fly ash, there appears to be a decrease in the portlandite content after 56 days, when compared to 7 days of hydration. This can be attributed to the pozzolanic reaction, where the portlandite from cement hydration is combining with the silica from the fly ash to form calcium silicate hydrate, or C-S-H. Quartz, or crystalline silica, is present for the mixtures with fly ash. It is also important to note that there is evidence that the fly ashes appear to accelerate the conversion of hemicarboaluminate to monocarboaluminate. The presence of monocarboaluminate is significant at 7 days, especially for the high calcium fly ash. At 56 days, there appears to be a significant amount of monocarboaluminate present and very little to no hemicarboaluminate left.

As shown, the same trends hold when PLC4 and PLC7 respectively, are used in combination with 20% class F fly ash.

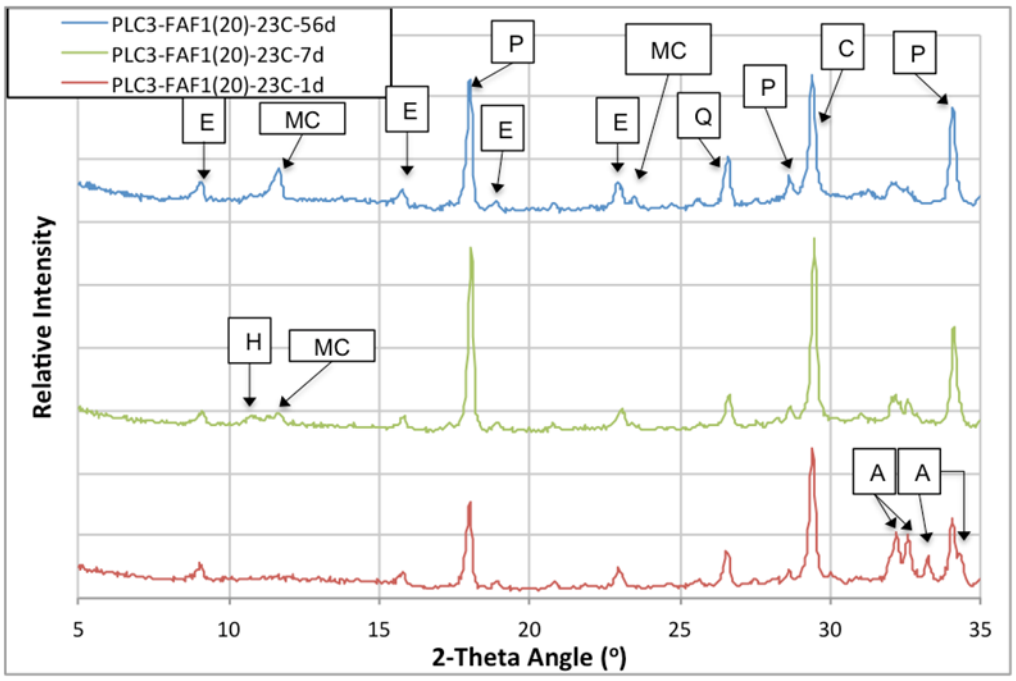

Figure 3.11: XRD Scans for PLC3-FAF1(20)-23C after 1, 7, and 56 Days

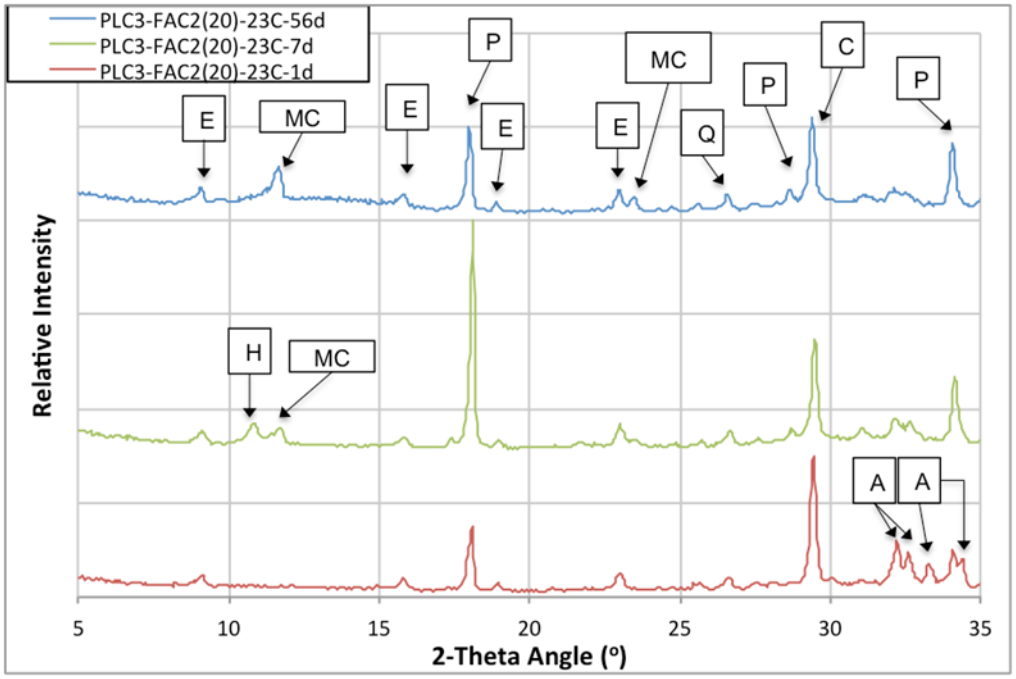

Figure 3.12: XRD Scans for PLC3-FAC2(20)-23C after 1, 7, and 56 Days

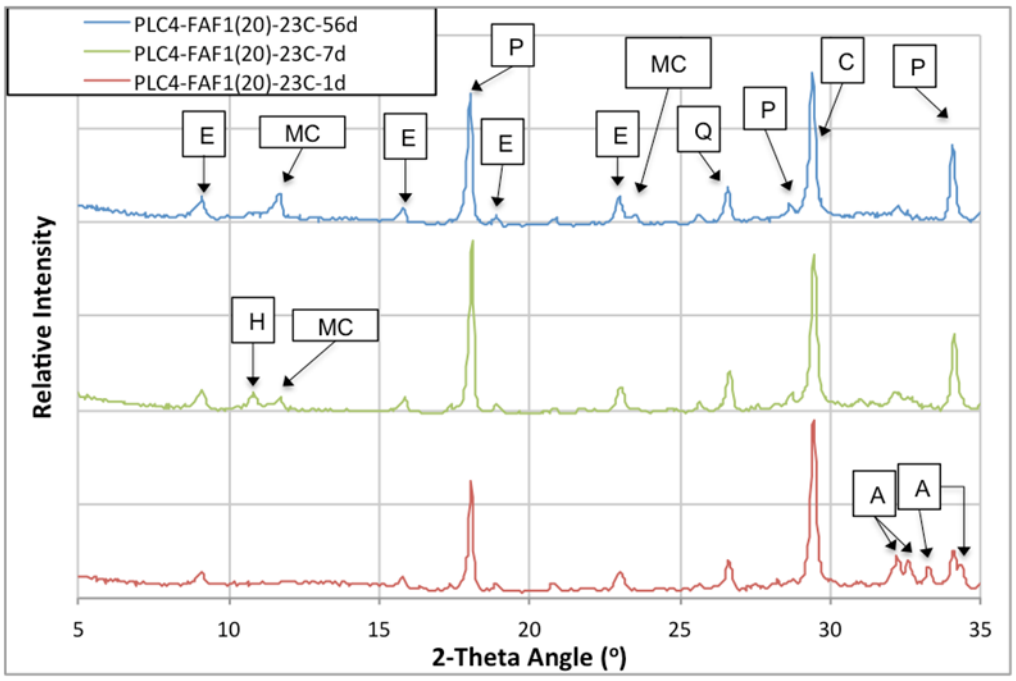

Figure 3.13: XRD Scans for PLC4-FAF1(20)-23C after 1, 7, and 56 Days

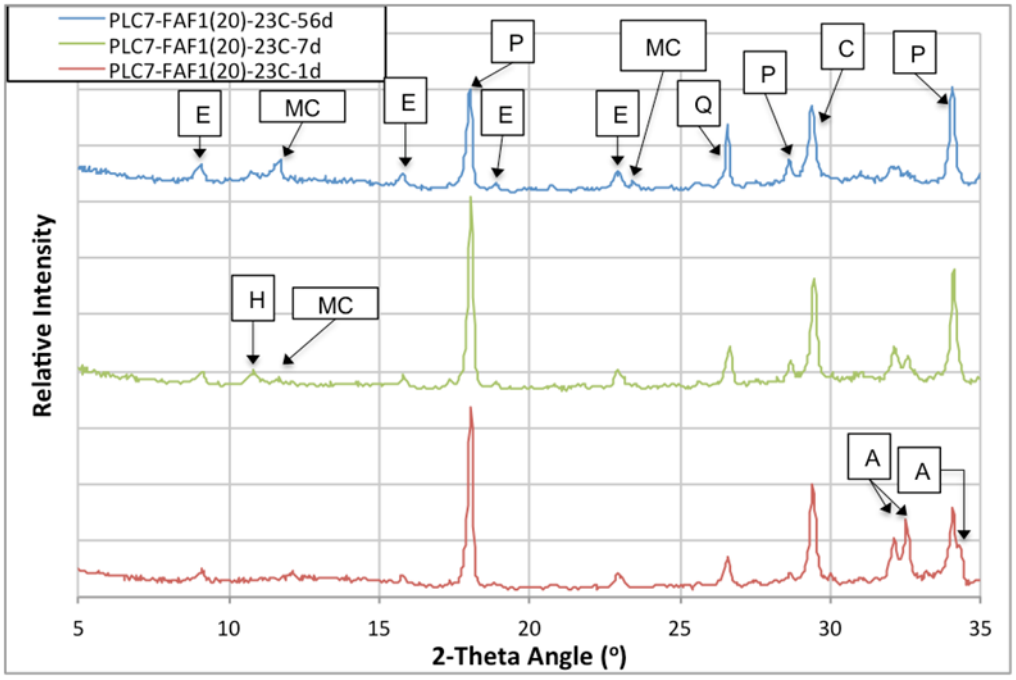

Figure 3.14: XRD Scans for PLC7-FAF1(20)-23C after 1, 7, and 56 Days

Figure 3.15 shows the XRD scans of PLC1 through PLC4 with a 20% cement replacement with class F fly ash, cured at 23 °C for 56 days. The control cement, PLC1 combined with fly ash, forms monosulfoaluminate as expected. Please note that a small amount of hemicarboaluminate appears

to be present after 56 days. In the future, it would be interesting to extend the curing for this mixture and stop hydration at a later age to see if the hemicarboaluminate eventually converts to monocarboaluminate.

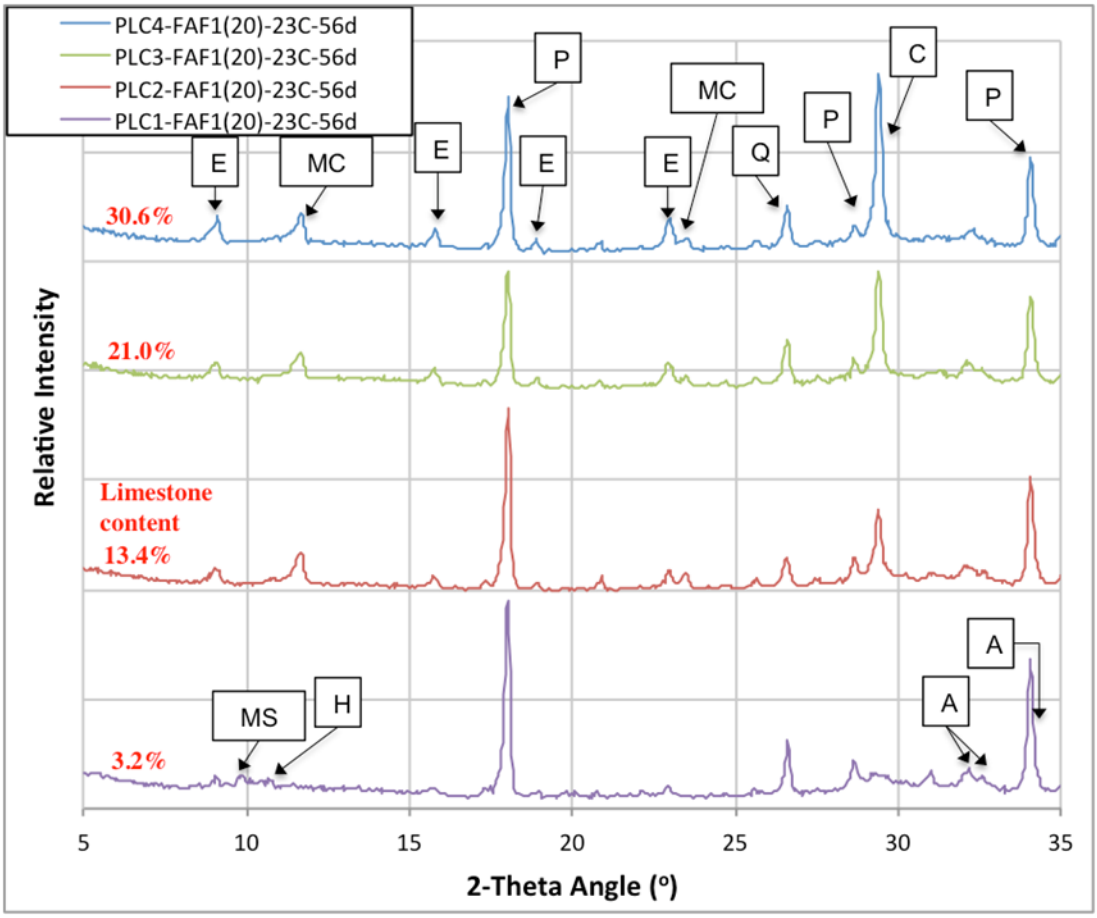

Figure 3.15: XRD Scans of PLC1-PLC4 with 20% Class F Fly Ash at 23 °C after 56 Days

There is not a significant effect of increasing the limestone content of the cement in terms of hydration product formation beyond a certain point. In other words, after enough limestone is added to promote the formation of carboaluminates, the same hydration products form whether the mixture includes 13% or 30% limestone in the cement. The higher limestone content mixture, PLC4-FAF1(20)-23C-56d, does appear to have more ettringite and monocarboaluminate present after 56 days, but quantitative XRD analysis using an internal reference should be able to verify this claim. If more limestone is present, it may encourage earlier formation of carboaluminates, by providing more available limestone particles to serve as nucleation and growth sites.

As shown in Figure 3.16, the addition of slag to the mixture does not appear to change the hydration product formation significantly. If anything, the addition of slag to the mixture appears to slow down the conversion from hemicarboaluminate to monocarboaluminate, since there appears to be

more hemicarboaluminate at 56 days for the mixture with 35% slag. The peaks for hemicarboaluminate and monocarboaluminate, which are both found in the range of 10.5-12 degrees 2θ, appear to broaden and combine with one another. Zajac et al. (2014) attribute this phenomenon to the formation of a "hemicarbonate containing additional carbonate, i.e. with a composition between hemicarbonate and monocarbonate," which was studied in depth by Runčevski et al. (2012) and which they named carbonated hemicarboaluminate. Runčevski's team was able to find that the carbonated hemicarboaluminate phase is "characterized by a larger amount of carbonate ion (at the expense of the hydroxyl anions)." The symbol "cH" has been assigned to label the carbonated hemicarboaluminate peak on the XRD plots.

If PLC7 is combined with 35% slag, the effect is essentially the same. As shown in Figure 3.17, hemicarboaluminate, carbonated hemicarboaluminate, and monocarboaluminate are all present after 7 and 56 days of hydration at a temperature of 23 ^{o}C.

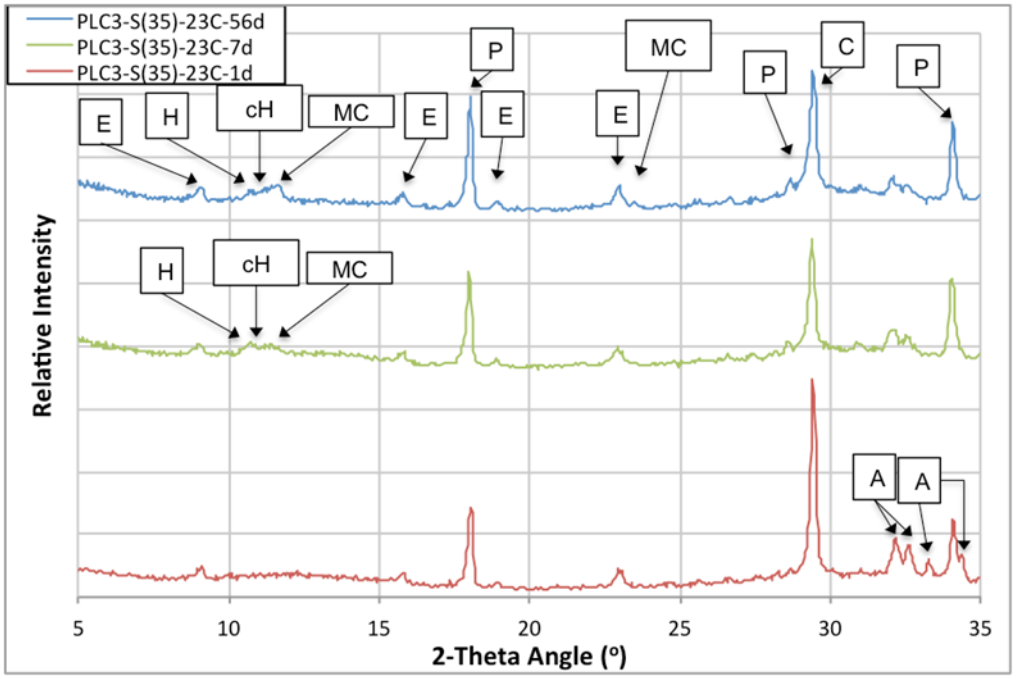

Figure 3.16: XRD Scans for PLC3-S(35)-23C after 1, 7, and 56 Days

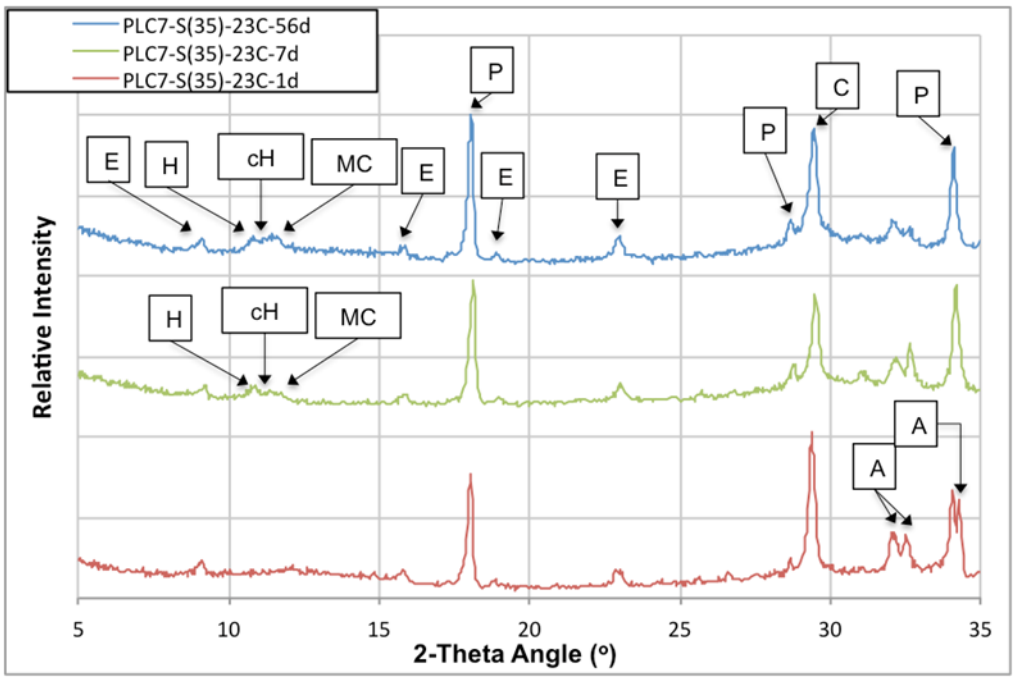

Figure 3.17: XRD Scans for PLC7-S(35)-23C after 1, 7, and 56 Days

3.5.1.3. Effect of Temperature on Straight Cement Mixtures

As shown in Table 3.4, several mixtures were cast and cured at constant temperatures of 5 °C and 38 °C to evaluate the effect of curing temperature on the formation of hydration products of portland limestone cement systems.

3.5.1.3.1. 38 °C

The plots of relative intensity vs. 2θ angle after 7 and 56 days for the straight cement mixtures cured at a constant temperature of 38 °C can be seen in Figure 3.18, which shows the XRD scan of PLC1 at the elevated curing temperature, shows that conversion of ettringite to monosulfate starts much earlier, when compared to a curing temperature of 23 °C. In fact, while there is still ettringite present after 56 days of curing at 23 °C, there is only a small amount of ettringite present after 7 days at the higher temperature, and all of the ettringite has converted after a curing period of 56 days.

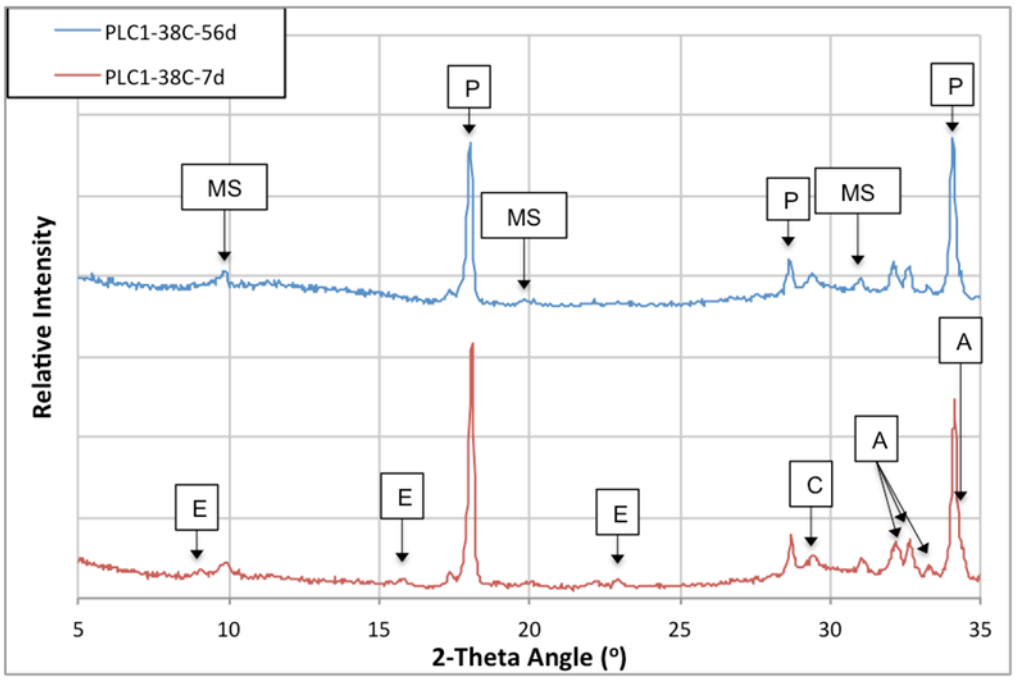

Figure 3.18: XRD Scans for PLC1 at 38 °C after 7 and 56 Days

The mixtures with PLC2, PLC3, and PLC4, are shown in Figures 3.19 through 3.21. PLC2 through PLC4 do not show significant conversion to monocarboaluminate at 56 days, as would be expected, based on the test results from the mixtures cured at 23 °C. The suppression of the monocarboaluminate phase may be attributed to the higher temperature, which has been reported by other researchers (Runčevski et al., 2012), where the hemicarboaluminate phase converts to carbonated hemicarboaluminate with increased temperature and low exposure to carbon dioxide. This would also explain the broadening of the peaks in the 10.5-12 degree 2-theta angle region, where hemicarboaluminate, carbonated hemicarboaluminate, and monocarboaluminate would be present. Another possibility would be that the monocarboaluminate has converted to another phase at the higher temperature, but further investigation would have to be done to verify this.

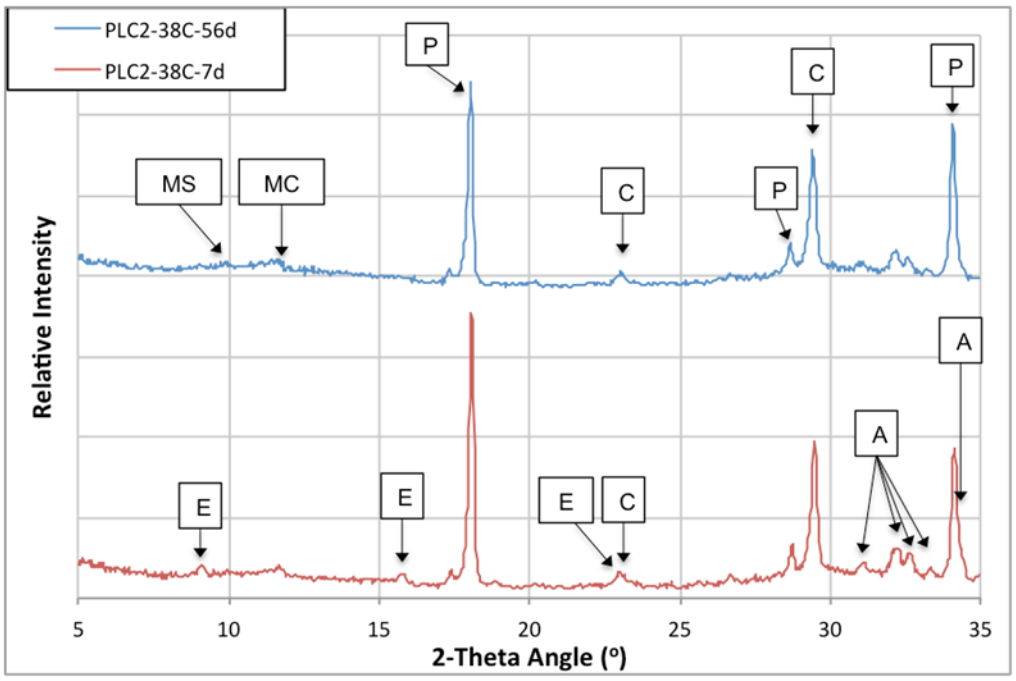

Figure 3.19: XRD Scans for PLC2 at 38 °C after 7 and 56 Days

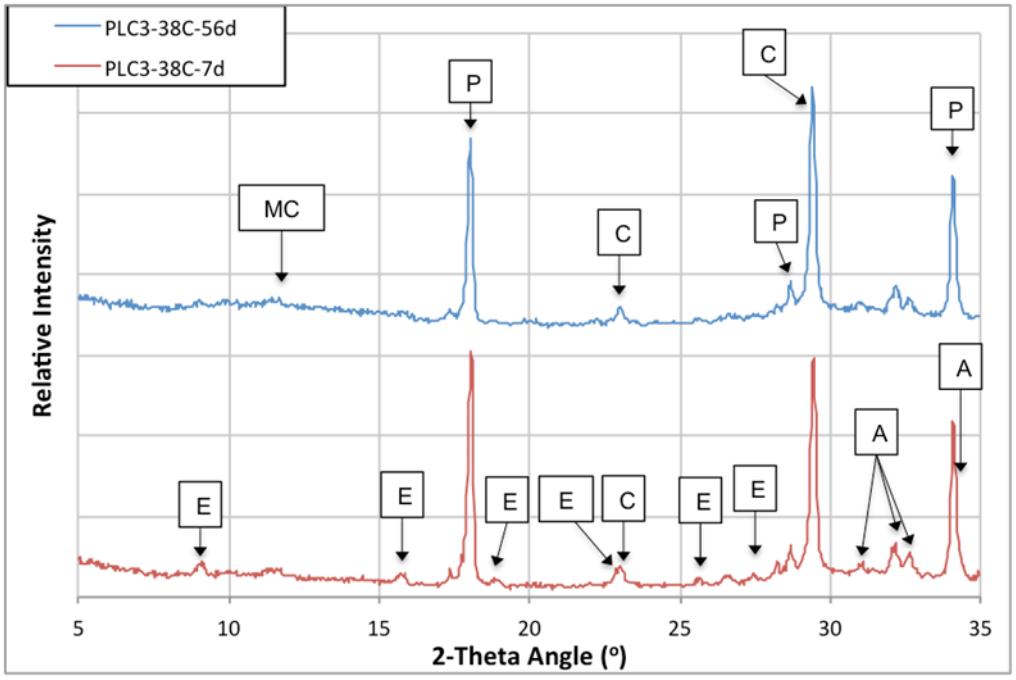

Figure 3.20: XRD Scans for PLC3 at 38 °C after 7 and 56 Days

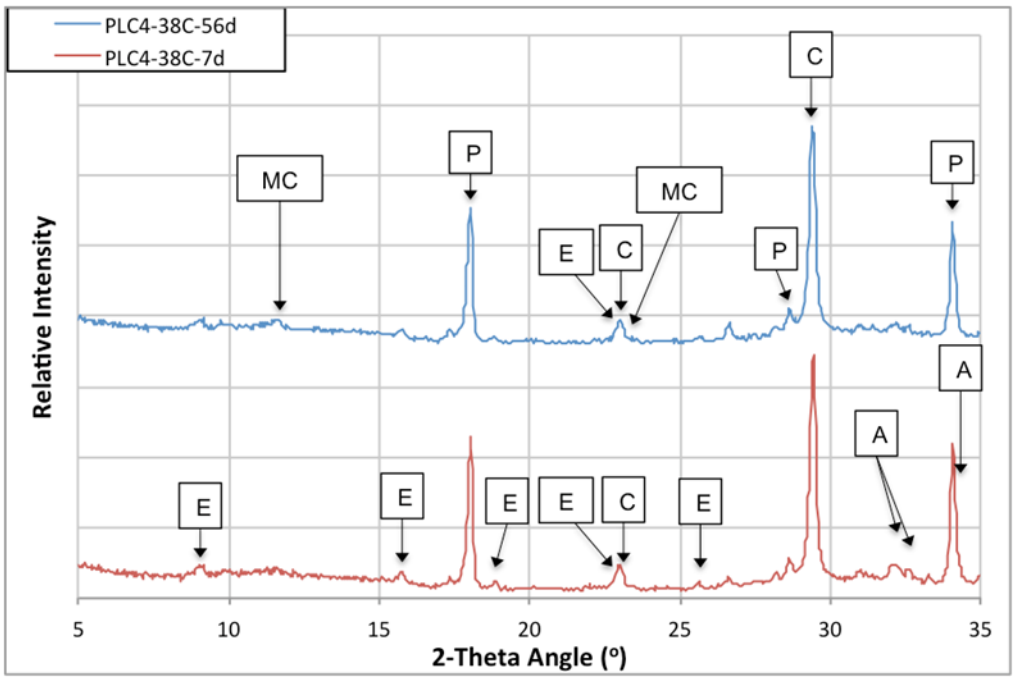

Figure 3.21: XRD Scans for PLC4 at 38 °C after 7 and 56 Days

The XRD scan of the sample made with PLC5 (Figure 3.22), the Type I/II cement that is the control cement produced by Cement Plant 2, is very similar to PLC1; the only difference is that the formation of monosulfoaluminate is less obvious for PLC5. For the mixtures with PLC6 and PLC7, the formation of monocarboaluminate is even less apparent than PLC2 through PLC4 after 56 days. In addition, PLC6 and PLC7 show a very small amount of monosulfoaluminate after 56 days of curing at 38 °C, which was not present for PLC6 and PLC7 after 56 days of curing at 23 °C (Figures 3.23 and 3.24).

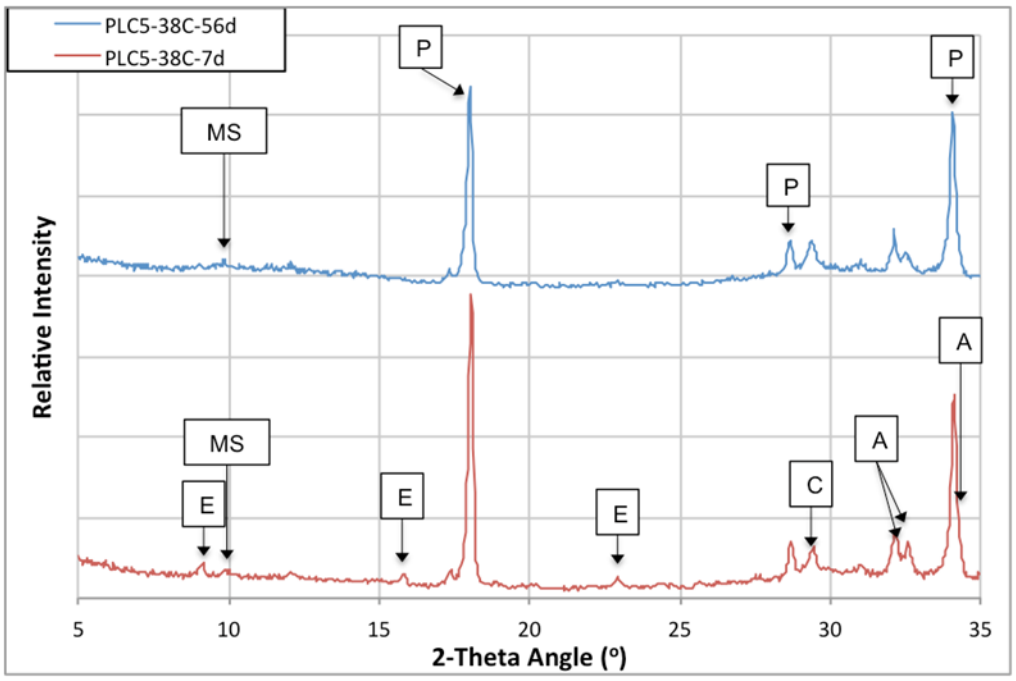

Figure 3.22: XRD Scans for PLC5 at 38 °C after 7 and 56 Days

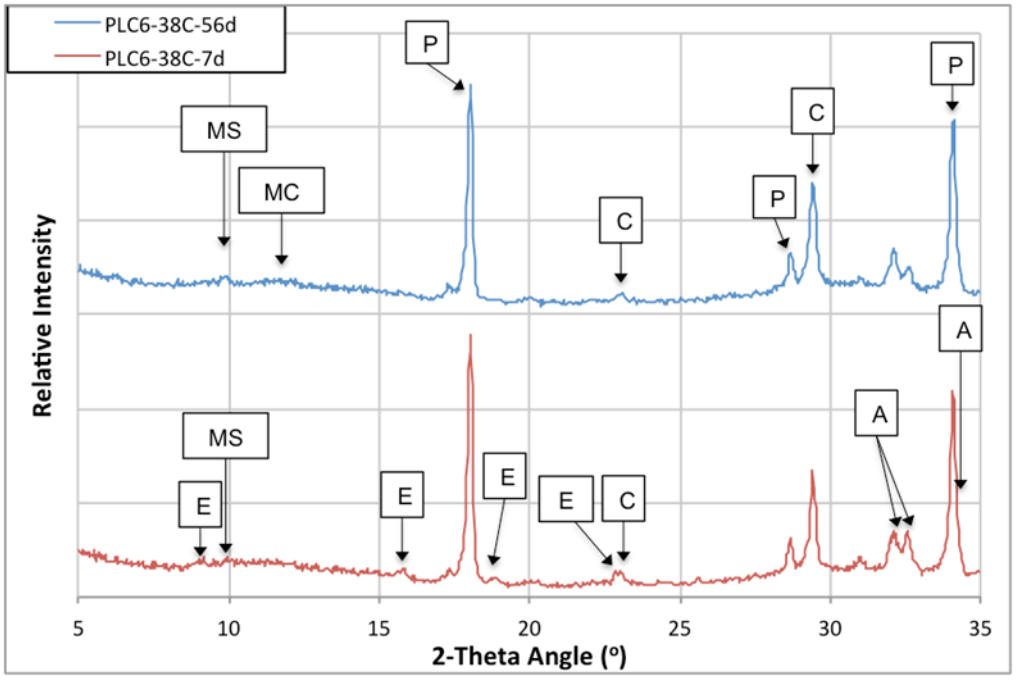

Figure 3.23: XRD Scans for PLC6 at 38 °C after 7 and 56 Days

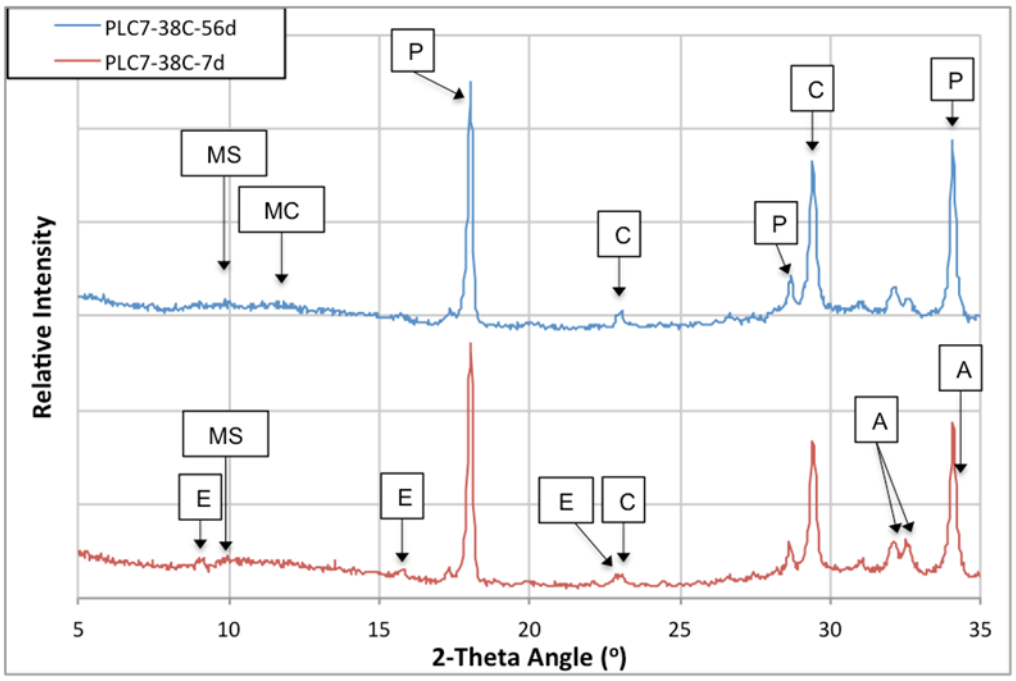

Figure 3.24: XRD Scans for PLC7 at 38 °C after 7 and 56 Days

3.5.1.3.2. 5 °C

The plots of relative intensity vs. 2θ angle after 7 and 56 days for the straight cement mixtures cured at a constant temperature of 5 °C can be seen in Figures 3.25 through 3.27. Interestingly, the mixture with PLC1 shows monosulfoaluminate and hemicarboaluminate after curing for 56 days at 5 °C, which did not occur at 23 °C or 38 °C.

The mixtures with PLC2, PLC3, and PLC4, are shown in Figures 3.26 through 3.28. These three mixtures show the formation of hemicarboaluminate and monocarboaluminate after 56 days. The PLC3 and PLC4 mixtures also show the formation of gismondine, a calcium aluminate silicate hydrate, which has been reported to form at room temperature in PLC pastes by past researchers (Voglis et al., 2005). The symbol "Gi" is used to label the gismondine peaks, which occur in very close proximity to the quartz peaks around 21 and 27 degrees. Formation of gismondine was only observed for the mixtures cured at 5 °C.

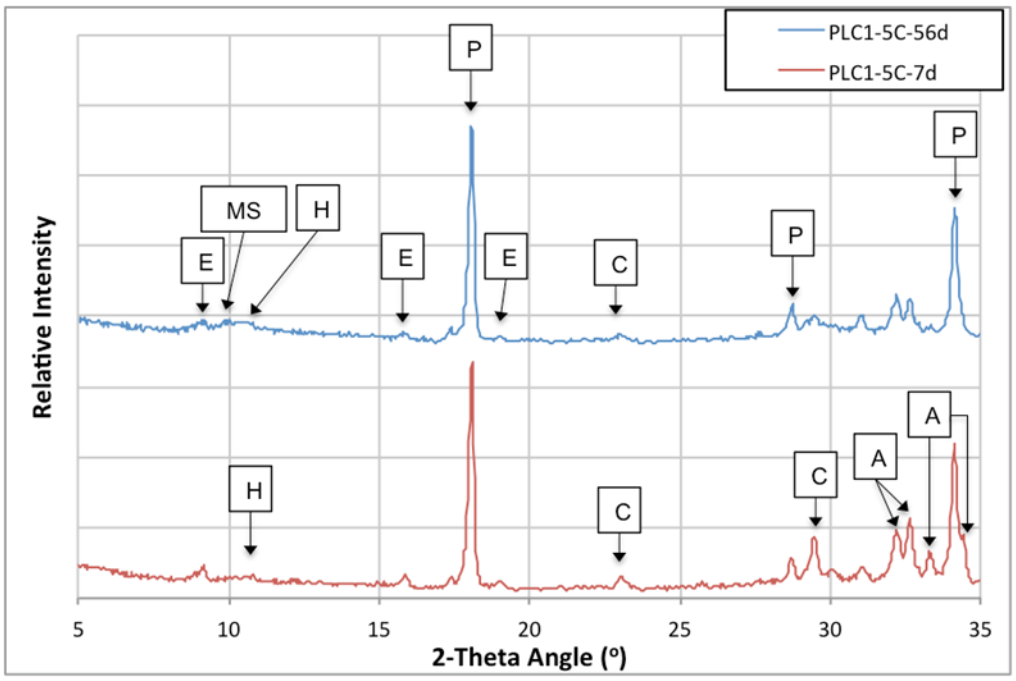

Figure 3.25: XRD Scans for PLC1 at 5 °C after 7 and 56 Days

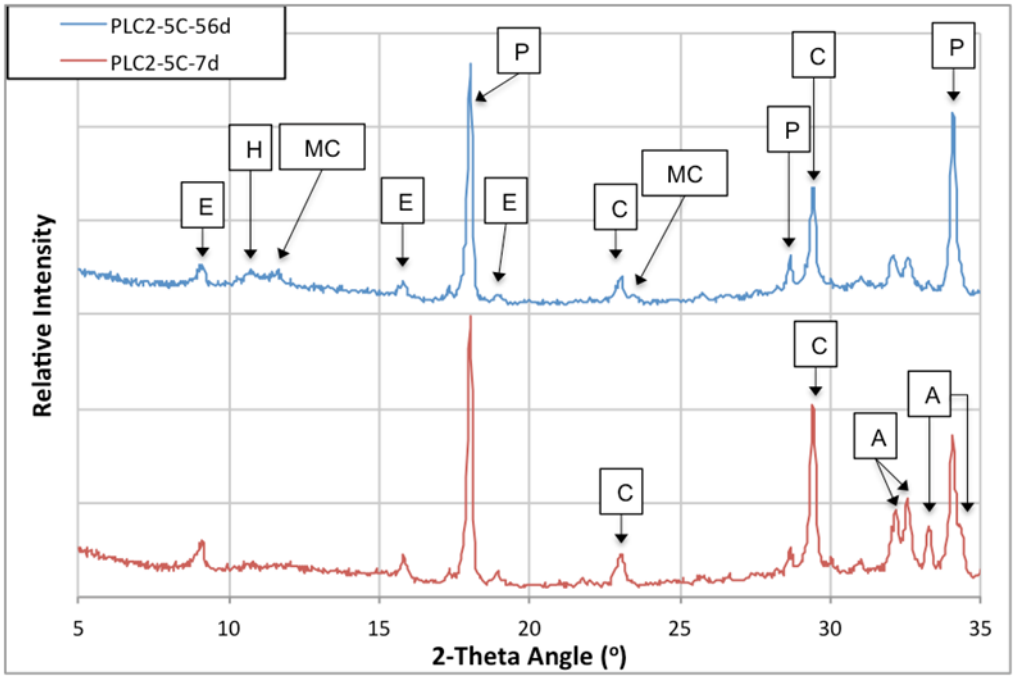

Figure 3.26: XRD Scans for PLC2 at 5 °C after 7 and 56 Days

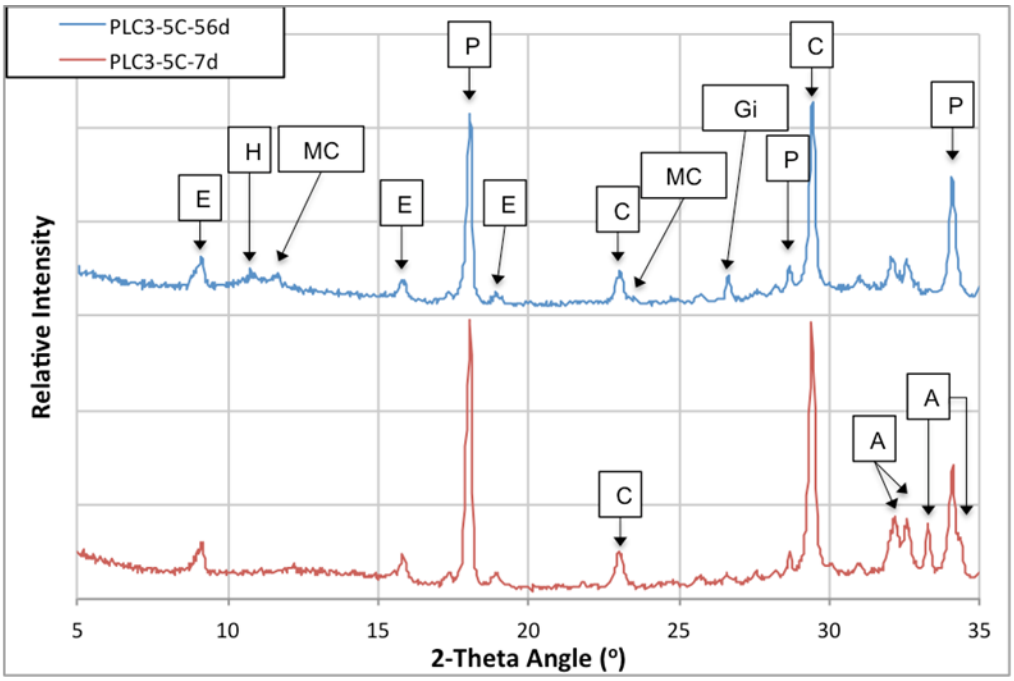

Figure 3.27: XRD Scans for PLC3 at 5 °C after 7 and 56 Days

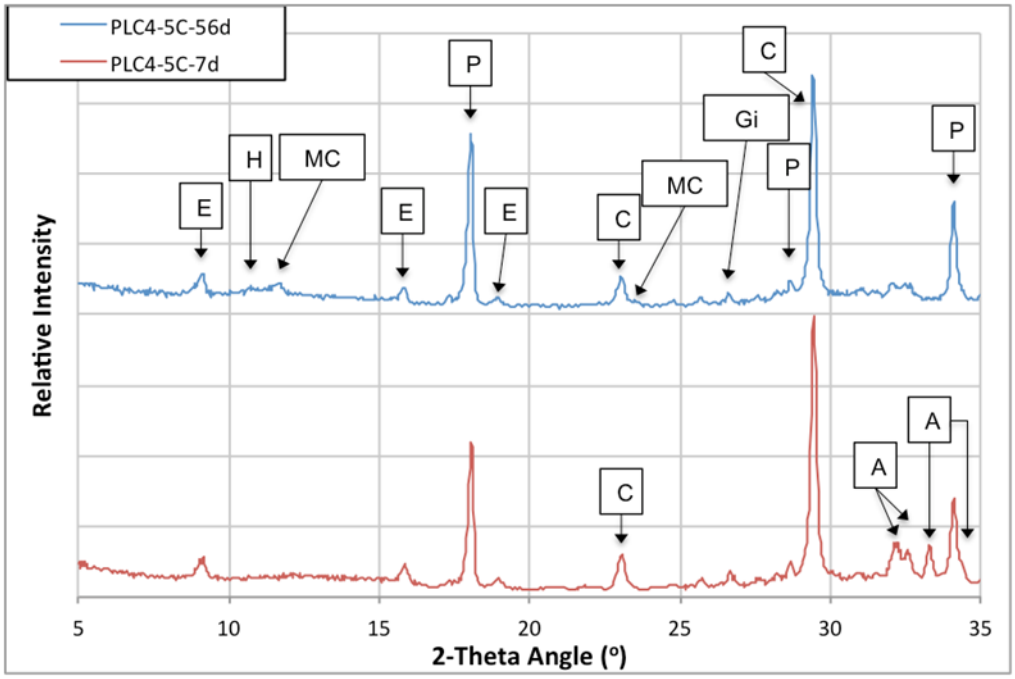

Figure 3.28 XRD Scans for PLC4 at 5 °C after 7 and 56 Days

Figure 3.29 shows the XRD scan of the PLC5 mixture. Very small amounts of hemicarboaluminate and monocarboaluminate are present after 56 days. It is expected that the amount of these phases would increase with increased curing

Srebrodol'skite, a phase with the chemical formula of $Ca_2Fe_2O_5$, has been associated with slag production (Ng et al., 2015). As can be seen in Figures 3.29 through 3.31, Srebrodol'skite is present in low quantities for mixtures with cements PLC5 through PLC7. It appears to hydrate slowly and, thus, is present only at early ages, especially when the low curing temperature of 5 ^oC slows the hydration reaction. Very small amounts of Srebrodol'skite also appear to be present for cements PLC5 through PLC7 at the curing temperature of 23 ^oC after 1 day of curing, and it is not present after 7 days. Gismondine is present in the PLC7 mixture after 7 days of curing at 5 ^oC, and it was not present anymore after hydration was stopped after curing for 56 days.

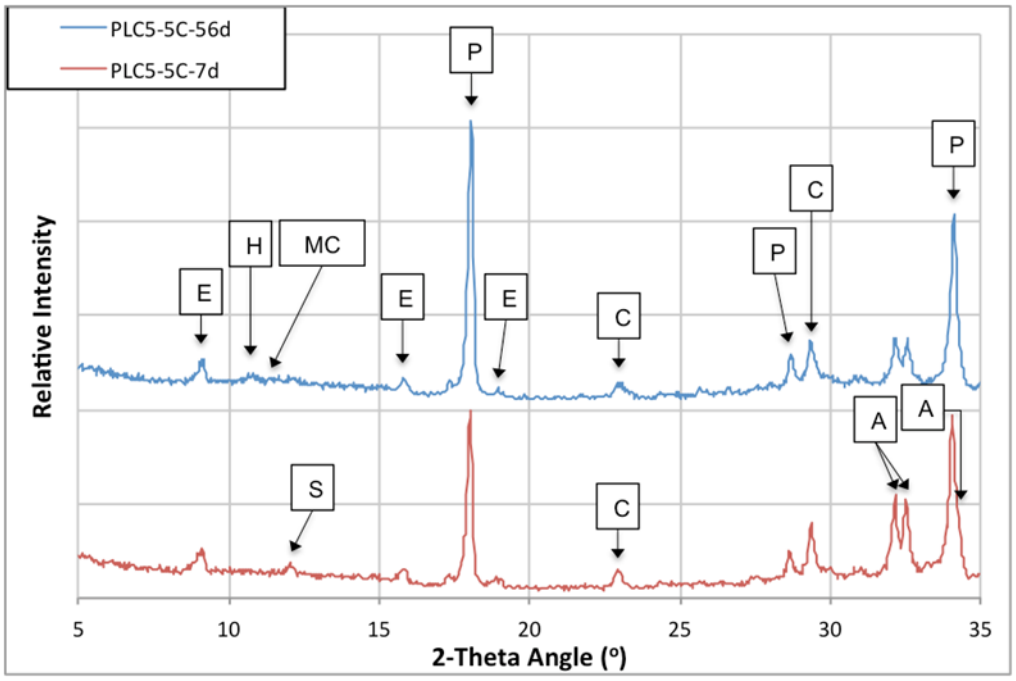

Figure 3.29: XRD Scans for PLC5 at 5 ^oC after 7 and 56 Days

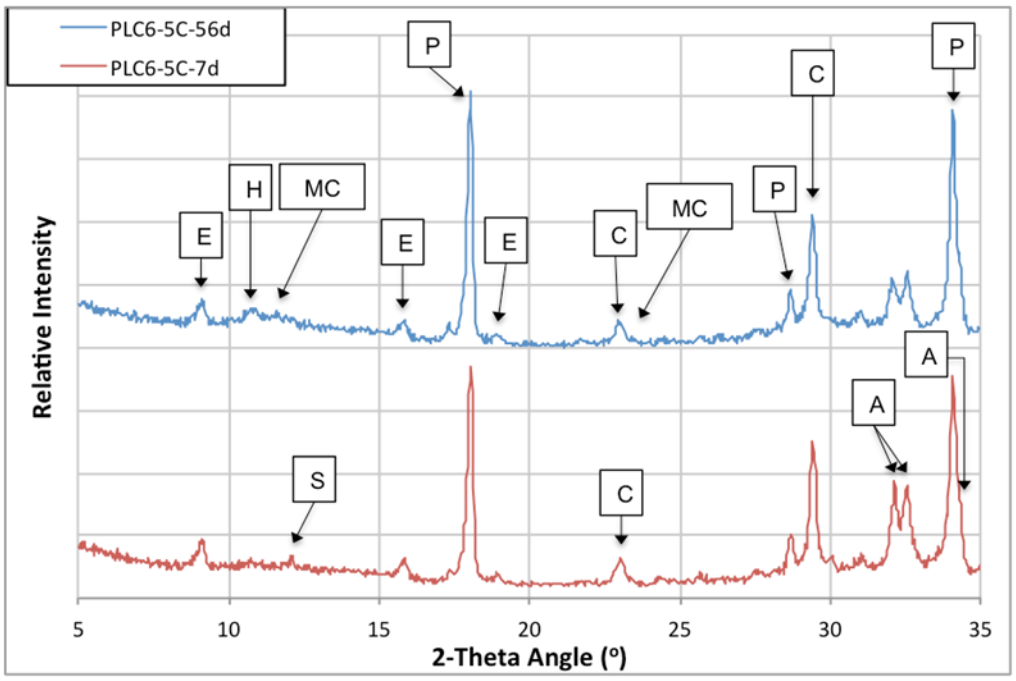

Figure 3.30: XRD Scans for PLC6 at 5 °C after 7 and 56 Days

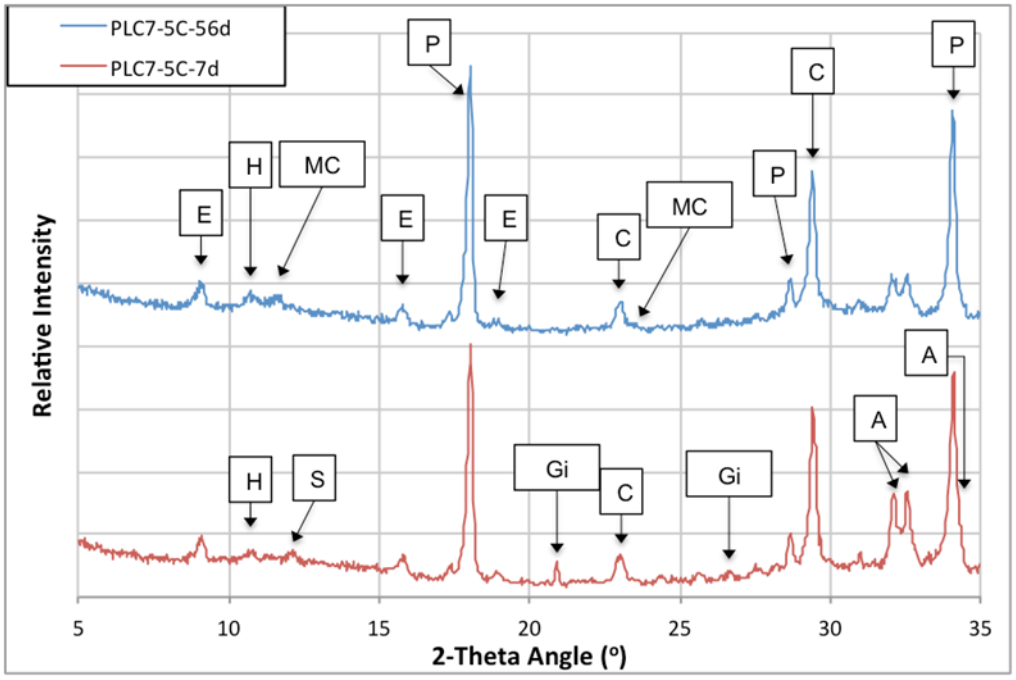

Figure 3.31: XRD Scans for PLC7 at 5 °C after 7 and 56 Days

3.5.1.4. Effect of Temperature on Mixtures Containing SCMs

Figure 3.32 shows the XRD scan of PLC3 combined with 20% class F fly ash cured at 5 ºC and Figure 3.33 shows the XRD scan of the same mixture cured at 38 ºC. When these two XRD scans are compared with the scan of the same mixture that was cured at 23 ºC, there does not appear to be any significant effect from the supplementary cementitious materials at the different temperatures. Figure 3.34 shows the XRD scans after curing for 56 days at the different temperatures. The small differences that are observed at these different temperatures can be attributed to temperature and not to the incorporation of SCMs.

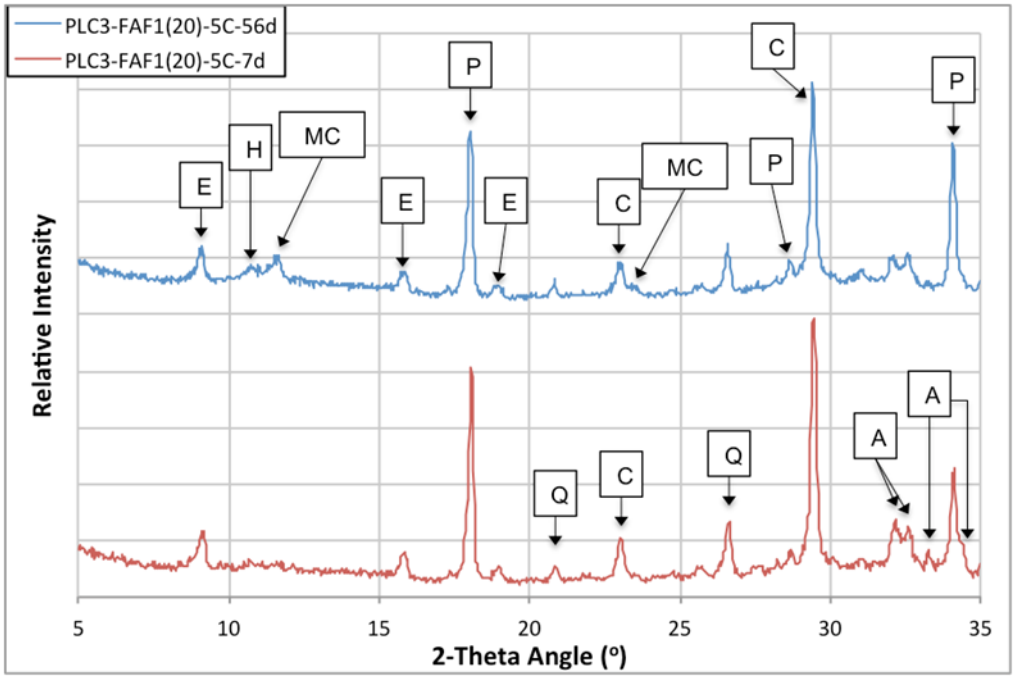

Figure 3.32: XRD Scan of PLC3-FAF1(20) at 5 ºC after 7 and 56 Days

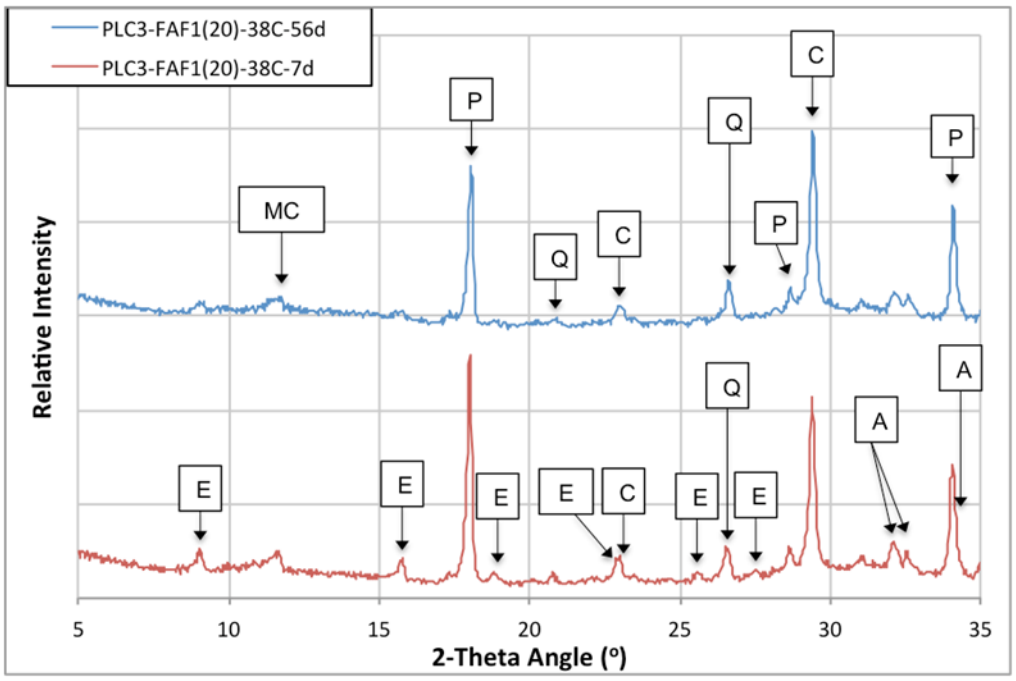

Figure 3.33: XRD Scan of PLC3-FAF1(20) at 38 °C after 7 and 56 Days

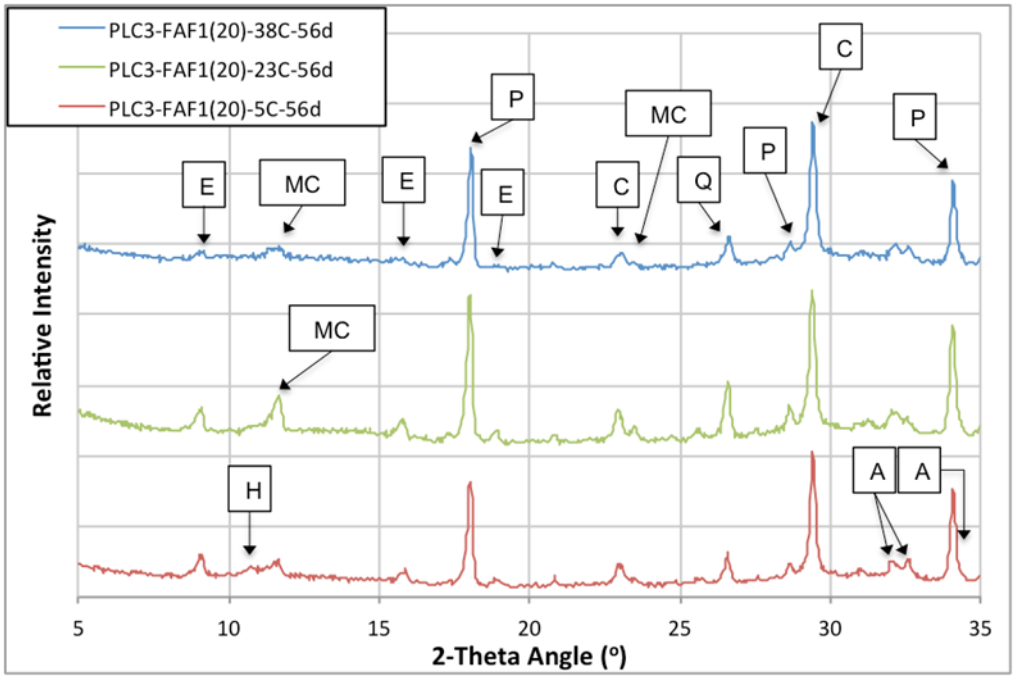

Figure 3.34: XRD Scan of PLC3-FAF1(20) after 56 Days Cured at Different Temperatures

3.6. GEMS Thermodynamic Modeling Software

This part of the study investigates the hydration products that form for the three different temperatures and compares them to predicted results using GEMS, a thermodynamic modeling software package that calculates phase equilibrium by using Gibbs free energy minimization techniques. In other words, the program is able to determine which reaction products form based on the amount of reactants, assuming that the temperature and pressure are known.

Although a detailed hydration analysis is possible using GEMS, the analysis can get very complicated, and is beyond the scope of this Final Report. The simple analysis that GEMS offers makes the assumption that the hydration reaction has been given enough time to reach equilibrium. In other words, 100% hydration has been achieved and all of the reactants have reacted to form products. Therefore, the simplified GEMS analysis will not show the presence of anhydrous cement phases whose presence was confirmed through XRD.

For this investigation, the following mixtures were modeled in GEMS: PLC1-0.45, PLC2-0.45, PLC3-0.45, and PLC4-0.45. The theoretical results provided by GEMS are compared to the experimental results that were presented in section 3.5.

Figure 3.35 shows the predicted phase composition of PLC1-0.45 and Table 3.6 shows the mass (in grams per 100 grams of cement) of each phase present. As expected, calcium silicate hydrate is the principal phase and the amount of C-S-H tends to decrease with increasing temperature. Since C-S-H is amorphous, it could not be detected in the XRD analysis. Also, since an internal standard was not used in the XRD analysis, it is only possible to say whether or not the predicted phases match the actual phases that were found through XRD.

The presence of ettringite, portlandite, and unreacted calcite in both analyses was expected. However, the presence of monocarboaluminate, in the GEMS analysis was surprising, as it was not detected through XRD. This is likely due to the assumption of 100% hydration. As mentioned earlier, researchers have reported the presence of monocarboaluminate even at low limestone contents, so it is probable that if the reaction was allowed to progress further by extending curing and then analyzing the sample using XRD, monocarbonate would be detected. The formation of $C_3(AF)S_{0.84}H$, which is a siliceous hydrogarnet with possible iron substitution, was overlooked in section 2.5, but the small peak around 17.4 degrees 2-theta angle indicating its presence is noticeable and can be seen in Figure 3.36. Siliceous hydrogarnet has been reported to form mainly at higher temperatures (greater than 50 ^{o}C), but it has been known to form in relatively low quantities at lower temperatures in the presence of $Fe(OH)_3$ (Deschner et al., 2013). While GEMS did not perfectly predict all of the phases that were observed using XRD analysis, it was still a very good approximation for a relatively simple analysis. A more detailed GEMS analysis that does not assume 100% hydration and shows the phase changes with time should more closely resemble the XRD results.

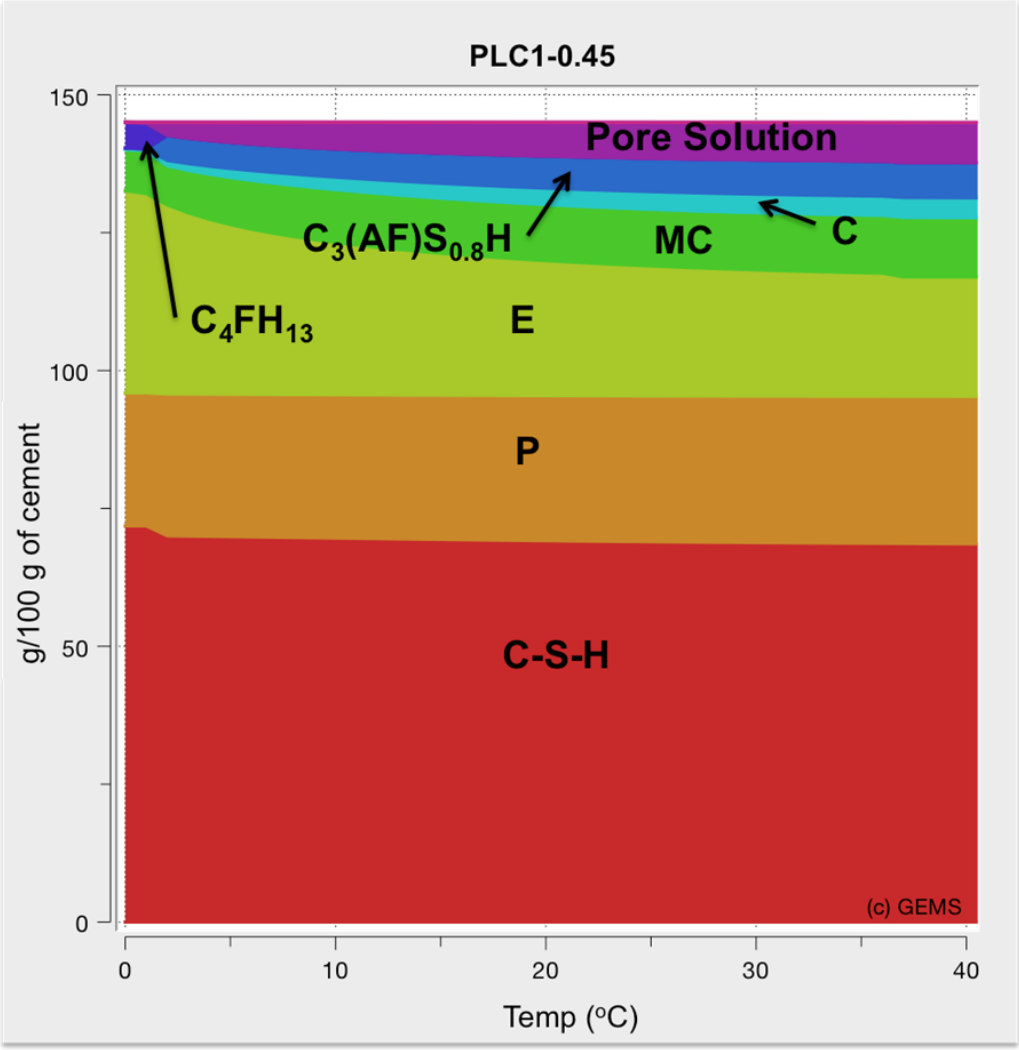

Figure 3.35: GEMS Analysis for PLC1-0.45

Table 3.6: Phase Composition of Hydrated Cement Paste (g/100g of cement) at Different Temperatures for PLC1-0.45 per GEMS Analysis

Phase	5 ºC	23 ºC	38 ºC
CSH	69.9	69.0	68.6
Portlandite	25.8	26.4	26.7
Ettringite	30.8	23.9	21.6
Monocarboaluminate	8.6	10.2	10.8
Hemicarboaluminate	0.0	0.0	0.0
Calcite	1.6	3.1	3.6
$C_3(AF)S_{0.84}H$	4.7	5.9	6.3
C_4FH_{13}	0.0	0.0	0.0
Pore Solution	3.6	6.4	7.3

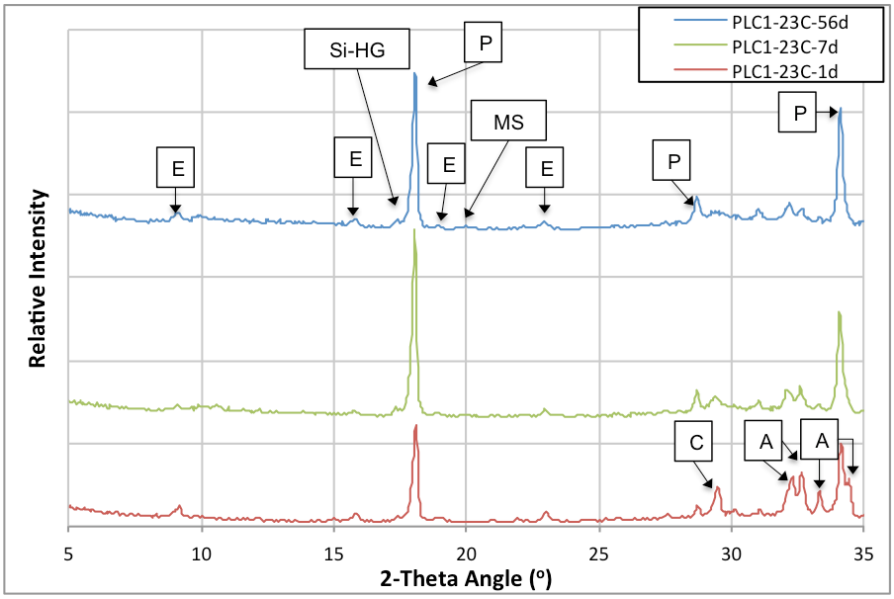

Figure 3.36: Revisited PLC1 Scan Showing the Presence of $C_3(AF)S_{0.84}H$, Labeled as "Si-HG"

Figures 3.37 through 3.39 show the GEMS analyses for PLC2-0.45, PLC3-0.45, and PLC4-0.45, respectively. The XRD results for PLC2-0.45 show the formation of monocarboaluminate after 56 days of curing at the three different temperatures. The GEMS model was able to predict well the phases that were observed using XRD analysis, the only exceptions being the anhydrous cement phases, which would be expected. It is also important to note that hemicarbonate is not detected in the simplified GEMS analysis. This is due to the fact that hemicarbonate converts to monocarboaluminate with time, as was discussed in the earlier sections.

For PLC3-0.45 and PLC4-0.45, it was surprising that GEMS did not show the formation of any monocarboaluminate, which implies that, at equilibrium, any previously formed

monocarboaluminate dissolves when the limestone content of the cement is relatively high. Further investigation is required in this regard.

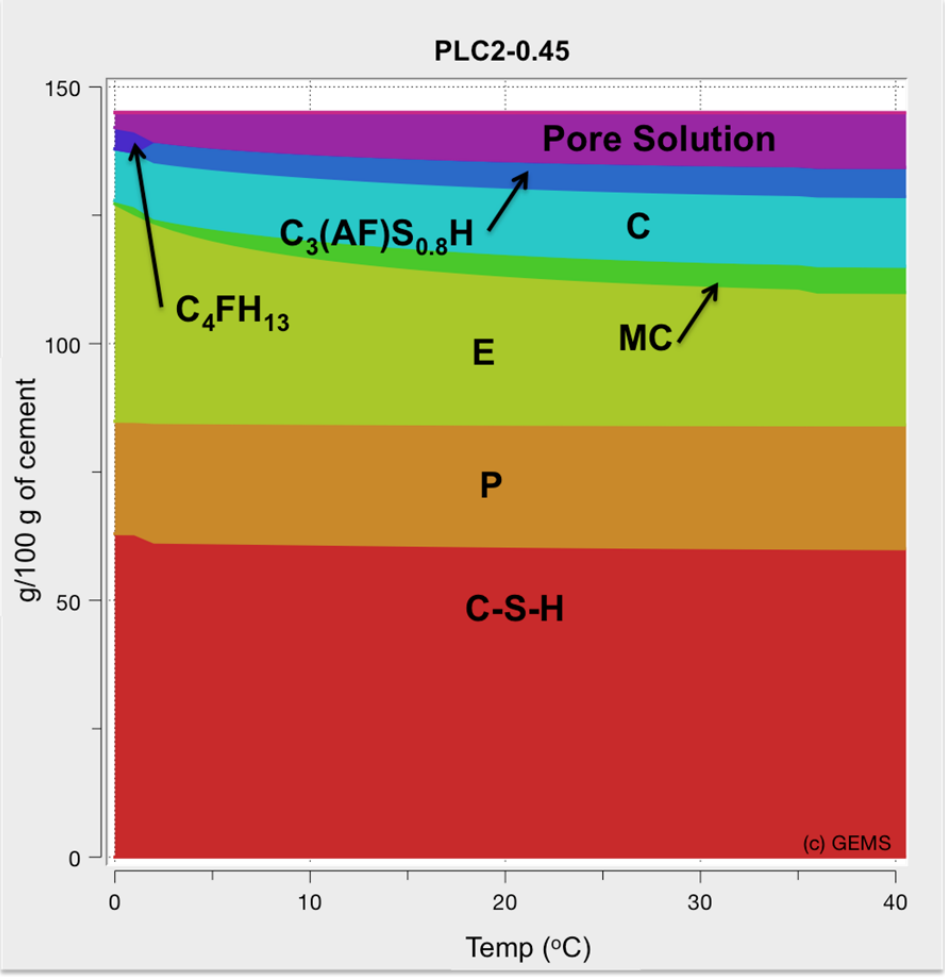

Figure 3.37: GEMS Analysis for PLC2-0.45

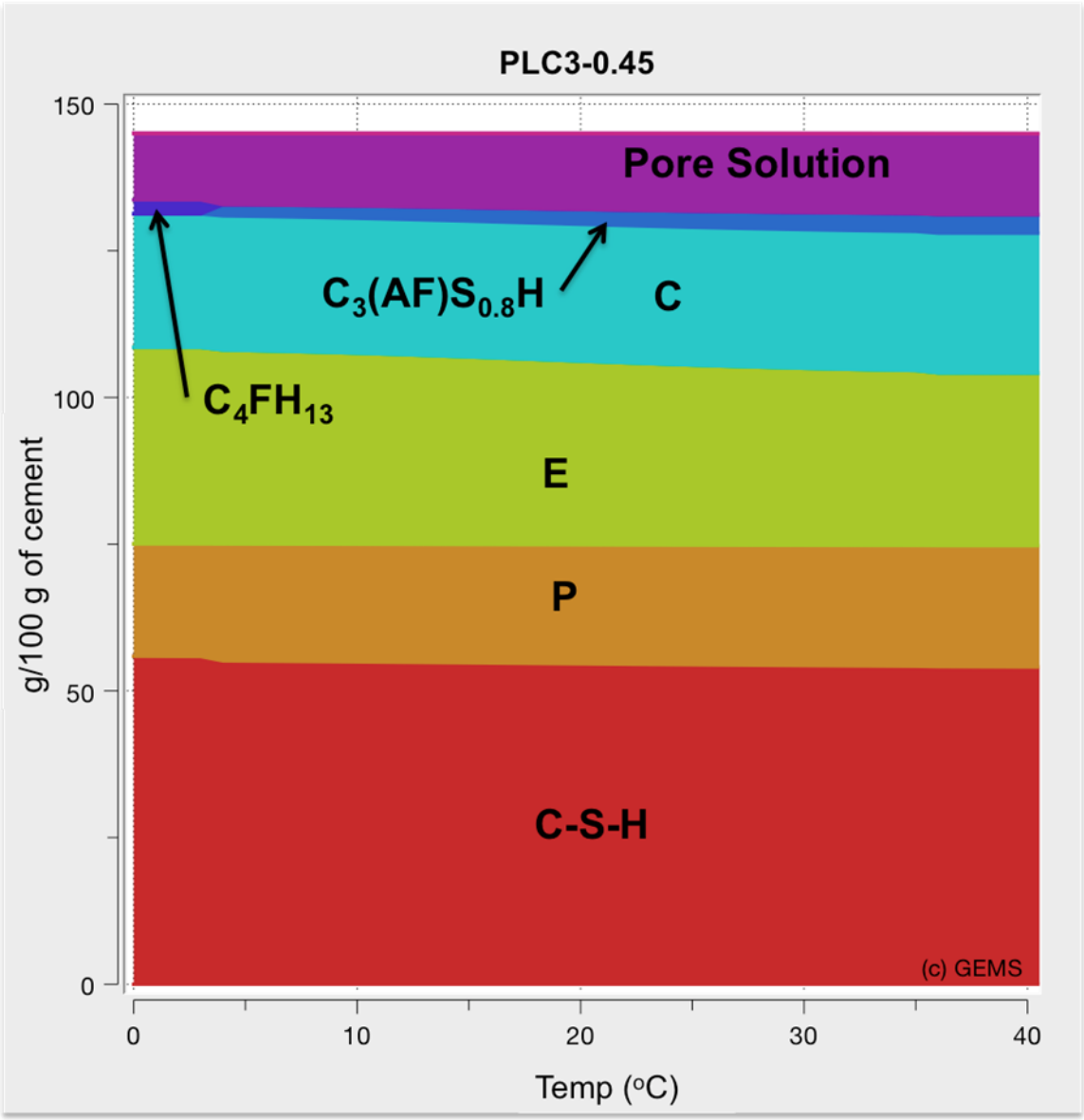

Figure 3.38: GEMS Analysis for PLC3-0.45

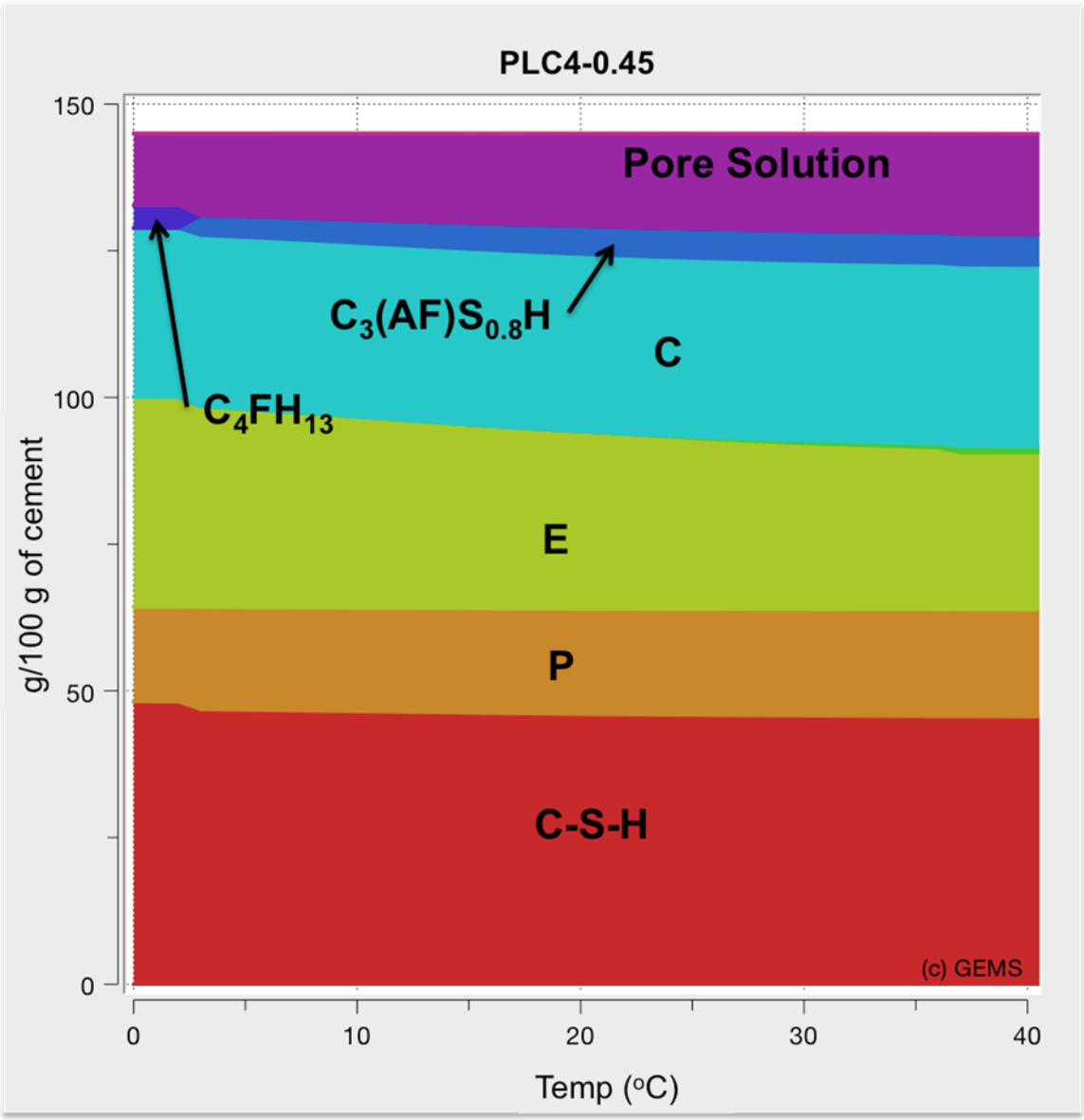

Figure 3.39: GEMS Analysis for PLC4-0.45

3.7. Conclusions and future work

The main objective of the investigation presented in this chapter was to determine the hydration products that form in portland limestone cement concrete systems with significant limestone interground with the cement. The effect of supplementary cementitious materials in combination with the high limestone contents, and the effect of temperature were also evaluated.

Twenty-eight different combinations of cements with increasing limestone contents and supplementary cementitious materials were used to cast cement paste samples at a water-to-

cementitious materials ratio of 0.45 and cured at 23 ^{o}C for 1, 7, and 56 days. Hydration was stopped after each curing period for each sample, the sample was pulverized and then analyzed using an x-ray diffractometer. Ten combinations were also cured at 5 ^{o}C and 38 ^{o}C and XRD analysis was performed after curing periods of 7 and 56 days.

The following conclusions can be made after analyzing the test results presented in the earlier sections:

- The observed phase assemblage for the mixtures in this study was in general agreement with the results reported by other researchers.
- When limestone is added to the system some of the limestone reacts to form carboaluminates, which are in addition to the hydration products that are typically formed in OPC systems. Carboaluminates include hemicarboaluminate, carbonated hemicarboaluminate, and monocarboaluminate.
- Only a portion of the limestone reacts and the rest is essentially inert filler. Nevertheless, the inner filler can still be beneficial by providing nucleation and growth sites for hydration products to form.
- The addition of limestone stabilizes ettringite at early ages and prevents a significant amount of conversion to monosulfoaluminate, resulting in the formation of carboaluminates instead.
- Monocarboaluminate formation appears to be suppressed at higher curing temperatures, where carbonated hemicarboaluminate appears to be more stable.
- The formation of gismondine, a calcium aluminate silicate hydrate, was observed at 7 days for the cements with higher limestone contents (PLC3, PLC4, and PLC7) at a curing temperature of 5 ^{o}C. More research is needed to fully understand the formation of gismondine.
- While a simplified GEMS analysis can be very useful, a more detailed hydration analysis in GEMS would be able to provide a better picture of how hydration changes with time. In the future, it is strongly recommended that the detailed analysis is done and compared to the XRD results presented in this chapter, especially for the mixtures with relatively high limestone contents.

In the future, the mixtures presented in this study should be replicated at different water-to-cementitious materials ratios to evaluate the effect of the limestone as the amount of water in the mixture changes. Additional intermediate analyses should be performed between 1 and 56 days to get a better picture of how the formation of hydration products changes with time. Curing should also extend past 56 days, especially at the lower curing temperature.

Chapter 4. Calorimetry of Portland Limestone Cement Systems

4.1. Isothermal Calorimetry

4.1.1. Introduction

Software programs such as ConcreteWorks use the activation energy as measured on pastes in isothermal calorimetry to predict thermal distributions in hydrating concrete. Consequently, a significant database of isothermal calorimetry at three different temperatures (40 °F, 73 °F, and 100 °F) was generated, which will allow for direct input into available models or predictive equations.

The physical presence of limestone particles has a profound effect on the hydration reactions. On the one hand, the increase in the w/clinker ratio increases the available space for the precipitation of hydration products, which can result in a higher degree of hydration [Scrivener, 2015]. In addition, Berodier and Scrivener [Berodier, 2014] showed that the presence of finely ground limestone increases the shearing between particles, which increases the number of C-S-H nucleation sites. In this context, it must be emphasized that the interparticle distance is of critical importance, which highlights the need to optimize the particle size distribution (PSD) of the system. Moreover, contrarily to limestone-free cements, once gypsum has been depleted, the available alumina reacts with calcite to form hemi and monocarboaluminate instead of monosulfoaluminate. This indirectly stabilizes ettringite, which results in a relative increase in the volume of hydrates [Lothenbach, 2008][Matschei, 2007][De Weerdt, 2011].

It has been shown that C-S-H tends to nucleate preferentially on the surface of the limestone particles, which further accelerates hydration. Several studies have shown that limestone is more efficient in accelerating the hydration reactions than other fillers such as fly ash, quartz, and slag [Berodier, 2014] [Oey, 2013]. Berodier and Scrivener [Berodier, 2014] proposed several explanations for the increased nucleation on the limestone surface. First, the increase in the calcium concentration in the pore solution due to the slight dissolution of limestone at early ages may shorten the induction period. Moreover, they have proposed that the arrangement of the calcium atoms on the limestone surface may provide a "templating" effect, which would facilitate the nucleation of C-S-H.

Generally, an increase in the cement fineness, limestone fineness, or in the filler content (finer than clinker) will tend to increase the rate of reaction [Simple methods to estimate the influence of limestone fillers on reaction and property evolution in cementitious materials]. The increase in the fineness of the binder increases the surface area available for reaction, resulting in an acceleration.

Together with this effect, the reduction in the interparticle distance due to the incorporation of finely ground limestone can decrease the time of initial set [Bentz, 2012].

4.1.2. Materials and Methods

In this section, seven cements were tested. Limestone was interground at one plant with a high-C3A clinker for the production of four cements—PLC1, PLC2, PLC3, and PLC4—which have limestone contents of 3.2%, 13.4%, 21.0%, and 30.6%, respectively. Analogously, other three cements were produced at another plant by intergrinding limestone with a lower-C3A clinker, and have limestone contents of 4.9%, 11.6%, and 15.5%, namely PLC5, PLC6, and PLC7, respectively. Moreover, several supplementary cementing materials (SCMs) were selected as partial replacement of the cements: one Class F fly ash, one class C fly ash, and slag. Table 4.1 shows the chemical composition of the cements and SCMs. Figure 4.1 shows the particle size distribution of the PLC1 to PLC7 cements.

Table 4.1: Chemical Composition of the Cements and SCMs

Material	PLC1	PLC2	PLC3	PLC4	PLC5	PLC6	PLC7	FA-F	FA-C2	Slag
Chemical analysis [%]										
SiO_2	19.8	18.6	18.1	16.9	19.9	19.0	19.5	53.2	32.4	36.1
Al_2O_3	5.5	5.2	4.7	4.7	4.7	4.6	5.0	18.0	17.3	8.0
Fe_2O_3	2.0	1.8	1.7	1.5	3.3	3.3	3.3	8.1	6.1	0.6
CaO	64.8	66.4	67.1	68.1	64.8	65.7	64.8	10.8	27.7	39.8
MgO	1.1	1.1	1.0	1.2	0.8	0.8	0.8	2.4	5.3	10.7
Na_2O	0.1	0.1	0.1	0.1	0.1	0.1	0.1	0.3	1.6	0.3
K_2O	0.6	0.5	0.6	0.4	0.6	0.7	0.6	1.1	0.3	0.5
SO_3	4.1	4.2	4.6	4.7	3.8	3.8	3.9	0.5	2.5	2.6
LOI	1.4	5.9	9.2	13.4	2.2	5.1	6.8	-	-	-
$CaCO_3$	3.2	13.4	21.0	30.6	4.9	11.6	15.5	-	-	-
Calculated phase composition (%) Rietveld analysis										
C_4AF	3.5	3.1	2.0	3.0	7.3	8.1	4.6	-	-	-
C_3A	9.2	7.6	6.5	6.0	4.2	2.9	3.8	-	-	-
C_3S	47.8	44.9	41.1	34.2	47.9	46.5	35.1	-	-	-
C_2S	20.9	16.8	17.8	13.6	22.4	28.7	24.6	-	-	-
$CaCO_3$	5.2	13.9	24.8	30.3	1.8	12	14.1	-	-	-

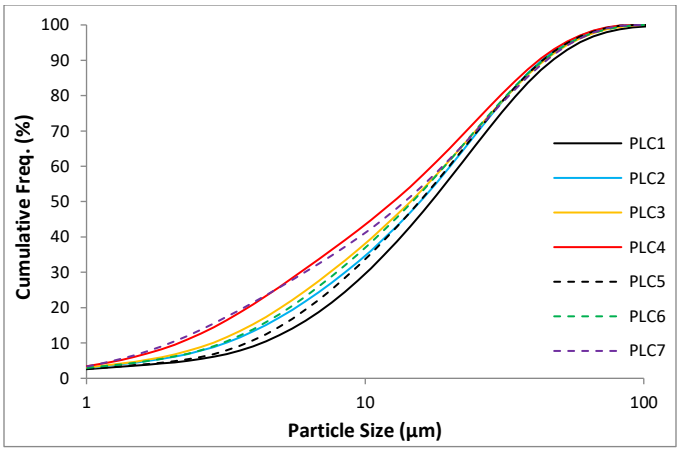

Figure 4.1: Particle Size Distribution of the PLC1 to PLC7 Cements

In this section, isothermal calorimetry at three different temperatures (40 °F, 73 °F, and 100 °F) was evaluated for the following mixtures:

- Control paste mixtures for all PCs and PLCs.
- Paste mixtures with each PLC with 20 percent Class F fly ash replacement.
- Paste mixtures with each PLC with 20 percent Class C fly ash replacement.
- Paste mixtures with each PLC with 35 percent slag replacement.

Paste samples of w/cm= 0.45 were prepared with 35 grams of cementitious material and tested using a modified version of a Grace AdiaCal isothermal calorimeter developed by Bentivegna (Bentivegna, 2012) at The University of Texas at Austin (UT Austin). The materials were pre-heated or pre-cooled to the specific testing temperature for 24 hours. The conditioned powders were placed in Grace AdiaCal TC sample holders and thoroughly mixed using a vibrating table for 30 seconds. Subsequently, water was added, the cup was sealed, and the materials were mixed on the vibrating table for 60 seconds. The specimens were immediately placed in the calorimeter. The heat of hydration was measured every 60 seconds for a period of 7 days.

Ea was calculated from the isothermal calorimetry data obtained at the three different temperatures selected. The rate of reaction was calculated as the slope of a best-fit line to the linear acceleration stage of the heat flow curve. Then, the natural logarithms of the reaction rates were plotted versus the inverse of the reaction temperatures. The negative of the slope of the best-fit line to the three data points was then multiplied by the natural gas constant R (8.314 J/mol/K) to obtain Ea. A detailed explanation of this procedure and other methods to calculate Ea can be found in [Poole, 2007].

4.1.3. Results

Table 4.2 presents the isothermal calorimetry data at 73 °F for all the paste mixtures evaluated. The data shown in the table includes the time to the main heat generation peak (corresponding to C3S hydration), the heat flow at the main peak, the calculated slope of the linear section of the curve in the acceleration stage, and the cumulative heat after 72 hours.

Table 4.2: Isothermal Calorimetry Data at 73°F

Mixture	Time to main peak (h)	Heat flow at main peak (mW/g)	Slope acceleration period (mW/g/h)	Cumulative heat after 72 hours (mJ/g)
PLC1	9.13	2.84	0.435	240759
PLC2	9.58	2.48	0.426	198097 (*)
PLC3	8.77	2.31	0.437	198193 (*)
PLC4	7.00	2.33	0.548	181395 (*)
PLC5	7.42	3.09	0.625	200181 (*)
PLC6	7.67	2.68	0.650	175817 (*)
PLC7	8.47	2.25	0.519	159147 (*)
PLC1+20% F	9.55	2.31	0.360	174348 (*)
PLC2+20% F	9.53	2.04	0.360	166394 (*)
PLC3+20% F	8.93	1.81	0.346	160723 (*)
PLC4+20% F	7.52	1.79	0.378	168526
PLC5+20% F	8.47	2.37	0.441	180153
PLC6+20% F	8.53	2.17	0.470	169928
PLC7+20% F	9.18	1.77	0.379	153779
PLC1+20% C2	11.48	2.35	0.347	217958
PLC2+20% C2	11.60	2.02	0.326	198311
PLC3+20% C2	11.05	1.79	0.298	189163
PLC4+20% C2	8.93	1.90	0.382	187554
PLC5+20% C2	9.08	2.46	0.436	191192
PLC6+20% C2	9.03	2.23	0.474	180587
PLC7+20% C2	9.82	1.86	0.378	167689
PLC1+35% Slag	8.72	2.19	0.375	187317
PLC2+35% Slag	8.77	1.85	0.344	171828
PLC3+35% Slag	8.32	1.67	0.322	167242
PLC4+35% Slag	6.72	1.62	0.374	152539
PLC5+35% Slag	6.80	2.36	0.537	172689
PLC6+35% Slag	7.33	2.01	0.476	134223 (*)
PLC7+35% Slag	7.87	1.63	0.366	123801 (*)

(*) Data collected up to 48 hours

The effects of limestone addition on the heat evolution of the paste mixtures was consistent among the neat cement and SCM-containing systems. The incorporation of limestone decreased the main heat flow peaks with respect to the Type I and Type I/II control mixtures. Similarly, the cumulative heat evolved up to 72 hours decreased with the increase in the limestone content for both high and moderate C3A systems. This was expected and it is a result of the dilution of the reactive clinker fraction.

In the case of the high-C3A mixtures, the time to the main heat generation peak was reduced when limestone contents greater than 20% were used. However, the same effect was not observed in the case of the PLC2 mixtures, which showed a delay in the time to the main peak of hydration together with a slower rate during the acceleration period. This indicates that the PLC2 cement may have not been optimized to the same degree as the PLC3 and PLC4 counterparts. The systems with the highest limestone content (PLC4) showed an increased rate of reaction during the acceleration stage with respect to the three lower-limestone systems. It must be remembered that the fineness of the cements increased as the interground limestone increased, as shown in Figure 4.1, which could explain the impact on the nucleation and growth of C-S-H. The same increase in reaction rates was not observed in the case of the moderate-C3A cements (PLC5, PLC6, and PLC7) with the increase in the limestone content. This effect was particularly surprising in the case of the PLC7 cement, which is much finer than both PLC5 and PLC6.

The time to the sulfate depletion peak exhibited a progressive delay with the increase in the limestone content from 3.2% in PLC1 to 30.6% in PLC4. This is believed to be a result of the increase in the SO3 % of the cements (from 4.1% in PLC1 to 4.7% in PLC4). In the case of the moderate C3A cements, this effect was only noticeable in the PLC7 system.

Isothermal calorimetry was also performed at 40°F and 100°F in order to obtain the parameters needed to calculate the apparent activation energy Ea of each system. The data for both temperatures are presented below in Table 4.3 and Table 4.4. The calculated apparent activation energies are shown in Table 4.5.

Table 4.3: Isothermal Calorimetry Data at 40°F

Mixture	Time to main peak (h)	Heat flow at main peak (mW/g)	Slope acceleration period (mW/g/h)	Cumulative heat after 72 hours (mJ/g)
PLC1	33.2	1.1	0.049	233387
PLC2	33.3	1.0	0.039	206326
PLC3	33.2	0.8	0.039	171384
PLC4	24.6	0.8	0.059	159188
PLC5	22.4	1.4	0.092	243464
PLC6	23.7	0.7	0.039	133534
PLC7	23.7	0.5	0.034	110748
PLC1+20% F	34.8	0.5	0.031	115652
PLC2+20% F	33.6	0.3	0.012	62115
PLC3+20% F	33.2	0.6	0.034	152014
PLC4+20% F	25.5	0.8	0.043	162342
PLC5+20% F	23.4	1.0	0.057	184540
PLC6+20% F	25.3	0.9	0.050	187374
PLC7+20% F	24.6	0.8	0.067	172798
PLC1+20% C2	36.6	0.9	0.037	207569
PLC2+20% C2	39.9	0.8	0.032	176241
PLC3+20% C2	35.2	0.7	0.036	161620
PLC4+20% C2	30.5	0.7	0.034	145680
PLC5+20% C2	25.6	1.0	0.063	199048
PLC6+20% C2	29.0	0.8	0.049	193251
PLC7+20% C2	28.1	0.9	0.054	197337
PLC1+35% Slag	29.2	1.0	0.050	214217
PLC2+35% Slag	31.2	0.7	0.032	165608
PLC3+35% Slag	26.8	0.7	0.036	137890
PLC4+35% Slag	24.3	0.8	0.044	152555
PLC5+35% Slag	21.2	1.0	0.060	181717
PLC6+35% Slag	25.6	0.8	0.042	169854
PLC7+35% Slag	25.6	0.6	0.040	133408

Table 4.4: Isothermal Calorimetry Data at 100°F

Mixture	Time to main peak (h)	Heat flow at main peak (mW/g)	Slope acceleration period (mW/g/h)	Cumulative heat after 72 hours (mJ/g)
PLC1	5.38	9.15	3.069	370200
PLC2	5.23	7.16	2.529	325822
PLC3	4.73	7.36	2.934	308947
PLC4	3.67	7.49	3.674	290067
PLC5	4.55	9.85	4.613	324493
PLC6	4.02	9.04	4.514	279083
PLC7	4.08	7.68	3.687	271926
PLC1+20% F	5.67	7.55	2.444	307393
PLC2+20% F	5.63	5.13	1.667	278376
PLC3+20% F	5.18	5.80	2.494	259157
PLC4+20% F	3.63	5.64	2.556	240979
PLC5+20% F	4.42	7.96	3.607	264449
PLC6+20% F	4.25	6.97	3.401	241604
PLC7+20% F	4.23	5.83	2.581	219024
PLC1+20% C2	6.17	7.27	2.287	318992
PLC2+20% C2	6.77	5.30	1.505	278774
PLC3+20% C2	5.80	5.96	2.223	280649
PLC4+20% C2	4.60	6.23	2.675	283453
PLC5+20% C2	5.07	8.32	3.758	294643
PLC6+20% C2	4.88	7.57	3.577	279589
PLC7+20% C2	4.82	6.09	2.510	243417
PLC1+35% Slag	4.85	6.83	2.399	299253
PLC2+35% Slag	4.85	5.90	2.314	268251
PLC3+35% Slag	4.77	5.07	1.953	252229
PLC4+35% Slag	3.50	5.04	2.401	239583
PLC5+35% Slag	4.02	7.06	3.315	253753
PLC6+35% Slag	3.90	6.07	3.165	233420
PLC7+35% Slag	3.98	5.15	2.351	225940

Table 4.5: Calculated Apparent Activation Energy E_a for All Mixtures

Mixture	Ea (J/mol)
PLC1	89,924
PLC2	90,772
PLC3	94,048
PLC4	89,775
PLC5	84,620
PLC6	104,058
PLC7	102,487
PLC1+20% F	95,187
PLC2+20% F	108,839
PLC3+20% F	93,150
PLC4+20% F	88,918
PLC5+20% F	89,849
PLC6+20% F	91,662
PLC7+20% F	78,891
PLC1+20% C2	89,849
PLC2+20% C2	84,370
PLC3+20% C2	89,342
PLC4+20% C2	94,713
PLC5+20% C2	88,128
PLC6+20% C2	93,067
PLC7+20% C2	83,364
PLC1+35% Slag	83,930
PLC2+35% Slag	92,959
PLC3+35% Slag	86,732
PLC4+35% Slag	87,122
PLC5+35% Slag	87,172
PLC6+35% Slag	94,248
PLC7+35% Slag	88,627

4.2. Chemical Shrinkage

4.2.1. Introduction

From the moment that water and cement are put in contact, the absolute volume of the hydrating cement paste decreases because the volume of the hydration products is smaller than the volume of the initial reactants (Barcelo et al. 2005) (Jensen and Hansen 2001) (Lura et al. 2003). This internal volume reduction is known as chemical shrinkage (Jensen and Hansen 2001).

Chemical shrinkage is commonly used to track the progression of hydration reactions. There are different test methods to measure chemical shrinkage. They are based on the measurement of the amount of water that is sorbed by the hydrating cement paste, which is kept in saturated conditions.

4.2.2. Procedure and Experimental Setup

To measure chemical shrinkage of cement paste specimens, the procedure specified in ASTM C1608 was used. The paste samples had a w/cm ratio of 0.45 and were mixed according to ASTM C305. The water used in the mix was previously de-aerated by boiling it and then stored at room temperature until the moment of the test. The mixed paste was placed in small plastic vials. A sample height of approximately 5 mm was used in this project as recommended by ASTM C1608. The sample was then consolidated in a vibrating table for a few seconds. The vial was filled with de-aerated water up to the top. A rubber stopper with a 2 ml capillary tube inserted in it was tightly positioned into the vial. As a result, the level of water inside the pipette rises. Following this step, red transmission oil was placed on top of the pipette in order to prevent evaporation. The sample was placed in a water bath at 23 °C to keep isothermal conditions. The amount of water that is absorbed by the sample was measured by monitoring the change in height (decrease) of water inside the tube with time. Tests were carried out at 23 °C for 7 days.

In this project, an automated system was used to monitor the height of water in the capillary tube. The data are captured by a web camera, which takes a picture of the samples every 5 minutes and is connected to a computer to store the images. All the pictures are then processed by image analysis software developed by Bishnoi at École Polytechnique Fédérale de Lausanne, Switzerland (2009), which uses the red oil as the reference point to determine the height of water in the capillary tube. Figure 4.2 shows the test setup at UT Austin. As shown in Figure 4.2, the sample holder placed on top of a water bath faces two webcams. As a result, this setup is capable of testing four mixes (3 samples per mix) at the same time. Foam insulation was used over the water bath to moderate evaporation and temperature changes.

Figure 4.2: Automated System at UT Austin for Continuous Measurement of Chemical Shrinkage

4.2.3. Results

Table 4.6 shows the mixture tested and the measured chemical shrinkage at the age of 1, 3, and 7 days since 30 min after initial contact of water + cement. Each individual value in Table 4.6 is the average of three samples measured by the automated setup previously described.

Table 4.6: Chemical Shrinkage Measured for Cement Paste Specimens

Mixture	Chemical Shrinkage (ml of H_2O/g. cem. mat)		
	1 day	3 days	7 days
PLC1	0.041	0.058	0.078
PLC2	0.038	0.053	0.069
PLC3	0.031	0.051	0.067
PLC4	0.030	0.050	0.066
PLC5	0.032	0.049	0.066
PLC6	0.034	0.048	0.065
PLC7	0.035	0.049	0.066
PLC1 + 20% F ash	0.039	0.058	0.070
PLC2 + 20% F ash	0.038	0.054	0.071
PLC3 + 20% F ash	0.032	0.050	0.065
PLC4 + 20% F ash	0.031	0.050	0.064
PLC5 + 20% F ash	0.033	0.051	0.069
PLC6 + 20% F ash	0.029	0.047	0.068
PLC7 + 20% F ash	0.027	0.044	0.066
PLC1 + 20% C ash	0.033	0.054	0.069
PLC2 + 20% C ash	0.032	0.056	0.073
PLC3 + 20% C ash	0.033	0.056	0.071
PLC4 + 20% C ash	0.030	0.050	0.070
PLC5 + 20% C ash	0.030	0.052	0.070
PLC6 + 20% C ash	0.034	0.053	0.072
PLC7 + 20% C ash	0.030	0.053	0.075
PLC1 + 35% Slag	0.040	0.060	0.087
PLC2 + 35% Slag	0.034	0.060	0.095
PLC3 + 35% Slag	0.038	0.064	0.092
PLC4 + 35% Slag	0.035	0.057	0.086
PLC5 + 35% Slag	0.041	0.063	0.094
PLC6 + 35% Slag	0.042	0.062	0.089
PLC7 + 35% Slag	0.035	0.056	0.085

As it can be observed, the chemical shrinkage measured showed a good correlation with the cumulative heat evolved up to 3 days. With further hydration, the SCM mixtures with high limestone exhibited a slightly higher increase in chemical shrinkage than the Type I and Type I/II counterpart systems. This could be attributed to the formation of monocarboaluminate from the reaction between the alumina provided by the SCM and the carbonate ions provided by the limestone. Further research is needed to examine the evolution in chemical shrinkage at later ages, especially in the case of the SCM systems, owing to their slow reaction kinetics.

4.3. Conclusions

The following conclusions can be made after analyzing the test results presented in this chapter:

- The effects of limestone addition on the heat evolution of the paste mixtures was consistent among the neat cement and SCM-containing systems.

- The incorporation of limestone decreased the main heat flow peaks with respect to the Type I and Type I/II control mixtures. Similarly, the cumulative heat evolved up to 72 hours decreased with the increase in the limestone content for both high and moderate C3A systems. This is a result of the dilution of the reactive clinker fraction.

- In the case of the high-C3A mixtures, the time to the main heat generation peak was reduced when limestone contents greater than 20% were used. However, the same effect was not observed in the case of the PLC2 mixtures, which showed a delay in the time to the main peak of hydration together with a slower rate during the acceleration period. This indicates that the PLC2 cement may have not been optimized to the same degree as the PLC3 and PLC4 counterparts.

- The systems with the highest limestone content (PLC4) showed an increased rate of reaction during the acceleration stage with respect to the three lower-limestone systems. It must be remembered that the fineness of the cements increased as the interground limestone increased, which could explain the impact on the nucleation and growth of C-S-H. The same increase in reaction rates was not observed in the case of the moderate-C3A cements (PLC5, PLC6, and PLC7) with the increase in the limestone content. This effect was particularly surprising in the case of the PLC7 cement, which is much finer than both PLC5 and PLC6.

- The time to the sulfate depletion peak exhibited a progressive delay with the increase in the limestone content from 3.2% in PLC1 to 30.6% in PLC4. This is believed to be a result of the increase in the SO3% of the cements (from 4.1% in PLC1 to 4.7% in PLC4). In the case of the moderate C3A cements, this effect was only noticeable in the PLC7 system.

- The chemical shrinkage measured showed a good correlation with the cumulative heat evolved up to 3 days. With further hydration, the SCM mixtures with high limestone exhibited a slightly higher increase in chemical shrinkage than the Type I and Type I/II counterpart systems. This could be attributed to the formation of monocarboaluminate from the reaction between the alumina provided by the SCM and the carbonate ions provided by the limestone.

- Further research is needed to examine the evolution in chemical shrinkage at later ages, especially in the case of the SCM systems, owing to their slow reaction kinetics.

Chapter 5. Mechanical Properties of Portland Limestone Cement Concrete Systems

5.1. Introduction

A thorough understanding of mechanical properties of concrete is essential in civil engineering practice. This chapter provides a brief overview of mechanical properties for ordinary portland cement concrete, followed by a summary of research-to-date on mechanical properties of PLC concrete.

Seven cements with varying limestone contents of up to approximately 30% limestone were used to evaluate how mechanical properties of portland limestone cement concrete systems differ from ordinary portland cement concrete. The mechanical properties that were studied in depth include compressive strength, tensile strength, and elastic modulus after curing the concrete mixtures for 1, 7, 28, and 91 days. The effects of limestone interaction with different supplementary cementitious materials and water-to-cementitious materials ratio were also investigated. Additionally, the mathematical models that are currently used to predict the elastic modulus and tensile strength, if the compressive strength is known, for OPC were tested for PLC systems. Finally, the electrical resistivity of the concrete was obtained at each testing age.

5.2. Review of Mechanical Properties

5.2.1. Ordinary Portland Cement Concrete

5.2.1.1. Compressive and Tensile Strength

It is well known that concrete is very strong in compression and weak in tension, as the tensile strength of concrete is approximately 10% the compressive strength (Mehta & Monteiro, 2006). According to Mindess et al. (2003), "compressive strength is widely considered to be the most important property of concrete." The 28-day concrete compressive strength is usually specified as the design strength in civil engineering projects, and the specified compressive strength for ordinary ready mix concrete is typically 20.7 to 41.4 MPa (3000-6000 psi) and 48.3 to 82.7 MPa (7000-12000 psi) for high-strength concrete (Wight, 2016).

According to Mindess et al. (2003), all of the following factors can affect concrete strength:

- **Water-to-cementitious materials ratio:** Generally, for well-compacted concrete, the compressive strength will increase as the w/cm decreases.

- **Age:** Due to the hydration reaction, as the concrete age increases, the compressive strength increases. The rate of strength increase will be dependent upon the rate of hydration and this assumes that water is available to allow hydration to continue

- **Cement type:** The chemical composition and fineness of cement play huge roles in compressive strength development. The C_3S phase is responsible for early strength, while the C_2S phase contributes to strength at later ages. Finer cement results in higher rates of strength gain due to the higher cement specific surface area that accelerates hydration

- **Supplementary cementitious materials:** The effect of SCMs on strength depends on chemical composition of each SCM and the replacement level of cement. Generally, most SCMs will result in slightly lower early strengths due to cement dilution (except in the case of silica fume), but higher later strengths can be expected at typical replacement levels due to the pozzolanic reaction and increased particle packing.

- **Chemical admixtures:** The effect of chemical admixtures on strength also depends on the type of admixture that is used and the use of the admixture. Air-entraining admixtures will reduce strength if the w/cm is not changed and water-reducing admixtures can increase strength even if the w/cm remains the same

- **Aggregates:** Aggregate properties play a huge role in strength since they can affect workability and bond strength at the aggregate-paste interface. Aggregate strength also becomes a factor in lightweight and high-strength concrete.

- **Interfacial transition zone (ITZ):** The strength of the ITZ can affect compressive strength by 10-15%, but the tensile strength can be affected by as much as 40%

- **Rate of loading:** Higher strength can be expected at increased loading rates, which are typical in seismic and high-wind loading applications.

5.2.1.2. Elastic Modulus

The structural concrete building code, ACI 318 (2014), allows the use of an empirical equation, shown in Equation 5.1, to predict the modulus of elasticity of normal weight concrete.

$$E_c = 57{,}000\sqrt{f'_c} \text{ (in psi)} \qquad \text{(Eq. 5.1)}$$

where Ec is the modulus of elasticity of concrete, and f'_c is the compressive strength of concrete.

There are a few factors that affect the modulus of elasticity of concrete. According to Mehta and Monteiro (2006), these factors include the interfacial transition zone, the elastic modulus of the cement paste, the degree of saturation in the concrete, the loading rate, and the aggregate porosity, size, shape, texture, grading and mineralogy.

5.2.2. Portland Limestone Cement Concrete

5.2.2.1. Compressive and Tensile Strength

According to Tennis et al. (2011), the compressive strength of PLC concrete is affected by the following factors:

- Quality and quantity of the limestone used to produce the PLC
- The clinker ingredients
- The particle size distribution of the PLC

Researchers have reported similar compressive strengths for PLCs with up to 15% limestone (Dhir et al., 2007; Ramezanianpour & Hooton, 2014) when compared to OPC concrete, provided that the PLC is ground finer. Alunno-Rosetti and Curcio (1997) showed that equivalent compressive strength between cements with 0% and 20% limestone was achieved by increasing the fineness of the cement from 345 m^2/kg to 480-490 m^2/kg. In small quantities (less than 10%), the addition of limestone has resulted in decreased porosity and increased compressive strength (Lothenbach et al., 2008; Ramezanianpour & Hooton, 2014). The decrease in porosity and increase in compressive strength have been attributed to the limestone providing nucleation and growth sites for hydration products, increasing particle packing, and the formation of carboaluminate hydrates, which were discussed in Chapter 3.

As noted by Tennis et al. (2011), there have been various investigations of the splitting tensile strength of concrete, and in general, the behavior of PLC concrete in splitting tension is very similar to that of OPC concrete. In other words, as Irassar et al. (2001) reported in their paper, "*tensile strength was affected more by the w/cm than the type of cement used."* They reported a splitting tensile strength of PLC concrete as approximately 10% of the compressive strength.

5.2.2.2. Elastic Modulus

Dhir et al. (2007) reported a decrease in the modulus of elasticity with increasing limestone content in the cement. However, the decrease in modulus of elasticity correlated to the decrease in compressive strength that is expected as the limestone content increases beyond 15%. This correlation seems to imply that predictive equations currently used to predict the modulus of elasticity of OPC concrete using the compressive strength are probably still valid for PLC concrete.

5.3. Materials

Concrete specimens were cast using water-to-cementitious materials ratios of 0.40 and 0.45. The cementitious materials include cements and supplementary cementitious materials (SCMs).

5.3.1. Cements

Cements PLC1 through PLC7, which have varying limestone contents, were used for this experimental investigation. For more information on the chemical composition and phase composition of all cements, please refer to section 2.1.

5.3.2. Supplementary Cementitious Materials

For this experimental investigation, the following supplementary cementitious materials were used: Class F fly ash, Class C fly ash 1, Grade 100 slag, and densified silica fume. Please refer to section 2.3 for information on the chemical composition of each SCM.

5.3.3. Aggregates

Manufactured limestone sand, natural river sand, and limestone gravel were used as aggregates for the concrete mixtures described in this chapter. Please refer to section 2.4 for more information on the different aggregates used.

5.3.4. Water

Potable tap water was used to mix concrete specimens for this study.

5.4. Mixture Proportions

5.4.1. Nomenclature

The nomenclature system discussed in section 2.6 is used in this chapter. The graphical representation of the nomenclature system provided in section 2.6 is provided again for convenience in Figure 5.1.

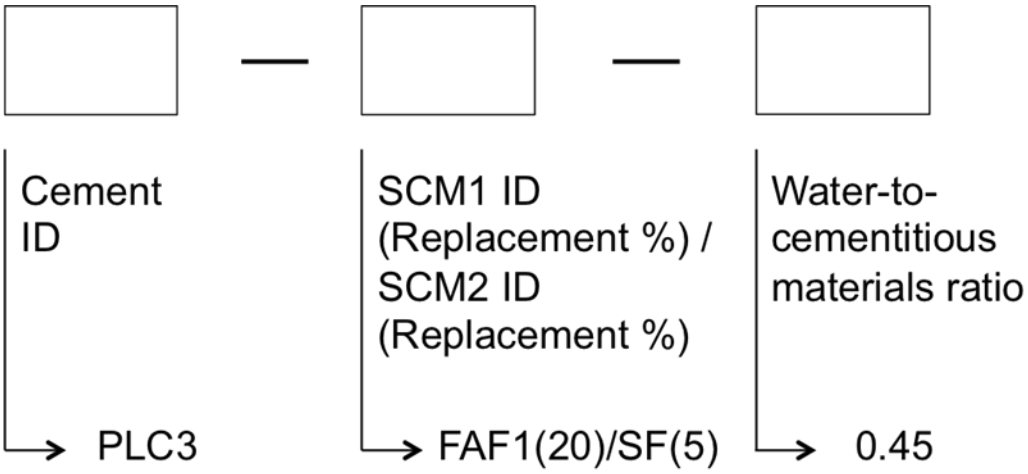

Figure 5.1: Graphical Representation of Nomenclature System

5.4.2. Test Matrix

Forty-two different concrete mixtures were tested. As shown in Table 5.1, the mixtures include straight cement mixtures and different combinations of cements and SCMs, including ternary blends of PLC, Class C fly ash, and densified silica fume. For all mixtures, the coarse aggregate fraction was 1048 kg/m^3 (1766 lb/yd^3), the fine aggregate fraction was 670 kg/m^3 (1129 lb/yd^3), the water content was 163 kg/m^3 (275 lb/yd^3) for the mixtures with a water-to-cementitious materials ratio of 0.45, and 145 kg/m^3 (244 lb/yd^3) for the mixtures with a water-to-cementitious materials ratio of 0.40. For some of the mixtures, limestone coarse aggregate and limestone sand were used, while for the remaining mixtures limestone coarse aggregate and natural river sand were incorporated into the mixture. The research sponsor wanted to limit the total limestone aggregate content in the concrete mixture to more closely mimic the pavement specification (e.g., to reduce polishing), and this was the reason for the change. Thus, some mixtures were repeated using different aggregates and the same cements to determine the effect of the change in fine aggregate. If the mixture ID is followed by a caret symbol (^), the mixture was repeated using both fine aggregates. If the mixture ID is followed by an asterisk symbol (*), the mixture was incorporated limestone sand only. If the mixture ID does not have any symbol after the ID, this is an indication that natural river sand was used for the concrete mixture.

Table 5.1: Mixture Proportions—Mass in kg/m^3 (Note 1 kg/m^3 = 1.69 lb/yd^3)

MIXTURE ID	Cement	FAF1	FAC1	S	SF
PLC1-0.45^	362.5	--	--	--	--
PLC2-0.45	362.5	--	--	--	--
PLC3-0.45^	362.5	--	--	--	--
PLC4-0.45^	362.5	--	--	--	--
PLC5-0.45	362.5	--	--	--	--
PLC6-0.45	362.5	--	--	--	--
PLC7-0.45^	362.5	--	--	--	--
PLC1-0.40	362.5	--	--	--	--
PLC2-0.40	362.5	--	--	--	--
PLC3-0.40	362.5	--	--	--	--
PLC4-0.40	362.5	--	--	--	--
PLC5-0.40	362.5	--	--	--	--
PLC6-0.40	362.5	--	--	--	--
PLC7-0.40	362.5	--	--	--	--
PLC1-FAF1(20)-0.45	290.1	72.4	--	--	--
PLC2-FAF1(20)-0.45	290.1	72.4	--	--	--
PLC3-FAF1(20)-0.45*	290.1	72.4	--	--	--
PLC4-FAF1(20)-0.45*	290.1	72.4	--	--	--
PLC5-FAF1(20)-0.45	290.1	72.4	--	--	--
PLC6-FAF1(20)-0.45	290.1	72.4	--	--	--
PLC7-FAF1(20)-0.45	290.1	72.4	--	--	--
PLC1-FAC1(30)-0.45	253.8	--	108.9	--	--
PLC2-FAC1(30)-0.45	253.8	--	108.9	--	--

MIXTURE ID	Cement	FAF1	FAC1	S	SF
PLC3-FAC1(30)-0.45	253.8	--	108.9	--	--
PLC4-FAC1(30)-0.45	253.8	--	108.9	--	--
PLC5-FAC1(30)-0.45	253.8	--	108.9	--	--
PLC6-FAC1(30)-0.45	253.8	--	108.9	--	--
PLC7-FAC1(30)-0.45	253.8	--	108.9	--	--
PLC1-S(35)-0.45	235.5	--	--	127.0	--
PLC3-S(35)-0.45*	235.5	--	--	127.0	--
PLC5-S(35)-0.45	235.5	--	--	127.0	--
PLC7-S(35)-0.45	235.5	--	--	127.0	--
PLC1-FAC1(25)/SF(5)-0.45	253.8	--	90.6	--	18.1
PLC3-FAC1(25)/SF(5)-0.45	253.8	--	90.6	--	18.1
PLC5-FAC1(25)/SF(5)-0.45	253.8	--	90.6	--	18.1
PLC7-FAC1(25)/SF(5)-0.45	253.8	--	90.6	--	18.1

5.5. Experimental Procedures

A total of sixteen 100 mm x 200 mm (4 in. x 8in.) cylinders were cast and cured following the requirements of ASTM C192 to obtain the compressive strength, elastic modulus, splitting tensile strength, and electrical resistivity for each mixture.

5.5.1. ASTM C39 Compressive Strength

Twelve cylinders were tested in accordance with ASTM C39 to obtain the compressive strength of each mixture at 1, 7, 28, and 91 days.

5.5.2. ASTM C469 Elastic Modulus

Four of the twelve cylinders that were cast to obtain the compressive strength of concrete (see section 5.5.1) were first used to obtain the modulus of elasticity of each concrete mixture at 28 and 91 days in accordance with the procedure described in ASTM C469.

5.5.3. ASTM C496 Tensile Strength

Four of the sixteen cylinders that were cast were used to obtain the splitting tensile strength of each mixture at 28 and 91 days, in accordance with the requirements specified in ASTM C496.

5.5.4. Electrical Resistivity

The electrical resistivity of two concrete cylinders per mixture was obtained prior to testing the cylinders in compression at each age (1, 7, 28, and 91 days). The equipment used was an RCON2 resistivity meter using a frequency of 10 KHz; the high frequency was used to obtain a low phase angle, resulting in a more accurate measurement, as recommended by the manufacturer.

Electrical resistivity is a measure of the pore structure connectivity, which is an indication of permeability, one of the most important factors in durability design. Electrical resistivity has good correlation with the rapid chloride permeability test (RCPT) outlined in ASTM C1202. The correlation between RCPT and electrical resistivity values can be seen in Table 5.2. Electrical resistivity also correlates well with the chloride diffusion coefficient test (ASTM C1556).

Table 5.2: RCPT and Electrical Resistivity Values (Source: Giatec Scientific)

Chloride Penetration	56-Day Rapid Chloride Permeability Charge Passed as per ASTM C1202 (Coulombs)	28-Day Bulk Electrical Resistivity of Saturated Concrete (kΩ*cm)
High	> 4,000	< 5
Moderate	2,000-4,000	5-10
Low	1,000-2,000	10-20
Very Low	100-1,000	20-200
Negligible	< 100	> 200

5.6. Results and Discussion

5.6.1. Compressive Strength

5.6.1.1. Straight Cement Mixtures

Figure 5.2 shows the compressive strength plotted as a function of age for the straight cement mixtures using the cements from Cement Plant 1 (PLC1-PLC4) at a water-to-cementitious materials ratio of 0.45. It is worth noting that PLC2, which has a limestone content of 13.2%, produces concrete with equivalent strength as the OPC control cement (PLC1). As the limestone content increases beyond 15%, the decrease in strength becomes more apparent.

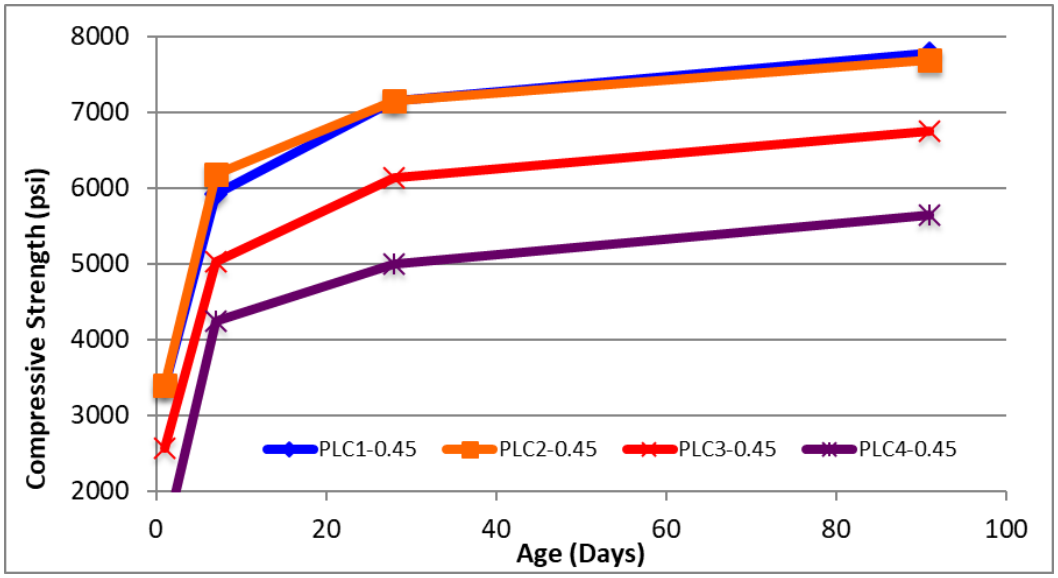

Figure 5.2: Compressive Strength vs. Age for Cement Plant 1 Straight Cement Mixtures at 0.45 w/cm (Note: 1000 psi = 6.9 MPa)

Figure 5.3 shows the compressive strength plotted as a function of age for the straight cement mixtures using the cements from Cement Plant 2 (PLC1-PLC4) at a water-to-cementitious materials ratio of 0.45. It is worth noting that PLC6, which has a limestone content of 11.6%, showed a decrease in compressive strength when compared to the control cement (PLC5) for Cement Plant 2. On the other hand, PLC7, which has a limestone content of 15.5%, had similar compressive strengths after curing for 7, 28, and 91 days. This can be attributed to the fineness of PLC7, which was optimized in an attempt to achieve equivalent strength.

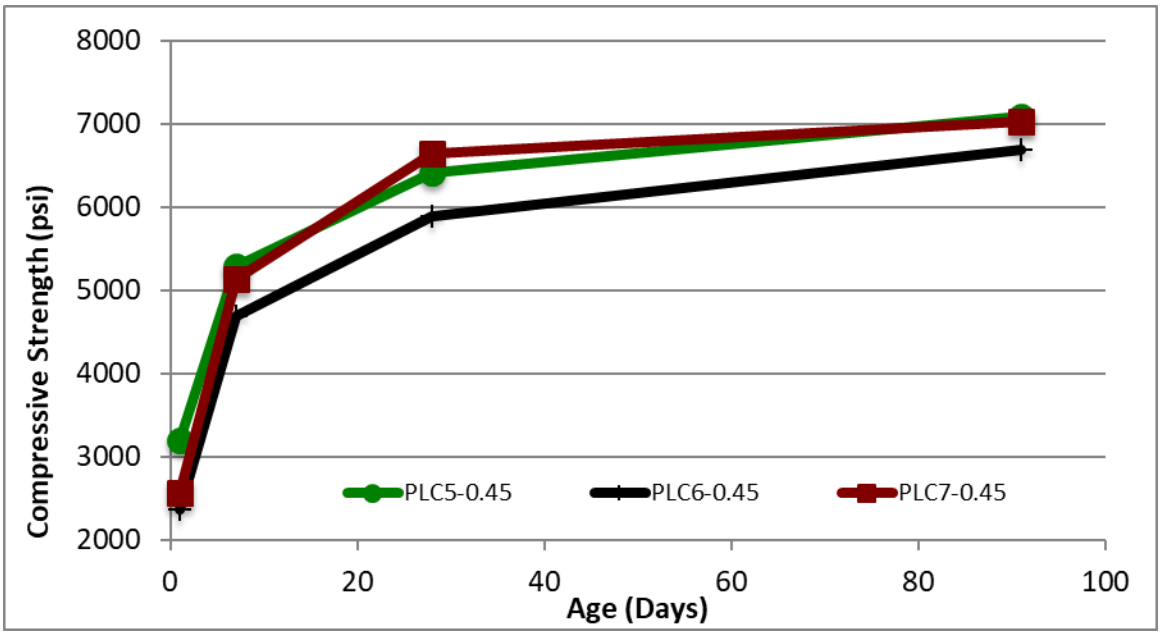

Figure 5.3: Compressive Strength vs. Age for Cement Plant 2 Straight Cement Mixtures at 0.45 w/cm (Note: 1000 psi = 6.9 MPa)

Figure 5.4 shows the compressive strength, normalized by clinker (including gypsum) content, plotted as a function of age for PLC1-PLC7 at a water-to-cementitious materials ratio of 0.45. Please note that all of the cement with high limestone contents, except for PLC4 (30.6% limestone), have a higher normalized compressive strength compared to the control cement for each plant. This is further evidence that a portion of the limestone powder reacts (as seen by the formation of carboaluminates in Chapter 2) and also increases the reactivity of the cement by providing nucleation and growth sites (Tennis et al., 2011).

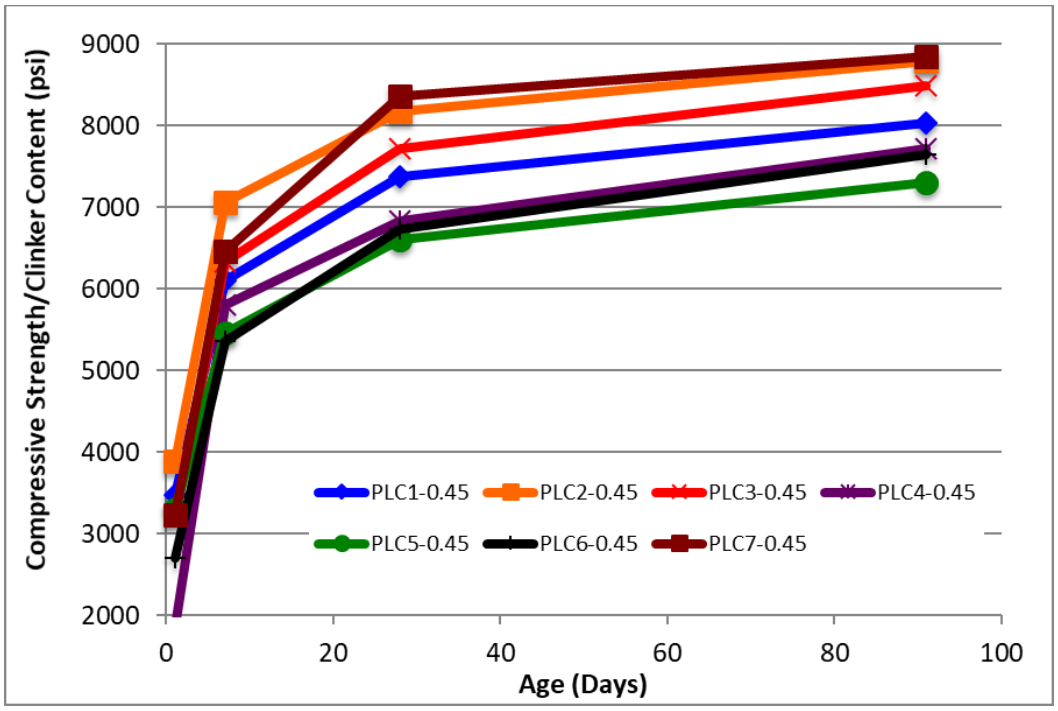

Figure 5.4: Compressive Strength Normalized by Clinker Content vs. Age for Straight Cement Mixtures at 0.45 w/cm (Note: 1000 psi = 6.9 MPa)

Figure 5.5 shows the 28-day compressive strength of the straight cement mixtures and Figure 5.6 shows the normalized 28-day compressive strength of the straight cement mixtures. Please note that the mixture with the lowest compressive strength, PLC4, was still able to reach 5000 psi at 28 days, which would be acceptable in the vast majority of structural engineering applications. Figure 5.6 shows the increased benefit, in terms of compressive strength, that the limestone addition provides.

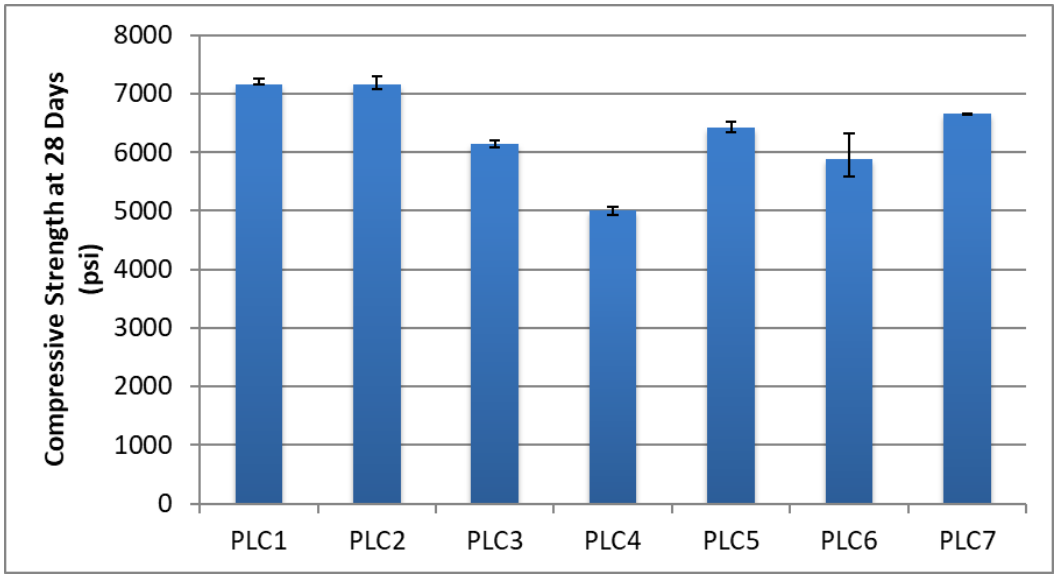

Figure 5.5: 28-Day Compressive Strength for Straight Cement Mixtures at 0.45 w/cm (Note: 1000 psi = 6.9 MPa)

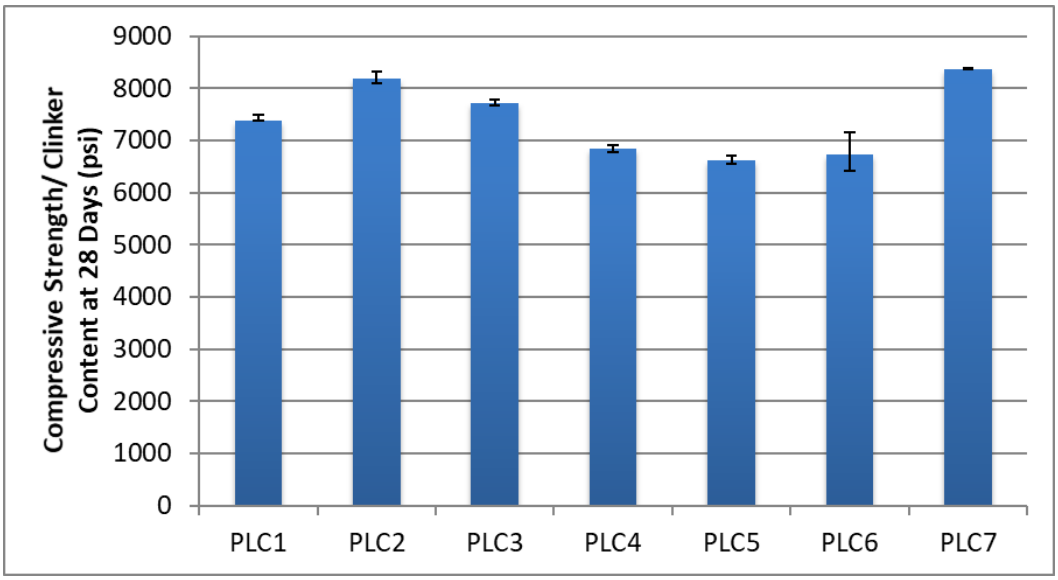

Figure 5.6: Normalized 28-Day Compressive Strength for Straight Cement Mixtures at 0.45 w/cm (Note: 1000 psi = 6.9 MPa)

Figure 5.7 shows the 28-day compressive strength plotted as a function of limestone content in the cement. Please note that there is not a significant decrease in compressive strength when the limestone content is less than about 15%.

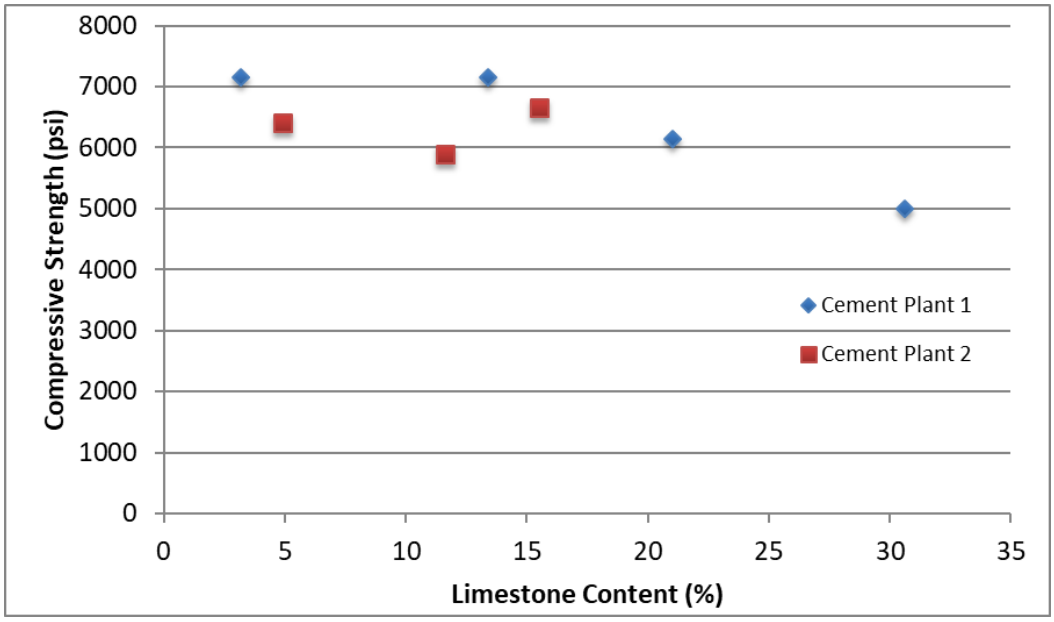

Figure 5.7: 28-Day Compressive Strength vs. Limestone Content for Straight Cement Mixtures at 0.45 w/cm (Note: 1000 psi = 6.9 MPa)

Figure 5.8 compares the compressive strength at 28 days for the straight cement mixtures at the water-to-cementitious materials ratios of 0.45 and 0.40. It is interesting that for PLC2 and PLC3, the 28-day compressive strength actually decreased when lowering the w/cm. Figure 5.9 shows the 91-day compressive strength for the straight cement mixtures at the water-to-cementitious materials ratios of 0.45 and 0.40. The 91-day compressive strengths of PLC2 and PLC3 at 0.40 have caught up to their respective strengths at 0.45 w/cm. The reason for the slower strength development for these two mixtures when the w/cm is lowered is unknown and needs further investigation.

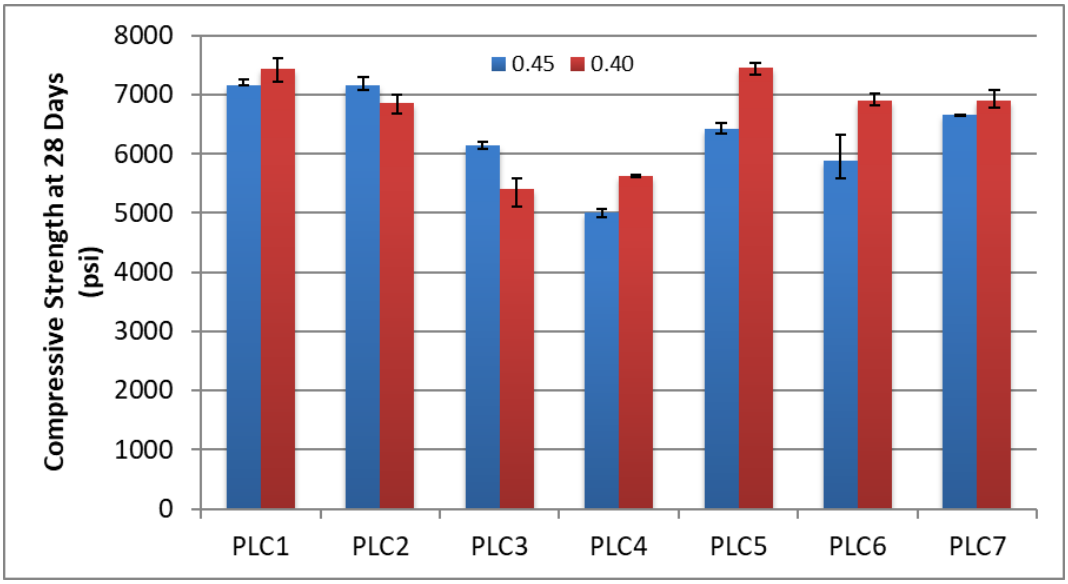

Figure 5.8: 28-Day Compressive Strength for Straight Cement Mixtures at 0.40 and 0.45 w/cm (Note: 1000 psi = 6.9 MPa)

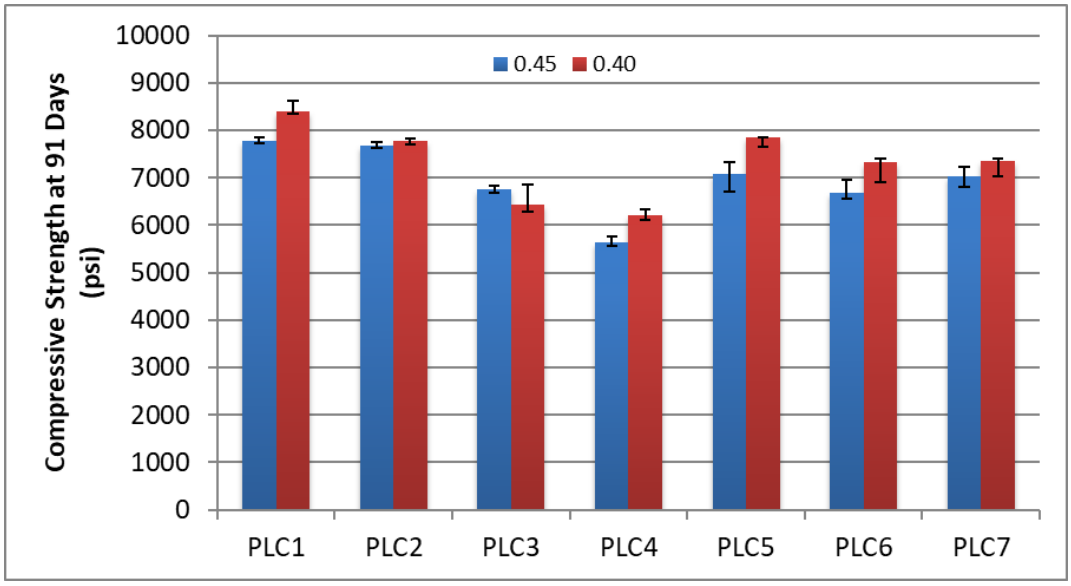

Figure 5.9: 91-Day Compressive Strength for Straight Cement Mixtures at 0.40 and 0.45 w/cm (Note: 1000 psi = 6.9 MPa)

Another method that could be used to normalize the compressive strength would be to calculate the effective water-to-cementitious materials ratio for each mixture using Equation 5.2. The concept of effective w/cm was developed in an attempt to calculate the equivalent w/cm that it would take to obtain an equivalent compressive strength, considering only the portland cement and gypsum portion of the cement and excluding the limestone powder portion.

$$\frac{w}{cm_{eff}} = \frac{w}{cm} * \frac{100 - LS_{control}}{100 - LS_{actual}} \quad \text{(Eq. 5.2)}$$

where w/cm is the water-to-cementitious materials ratio of the cement that is being normalized, $LS_{control}$ is the limestone content of the control cement, and LS_{actual} is the limestone content of the cement being normalized. For example, to calculate the effective w/cm for the concrete mixture using PLC2, w/cm is equal to 0.45, $LS_{control}$ is 3.2 (the limestone content of PLC1, the control cement), LS_{actual} is 13.4 (the limestone content of PLC2), resulting in an effective w/cm of 0.50. Table 5.3 provides the effective w/cm for straight cement mixtures.

Table 5.3: Effective w/cm for Straight Cement Mixtures

Mixture ID	Effective w/cm
PLC1-0.45	0.45
PLC2-0.45	0.50
PLC3-0.45	0.55
PLC4-0.45	0.63
PLC5-0.45	0.45
PLC6-0.45	0.48
PLC7-0.45	0.51
PLC1-0.40	0.40
PLC2-0.40	0.45
PLC3-0.40	0.49
PLC4-0.40	0.56
PLC5-0.40	0.40
PLC6-0.40	0.43
PLC7-0.40	0.45

Figure 5.10 shows the development of compressive strength with age for the mixtures that have approximately the same effective w/cm. Please note that the compressive strengths are very similar and thus, the concept of effective w/cm is valid for these mixtures.

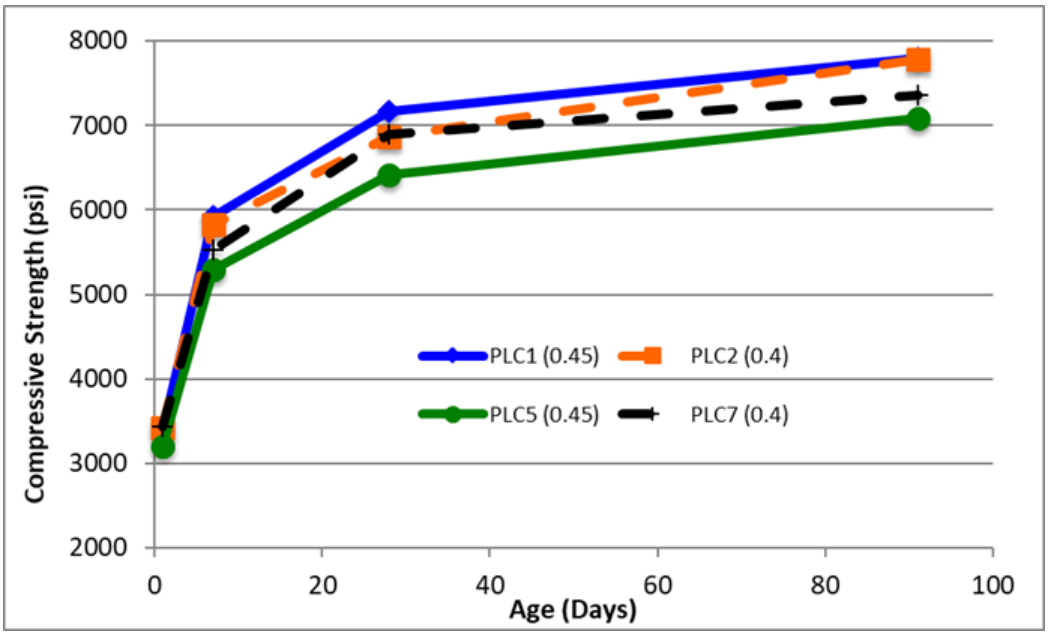

Figure 5.10: Compressive Strength vs. Age for Mixtures with Effective w/cm = 0.45 (Note: 1000 psi = 6.9 MPa)

Figure 5.11 shows the 28-day compressive strength plotted as function of effective w/cm for the straight cement mixtures with actual w/cm of 0.4 and 0.45. As expected, the compressive strength decreases as the effective w/cm increases. For concrete mixtures incorporating high limestone PLCs, the effective w/cm is a better indicator of compressive strength.

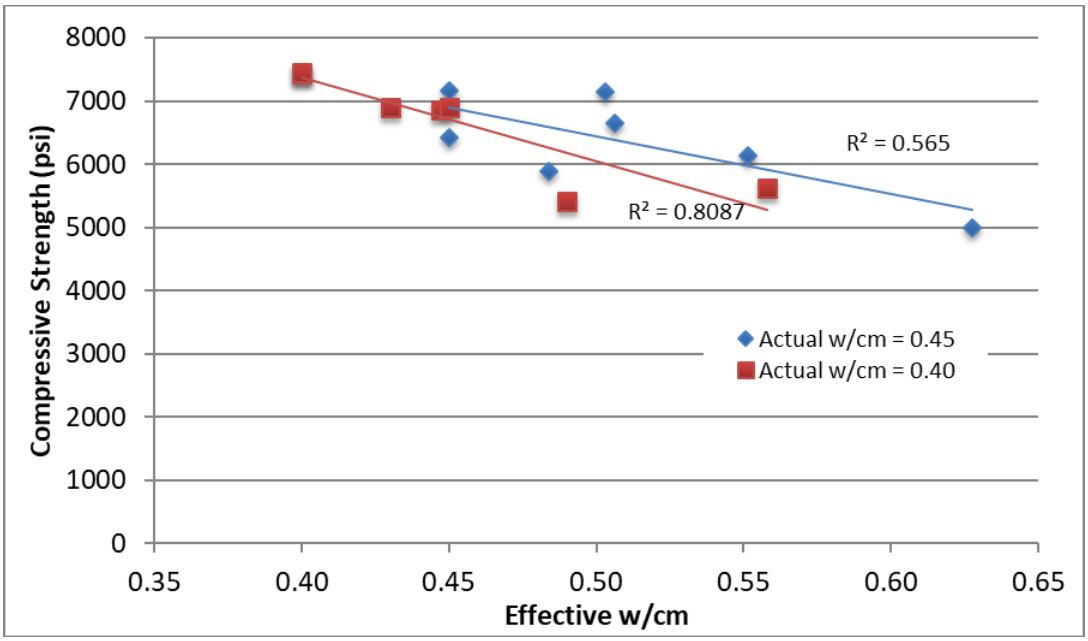

Figure 5.11: 28-Day Compressive Strength vs. Effective w/cm (Note: 1000 psi = 6.9 MPa)

5.6.1.2. Effect of SCMs

Figures 5.12 through 5.15 show the 28-day compressive strength for the several different combinations of PLCs and supplementary cementitious materials at various replacement levels. The same general trend can be observed regardless of type of SCM that is used: as the limestone content of the cement increases, the compressive strength decreases.

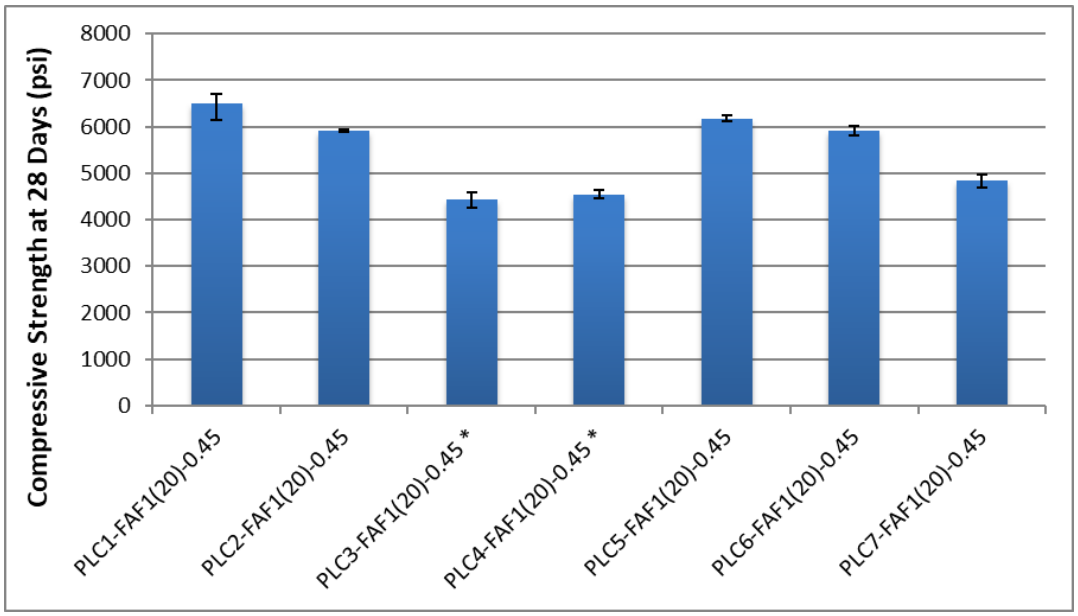

*Figure 5.12: 28-Day Compressive Strength for Mixtures with 20% Class F Fly Ash (*Limestone sand; Note: 1000 psi = 6.9 MPa)*

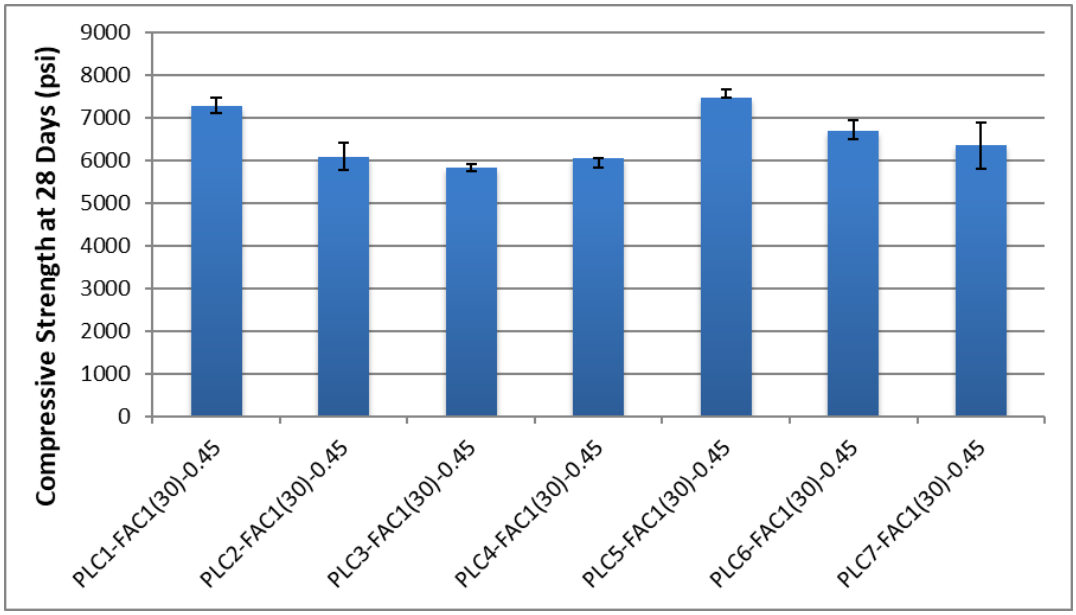

Figure 5.13: 28-Day Compressive Strength for Mixtures with 30% Class C Fly Ash (Note: 1000 psi = 6.9 MPa)

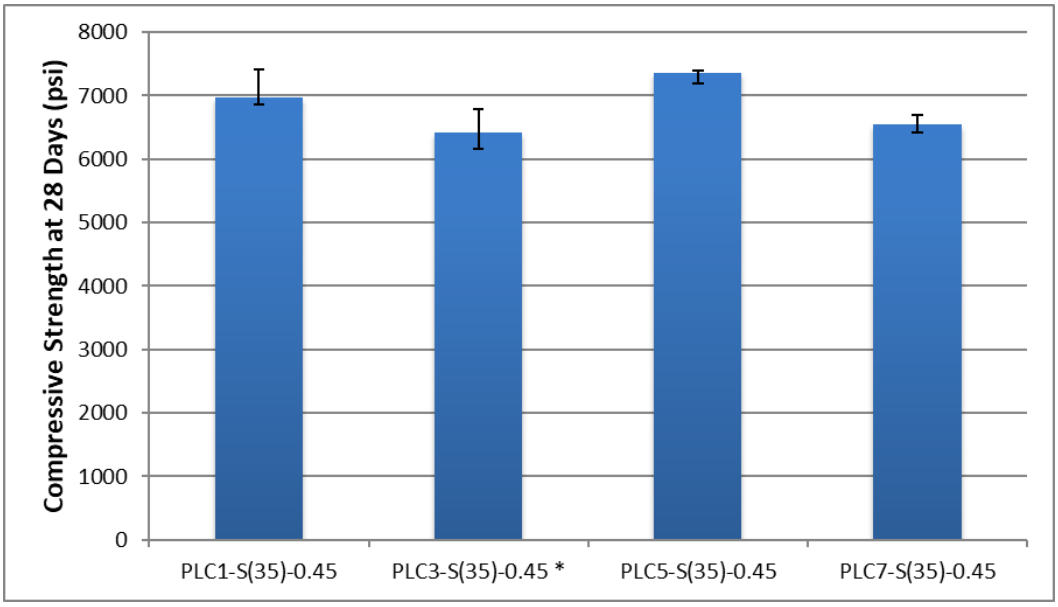

*Figure 5.14: 28-Day Compressive Strength for Mixtures with 35% Slag (*Limestone sand; Note: 1000 psi = 6.9 MPa)*

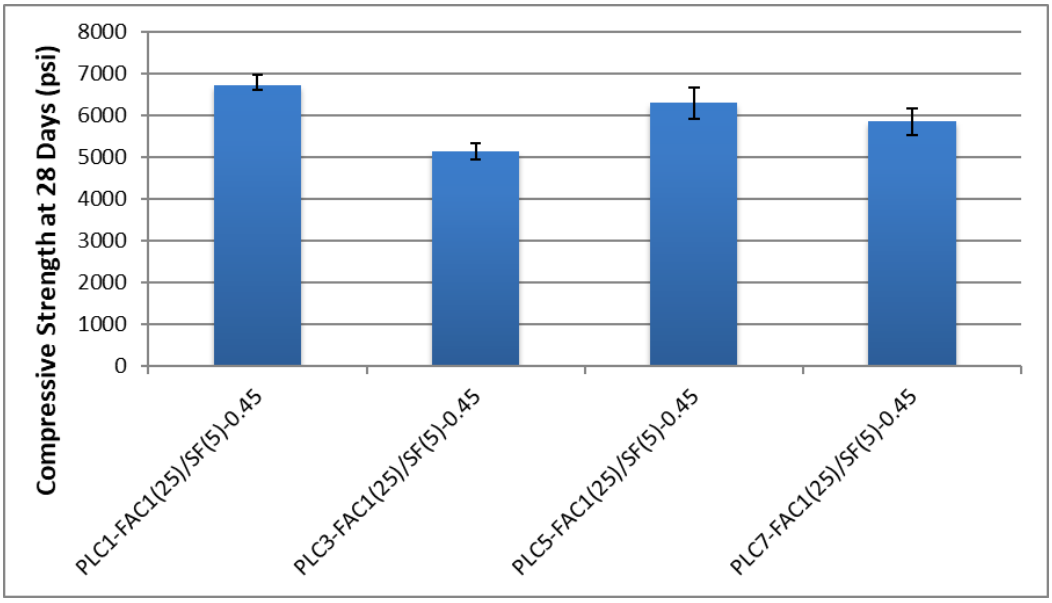

Figure 5.15: 28-Day Compressive Strength for Mixtures with 25% Class C Fly Ash and 5% Densified Silica Fume (Note: 1000 psi = 6.9 MPa)

Figure 5.16 shows PLC4 combined with different types of SCMs and Figure 5.17 shows PLC7 combined with different types of SCMs. There is not a clear effect from combining SCMs with high limestone content PLCs. The addition of Class F fly ash decreased the 28-day compressive strength in both cases. The incorporation of class C fly ash into the mixture resulted in about a 20% increase in compressive strength for the mixture with PLC4, but the compressive strength for PLC7 and class C fly ash were about the same.

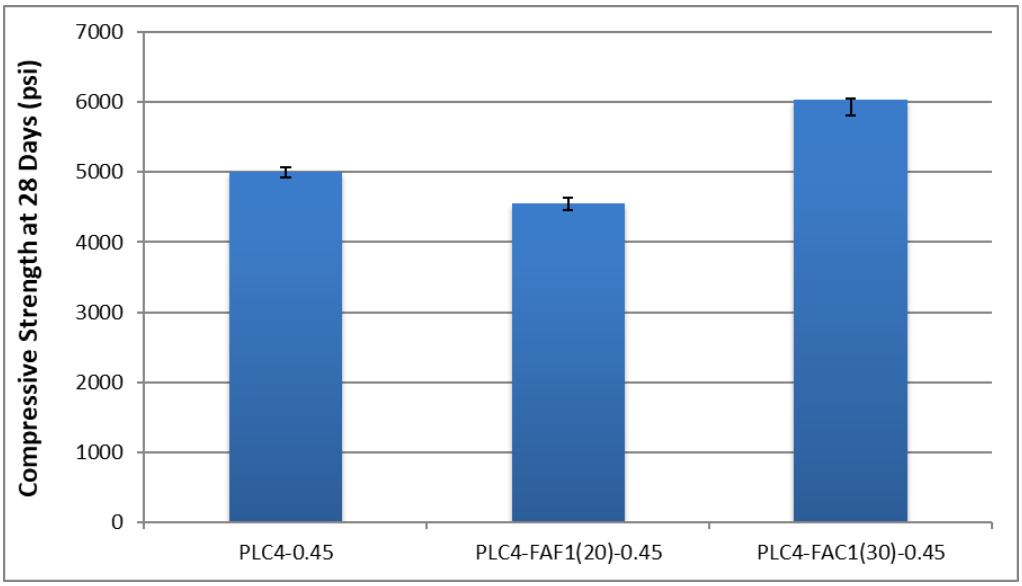

Figure 5.16: 28-Day Compressive Strength for Mixtures with PLC4 and SCMs (Note: 1000 psi = 6.9 MPa)

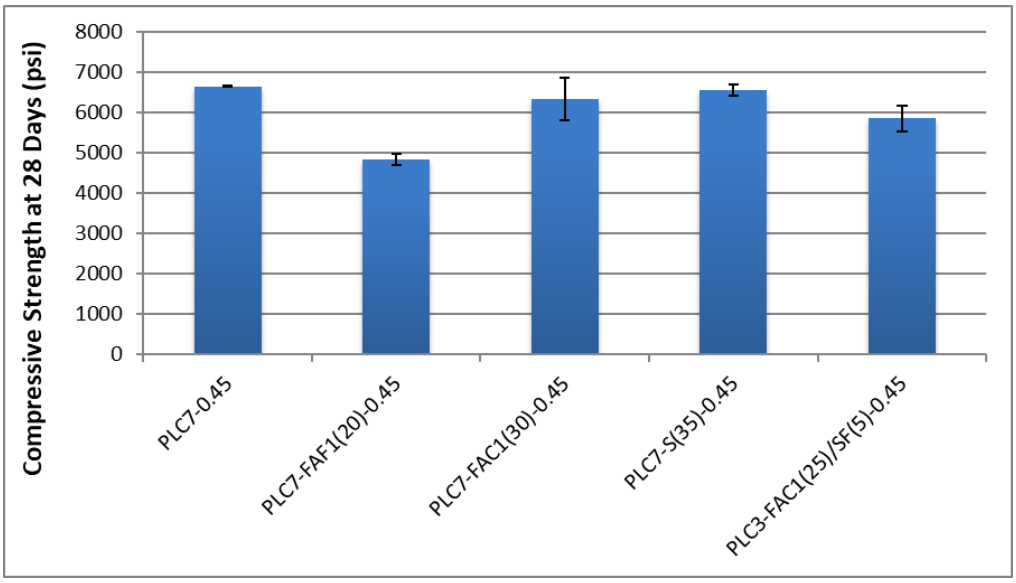

Figure 5.17: 28-Day Compressive Strength for Mixtures with PLC7 and SCMs (Note: 1000 psi = 6.9 MPa)

5.6.2. Tensile Strength

Figure 5.18 shows the ratio of tensile strength to compressive strength at 28 and 91 days for the straight cement mixtures. For the mixtures made with cements from Cement Plant 1 (PLC1-PLC4), the tensile to compressive strength ratio varied from about 8.3% to 10.8% and increases as the limestone content increases. For the mixtures made with cements from Cement Plant 2 (PLC5-PLC7), the tensile to compressive strength ratio varied 8.3% to 10.1% and also increased as the limestone content increased.

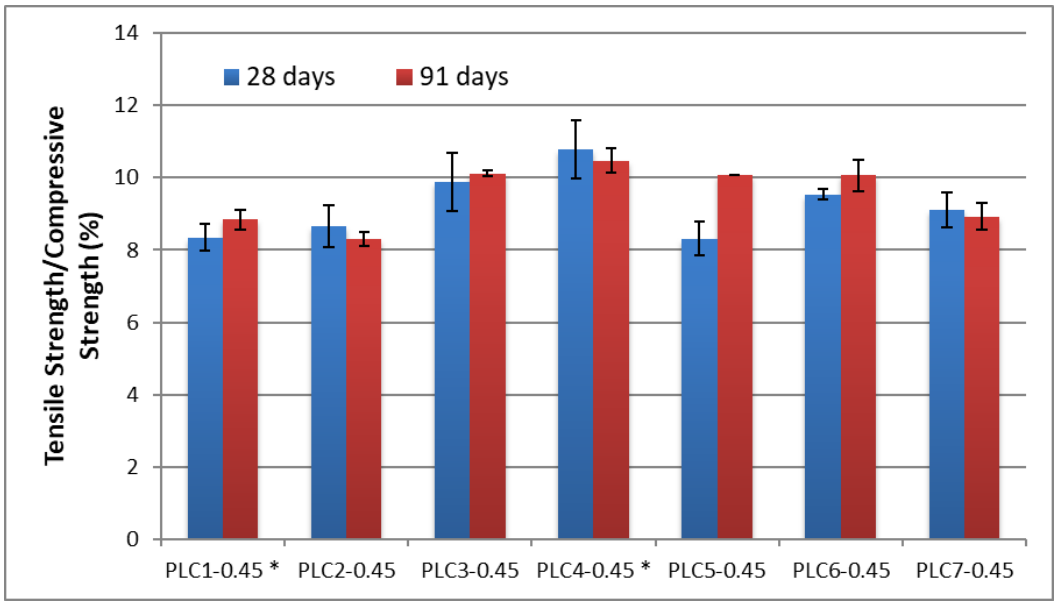

Figure 5.18: Tensile Strength to Compressive Strength Ratio at 28 and 91 Days for Straight Cement Mixtures at w/cm = 0.45

The effect of increasing limestone content combined with the addition of Class C fly ash can be seen in Figure 5.19. The tensile to compressive strength ratio varies from 8.1% and 10.5%, giving about the same range as PLCs without fly ash. Figure 5.20 shows the effect of different supplementary cementitious materials when they are combined with PLC7, which has a limestone content of about 15%. Please note that the addition of supplementary cementitious materials, regardless of SCM type, led to an increase in the ratio of tensile to compressive strength, presumably due to the improvements within the interfacial transition zone (ITZ) (Mindess et al., 2003).

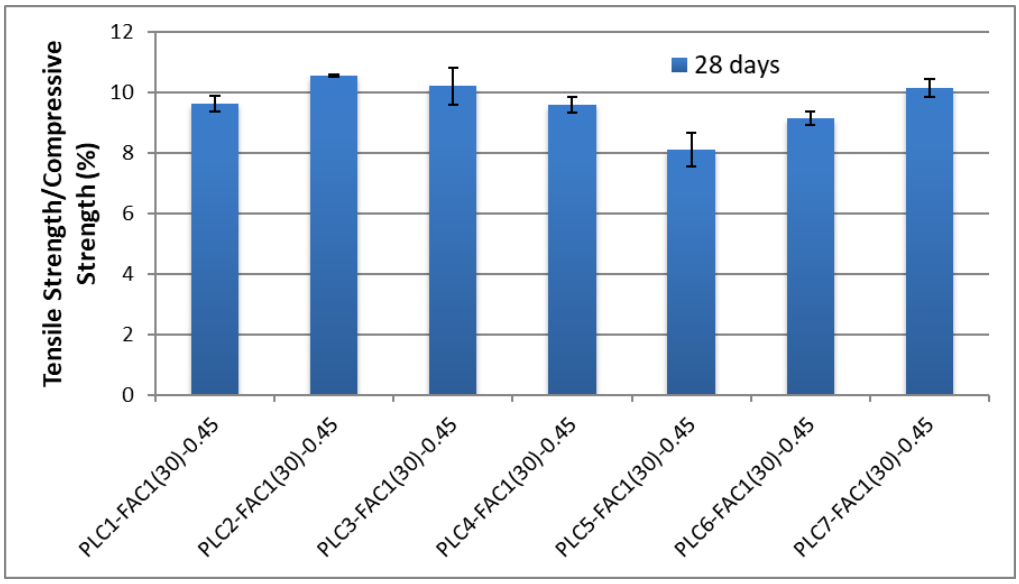

Figure 5.19: Tensile Strength to Compressive Strength Ratio at 28 Days for PLCs with 30% Class C Fly Ash at w/cm = 0.45

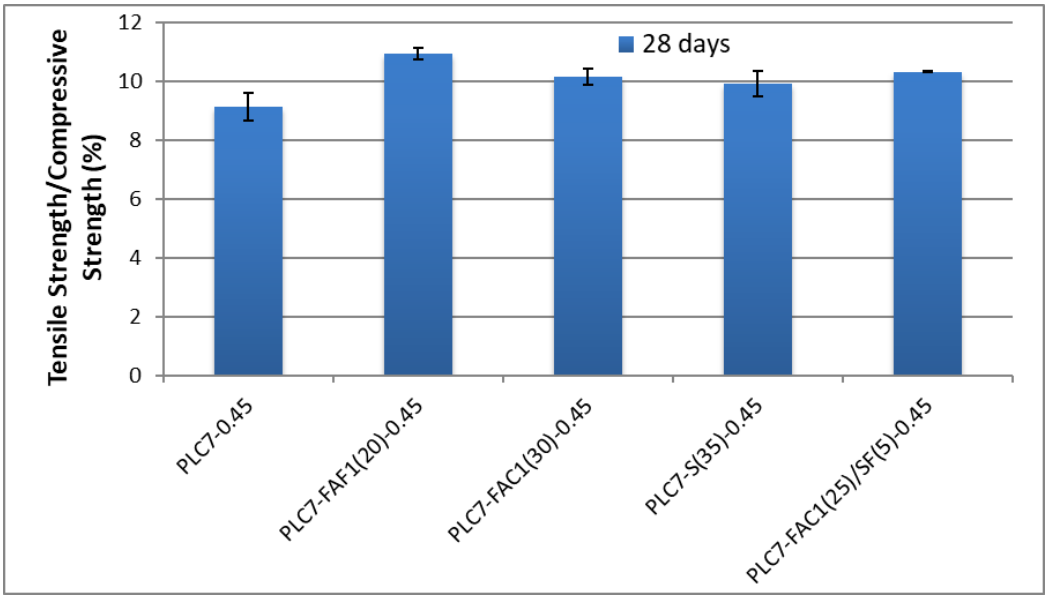

Figure 5.20: Tensile Strength to Compressive Strength Ratio at 28 Days for PLC7 with Different SCMs at w/cm = 0.45

5.6.3. Elastic Modulus

Figure 5.21 shows the ratio of predicted to experimental elastic modulus at 28 days for PLC1-PLC7 at water-to-cementitious materials ratios of 0.40 and 0.45. Equation 5.1 was used to predict the elastic modulus based on the 28-day compressive strength. Please note that a ratio of 1.0 means

that the predictive equation is very accurate and a ratio below 1.0 would be a conservative prediction of modulus of elasticity in terms of structural design.

For the straight cement mixtures, the effect of increasing limestone content does not have a conclusive effect on the ratio of predicted-to-experimental elastic modulus. Please note that for the mixtures with a w/cm of 0.40, the ratio is essentially the same regardless of limestone content in the cement. Also of importance is the fact that the ratios range from 0.85 to about 1.0 when all the mixes at both of the water-to-cementitious materials ratios are considered, indicating that Equation 3.1 is accurate and conservative for predicting the elastic modulus of PLC concrete at high limestone contents. This is in agreement with results reported by other researchers (Tennis et al., 2011).

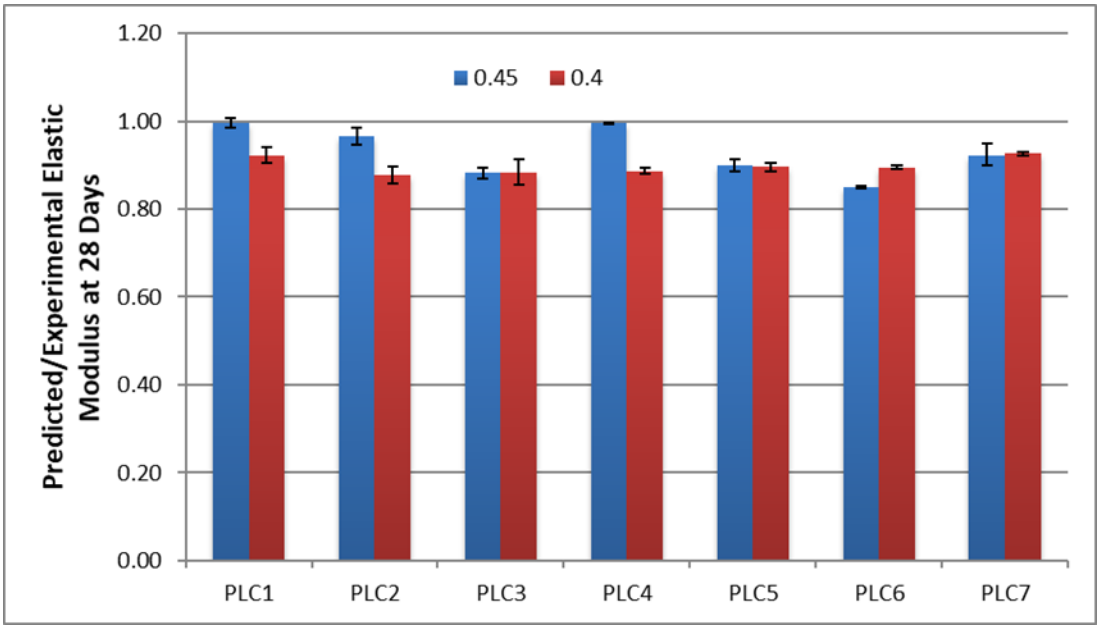

Figure 5.21: Ratio of Predicted to Experimental Elastic Modulus at 28 Days for Straight Cement Mixtures at w/cm = 0.40 and w/cm = 0.45

Figure 5.22 shows the ratio of predicted to experimental elastic modulus at 28 days for PLC1-PLC7 when combined with 30% Class C fly ash at a w/cm of 0.45. The incorporation of fly ash into the mixtures leads to insignificant differences in the predicted-to-experimental ratios of elastic moduli when compared to the mixtures without fly ash. Equation 3.1 is still valid and provides a conservative approach to predicting the modulus of elasticity given compressive strength even at extremely low clinker contents, as is the case for PLC4-FAC1(30)-0.45, when the clinker and gypsum content is approximately 40% of the total powder material weight.

Figure 5.23 shows the ratio of predicted to experimental elastic modulus at 28 days for PLC7 when combined with different supplementary cementitious materials at a w/cm of 0.45. The ratio does not change significantly, regardless of SCM used or the SCM replacement level.

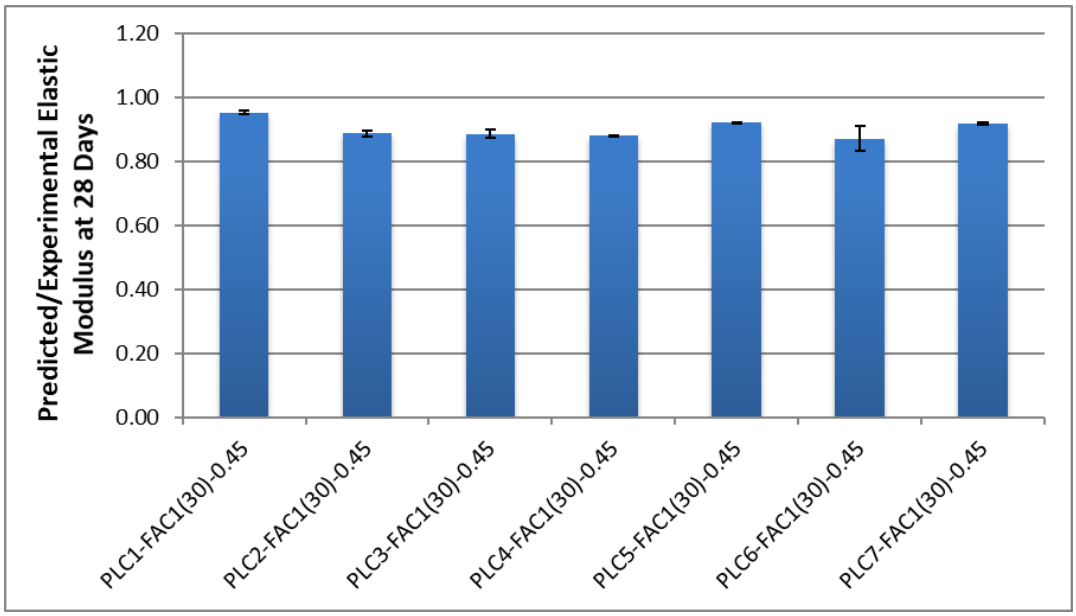

Figure 5.22: Ratio of Predicted to Experimental Elastic Modulus at 28 Days for PLCs with 30% Class C Fly Ash at w/cm = 0.45

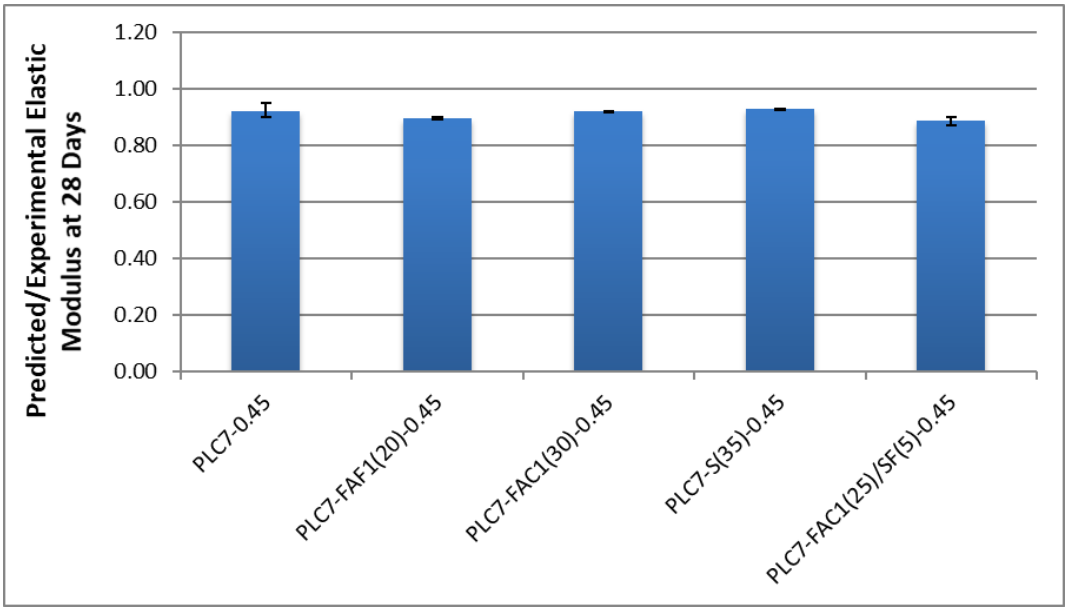

Figure 5.23: Ratio of Predicted to Experimental Elastic Modulus at 28 Days for PLC7 with Different SCMs at w/cm = 0.45

5.6.4. Electrical Resistivity

Figures 5.24 and 5.25 show the development of electrical resistivity as a function of curing duration for PLC1 to PLC4 at water-to-cementitious materials ratios of 0.45 and 0.40, respectively. The electrical resistivity of the control cement, PLC1, is higher at both water-to-cementitious materials ratios, and the resistivity decreases at higher limestone contents. As expected, the electrical resistivity decreases as the water-to-cementitious materials ratio decreases.

It is also worth noting that the electrical resistivity development curves are very similar to the compressive strength development curves, which are shown in section 5.6.1.

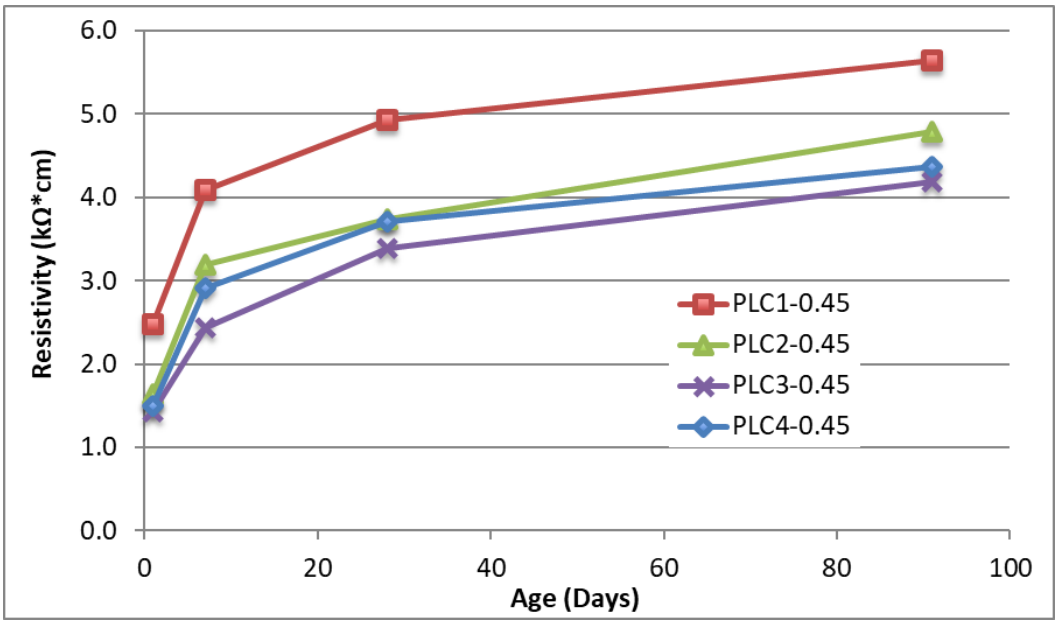

Figure 5.24: Electrical Resistivity vs. Age for PLC1-PLC4 at w/cm = 0.45

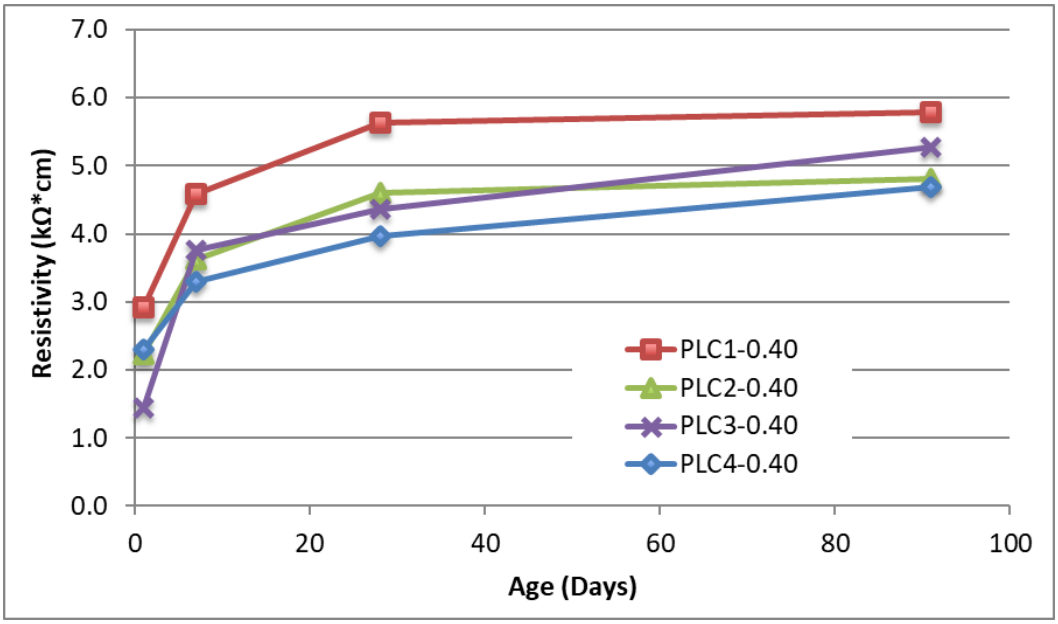

Figure 5.25: Electrical Resistivity vs. Age for PLC1-PLC4 at w/cm = 0.40

Figures 5.26 and 5.27 show the development of electrical resistivity as a function of curing duration for PLC5 to PLC7 at water-to-cementitious materials ratios of 0.45 and 0.40, respectively. At w/cm equal to 0.45, the resistivity is the same for PLC5 and PLC6 and slightly lower for PLC7. If the w/cm is lowered to 0.40, the electrical resistivity increases for all mixtures and they all have approximately the same electrical resistivity.

Please note that most of these mixtures have a resistivity value less than 5 kΩ*cm, which is about equal to a 4,000 coulomb charge passed in the RCPT per ASTM C1202. High chloride penetration would be expected for the majority of these mixes, even at a relatively low water-to-cementitious materials ratio of 0.40.

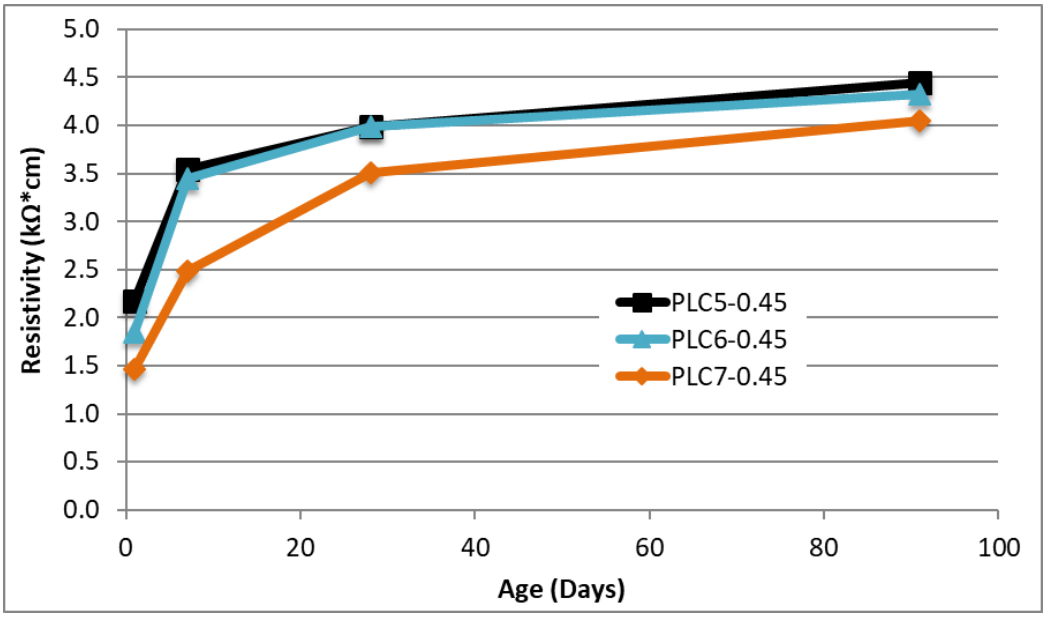

Figure 5.26: Electrical Resistivity vs. Age for PLC5-PLC7 at w/cm = 0.45

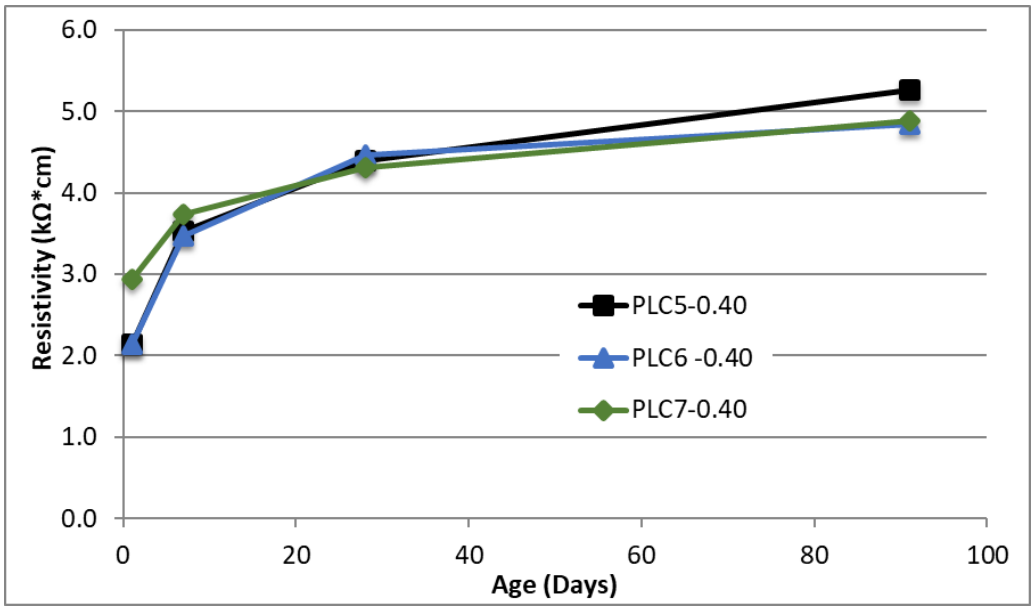

Figure 5.27: Electrical Resistivity vs. Age for PLC5-PLC7 at w/cm = 0.40

The 28-day and 91-day electrical resistivity values for the straight cement mixtures are tabulated in Table 5.4. Figure 5.28 shows the electrical resistivity values plotted as a function of effective w/cm. It is evident that the electrical resistivity decreases as the effective w/cm increases. The same trend was observed for compressive strength as the w/cm increased; however, the correlation for electrical resistivity with effective w/cm is not as strong.

Table 5.4: 28-day and 91-day Electrical Resistivity Values for Straight Cement Mixtures

Mixture ID	Effective w/cm	28-Day Resistivity (kΩ*cm)	91-Day Resistivity (kΩ*cm)
PLC1-0.45	0.45	4.93	5.65
PLC2-0.45	0.50	3.73	4.79
PLC3-0.45	0.55	3.39	4.19
PLC4-0.45	0.63	3.71	4.37
PLC5-0.45	0.45	3.99	4.45
PLC6-0.45	0.48	3.99	4.33
PLC7-0.45	0.51	3.51	4.05
PLC1-0.40	0.40	5.63	5.79
PLC2-0.40	0.45	4.61	4.81
PLC3-0.40	0.49	4.37	5.27
PLC4-0.40	0.56	3.97	4.69
PLC5-0.40	0.40	4.39	5.27
PLC6-0.40	0.43	4.47	4.85
PLC7-0.40	0.45	4.31	4.89

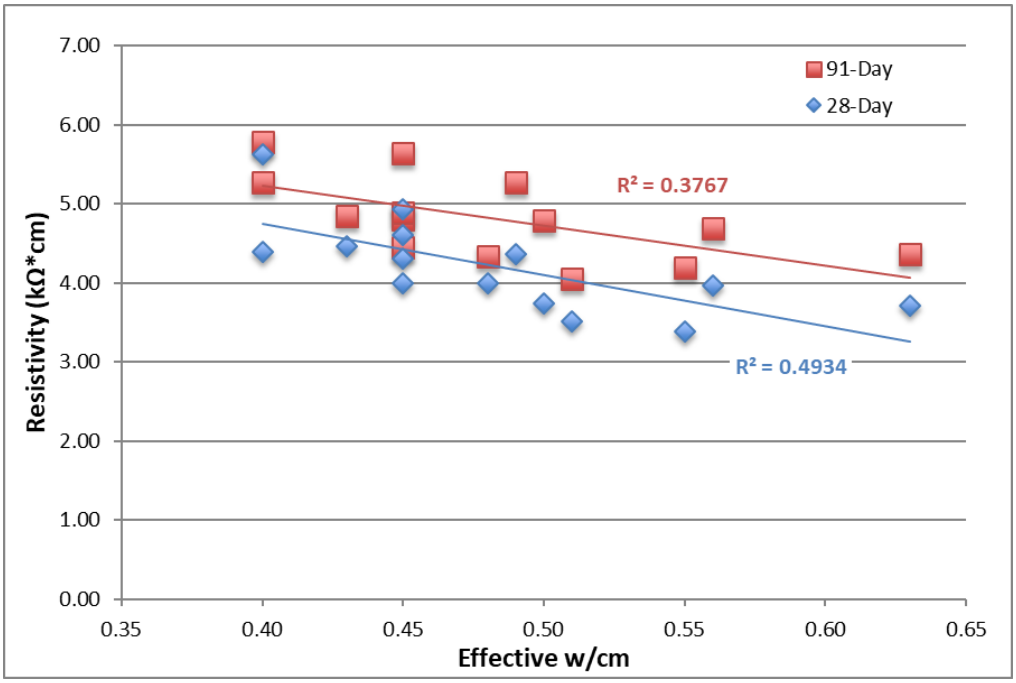

Figure 5.28: 28-day and 91-day Electrical Resistivity vs. Effective w/cm for Straight Cement Mixtures

Figure 5.29 shows the development of electrical resistivity as a function of curing duration for PLC1 to PLC4 when 30% Class C fly ash is incorporated into the mixtures at water-to-cementitious materials ratios of 0.45. The control mix, PLC1-0.45, which had the highest electrical resistivity values out of all mixes without SCMs, is included for reference. Please note that the

addition of fly ash is not beneficial at early ages, likely due to cement dilution effects, but it is beneficial at later ages. Please note that all of the electrical resistivity values for the mixtures with fly ash are very similar, despite the very different limestone content of the cements. The same trends are observed in Figure 5.30, where the cements from Cement Plant 2, PLC5-PLC7, were used in the concrete mixtures.

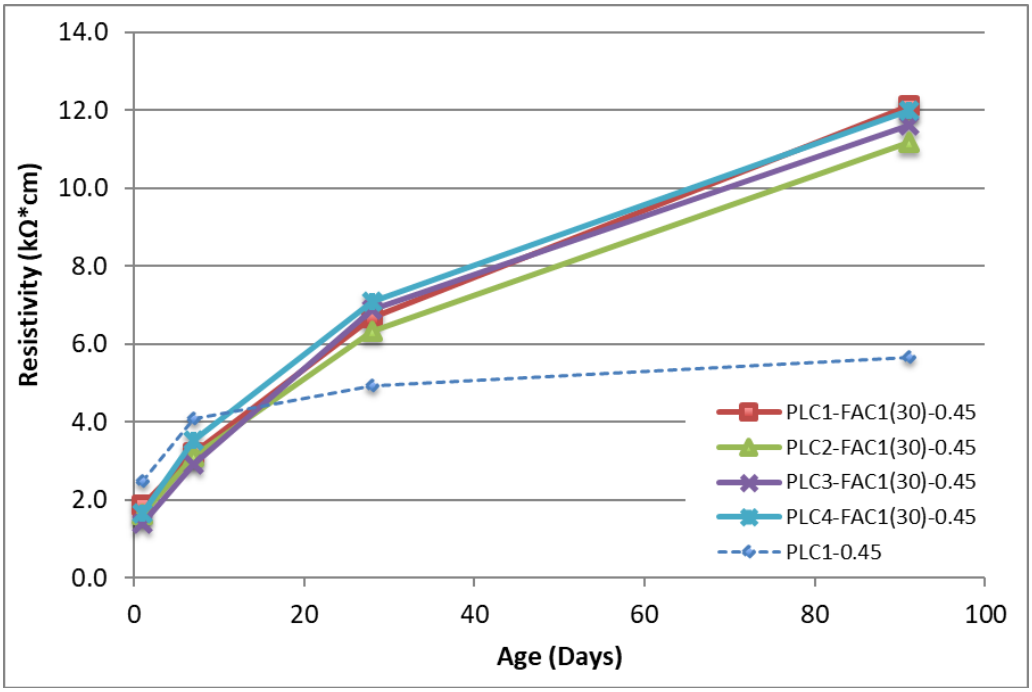

Figure 5.29: Electrical Resistivity vs. Age for PLC1-PLC4 Combined with 30% Class C Fly Ash at w/cm = 0.45

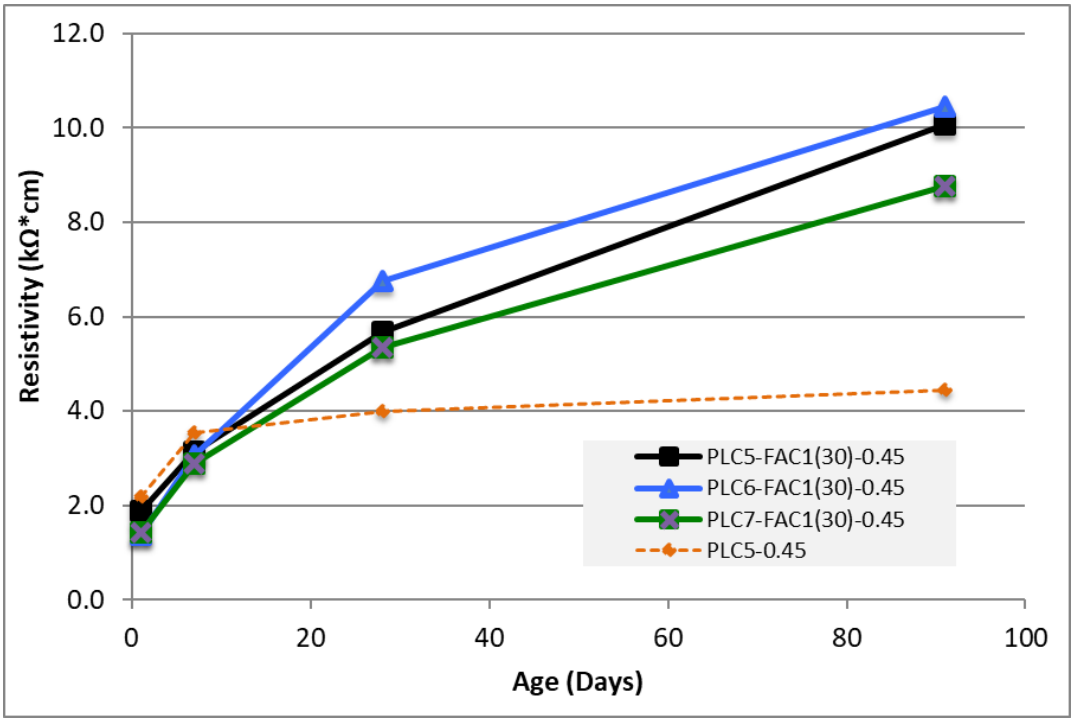

Figure 5.30: Electrical Resistivity vs. Age for PLC5-PLC7 Combined with 30%

Figure 5.31 shows the electrical resistivity plotted as a function of curing age for ternary mixtures with different PLCs, 25% Class C fly ash, and 5% silica fume. It is important to note that these ternary blends achieved the highest electrical resistivity values at 91 days of all the mixtures that were tested. The early age resistivity values are on par with the control, probably due to the high reactivity of the silica fume having the greatest impact at 1 and 7 days. The later age values can be attributed to the pozzolanic reaction from the fly ash creating secondary C-S-H, leading to decreases in porosity and pore connectivity.

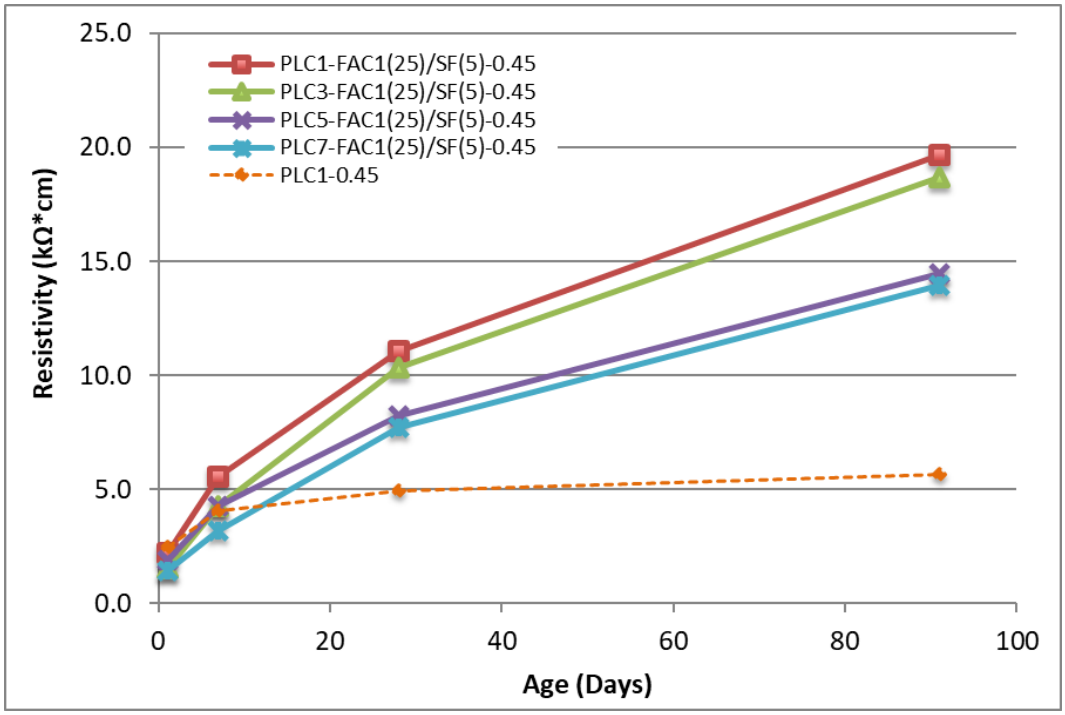

Figure 5.31: Electrical Resistivity vs. Age for Ternary Blends of PLCs Combined with 25% Class C Fly Ash and 5% Silica Fume at w/cm = 0.45

Figure 5.32 shows the effect of lowering the w/cm and addition of SCMs into the mixture with PLC7, which has about 15% limestone. Lowering the w/cm from 0.45 to 0.40 increases the electrical resistivity slightly when compared with the control mixture (PLC7-0.45), and provides the most benefit at early ages. The addition of either 20% Class F fly ash or 30% Class C fly ash has the same impact on electrical resistivity, and moderate chloride penetration can be expected. The incorporation of slag increases resistivity significantly at early and later ages. As already mentioned, the most beneficial results came from the ternary blend of 25% class C fly ash and 5% silica fume. If the slag mixture or the ternary blend were subjected to ASTM C1202, a charge passed of 1,000 to 2,000 coulombs would be expected; thus, a classification of low chloride penetrability is possible with high limestone content cements. These results are in agreement with what other researchers have reported in the past (Thomas et al., 2010).

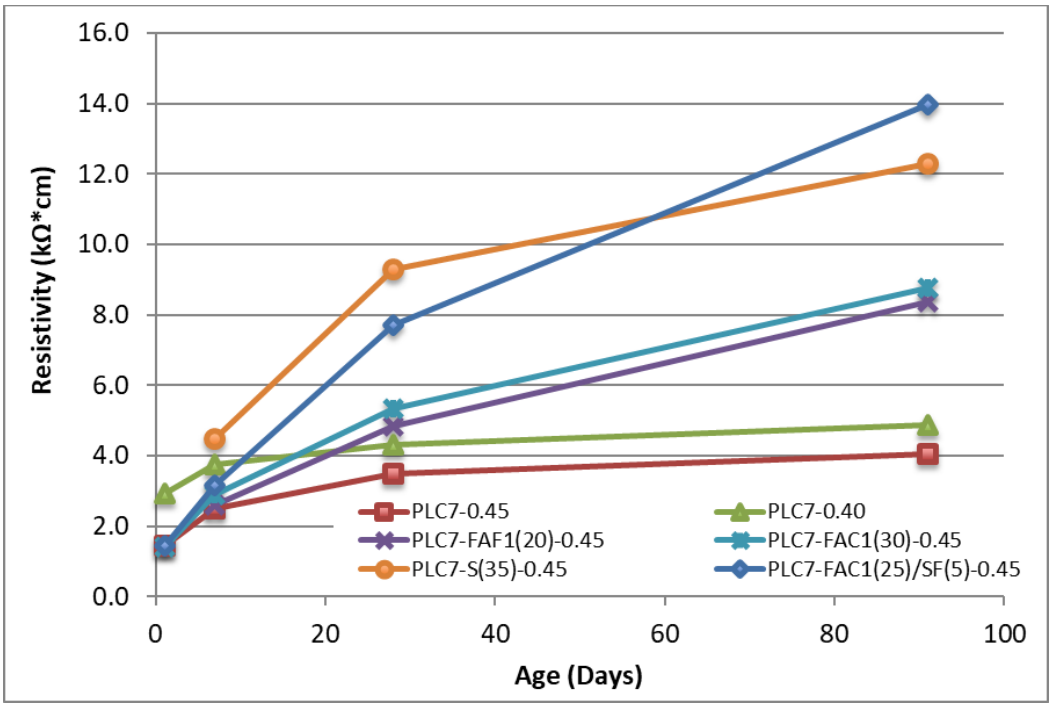

Figure 5.32: Electrical Resistivity vs. Age for PLC7 Combined with Different SCMs at w/cm = 0.45

5.7. Conclusions and Future Work

The main goal of the investigations presented in this chapter was to evaluate how the mechanical properties and the electrical resistivity development are affected by using PLCs with significant limestone contents. The effects of supplementary cementitious materials in combination with the high limestone contents and water-to-cementitious materials ratio were also evaluated.

The following conclusions can be made from the results presented in section 5.6,

- Similar compressive strengths to OPC concrete can be achieved with up to 15% limestone, provided that the portland limestone cements are finely ground to overcome the cement dilution effect.
- The effective w/cm is a better indicator of the compressive strength of PLC concrete than the actual w/cm.
- Equivalent strength is possible for the high limestone contents if the actual w/cm is lowered to match the effective w/cm.
- The effect of the addition of supplementary cementitious materials to high limestone content PLCs on compressive strength was not clear and needs to be investigated further.
- Cements with high limestone contents result in increased tensile strength.

- The addition of SCMs appears to have a beneficial effect on PLC concrete, even at high limestone contents.
- The modulus of elasticity of PLC concrete decreases as the limestone content increases.
- The equation currently used in the structural concrete building code to predict elastic modulus based on compressive strength is accurate and conservative even at low clinker and gypsum contents of less than 50%.
- The addition of limestone decreases the electrical resistivity of a concrete mixture, meaning that a higher permeability should be expected of PLC concrete.
- Good quality, low permeability concrete can be produced with high limestone content PLCs with the help of supplementary cementitious materials. The beneficial effect of SCM additions on the electrical resistivity is easily able to overcome the detrimental effect of limestone on electrical resistivity.

Chapter 6. Drying Shrinkage of Portland Limestone Cement Concrete Systems

6.1. Introduction

Drying shrinkage is a very important design consideration for concrete structures and pavements. This chapter provides background information on drying shrinkage of OPC concrete systems, the mechanism behind it, and presents some of the research-to-date on the drying shrinkage of PLC concrete systems.

Seven cements with varying limestone contents up to approximately 30% limestone were tested following ASTM C157 to determine the role that increasing limestone content in the cement plays in the drying shrinkage of the concrete. Different combinations of cements and supplementary cementitious materials (SCMs) were also tested to determine if there is any interaction between the PLCs and SCMs that affects the drying shrinkage of the concrete system. Finally, existing models that are currently used to predict the amount of drying shrinkage in a concrete system are tested to determine if the existing models can be applied to PLC concrete systems.

6.2. Review of Drying Shrinkage

Drying shrinkage occurs when hardened concrete loses moisture to the surrounding environment, which will result in a strain that must be accounted for in structural design (Mehta and Monteiro, 2006).

6.2.1. Mechanism of Drying Shrinkage

Drying shrinkage generally occurs when water is lost from the capillary pores that are smaller than 50 nm (Mehta and Monteiro, 2006). As water is lost from the small capillary pores, menisci form due to surface tension, and the walls of the pores are pulled inward, resulting in shrinkage (Mindess et al., 2003).

6.2.2. Drying Shrinkage in OPC

There are several factors that affect drying shrinkage of concrete including: volume fraction of the hydrated cement paste, the elastic modulus of the aggregate, and the relative humidity of the environment. For typical concrete, the typical drying shrinkage values are in the range of 400 to 1000 microstrain. Since the volume instability occurs in the hydrated cement paste, minimizing the cement paste volume will result in lower drying shrinkage values (closer to 400 microstrain).

According to Mindess et al. (2003) and Mehta & Monteiro (2006), the following methods can be used to minimize the amount of drying shrinkage:

- Minimizing the paste volume
- Use of aggregate with higher elastic moduli
- Use of shrinkage reducing admixtures (SRAs)
- Use of shrinkage-compensating cement
- Lowering the water content of the concrete mixture
- Use of steel fibers

6.2.3. Drying Shrinkage in PLC—Research to Date

Adams and Race (1990) measured shrinkage on mortar samples with limestone additions of up to 5% and reported a small increase in drying shrinkage when limestone was added. Bucher et al. (2008) reported the opposite trend in mortar specimens, as they reported lower drying shrinkage values with 5% and 10% limestone contents in the cement. Alunno-Rosetti and Curcio (1997) measured the drying shrinkage of PLC concrete with up to 20% limestone at 900 days (approximately 30 months) and found that the drying shrinkage was about the same as that of concrete with 0% limestone. Dhir et al. (2007) measured the drying shrinkage at 90 days of concrete made with up to 45% limestone content in the cement and reported decreased drying shrinkage values as the limestone was increased. Figure 6.1 shows the drying shrinkage reported by Dhir et al. (2007), plotted as a function of the limestone content in the cement. Please note that the limestone content of the control cement was not reported, but it is estimated to be around 2%, based on the reported loss-on-ignition (LOI) value of 0.90.

Hooton et al. (2010) also reported lower drying shrinkage values for concrete made with cement containing 10 and 15% limestone after a drying period of one year, when compared to the control. In the same study, the use of slag was also reported to decrease drying shrinkage.

In a comprehensive drying shrinkage study by Kwan et al. (2013), the research team reported a decrease in drying shrinkage as an increasing percent of OPC was replaced with limestone filler, for a wide range of water-to-cementitious materials ratios. Kwan et al. attributed the decrease in drying shrinkage to the decrease in cement content leading to a smaller volume of hydrated cement paste, which is the component of concrete that contributes the most to shrinkage.

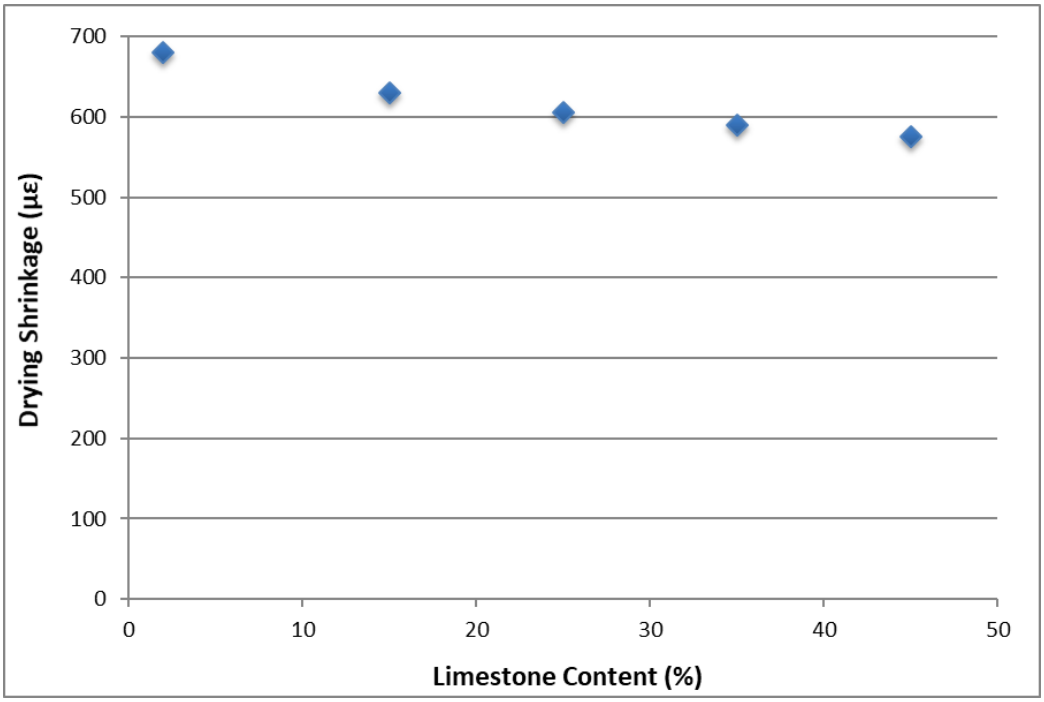

Figure 6.1: Drying Shrinkage vs. Limestone Content of Cement at w/cm = 0.60 after 90 Days (adapted from Dhir et al., 2007)

6.3. Materials

Concrete specimens were cast using a water-to-cementitious materials ratio of 0.45. The cementitious materials include cements and supplementary cementitious materials (SCMs).

6.3.1. Cements

Cements PLC1 through PLC7, which have varying limestone contents, were used for this experimental investigation. For more information on the chemical composition and phase composition of all cements, please refer to section 2.1.

6.3.2. Supplementary Cementitious Materials

For this experimental investigation, the following supplementary cementitious materials were used: Class F fly ash 1, Class C fly ash 1, Class C fly ash 2, Grade 100 slag, and densified silica fume. Please refer to section 2.3 for information on the chemical composition of each SCM.

6.3.3. Aggregates

Manufactured limestone sand and crushed limestone rock were used as fine aggregate and coarse aggregate, respectively, for the concrete mixtures described in this chapter. Please refer to section 2.4 for more information on both aggregates.

6.3.4. Water

Potable tap water was used to mix concrete specimens for this study.

6.4. Mixture Proportions

6.4.1. Nomenclature

The nomenclature system discussed in section 2.6 is used in this chapter. The graphical representation of the nomenclature system provided in Figure 2.6 is provided again for reference in Figure 6.2. Since all of the mixtures in this study were cast at a constant w/cm of 0.45, the last part of the nomenclature system (-0.45) has been dropped for the figures in this chapter in an attempt to make the labels bigger and easier to read.

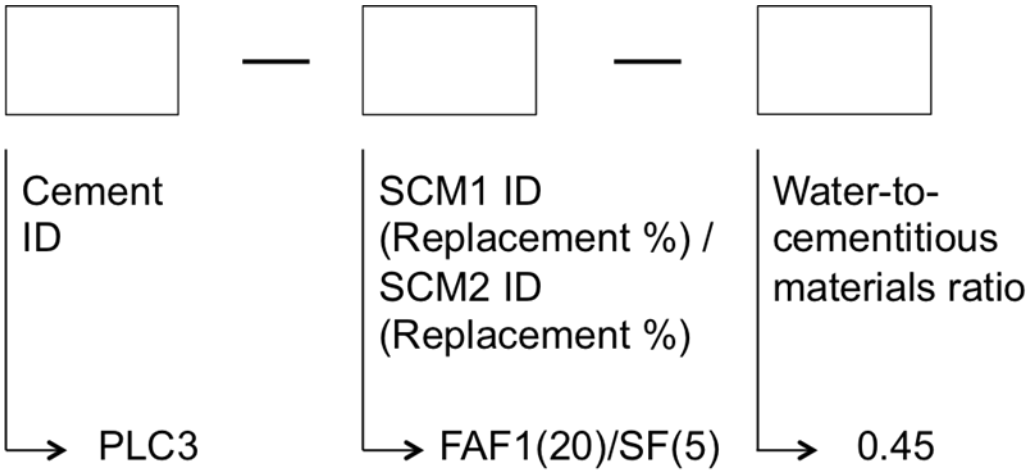

Figure 6.2: Graphical Representation of Nomenclature System

6.4.2. Test Matrix

Twenty different concrete mixtures were tested. As shown in Table 6.1, the mixtures include straight cement mixtures and different combinations of cements and SCMs, including ternary blends of PLC, class C fly ash, and densified silica fume. For all mixtures, the coarse aggregate fraction was 1048 kg/m^3 (1766 lb/yd^3), the fine aggregate fraction was 670 kg/m^3 (1129 lb/yd^3), the water content was 163 kg/m^3 (275 lb/yd^3), and the water-to-cementitious materials ratio was a constant 0.45.

Table 6.1: Mixture Proportions—Mass in kg/m³ (Note 1 kg/m³ = 1.69 lb/yd³)

MIXTURE ID	Cement	FAF1	FAC1	FAC2	S	SF
PLC1-0.45	362.5	--	--	--	--	--
PLC2-0.45	362.5	--	--	--	--	--
PLC3-0.45	362.5	--	--	--	--	--
PLC4-0.45	362.5	--	--	--	--	--
PLC5-0.45	362.5	--	--	--	--	--
PLC6-0.45	362.5	--	--	--	--	--
PLC7-0.45	362.5	--	--	--	--	--
PLC3-FAF1(20)-0.45	290.1	72.4	--	--	--	--
PLC3-FAC1(20)-0.45	290.1	--	72.4	--	--	--
PLC3-FAC1(40)-0.45	217.7	--	144.8	--	--	--
PLC3-S(35)-0.45	235.5	--	--	--	127.0	--
PLC3-FAC1(20)/SF(5)-0.45	271.7	--	72.4		--	18.4
PLC3-FAC2(20)-0.45	290.1	--	--	72.4	--	--
PLC3-FAC2(40)-0.45	217.7	--	--	144.8	--	--
PLC3-FAC2(20)/SF(5)-0.45	271.7	--	--	72.4	--	18.4
PLC4-FAF1(20)-0.45	290.1	72.4	--	--	--	--
PLC7-FAF1(20)-0.45	290.1	72.4	--	--	--	--
PLC7-FAC2(20)-0.45	290.1	--	--	72.4	--	--
PLC7-S(35)-0.45	235.5	--	--	--	127.0	--
PLC7-FAC2(20)/SF(5)-0.45	271.7	--	--	72.4	--	18.4

6.5. Experimental Procedures

6.5.1. ASTM C157

Three concrete prisms were cast for each mixture following the procedures described in ASTM C157. The prism dimensions are 75 x 75 x 285 mm (3 x 3 x 11.25 in.) with a stainless steel gauge stud embedded at each end of the prism to provide a 250 mm (10 in.) gauge length for length change measurements.

The prisms were de-molded after 23.5 hours and placed in saturated limewater solution until the prisms reached an age of 28 days. After 28 days of curing, the initial specimen length was measured and the prisms were stored in a drying room where the temperature was maintained at 23 +/- 2 ºC (73+/- 3 ºF). Subsequent readings were taken after 4, 7, 14, and 28 days, and after 8, 16, 26, 38, and 52 weeks of time stored in the drying room.

6.6. Results and Discussion

6.6.1. Straight Cement Mixtures

Plots of the drying shrinkage as a function of drying time for all of the straight cement mixtures are shown in Figures 6.3 and 6.4. All the mixtures followed the same general trends. The rate of water loss is much greater during the first 28 days, leading to most of the drying shrinkage occurring in this period. The prisms reach equilibrium, i.e. they stop shrinking (or exhibit very little shrinkage), after approximately 100 days of drying. Please note that the cements with higher limestone contents shrink faster at early ages, but the ultimate drying shrinkage value is approximately the same or less when compared to the control cements with relatively low limestone contents.

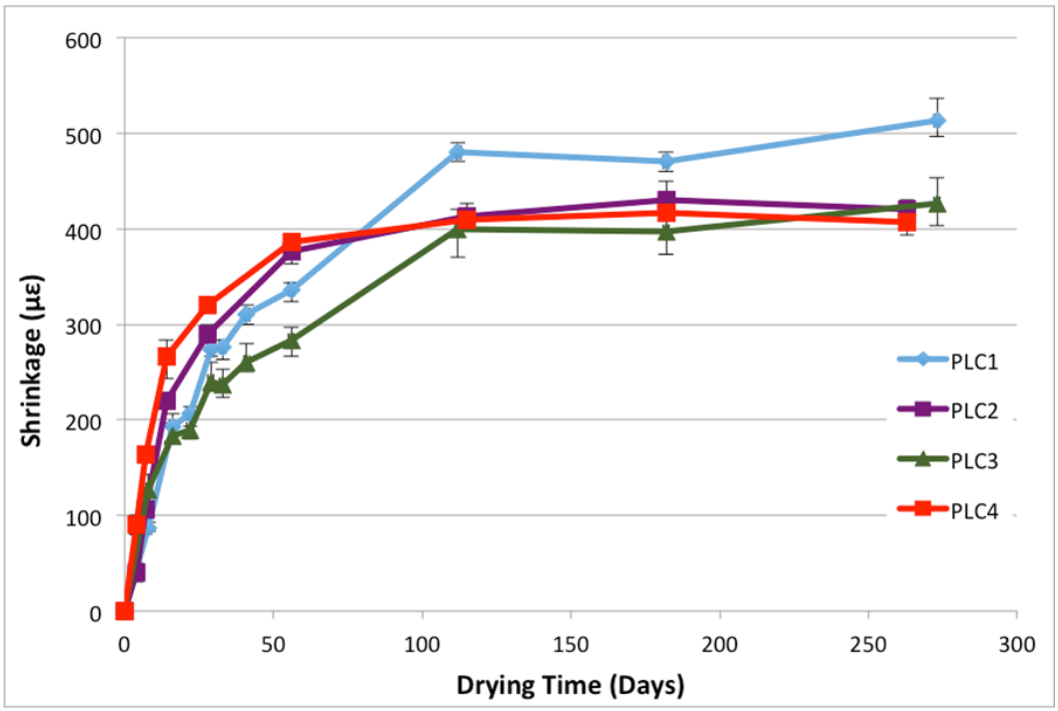

Figure 6.3: Shrinkage vs. Drying Time for Straight Cement Mixtures using Cements from Cement Plant 1

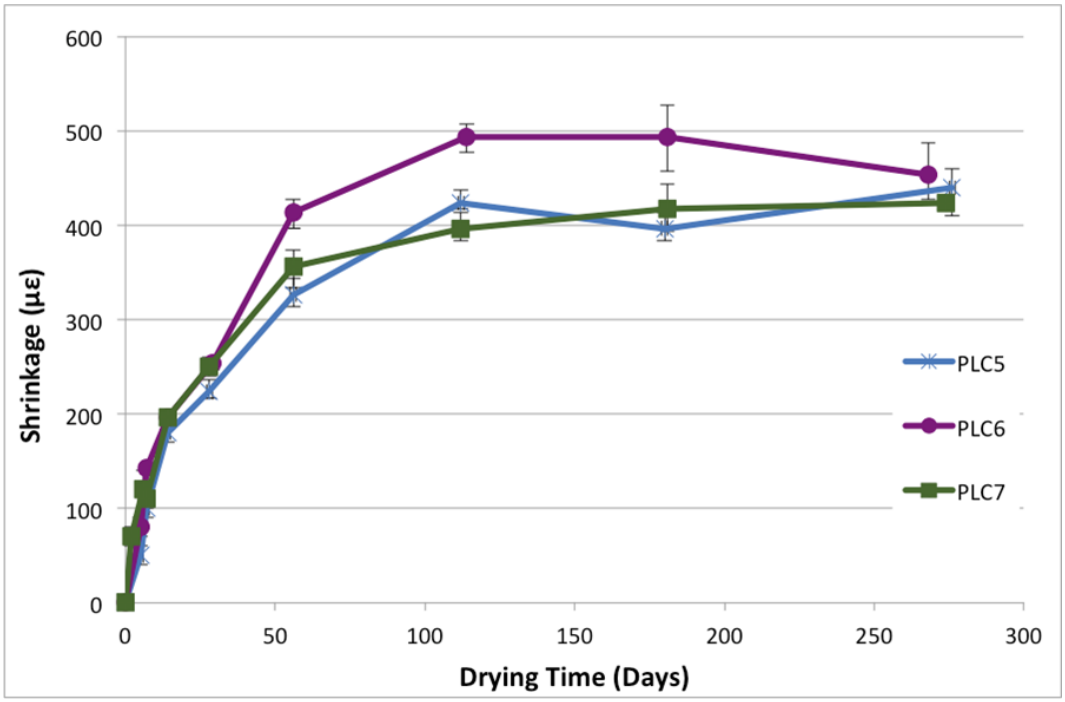

Figure 6.4: Shrinkage vs. Drying Time for Straight Cement Mixtures using Cements from Cement Plant 2

Figure 6.5 shows the drying shrinkage plotted as a function of limestone content for the straight cement mixtures investigated in this study. The data generated by Dhir et al. (2007) is also presented for reference. Dhir et al. used a higher water-to-cementitious materials ratio for their mixtures and thus, as expected, they reported higher shrinkage values compared to the mixtures in this study. However, please note that the same trend is observed for the mixtures in this study that came from Cement Plant 1: as the limestone content increases, the drying shrinkage value decreases slightly. It is expected that this trend would have still held if Cement Plant 2 had been able to produce a PLC with a higher limestone content.

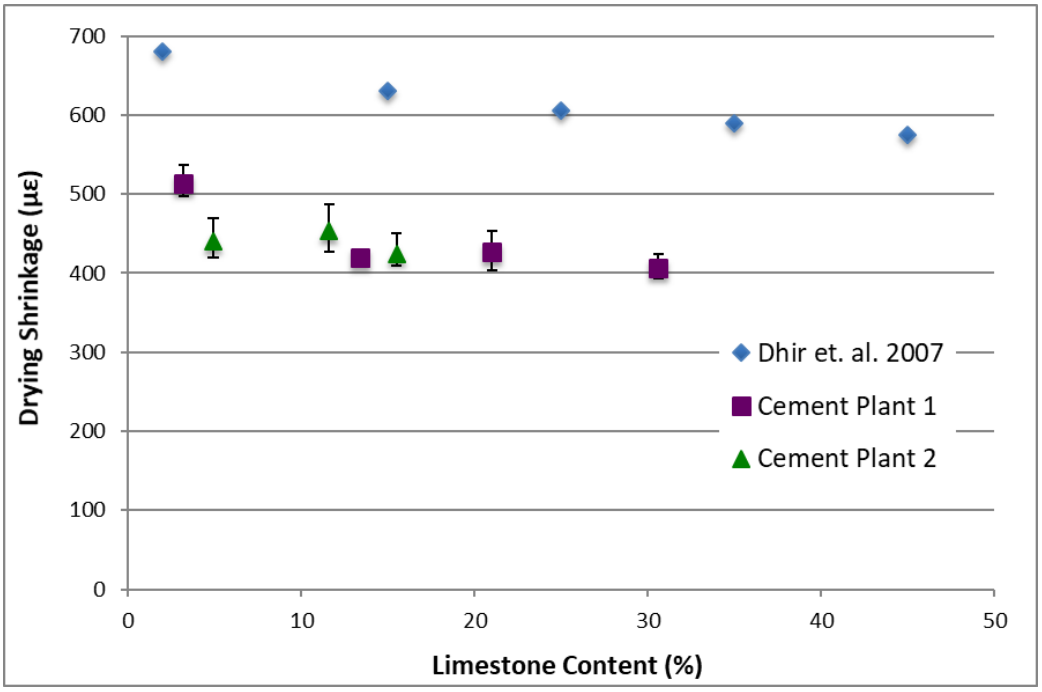

(Note: Dhir et al., 2007 shows drying shrinkage for w/cm = 0.6 at 90 days and Cement Plant 1 and Cement Plant 2 data show drying shrinkage for w/cm = 0.45 after 270 days of drying)

Figure 6.5: Drying Shrinkage vs. Limestone Content of Cement

Figure 6.6 shows the drying shrinkage after 270 days of drying plotted as function of effective water-to-cementitious materials ratio for the straight cement mixtures investigated in this study. The effective w/cm was calculated using Equation 6.1, which normalizes the w/cm by the limestone content of the cement.

$$\frac{w}{cm_{eff}} = \frac{w}{cm} * \frac{100 - LS_{control}}{100 - LS_{actual}} \qquad \text{(Eq. 6.1)}$$

where w/cm is the water-to-cementitious materials ratio of the cement that is being normalized, $LS_{control}$ is the limestone content of the control cement, and LS_{actual} is the limestone content of the cement being normalized. For example, to calculate the effective w/cm for the concrete mixture using PLC2, w/cm is equal to 0.45, $LS_{control}$ is 3.2 (the limestone content of PLC1, the control cement), LS_{actual} is 13.4 (the limestone content of PLC2), resulting in an effective w/cm of 0.50.

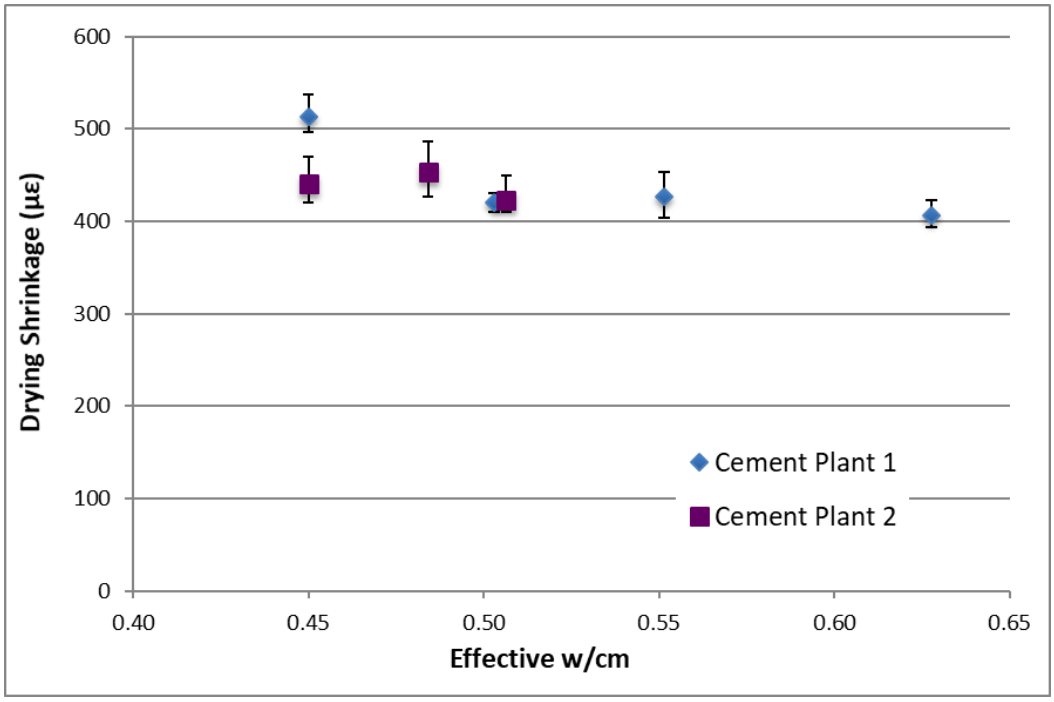

Figure 6.6: Drying Shrinkage After 270 Days of Drying vs. Effective Water-to-Cementitious Materials Ratio

Figure 6.7 compares the drying shrinkage of all straight cement mixtures after 270 days of drying time. Note that for the cements manufactured in Cement Plant 1, the drying shrinkage of the PLCs with higher limestone contents (PLC2, PLC3, and PLC4) is lower than that of OPC. However, for the cements made in Cement Plant 2, the drying shrinkage of the high limestone cements (PLC6 and PLC7) was about the same as that of the control (PLC5). Please note that all mixtures exhibit what would be considered fairly low drying shrinkage values. Since the w/cm used in this study was 0.45, the low drying shrinkage values are expected and they would likely meet the drying shrinkage requirements specified by state Department of Transportation (DOT) agencies for concrete pavements.

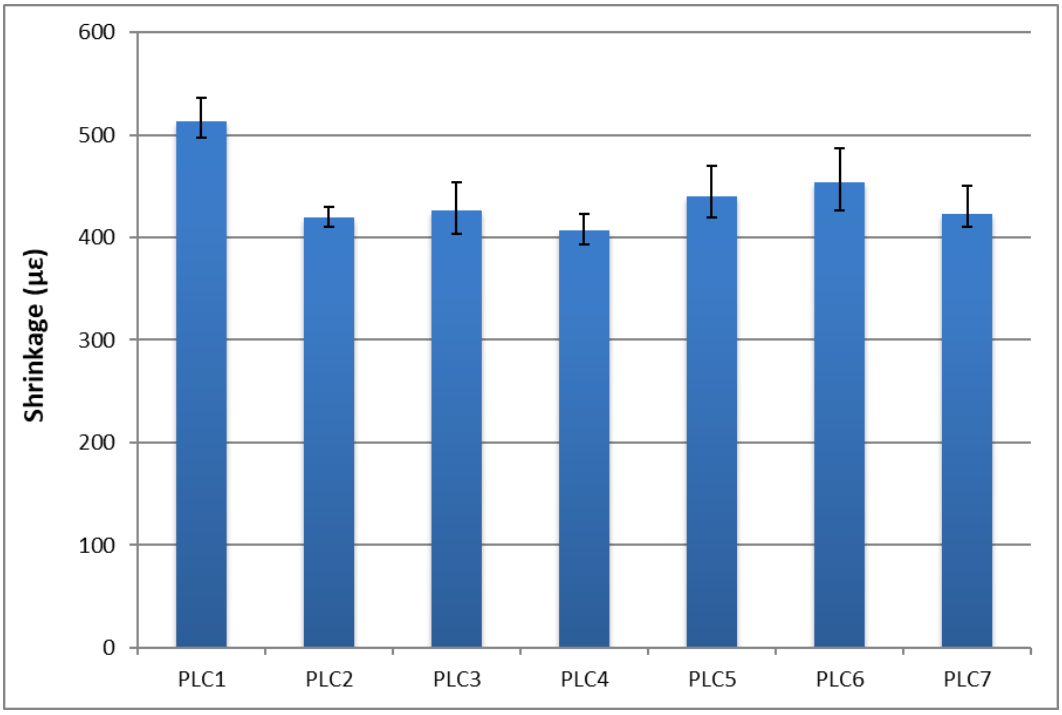

Figure 6.7: Drying Shrinkage at 270 Days for Straight Cement Mixtures (w/cm = 0.45)

6.6.2. Effect of SCMs on Drying Shrinkage

In order to assess the effect of combining PLCs and SCMs on drying shrinkage, several PLC and SCM combinations were tested. Ternary mixtures of high limestone PLCs, Class C fly ash, and silica fume were also added to the test matrix.

Figure 6.8 shows the drying shrinkage after 270 days of drying for different combinations of PLC3 with SCMs. The addition of SCMs into the system did not have a clear effect on drying shrinkage. Depending on the SCM, the drying shrinkage value decreased, remained about the same, or increased when compared to that of the straight PLC3 mixture. The ternary mixtures were also inconclusive, as one of them slightly reduced the drying shrinkage and the other one increased it marginally.

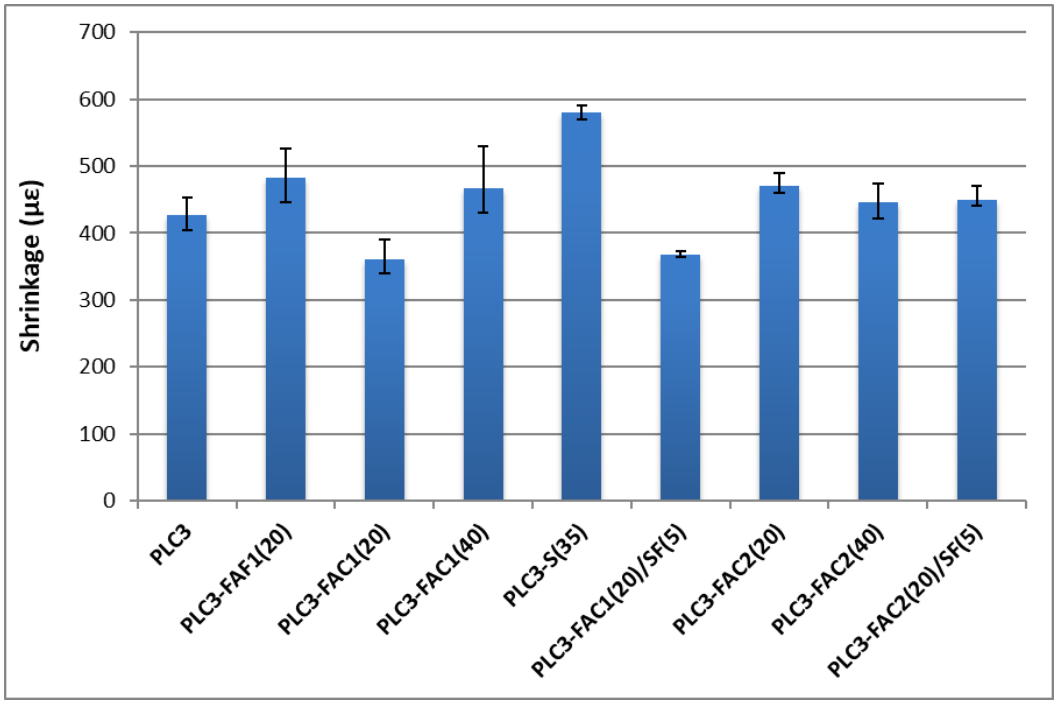

Figure 6.8: Drying Shrinkage at 270 Days for Different Combinations of PLC3 with SCMs (w/cm = 0.45)

Figure 6.9 shows the drying shrinkage after 270 days of drying for different combinations of PLC7 with SCMs. In this case, the addition of SCMs to the system caused the drying shrinkage values to either remain about the same or increase slightly.

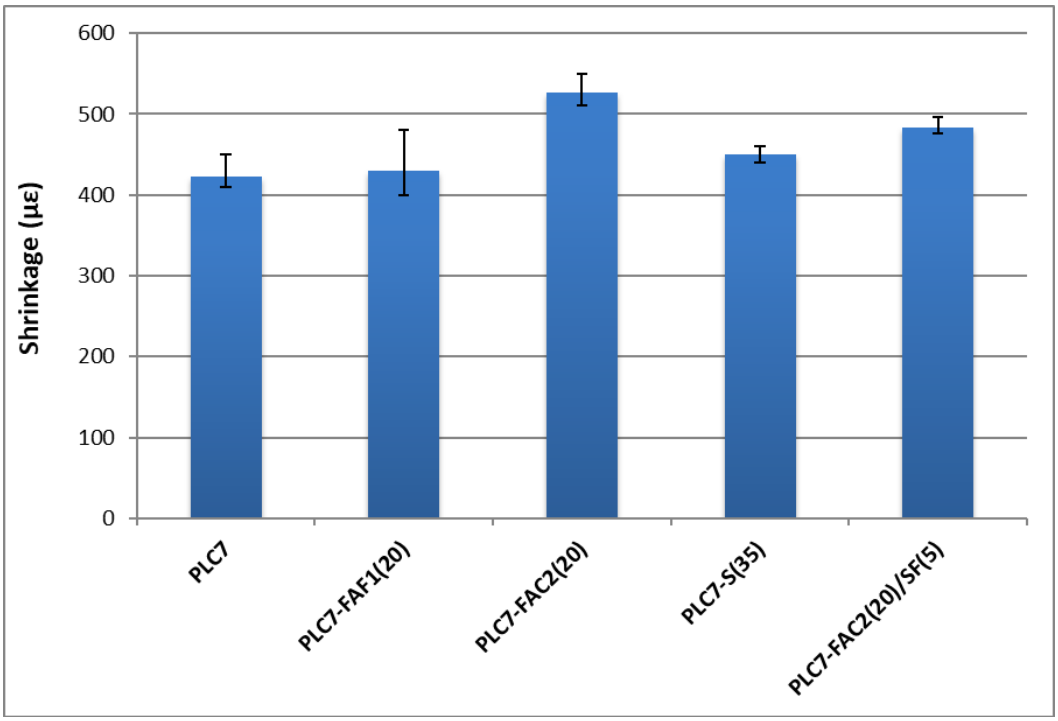

Figure 6.9: Drying Shrinkage at 270 Days for Different Combinations of PLC7 with SCMs (w/cm = 0.45)

Figure 6.10 shows the drying shrinkage after 270 days of drying for different combinations of PLCs with 20% class F fly ash. Again, the addition of class F fly ash to the system does not help to reduce the drying shrinkage when compared to the mixture using the same cement but without any fly ash.

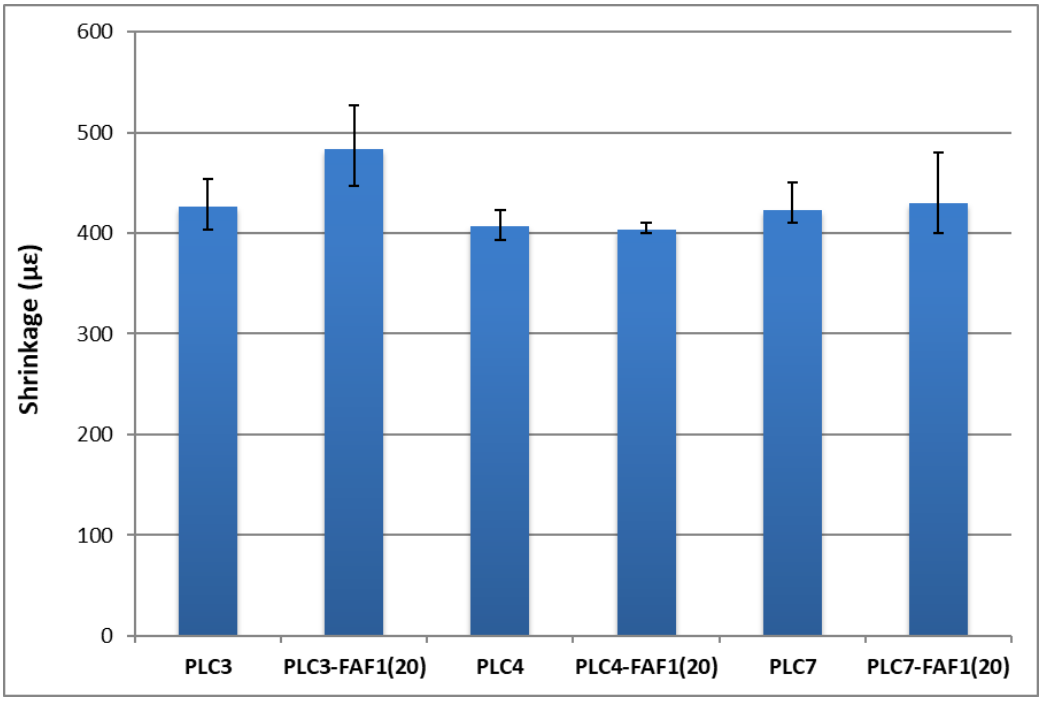

Figure 6.10: Drying Shrinkage at 270 Days for Different Combinations of PLCs with 20% Class F Fly Ash (w/cm = 0.45)

6.6.3. Comparison to Drying Shrinkage Model

Several shrinkage models were tested using experimental data generated by Pesek et al. (2017) and they determined that the B3 model proposed by Bazant & Baweja (2000) was the best predictor of shrinkage. The B3 model is incorporated into the ConcreteWorks software package, which is used to assess cracking potential of different concrete mixtures due to shrinkage, thermal effects, and delayed ettringite formation. The experimental values of drying shrinkage obtained in this study are compared to the values predicted by the B3 model; Table 6.2 shows the values for the concrete mixtures made with the cements from Cement Plant 1. Table 6.3 shows the measured and predicted shrinkage values, and the percent error, for the mixtures made with the cements from Cement Plant 2.

Table 6.2: Measured Shrinkage, Predicted Shrinkage, and Percent Error for Cement Plant 1 Mixtures

MIX ID	Measured Shrinkage (με)	Predicted Shrinkage (με)	Percent Error (%)
PLC1	513	483	6.0
PLC2	420	477	-13.6
PLC3	427	498	-16.6
PLC4	407	499	-22.6
PLC3-FAF1(20)	483	511	-5.6
PLC3-FAC1(20)	360	497	-38.2
PLC3-FAC1(40)	467	487	-4.5
PLC3-S(35)	580	485	16.4
PLC3-FAC1(20)/SF(5)	367	490	-33.5
PLC4-FAF1(20)	403	509	-26.1

The B3 model provides a reasonable drying shrinkage prediction for the Type I cement concrete mixture (PLC1). However, the B3 model overestimates the amount of drying shrinkage in PLC concrete, and the magnitude of the over prediction increases as the limestone content in the cement increases. When SCMs are incorporated into the mixture, the model generally predicts much higher shrinkage values than were measured. The only exception was the mixture with slag, where the actual drying shrinkage was much higher than predicted.

Table 6.3: Measured Shrinkage, Predicted Shrinkage, and Percent Error for Cement Plant 2 Mixtures

MIX ID	Measured Shrinkage (με)	Predicted Shrinkage (με)	Percent Error (%)
PLC5	440	449	-2.0
PLC6	453	454	-0.1
PLC7	423	452	-6.9
PLC7-FAF1(20)	430	466	-8.5
PLC7-FAC2(20)	527	449	14.7
PLC7-S(35)	450	447	0.6
PLC7-FAC2(20)/SF(5)	483	454	6.0

The B3 model predicted very accurately the drying shrinkage of the straight cement mixtures, even as the limestone content increased. It is important to note that cements PLC5 through PLC7 have a low C_3A content, and thus, these cements are designated as Type I/II cements. The B3 model

recognizes that Type II cements generally experience less drying shrinkage, and there is a cement type factor that was used when calculating the expected shrinkage values. When supplementary cementitious materials are incorporated into the mixture, that model is still fairly accurate.

If a more in-depth study is conducted in the future, a PLC cement (clinker) factor could be obtained and incorporated into the B3 model to better predict the drying shrinkage of PLCs with high limestone contents. This factor could be modified further to account for the combination of different SCMs with high limestone content PLCs.

6.7. Conclusions and Future Work

The main purpose of the investigation presented in this chapter was to evaluate the drying shrinkage that can be expected of PLC concrete and to compare it to OPC. A secondary purpose of this study was to evaluate how accurately the B3 model presented by Bazant and Baweja would be able to predict the drying shrinkage of PLC concrete. Seven straight cement mixtures with a range of limestone contents between 3.2% and 30.6% were evaluated following ASTM C157. In addition, thirteen mixtures with a combination of high limestone PLCs and supplementary cementitious materials were also evaluated.

The following conclusions can be made after analyzing the test results presented in the earlier sections:

- As the limestone content in the cement increases, the drying shrinkage of the concrete specimens will generally decrease, everything else being equal.
- There is no clear trend when SCMs are added to the mixture.
- The B3 model generally overestimates the amount of drying shrinkage that can be expected of PLC concrete.
- The overestimation error generally increases as the limestone content in the cement increases and/or if SCMs are added to the mixture.

In the future, the mixtures presented in this study should be replicated at different water-to-cementitious materials ratios to evaluate the effect of the limestone as the amount of water in the mixture changes. The following water-to-cementitious materials ratios are recommended: 0.35, 0.40, 0.50, and 0.60. The generation of this data would also be helpful in obtaining a PLC cement factor that could be incorporated into the B3 model, allowing for better drying shrinkage predictions of PLC concrete.

Chapter 7. Corrosion and Chloride Diffusion of Portland Limestone Cement Concrete Systems

7.1. Introduction

This chapter presents the findings from a study on the resistance to chloride ion penetration of portland limestone cement concrete systems and the impact on corrosion of reinforcing steel. Five cements with limestone contents of 3.2%, 4.9%, 15.5%, 21.0%, and 30.6%, in combination with different supplementary cementitious materials, were used to fabricate eleven different concrete specimens at a constant water-to-cementitious materials ratio of 0.45. The specimens were placed in a marine environment and the rate of corrosion was monitored periodically using half-cell potential measurements.

In addition to casting specimens for exposure in a marine environment, a concrete cylinder was cast for each mixture to obtain the chloride diffusion coefficient following the procedure outlined in ASTM C1556.

7.2. Review of Corrosion and Chloride Diffusion

7.2.1. Corrosion of OPC

Corrosion of steel reinforcement is the major concrete durability problem and the only mechanism that affects the steel and not the concrete itself. Corrosion is an electrochemical process that forms rust and leads to concrete cracking and spalling (Mindess et al., 2003). The formation of rust can occupy as much as six times the original volume of the original reinforcement (Mehta and Monteiro, 2006).

There are four basic requirements for corrosion:

- Galvanic couple: Anodic & cathodic areas that have different galvanic potential
- Electrical connectivity between anode and cathode
- Water to drive the cathodic reaction
- Oxygen to drive the cathodic reaction

The anodic reaction occurs at the anode, and the cathodic reaction occurs at the cathode. The anodic and cathodic reactions are shown in Equations 7.1 and 7.2, respectively (Mindess et al., 2003).

$$Fe \rightleftarrows 2e^{-} + Fe^{2+} \qquad \text{(Eq. 7.1)}$$

$$^1/_2\, O_2 + H_2O + 2e^- \rightleftarrows\ 2OH^-$$ (Eq. 7.2)

Although the four basic corrosion requirements are typically present in concrete, reinforcing steel in concrete does not usually corrode because a passivation layer protects it. The passivation layer is stable at high pH levels above 11.5 and it will keep protecting the reinforcement as long as the passivation layer is not destroyed (Mindess et al., 2003).

There are two mechanisms that can lead to the destruction of the passivation layer. The first mechanism is concrete carbonation, a natural process that lowers the pH of concrete from above 13 to about 8. Carbonation is discussed in detail in Chapter 8 of this Final Report. The second mechanism is the penetration of chloride ions into the concrete that can break down the passivation layer, even at high pH levels (Mindess et al., 2003).

Corrosion will not occur if any of the four basic requirements are missing, or if the concrete is protected from carbonation and chloride penetration. Thus, according to Mindess et al. (2003), corrosion mitigation strategies can be divided into the following categories:

- Reduction of the permeability of concrete: Lower permeability leads to reduced carbonation rate, lower chloride diffusion, and less water and oxygen available to drive the cathodic reaction
- Protective membranes on the concrete: Same approach as reducing concrete permeability
- Protective coatings on the steel: Epoxy coatings have been used in the past to try to protect the steel reinforcement. The effectiveness of epoxy-coated steel reinforcement is an issue that is hotly debated and some state departments of transportation have banned the use of epoxy-coated reinforcement since research has shown that epoxy coatings can actually speed up the onset of corrosion and the corrosion rate
- Suppression of the electrochemical reaction: This strategy includes the use of cathodic protection and/or corrosion inhibitors.

7.2.2. Chloride Diffusion of OPC

As mentioned in the previous section, if enough chloride ions reach the depth of the steel reinforcement, the passivation layer will be destroyed corrosion may initiate, provided that there is enough water and oxygen to drive the cathodic reaction. The minimum chloride concentration to initiate corrosion is called the critical chloride concentration or the chloride threshold. There is no general consensus among researchers regarding the exact value of the critical chloride concentration, but it is typically cited to be in the range of 0.6 to 1.2 kilograms (1.0 to 2.0 pounds) of chloride per cubic meter (cubic yard) of concrete (Mindess et al., 2003), which translates to approximately 0.026% to 0.051% of chlorides by mass of concrete, assuming a concrete density

of 2350 kg/m^3 (147 lb/ft^3). In this chapter, the critical chloride concentration is assumed to be 0.07% by mass of concrete, which is the same assumption made in the service-life modeling software package ConcreteWorks.

When concrete is exposed to a source of chlorides, such as seawater, the chloride ions will penetrate the concrete following Fick's second law of diffusion, which is shown in Equation 7.3.

$$\frac{\partial C}{\partial t} = D_a \frac{\partial^2 C}{\partial x^2} \quad \text{(Eq. 7.3)}$$

where C is the concentration, t is the time, D_a is the diffusion coefficient, and x is equal to the depth.

The diffusion coefficient can be found by solving the partial differential equation, and the solution is shown in Equation 7.4 (ASTM C1556, 2016),

$$C(x,t) = C_s - (C_s - C_i) * \text{erf}\left(\frac{x}{\sqrt{4 * D_a * t}}\right) \quad \text{(Eq. 7.4)}$$

where C is equal to the chloride concentration at depth x and exposure time t, C_s is equal to the projected chloride concentration at the surface of the specimen determined by a nonlinear regression analysis, C_i is the initial chloride-ion concentration, and erf is the error function.

Although the incorporation of fly ash into a concrete mixture lowers the critical chloride concentration, the reduction in permeability provided by fly ash overcomes the lower critical chloride concentration and thus reduces the risk of corrosion (Thomas, 1996). The addition of slag also reduces the chloride diffusion coefficient and provides better protection for the steel reinforcement in a marine environment (Hooton et al., 2010).

Measuring the diffusion coefficient of a given concrete mixture is possible by following the requirements established in ASTM C1556, but the process can be time-consuming, tedious, and expensive. Alternative methods that correlate very well with ASTM C1556 are available and are faster and more convenient. These methods include ASTM C1202, otherwise known as the rapid chloride permeability test, and electrical resistivity, which was discussed in section 3.5.4.

7.2.3. Corrosion Potential and Chloride Diffusion of PLC

A number of researchers have investigated the corrosion potential and resistance to chloride ion penetration of portland limestone cement concrete. Tsivilis et al. (2000) tested cements with 0%, 10%, 15%, 20%, and 35% limestone contents with a w/cm of 0.50 and measured the half-cell potential, which is a measure of the probability that active corrosion is occurring, of specimens exposed to 3% sodium chloride solution for nine months. They found that corrosion probability decreased as the limestone content increased, and these results were verified by measuring the

mass loss of the reinforcement bars with increasing time of exposure, where the higher limestone content mixtures were the best performers. In the same study, Tsivilis et al. also measured the charge passed using the rapid chloride permeability test (ASTM C1202) of concrete specimens cast using w/cm of 0.7 (0.62 for the mixture with 35% limestone) and found that that the charge passed did not change significantly as the limestone content increased, as can be seen in Table 7.1.

Irassar et al. (2001) found that the diffusion coefficient generally increased as the limestone content in the cement increased in their specimens, but that increasing the w/cm had a much larger effect than increasing the limestone content. Lollini et al. (2014) also reported the same trends obtained using the Rapid Chloride Migration Test on 28-day samples at different water-to-cementitious materials ratios for cements with 15% and 30% limestone. It is important to note that in both of the studies referenced, the compressive strengths of the PLC concretes were lower than the OPC concretes.

Ramezanianpour et al. (2009) reported lower values of electrical charge passed using RCPT for concretes containing between 10% and 15% limestone. Hooton et al. (2010) also performed RCPT and reported very similar values for concretes with made with up to 15% limestone; the same trend was observed when slag was incorporated into the mixtures. In the same study, Hooton's team also calculated the chloride diffusion coefficients using ASTM C1556, and showed that increasing the limestone content to 15% was not detrimental in terms of chloride penetration.

After reviewing a number of published studies, Tennis et al. (2011) proposed that that equivalent chloride resistance can be expected of PLC concrete with up to 15% limestone, provided that equivalent 28-day strength is achieved.

Table 7.1: RCPT Results of Concretes with Increasing Limestone Content (Adapted from Tsivilis et al., 2000)

Limestone Content of Cement (%)	w/cm	Charge Passed (Coulombs)
0	0.70	6100
10	0.70	5800
15	0.70	6000
20	0.70	6400
35	0.62	6600

7.3. Materials

Concrete specimens were cast using a water-to-cementitious materials ratio of 0.45. The cementitious materials include cements and supplementary cementitious materials (SCMs).

7.3.1. Cements

Cements PLC1 through PLC7, which have varying limestone contents, were used for this experimental investigation. For more information on the chemical composition and phase composition of all cements, please refer to section 2.1.

7.3.2. Supplementary Cementitious Materials

For this experimental investigation, the following supplementary cementitious materials were used: Class F fly ash 1, Class C fly ash 1, Grade 100 slag, and densified silica fume. Please refer to section 2.3 for information on the chemical composition of each SCM.

7.3.3. Aggregates

Manufactured limestone sand and crushed limestone rock were used as fine aggregate and coarse aggregate, respectively, for the concrete mixtures described in this chapter. Please refer to section 2.4 for more information on both aggregates.

7.3.4. Water

Potable tap water was used to mix concrete specimens for this study.

7.4. Mixture Proportions

7.4.1. Nomenclature

The nomenclature system discussed in section 2.6 is used in this chapter. The graphical representation of the nomenclature system provided in Figure 2.6 is provided again for convenience in Figure 7.1.

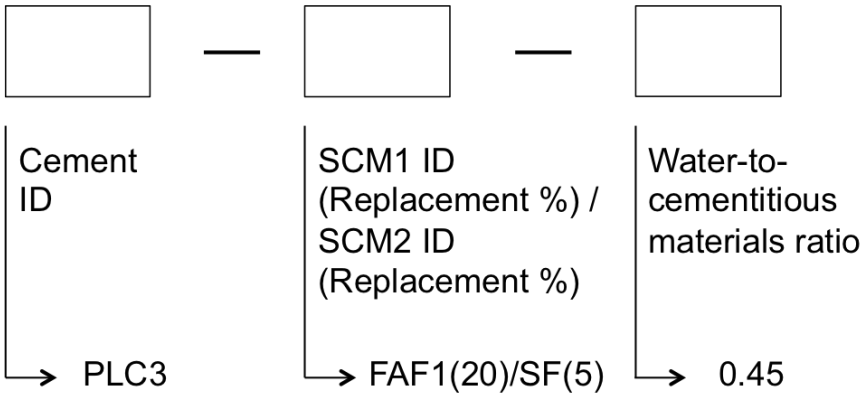

Figure 7.1: Graphical Representation of Nomenclature System

7.4.2. Test Matrix

Eleven different concrete mixtures were tested. As shown in Table 7.2, the mixtures include five straight cement mixtures and six different combinations of cements and SCMs, including one ternary blend of PLC, Class C fly ash 1, and densified silica fume. For all mixtures, the coarse aggregate fraction was 1048 kg/m^3 (1766 lb/yd^3), the fine aggregate fraction was 670 kg/m^3 (1129 lb/yd^3), the water content was 163 kg/m^3 (275 lb/yd^3), and the water-to-cementitious materials ratio was a constant 0.45.

Table 7.2: Mixture Proportions—Mass in kg/m^3 (Note 1 kg/m^3 = 1.69 lb/yd^3)

MIXTURE ID	Cement	FAF1	FAC1	FAC2	S	SF
PLC1-0.45	362.5	--	--	--	--	--
PLC3-0.45	362.5	--	--	--	--	--
PLC4-0.45	362.5	--	--	--	--	--
PLC5-0.45	362.5	--	--	--	--	--
PLC7-0.45	362.5	--	--	--	--	--
PLC3-FAF1(20)-0.45	290.1	72.4	--	--	--	--
PLC3-FAC1(20)-0.45	290.1	--	72.4	--	--	--
PLC3-FAC1(40)-0.45	217.7	--	144.8	--	--	--
PLC3-S(35)-0.45	235.5	--	--	--	127.0	--
PLC3-FAC1(20)/SF(5)-0.45	271.7	--	72.4		--	18.4
PLC4-FAF1(20)-0.45	290.1	72.4	--	--	--	--

7.5. Experimental Procedures

7.5.1. Marine Exposure Site

A marine exposure site was recently developed in Port Aransas, Texas located within the Marine Science Institute at UT Austin. Researchers affiliated with UT Austin are currently using the exposure site to investigate the marine environment effects on corrosion of steel reinforcement, alkali-silica reaction, and carbonation. The exposure site can be seen in Figure 7.2.

Figure 7.2: Carbonation and ASR Exposure Sites (left) and Corrosion Specimens Hanging from Seawall (right)

7.5.2. Corrosion Potential Evaluation

Two 305 x 140 x 1118 mm (12 x 5.5 x 44 in.) concrete blocks were cast for each mixture. One of the blocks is unreinforced and will be used in the future to calculate the chloride diffusion coefficients for all mixtures. The second block was reinforced with four #4 bars, which have a diameter of 12.7 mm (0.5 in.), having four different clear cover depths of 12.7, 25.4, 38.1, and 50.8 mm (0.5, 1, 1.5, and 2 in.). A schematic showing the cross-sectional view of the marine exposure blocks is shown in Figure 7.3. A stainless steel threaded rod, long enough to protrude from the concrete, was attached to each reinforcing bar to provide the electrical connection required for half-cell potential measurements (Figure 7.4).

All of the blocks were hung off the seawall, as seen in Figure 7.2, using a stainless steel hook cast within the concrete block and a chain that is fixed to the seawall. The blocks were wet-cured using saturated burlap and polyethylene sheeting for seven days, after which the burlap was removed and the blocks were then covered with polyethylene until an age of 28 days was reached.

The blocks were then taken to the marine exposure site, and initial half-cell potential measurements were taken before half of the block was immersed in the sea. The blocks were only partially submerged to simulate concrete exposure in the splash zone, which is known to have the highest corrosion rates due to the excess availability of moisture and oxygen to drive the cathodic reaction. The blocks were monitored as often as possible, when the research team was able to return to the exposure site.

The half-cell potential readings were taken using a copper/copper-sulfate reference electrode, and the procedure can be seen in Figure 7.5. It is important to note that, as explained in ASTM C876, half-cell potential readings only indicate the probability that active corrosion is occurring at the time of measurement, based on the magnitude of the reading; therefore, potential readings should only be used as a tool to determine if more investigation is warranted. The results of half-cell potential can be interpreted using Table 7.3. Usually, when half-cell potential readings indicate a high likelihood that corrosion is occurring, there will also be cracking following the reinforcement pattern and visible rust-staining, which is more evidence that corrosion is indeed taking place.

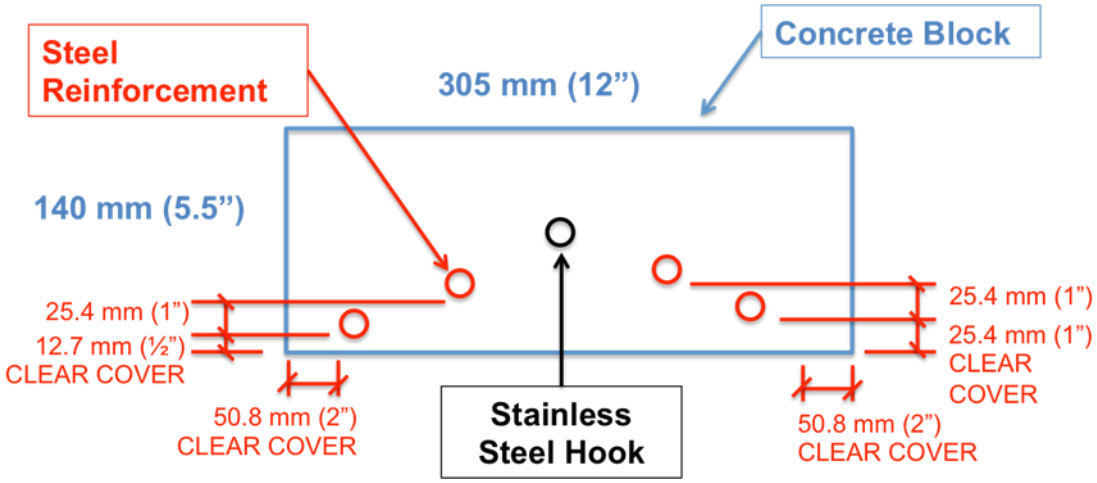

Figure 7.3: Cross-Sectional View of Reinforced Concrete Block used to Monitor Corrosion Potential

Figure 7.4: Cross-Sectional View of Actual Specimen after Being Pulled Out of Seawater

Figure 7.5: Half-Cell Potential Measurement Procedure

Table 7.3: Relationship Between Half-Cell Potential Measurements and Corrosion Probability (ASTM C876)

Half-Cell Potential Reading (mV)	Percentage Chance of Active Corrosion
< -350	90%
-350 to -200	50%
> -200	10%

The research team noticed that abrasion/erosion became an issue created by the wave action and the close proximity of the block to the seawall. The blocks with higher limestone contents appeared to be the most affected by abrasion/erosion, but no formal data can be reported, as abrasion was not considered for this study. Rubber tires were added in an attempt to protect the blocks from further damage, but most of the tires and even some of the blocks were lost after Hurricane Harvey devastated the area in August 2017.

7.5.3. Chloride Diffusion

In addition to casting the two concrete blocks for seawater exposure, a 100 x 200 mm (4 x 8 in.) concrete cylinder was cast for each mixture to obtain the chloride diffusion coefficient for each

mixture, following the procedure established in ASTM C1556. All cylinders were cured for 28 days before they were immersed in a sodium chloride solution (165 g of sodium chloride per liter of solution) for 91 days. The cylinders were coated with an epoxy so as to only allow chloride penetration from the finished surface. Once the cylinders were exposed to the sodium chloride solution for 91 days, the cylinders were rinsed with tap water and they were allowed to dry for 24 hours before each cylinder was ground in layers as shown in Table 7.4. A 3-gram powder sample was collected from each layer and combined with 20 mL of acetic acid digestion solution to extract the acid-soluble chloride ions from each sample. After allowing enough time for acid digestion, the sample was analyzed using a James Instruments CL-3000 chlorimeter with a chloride-ion specific electrode and the chloride concentration, as a percentage of concrete mass, was obtained.

Table 7.4: Layer Depths Used to Determine Chloride Diffusion Coefficient (Adapted from ASTM C1556, 2016)

Layer	Depth Intervals (mm)	Layer Mid-depth (mm)
1	0-1	0.5
2	1-3	2
3	3-5	4
4	5-7	6
5	7-9	8
6	9-12	10.5
7	12-15	13.5
8	15-18	16.5
9	18-22	20

7.6. Results and Discussion

7.6.1. Corrosion Potential

The half-cell potential measurements of the marine blocks made with the straight cement mixtures can be seen in Table 7.5. For the cements from Cement Plant 1 (PLC1, PLC3, and PLC4) the corrosion potential increases as the limestone content increases. The results are surprising, given the fact that the calculated chloride diffusion coefficient for PLC3-0.45, as presented in section 7.6.2, is almost the same as for PLC1-0.45, and for PLC4-0.45 the diffusion coefficient is actually 20% lower compared to PLC1-0.45. There are a few explanations that could explain the disconnect between the corrosion potential and the chloride diffusion coefficients. First, the calculated chloride coefficient is based on a cylinder that is not subjected to the same exposure conditions as the marine block. Second, the fact that the marine blocks are partially submerged, which is purposefully done in order to accelerate the corrosion process attributed to the splash zone effect, likely resulted in increased chloride diffusion that appears to affect the cements with higher limestone content the most. Finally, the wave action that led to abrasion of the concrete specimens before the protective tires were installed, led to premature deterioration and reduction of the

concrete cover. PLC concrete has been reported to be less resistant to abrasion (Dhir et al., 2007). Unfortunately, blocks PLC1-0.45 and PLC3-0.45 were lost after August 2017 due to Hurricane Harvey and future monitoring is probably not going to be possible.

For PLC5-0.45 and PLC7-0.45, it is difficult to make a definitive conclusion whether or not the increased limestone affected the corrosion potential due to the fact that the potential readings were taken after significantly different exposure periods. To further complicate things, PLC5-0.45 and PLC7-0.45 had the highest and lowest diffusion coefficients, respectively, as shown in section 7.6.2. Therefore, a direct comparison between the two mixtures is difficult at this time.

Table 7.5: Half-Cell Potential Measurements of Marine Blocks (Straight Cement Mixtures) (Note: 25.4 mm = 1 in.)

Mix:	PLC1-0.45				
Date	Exposure Time (Days)	Reading (mV) Cover			
		12.7 mm	25.4 mm	38.1 mm	50.8 mm
1/12/16	0	-21	-28	-52	-51
8/2/16	203	-311	-69	-74	-67
5/17/17	491	-510	-430	-370	-20
Lost due to Hurricane Harvey					
Mix:	**PLC3-0.45**				
Date	Exposure Time (Days)	Reading (mV) Cover			
		12.7 mm	25.4 mm	38.1 mm	50.8 mm
1/12/16	0	-28	-30	-50	-34
8/2/16	203	-301	-322	-192	-103
5/17/17	491	-480	-390	-420	-350
Lost due to Hurricane Harvey					
Mix:	**PLC4-0.45**				
Date	Exposure Time (Days)	Reading (mV) Cover			
		12.7 mm	25.4 mm	38.1 mm	50.8 mm
8/2/16	0	-158	-157	-158	-155
5/17/17	288	-550	-510	-550	-430
4/11/18	617	-588	-555	-522	-514
Mix:	**PLC5-0.45**				
Date	Exposure Time (Days)	Reading (mV) Cover			
		12.7 mm	25.4 mm	38.1 mm	50.8 mm
3/17/16	0	-82	-89	-102	-85
8/2/16	138	-311	14	-107	72
5/17/17	426	-470	-350	-340	20
4/11/18	755	-733	-422	-390	-356

Table continues on next page

Mix:	PLC7-0.45				
Date	Exposure Time (Days)	Reading (mV)			
		Cover			
		12.7 mm	25.4 mm	38.1 mm	50.8 mm
8/2/16	0	-118	-98	-164	-156
5/17/17	288	-510	-560	-350	-140
4/11/18	617	-567	-586	-520	-504

Table 7.6 shows the half-cell potential measurements of the marine blocks where SCMs were combined with PLC3 and PLC4. The addition of supplementary cementitious materials, as expected, proved to be beneficial in terms of reducing the corrosion potential at a given age. It can be observed that all four of the reinforcement bars for PLC3-0.45, even the one with a 50.8 mm clear cover, were likely probably corroding after 491 days of exposure. Every mixture with PLC3 in combination with supplementary cementitious materials limited the high likelihood of corrosion activity to the reinforcement bars with that had the least amount of clear cover depth. The best performer was the ternary blend that combined PLC3, 20% Class C fly ash 1, and 5% densified silica fume, followed by PLC3-FAC1(40)-0.45, and PLC3-S(35)-0.45.

Similarly, the addition of Class F fly ash considerably reduced the corrosion potential of PLC4-0.45, which performed very poorly, as there was evidence that even the reinforcement bar with 50.8 mm of clear cover was corroding after only 288 days (approximately 9.5 months). The addition of Class F fly ash at a 20% replacement level limited the high corrosion potential to the two bars with 12.7 mm and 25.4 mm of clear cover for the same exposure period. After 617 days of exposure (~21 months) the corrosion potential of the bar with 50.8 mm of clear cover was still low.

Table 7.6: Half-Cell Potential Measurements of Marine Blocks (Combination of PLCs with SCMs)
(Note: 25.4 mm = 1 in.)

Mix:	PLC3-FAF1(20)-0.45				
Date	Exposure Time (Days)	Reading (mV)			
		Cover			
		12.7 mm	25.4 mm	38.1 mm	50.8 mm
1/12/16	0	-13	-31	-47	-39
8/2/16	203	-363	-295	-51	-69
5/17/17	491	-470	-430	-260	-90
4/11/18	820	-566	-458	-404	36
Mix:	**PLC3-FAC1(20)-0.45**				
Date	Exposure Time (Days)	Reading (mV)			
		Cover			
		12.7 mm	25.4 mm	38.1 mm	50.8 mm
2/5/16	0	-59	-71	-79	-83
8/2/16	179	-360	-296	-75	-107
5/17/17	467	-680	-430	-180	-160
4/11/18	796	-577	-515	-250	3
Mix:	**PLC3-FAC1(40)-0.45**				
Date	Exposure Time (Days)	Reading (mV)			
		Cover			
		12.7 mm	25.4 mm	38.1 mm	50.8 mm
3/17/16	0	-14	-27	-41	-39
8/2/16	138	-458	-160	7	-117
5/17/17	426	-440	-250	140	100
4/11/18	755	-577	-314	-35	-67
Mix:	**PLC3-FAC1(20)/SF(5)-0.45**				
Date	Exposure Time (Days)	Reading (mV)			
		Cover			
		12.7 mm	25.4 mm	38.1 mm	50.8 mm
2/5/16	0	-46	-52	-50	-42
8/2/16	179	-363	-143	-102	-82
5/17/17	467	-510	-430	-50	-30
Lost due to Hurricane Harvey					

Mix:	PLC3-S(35)-0.45				
Date	Exposure Time (Days)	Reading (mV)			
		Cover			
		12.7 mm	25.4 mm	38.1 mm	50.8 mm
1/12/16	0	-37	-59	-220	-103
8/2/16	203	-354	-209	-192	-145
5/17/17	491	-500	-390	-170	-200
4/11/18	820	-625	-438	-273	-27
Mix:	**PLC4-FAF1(20)-0.45**				
Date	Exposure Time (Days)	Reading (mV)			
		Cover			
		12.7 mm	25.4 mm	38.1 mm	50.8 mm
8/2/16	0	-134	-145	-140	-145
5/17/17	288	-480	-430	-100	-40
4/11/18	617	-576	-584	-408	-98

7.6.2. Chloride Diffusion

The plots of chloride concentration as a function of depth, and the nonlinear regression line obtained by following ASTM C1556, for the straight cement mixtures are shown in Figures 7.6 through 7.16. The plots of chloride concentration vs. depth and nonlinear regression line for the different combinations of PLCs and SCMs are provided as well.

The nonlinear regression line, which is obtained in accordance with ASTM C1556 by minimizing the sum of squares error, is a function of the chloride concentration at the surface and the chloride diffusion coefficient for each mixture. The line is shown on each plot to provide a visual estimate of the error, and the equation for the line is shown in the top right corner of each plot.

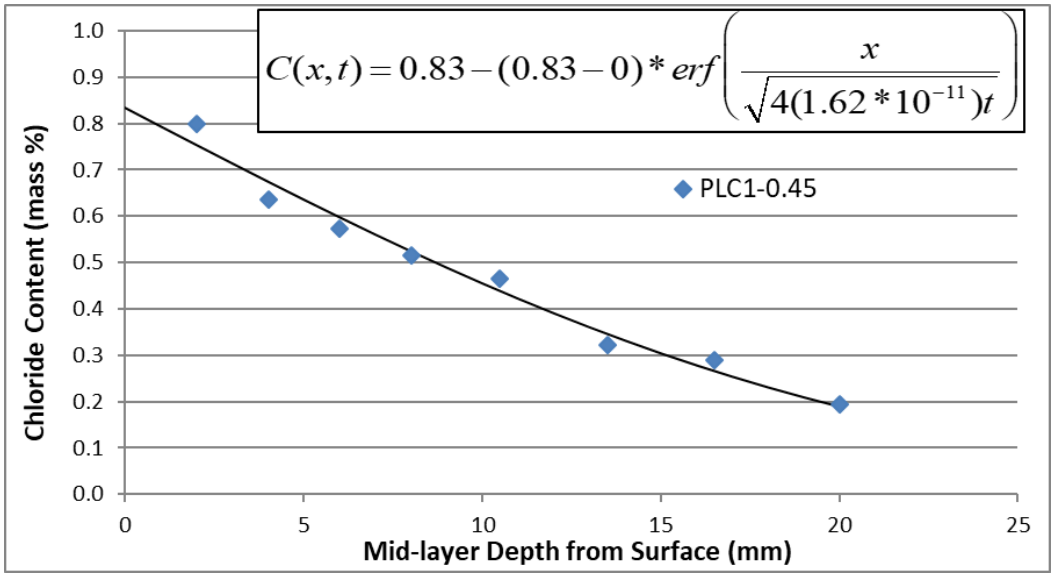

Figure 7.6: Chloride Content vs. Depth for PLC1-0.45 (Note 25.4 mm = 1 in.)

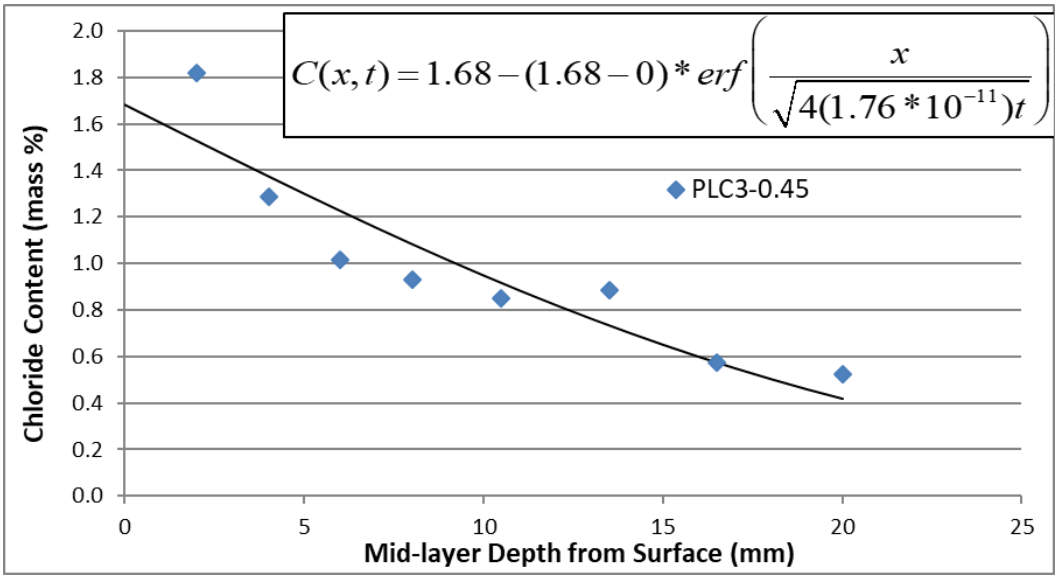

Figure 7.7: Chloride Content vs. Depth for PLC3-0.45 (Note 25.4 mm = 1 in.)

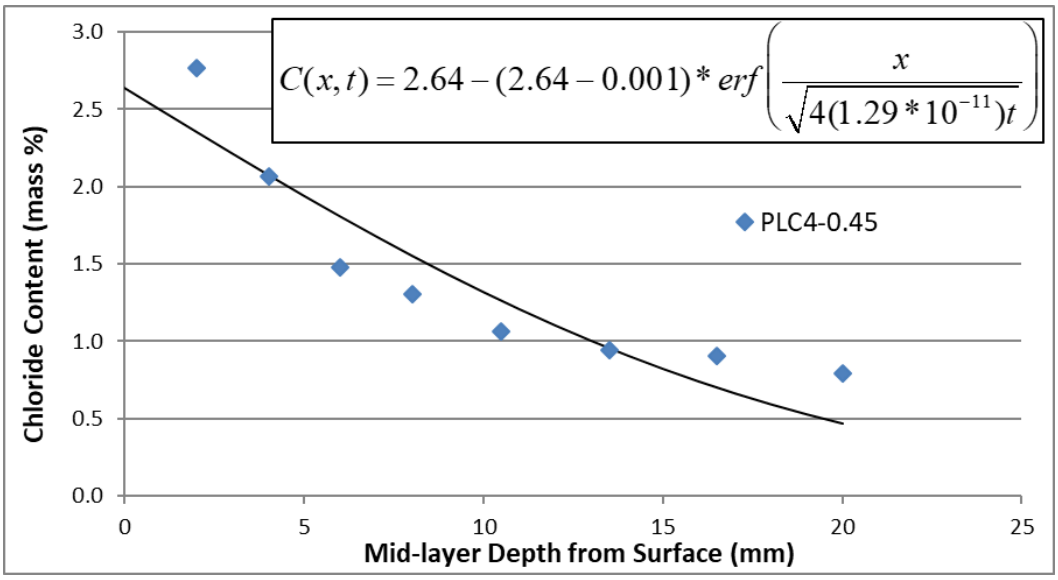

Figure 7.8: Chloride Content vs. Depth for PLC4-0.45 (Note 25.4 mm = 1 in.)

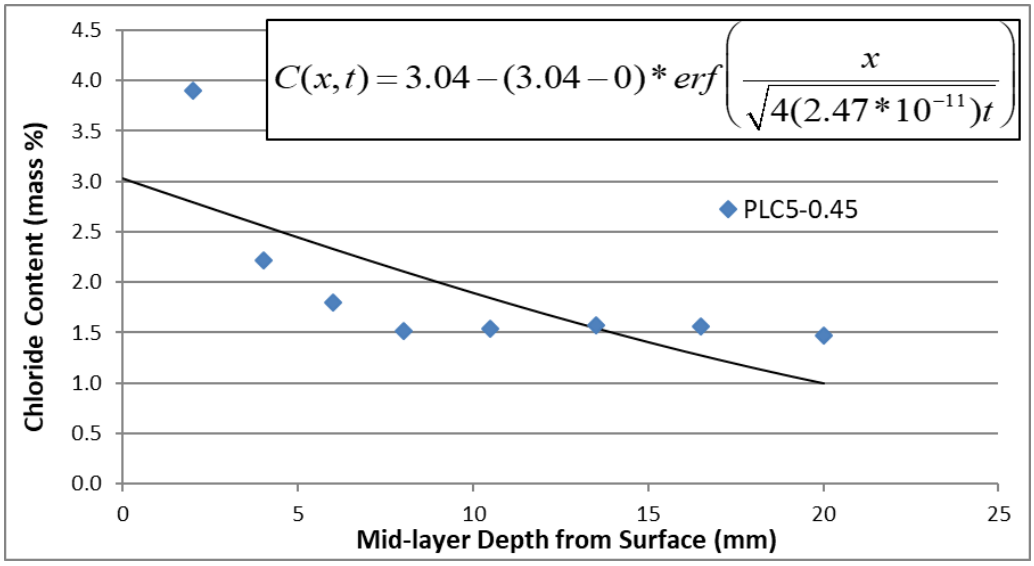

Figure 7.9: Chloride Content vs. Depth for PLC5-0.45 (Note 25.4 mm = 1 in.)

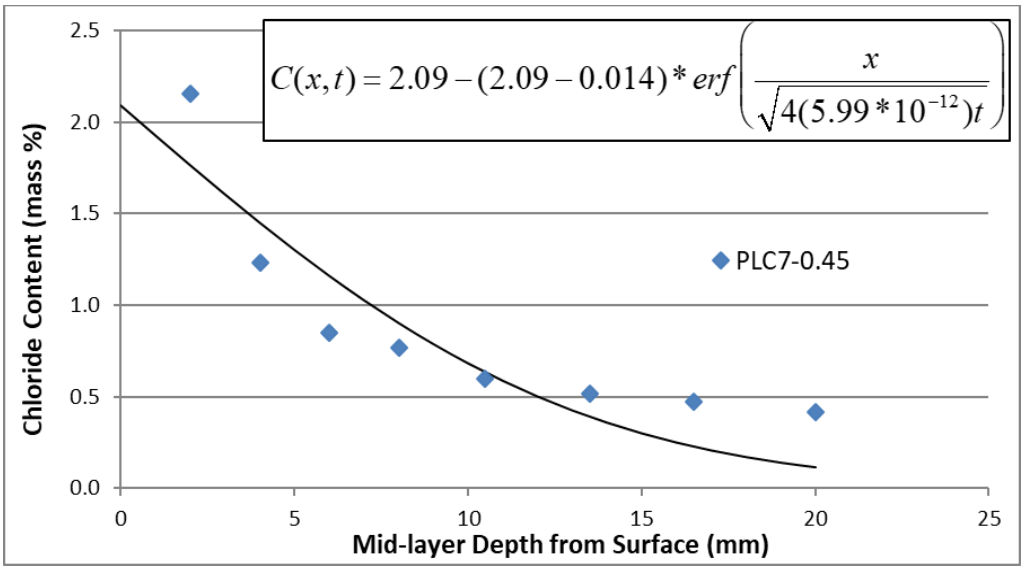

Figure 7.10: Chloride Content vs. Depth for PLC3-FAF1(20)-0.45 (Note 25.4 mm = 1 in.)

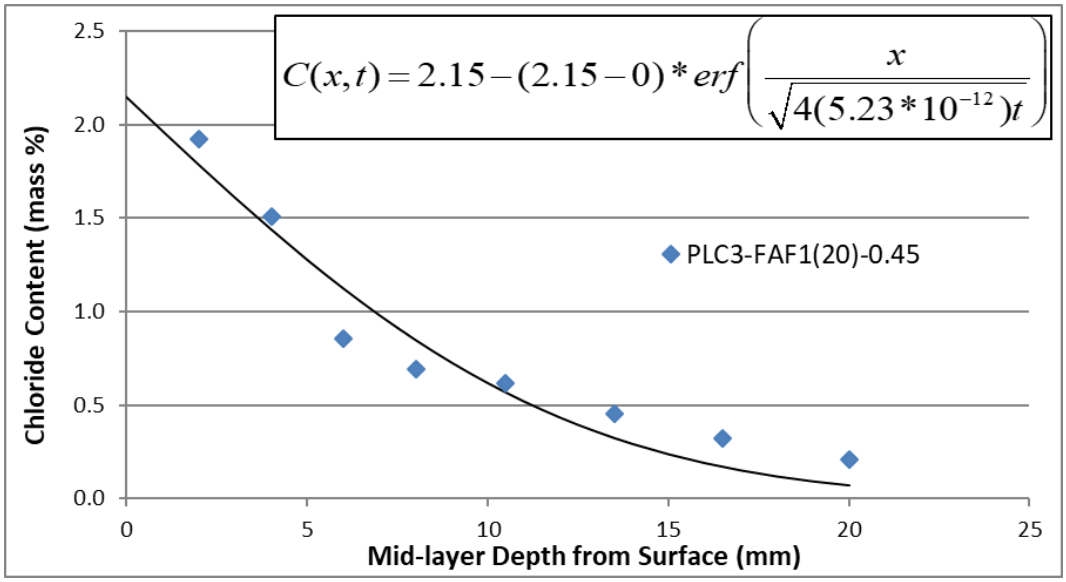

Figure 7.11: Chloride Content vs. Depth for PLC3-FAF1(20)-0.45 (Note 25.4 mm = 1 in.)

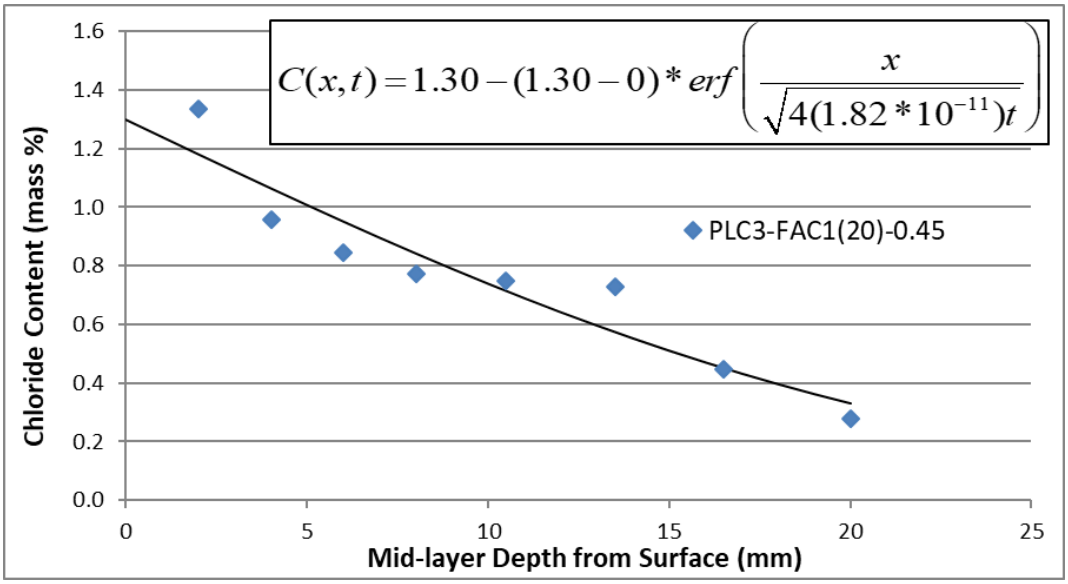

Figure 7.12: Chloride Content vs. Depth for PLC3-FAC1(20)-0.45 (Note 25.4 mm = 1 in.)

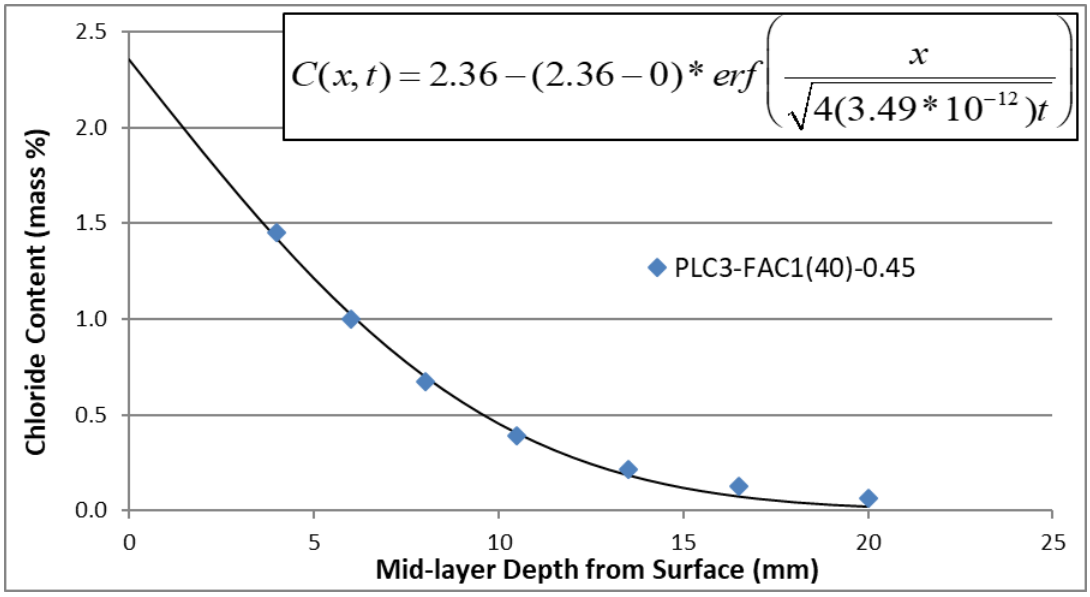

Figure 7.13: Chloride Content vs. Depth for PLC3-FAC1(40)-0.45 (Note 25.4 mm = 1 in.)

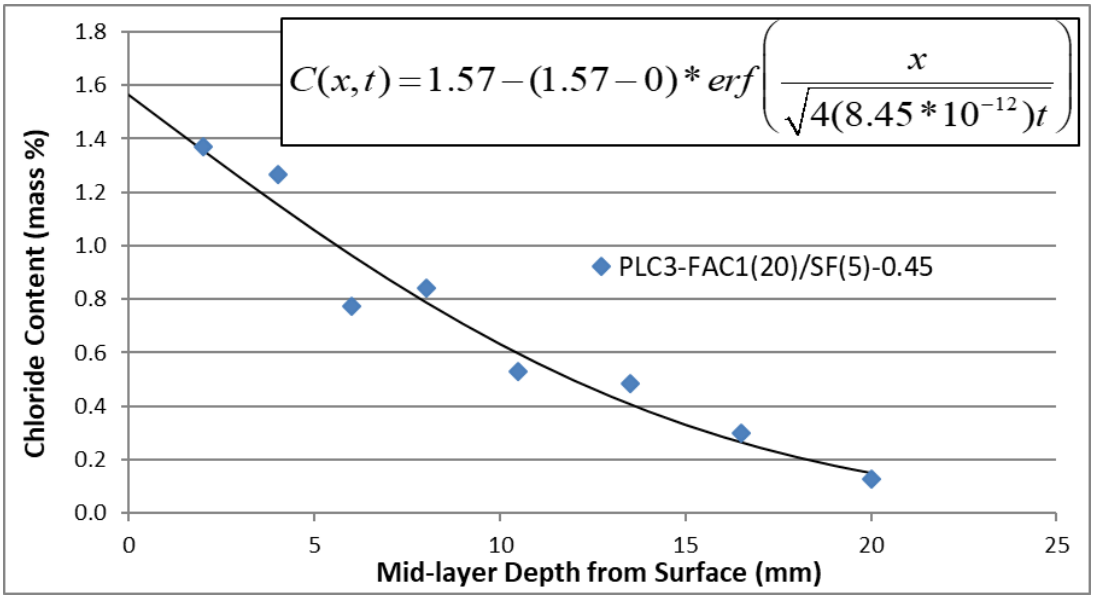

Figure 7.14: Chloride Content vs. Depth for PLC3-FAC1(20)/SF(5)-0.45 (Note 25.4 mm = 1 in.)

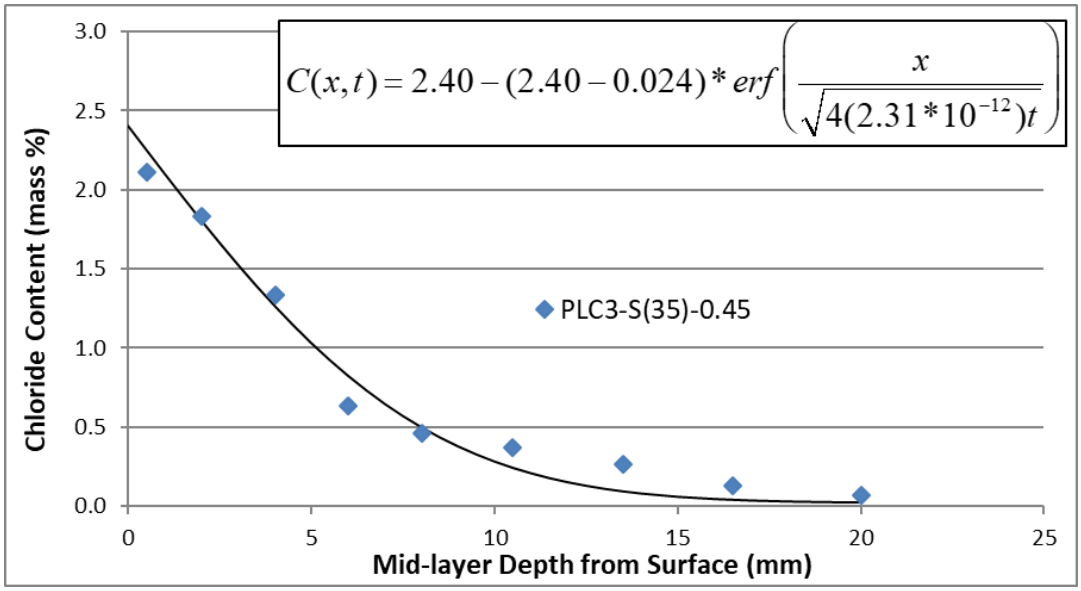

Figure 7.15: Chloride Content vs. Depth for PLC3-S(35)-0.45 (Note 25.4 mm = 1 in.)

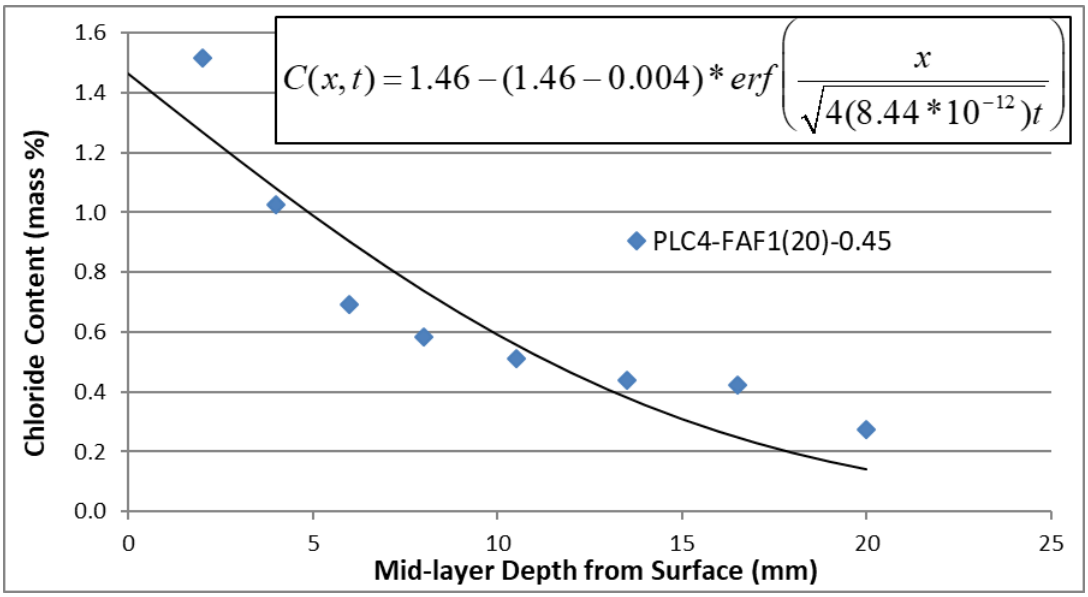

Figure 7.16: Chloride Content vs. Depth for PLC4-FAF1(20)-0.45 (Note 25.4 mm = 1 in.)

Table 7.7 summarizes the experimental diffusion coefficients for the straight cement mixtures. The diffusion coefficient of the PLC3-0.45 mixture, which has 21.0% limestone in the cement, is not significantly higher than that of the control mixture, PLC1-0.45. It is important to note that the 28-day compressive strengths for PLC1-0.45 and PLC3-0.45 are 49 and 42 MPa (7200 and 6100 psi), respectively, and thus, the diffusion coefficient was expected to be higher for PLC3-0.45. Following the same logic, the low diffusion coefficient of PLC4-0.45 was even more surprising, given the fact that the 28-day compressive strength was approximately 34 MPa (5000 psi) due to the high limestone content (31%). The cements from Cement Plant 2, PLC5 and PLC7 did not give expected results either. The 28-day compressive strengths of PLC5-0.45 and PLC7-0.45 are essentially equivalent (45 MPa [6500 psi]), however, the chloride diffusion coefficients obtained using the ASTM C1556 procedure were significantly different. In fact, the diffusion coefficient of PLC5-0.45 was the highest of all the straight cement mixtures, while PLC7-0.45 had the lowest diffusion coefficient. Further investigation in the future is needed to identify the key parameters that affect the chloride diffusion coefficients for portland limestone cement concrete systems.

The service-life modeling software package ConcreteWorks was used to predict the diffusion coefficient for each mixture. The predictive equation used by the software to estimate the diffusion coefficient, which uses the mixture design parameters, was not very accurate for any of the mixtures. The predicted diffusion coefficients are also shown in Table 7.7.

Table 7.7: Experimental and Predicted Diffusion Coefficients for Straight Cement Mixtures

Mixture ID	D_{EXP} ($m^2/s*10^{-12}$)	D_{PRED} ($m^2/s*10^{-12}$)	% Error
PLC1-0.45	16.2	10.9	32.7
PLC3-0.45	17.6	10.9	38.1
PLC4-0.45	12.9	10.9	15.5
PLC5-0.45	24.7	10.9	55.9
PLC7-0.45	5.99	10.9	-82.0

Since ConcreteWorks does not yet have portland limestone cement data built into the software, the predicted diffusion coefficient is the same, regardless of limestone content. The concept of effective water-to-cementitious materials ratio, which has already been discussed in Chapters 3 and 4 of this Final Report, was used in lieu of the actual w/cm of each mixture to see if this would provide a better prediction of the diffusion coefficient and the results are shown in Table 7.8. The estimated chloride diffusion coefficients did not improve after adjusting the mixture parameters to reflect the effective w/cm; further investigation is needed to figure out how ConcreteWorks can be modified, if at all, to be able to better estimate the chloride diffusion coefficients of PLC concrete.

Table 7.8: Experimental and Predicted (Based on Effective w/cm) Diffusion Coefficients for Straight Cement Mixtures

Mixture ID	D_{EXP} ($m^2/s*10^{-12}$)	Effective w/cm	$D_{PRED,\ Eff\ w/cm}$ ($m^2/s*10^{-12}$)	% Error
PLC1-0.45	16.2	0.45	10.9	32.7
PLC3-0.45	17.6	0.55	15.6	11.4
PLC4-0.45	12.9	0.63	20.8	-61.2
PLC5-0.45	24.7	0.45	10.9	55.9
PLC7-0.45	5.99	0.51	13.5	-125.4

Tennis et al. (2011) suggested that similar chloride diffusion resistance could be achieved for PLC concrete provided that the mixture is adjusted to achieve equivalent strength of OPC concrete. As a way to test this theory, diffusion coefficients and 28-day compressive strengths were plotted as a function of effective w/cm for the straight cement mixtures and the results are shown in Figure 7.17. It was expected that the chloride diffusion coefficient would increase as the compressive strength decreased and vice-versa, but clearly this is not the case.

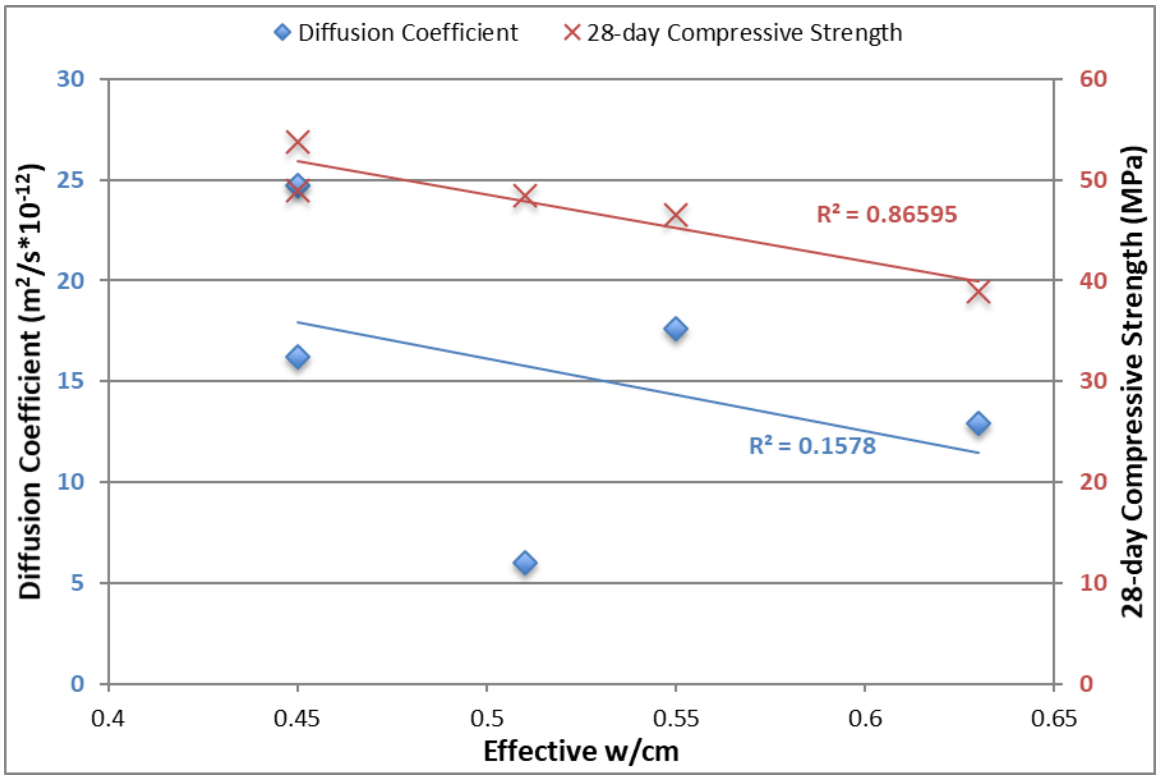

Figure 7.17: Diffusion Coefficients and 28-day Compressive Strength vs. w/cm for Straight Cement Mixtures

As was discussed in sections 7.5.4 and 7.2.2, chloride diffusion and electrical resistivity are known to correlate very well. Unfortunately, electrical resistivity was tested for the cylinders used to determine compressive strength, as presented in Chapter 3, and not for the cylinders used for the chloride diffusion study presented in this chapter. The only difference between the mixture designs is that natural river sand was used to determine compressive strength and manufactured limestone sand was used to determine the chloride diffusion coefficient. Since there was interest in testing the correlation between resistivity and chloride diffusion and presenting the results in this chapter, PLC4-0.45 and PLC7-0.45 were cast with manufactured limestone sand and the electrical resistivity was obtained at 28 days and 91 days. The results are tabulated in Tables 7.9 and 7.10. The mixtures with manufactured limestone sand yield lower electrical resistivity than the mixtures with natural river sand, as the average ratio of limestone sand to river sand ratio is 0.84.

Table 7.9: Comparison of Electrical Resistivity at 28 and 91 Days for PLC4-0.45 using Different Fine Aggregates (Values in kΩ*cm)

Testing Age	PLC4-0.45 (River Sand)	PLC4-0.45 (Limestone Sand)	Limestone to River Ratio
28-day	3.71	2.82	0.76
91-day	4.37	3.59	0.82

Table 7.10: Comparison of Electrical Resistivity at 28 and 91 Days for PLC7-0.45 using Different Fine Aggregates (Values in kΩ*cm)

Testing Age	PLC7-0.45 (River Sand)	PLC7-0.45 (Limestone Sand)	Limestone to River Ratio
28-day	3.51	3.03	0.86
91-day	4.05	3.65	0.90

Figure 7.18 shows the diffusion coefficients and 91-day electrical resistivity values plotted as functions of effective w/cm. Please note that the electrical resistivity values are for the mixtures with natural river sand and that they have been multiplied by 0.84, as explained in the previous paragraph, to obtain a fair comparison. It is important to note that the electrical resistivity and chloride diffusion coefficients both decrease as the effective water-to-cementitious materials ratio increases. Higher electrical resistivity is associated with lower chloride diffusivity and thus, there is a disconnect between chloride diffusion and resistivity for the PLC mixtures investigated in this study.

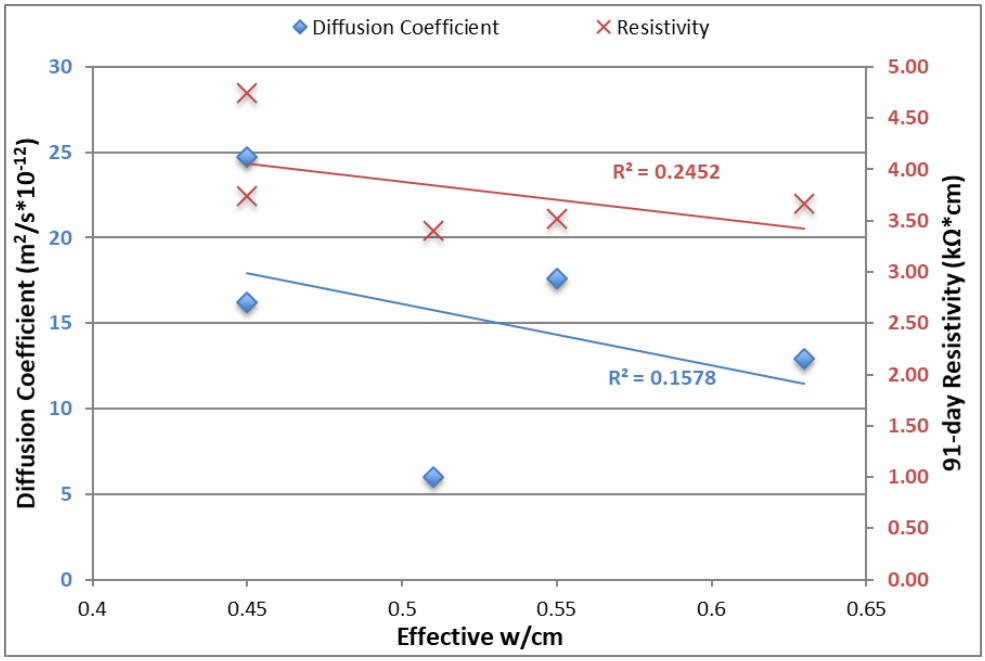

Figure 7.18: Diffusion Coefficients and 91-day Compressive Strength vs. w/cm for Straight Cement Mixtures

Figure 7.18 shows the experimental and predicted diffusion coefficients for the mixtures where PLC3 and PLC4 are combined with different supplementary cementitious materials. The addition of SCMs resulted in decreased diffusion coefficients for PLC3 and PLC4, the only exception being the incorporation of Class C fly ash at a 20% replacement level of PLC3, which increased the diffusion slightly. Nevertheless, as seen by the half-cell potential measurements, even PLC3-FAC1(20)-0.45 reduced the corrosion potential of PLC3-0.45, which can be attributed to the diffusion coefficient decaying over time at a faster rate when fly ash is added to the mixture. The addition of 35% slag, 40% Class C fly ash, 20% Class F fly ash, and the ternary blend of 20% class C fly ash, 5% densified silica fume, and PLC3 all reduced the diffusion coefficient by an order of magnitude; however, it was expected that the addition of silica fume would result in a higher decrease in the diffusion coefficient. The addition of slag resulted in the lowest chloride diffusivity out of all the mixtures, which was expected, due to the widespread use of slag in marine environments for its well-documented effect of minimizing concrete permeability.

It is important to note that ConcreteWorks assumes that the addition of fly ash or slag does not change the 28-day diffusion coefficient, based on inconclusive research. The benefit of fly ash and slag comes from the reduction in permeability that is achieved over time with curing, and ConcreteWorks accounts for this by using a decay coefficient that is built into the program. In the case of silica fume, ConcreteWorks does assume that the 28-day diffusion coefficient is reduced, based on previous research. The decay values assumed by the software package for each mixture with cement and a particular SCM are provided in Table 7.11 for reference. For the straight cement mixtures, ConcreteWorks assumes a decay coefficient of 0.26, with no distinction between OPC and PLC.

Table 7.11: Experimental and Predicted Diffusion Coefficients for Combinations of PLCs and SCMs

Mixture ID	D_{EXP} ($m^2/s*10^{-12}$)	D_{PRED} ($m^2/s*10^{-12}$)	% Error	Decay Value
PLC3-FAF1(20)-0.45	5.23	10.9	-108.4	0.42
PLC3-FAC1(20)-0.45	18.2	10.9	40.1	0.42
PLC3-FAC1(40)-0.45	3.49	10.9	-212.3	0.58
PLC3-FAC1(20)/SF(5)-0.45	8.45	3.4	59.8	0.42
PLC3-S(35)-0.45	2.31	10.9	-371.9	0.46
PLC4-FAF1(20)-0.45	8.44	10.9	-29.1	0.42

It is clear that the diffusion coefficient estimates provided by ConcreteWorks are not accurate enough to be used reliably for combinations of PLC concrete systems. However, service-life modeling calculations can still be obtained using ConcreteWorks by overriding the program and inputting the actual chloride diffusion coefficient for any given mixture. In order to test the validity of overriding the program to verify if an accurate prediction of corrosion initiation can be obtained with ConcreteWorks, the experimental diffusion coefficients were input into the software. Using

the actual diffusion coefficients and the decay values assumed by the software, it was possible to obtain chloride concentrations plotted as a function of exposure time for the different mixtures. Assuming that a critical chloride concentration of 0.07% as a mass of concrete initiates corrosion, the predicted time to corrosion initiation was obtained for each mixture and the results were then compared to the half-cell potential measurements to test the validity of the predictions. The plots of predicted chloride concentrations as a function of time can be seen in Figures 7.19 and 7.20.

Table 7.12 compares the approximate time, in years, that it took corrosion to probably initiate on the reinforcement bar with 38.1 mm of concrete cover, based on half-cell potential measurements, to the estimated time that it would take for the critical chloride concentration to reach a depth of 38.1 mm, which is associated with corrosion initiation. The estimate that ConcreteWorks gives agrees with 5 out of the 11 mixtures. If half-cell potential measurements were conducted more frequently, a more accurate analysis between predicted and actual corrosion initiation exposure times would be possible.

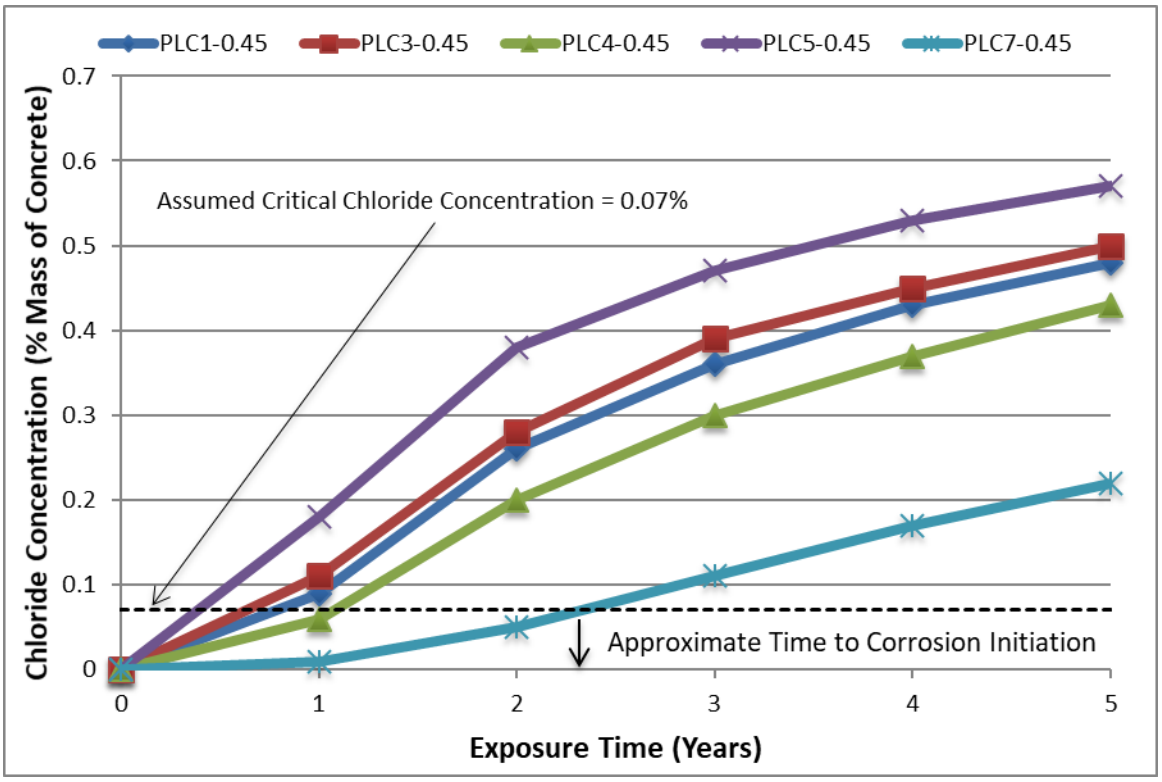

Figure 7.19: Predicted Chloride Concentrations vs. Exposure Time for Straight Cement Mixtures (Data Courtesy of ConcreteWorks)

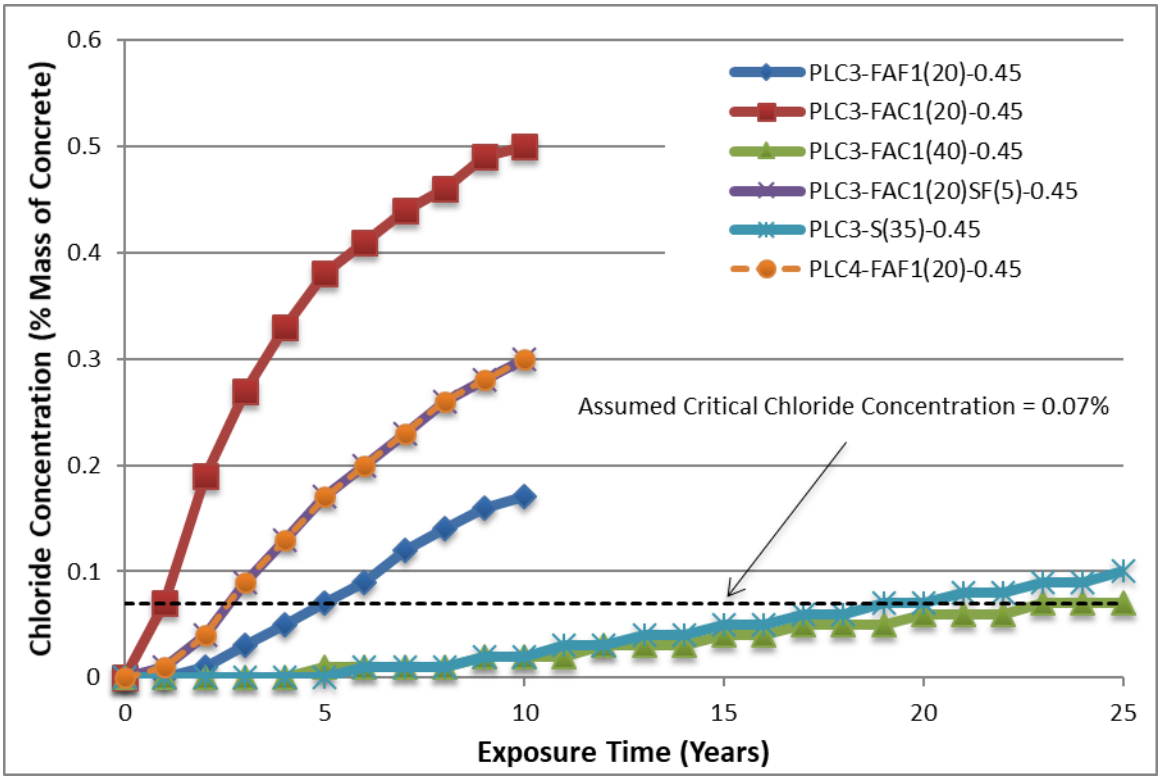

Figure 7.20: Predicted Chloride Concentrations vs. Exposure Time for PLC and SCM Combinations (Data Courtesy of ConcreteWorks)

Table 7.12 Comparison of Half-Cell Potential Measurements to ConcreteWorks Predictions

Mixture ID	Approx. Time to Reach 90% Probability of Corrosion in 38.1 mm Bar (Years)	Calculated Time in ConcreteWorks for Critical Chloride Threshold to Reach 38.1 mm (Years)	Does Prediction Make Sense?
PLC1-0.45	>0.6 and <1.3	0.8	Yes
PLC3-0.45	>0.6 and <1.3	0.6	Yes
PLC4-0.45	>0 and <0.8	1.2	No
PLC5-0.45	~1.2	0.4	No
PLC7-0.45	>0 and <0.8	2.3	No
PLC3-FAF1(20)-0.45	>1.3 and <2.2	5.0	No
PLC3-FAC1(20)-0.45	>2.2	1.0	No
PLC3-FAC1(40)-0.45	>2.2	24	Yes
PLC3-FAC1(20)/SF(5)-0.45	>2.2	2.6	Yes
PLC3-S(35)-0.45	>2.2	19.7	Yes
PLC4-FAF1(20)-0.45	>0.8 and <1.7	2.6	No

7.7. Conclusions and Future Work

The objective of the study presented in this chapter was to determine if portland limestone cement concrete, with high limestone content, presents a higher risk of chloride-induced corrosion which is common in marine environments and also in transportation infrastructure and parking garages where de-icing salts are frequently used.

Taking into consideration the half-cell potential measurements and the experimental chloride diffusion coefficients that were determined for eleven concrete mixtures with and without supplementary cementitious materials, the following conclusions can be drawn:

- When compared to the control mixtures, similar or, in some cases, lower diffusion coefficients were observed for straight cement mixtures even at high limestone contents.
- The addition of supplementary cementitious materials significantly reduces the chloride diffusion coefficients even for mixtures with significant limestone contents. The chloride diffusion coefficients were reduced by about one order of magnitude for the majority of SCMs.
- In the future, research should focus on advancing prediction models that can more accurately estimate the diffusion coefficients for PLC concrete systems.
- Contrary to previous research findings, the balance of data obtained during this investigation seems to indicate that the corrosion potential increases as the limestone content increases, even though the diffusion coefficients are similar or lower. Possible explanations could include:
- PLC concrete systems are more susceptible to abrasion that should be expected in marine environments. Abrasion can lead to a significant decrease in concrete cover and corrosion initiation may occur faster than laboratory tests may indicate.
- The critical chloride concentration for PLC concrete is lower than for OPC concrete.
- The addition of SCMs does increase the protection against corrosion potential for mixtures with significant limestone contents.
- Provided that SCMs in sufficient quantity are used in combination with adequate concrete cover and possibly lowering the w/cm, it is possible that PLC concrete systems could be used in highly aggressive chloride environments, but more research should verify this conclusion.
- ConcreteWorks was not able to predict the chloride diffusion coefficient for PLC concrete systems with accuracy.

- ConcreteWorks was able to, with some degree of success, provide an estimate of time to corrosion initiation, provided that actual chloride diffusion coefficients are used in the program instead of those predicted by the software.
- Future research should focus on identifying means and methods to enable concrete producers to use ConcreteWorks to better predict the service-life of PLC concrete systems subjected to chloride environments.

Chapter 8. Carbonation of Portland Limestone Cement Concrete Systems

8.1. Introduction

This chapter presents the findings from a thorough study on the natural carbonation of portland limestone cement concrete. A brief summary of concrete carbonation is presented and how it changes when cements with high limestone contents are used in lieu of ordinary portland cement.

Twelve straight cement mixtures at three different water-to-cementitious materials ratios and eighteen mixtures with different combinations of cements, which have varying limestone contents in the approximate range of 3% to 30%, and supplementary cementitious materials at a constant w/cm were cast and tested.

Three exposure sites with different weather exposure conditions in the state of Texas were used in this investigation. The depth of carbonation was measured every six months for each mixture.

Lastly, the development of an accelerated carbonation chamber, preliminary results, and plans for future research are presented at the end of the chapter.

8.2. Review of Carbonation

8.2.1. Carbonation of OPC

Carbonation is a natural process that occurs when concrete is exposed to carbon dioxide, which is present in air at a concentration of approximately 0.04%. Carbon dioxide reacts with the calcium bearing phases present in hydration products and anhydrous cement to produce calcium carbonate, as shown in Equations 8.1 to 8.4 (Peter et al., 2008).

$$Ca(OH)_2 + CO_2 \rightarrow CaCO_3 + H_2O \quad \text{(Eq. 8.1)}$$

$$(3CaO \cdot 2SiO_2 \cdot 3H_2O) + 3CO_2 \rightarrow (3CaCO_3 \cdot 2SiO_2 \cdot 3H_2O) \quad \text{(Eq. 8.2)}$$

$$(2CaO \cdot SiO_2) + 2CO_2 + nH_2O \rightarrow (SiO_2 \cdot nH_2O) + 2CaCO_3 \quad \text{(Eq. 8.3)}$$

$$(3CaO \cdot SiO_2) + 3CO_2 + nH_2O \rightarrow (SiO_2 \cdot nH_2O) + 3CaCO_3 \quad \text{(Eq. 8.4)}$$

The carbonation reaction causes the pH of the concrete to decrease from typical values above 13 for concrete at early ages to below 9.0 (Heiyantuduwa et al., 2006). Valcuende and Parra (2010) reported an approximate pH of 8.3. The drop in pH causes the passivation layer of steel reinforcement, which is stable at high pH levels, to break down and this increases the potential of carbonation-induced corrosion. Phenolphthalein solution, a pH indicator that turns purple at pH

levels above 9.2 and remains colorless below 9.2, can be used to quickly identify carbonated concrete. A schematic showing the spraying of phenolphthalein solution can be seen in Figure 8.1.

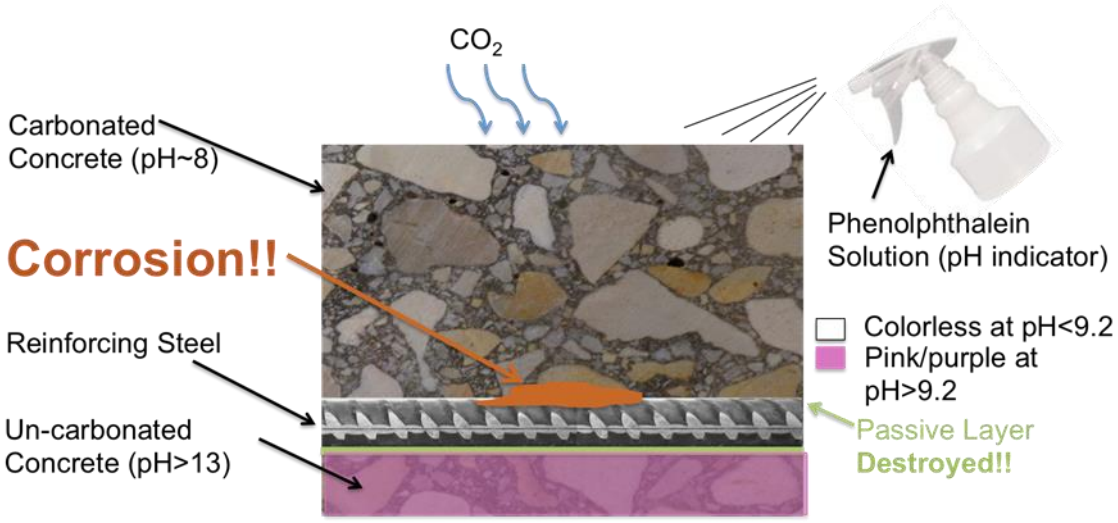

Figure 8.1: Schematic of Carbonation-Induced Corrosion and Use of Phenolphthalein Solution

Carbonation is also associated with densification of the concrete matrix for ordinary portland cement concrete, leading to carbonation shrinkage, and an increase in strength and dimensional stability. The precast industry uses carbonation to its advantage by exposing precast elements to high concentrations of carbon dioxide, known as carbonation curing, to increase strength and reduce shrinkage before the precast element is in service (Mindess et al., 2003).

The consumption of calcium hydroxide, shown in Equation 6.1, is the fastest carbonation reaction that occurs. Intuitively, it would make sense that the rate of concrete carbonation would be faster in concrete with lower levels of calcium hydroxide, but many researchers have actually proven that the exact opposite is true. Thomas and Matthews (1992) reported higher carbonation rates in concrete that incorporated fly ash, where calcium hydroxide would be converted to calcium silicate hydrate through the pozzolanic reaction.

Several models have been proposed to predict the carbonation rate of a concrete mixture; Zhou et al. (2014) provide a good summary of the models. One such model, which is based on an empirical relationship observed by a number of researchers, is shown in Equation 8.5.

$$x = k\sqrt{t} \qquad \text{(Eq. 8.5)}$$

where x is equal to the measured depth of carbonation in mm, k is the carbonation coefficient ($mm/year^{1/2}$), and t is the time, in years, when the depth of carbonation is measured. Once the carbonation coefficient for a given mixture is found empirically, the depth of carbonation at any other time t can be estimated.

According to Thomas & Matthews (1992), the carbonation coefficient can be predicted if the following parameters are known:

- Ambient temperature during casting
- Curing period length
- Exposure conditions (temperature, relative humidity)
- Fly ash content
- Nominal concrete strength

Typical carbonation coefficients that can be predicted using the Thomas and Matthews model are in the order of 0-15 mm/year$^{1/2}$ (0-0.59 in/year$^{1/2}$).

A more recent study by Galan et al. (2010) presents the carbonation coefficients for mixtures at water-to-cementitious materials ratios of 0.45 and 0.60 on cements with clinker percentages ranging from 5% to 100%. The cements were combined with the following materials as clinker replacement: limestone, fly ash, limestone and fly ash combined, slag, pozzolans, and a combination of slag and fly ash. The reported carbonation coefficients ranged from about 1 to as high as 14 mm/year$^{1/2}$ (0.04-0.55 in/year$^{1/2}$). Valcuende and Parra (2010) reported a similar range of carbonation coefficient values in their study.

8.2.2. Carbonation of PLC

Previous researchers have reported that increasing the limestone content of the cement increases the rate of carbonation if the water-to-cementitious materials ratio is held constant. However, if the mixtures are adjusted to achieve equivalent strength, the rate of carbonation can be expected to remain the same, regardless of limestone content (Tennis et al., 2011).

There does not appear to be sufficient published data on the carbonation of mixtures made with high limestone content PLCs combined with supplementary cementitious materials to conclude the effect of SCM additions to PLC systems. However, it is expected that the carbonation of these PLC systems increases as the SCM content increases (Hooton et al., 2007).

8.3. Materials

8.3.1. Cements

Cements PLC1 through PLC7, which have varying limestone contents, were used for this experimental investigation. For more information on the chemical composition and phase composition of all cements, please refer to section 2.1.

8.3.2. Supplementary Cementitious Materials

For this experimental investigation, the following supplementary cementitious materials were used: Class F fly ash 1, Class C fly ash 1, Class C fly ash 2, Grade 100 slag, and densified silica fume. Please refer to section 2.3 for information on the chemical composition of each SCM.

8.3.3. Aggregates

Manufactured limestone sand and crushed limestone rock were used as fine and coarse aggregates for the concrete mixtures described in this chapter. Please refer to section 2.4 for more information on both aggregates.

8.3.4. Water

Potable tap water was used to mix concrete specimens for this study.

8.4. Mixture Proportions

8.4.1. Nomenclature

The nomenclature system discussed in section 2.6 is used in this chapter. The graphical representation of the nomenclature system provided in Figure 2.6 provided again for reference in Figure 8.2.

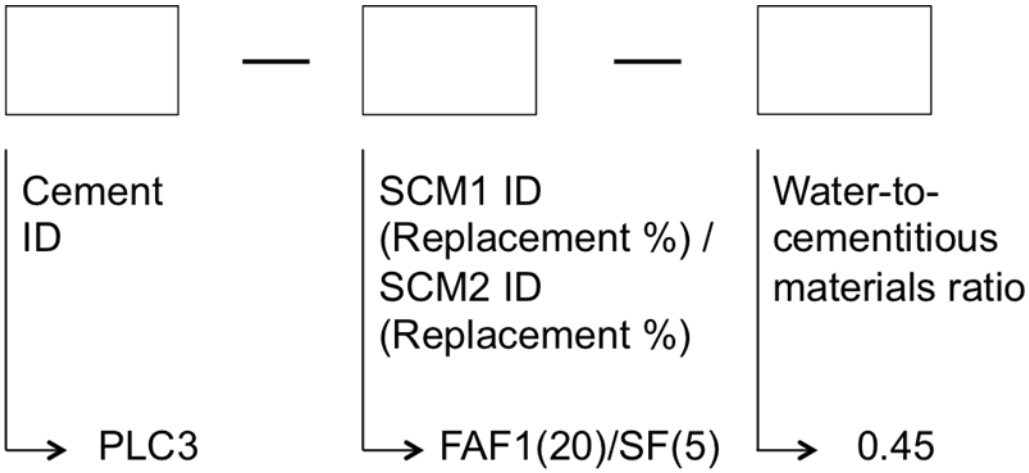

Figure 8.2: Nomenclature Used in This Chapter

8.4.2. Test Matrix

Thirty-four different concrete mixtures were tested. As shown in Table 8.1, the mixtures include straight cement mixtures and different combinations of cements and SCMs, including ternary

blends of PLC, Class C fly ash, and densified silica fume. For all mixtures, the coarse aggregate fraction was 1048 kg/m^3 (1766 lb/yd^3), and the fine aggregate fraction was 670 kg/m^3 (1129 lb/yd^3). The water contents were 145 kg/m^3 (244 lb/yd^3), 163 kg/m^3 (275 lb/yd^3), and 181 kg/m^3 (306 lb/yd^3), for the water-to-cementitious materials ratios of 0.40, 0.45, and 0.50, respectively.

Table 8.1: Mixture Proportions—Mass in kg/m^3 (Note 1 kg/m^3 = 1.69 lb/yd^3)

MIXTURE ID	Cement	FAF1	FAC1	FAC2	S	SF
PLC1-0.40/0.45/0.50	362.5	--	--	--	--	--
PLC2-0.45	362.5	--	--	--	--	--
PLC3-0.45	362.5	--	--	--	--	--
PLC4-0.40/0.45/0.50	362.5	--	--	--	--	--
PLC5-0.40/0.45/0.50	362.5	--	--	--	--	--
PLC6-0.45	362.5	--	--	--	--	--
PLC7-0.40/0.45/0.50	362.5	--	--	--	--	--
PLC1-FAF1(20)-0.45	290.1	72.4	--	--	--	--
PLC3-FAF1(20)-0.45	290.1	72.4	--	--	--	--
PLC4-FAF1(20)-0.45	290.1	72.4	--	--	--	--
PLC5-FAF1(20)-0.45	290.1	72.4	--	--	--	--
PLC7-FAF1(20)-0.45	290.1	72.4	--	--	--	--
PLC3-FAC1(20)-0.45	290.1	--	72.4	--	--	--
PLC3-FAC1(40)-0.45	217.7	--	144.8	--	--	--
PLC1-FAC2(20)-0.45	290.1	--	--	72.4	--	--
PLC3-FAC2(20)-0.45	290.1	--	--	72.4	--	--
PLC3-FAC2(40)-0.45	217.7	--	--	144.8	--	--
PLC4-FAC2(20)-0.45	290.1	--	--	72.4	--	--
PLC5-FAC2(20)-0.45	290.1	--	--	72.4	--	--
PLC7-FAC2(20)-0.45	290.1	--	--	72.4	--	--
PLC3-S(35)-0.45	235.5	--	--	--	127.0	--
PLC7-S(35)-0.45	235.5	--	--	--	127.0	--
PLC3-FAC2(20)/SF(5)-0.45	271.7	--	--	72.4	--	18.4
PLC3-FAC2(20)/SF(5)-0.45	271.7	--	--	72.4	--	18.4

8.5. Experimental Procedures

8.5.1. Exposure Site Development

Three carbonation exposure sites in the state of Texas were used for this study. The first exposure site, located in the city of Austin, already existed by the time that this research project was initiated. Two additional sites were developed as part of this research project to study the effect of different weather exposure conditions on carbonation of PLC concrete. The location of the three exposure

sites can be seen in Figure 8.3 and the average weather conditions for each exposure site are shown in Table 8.2.

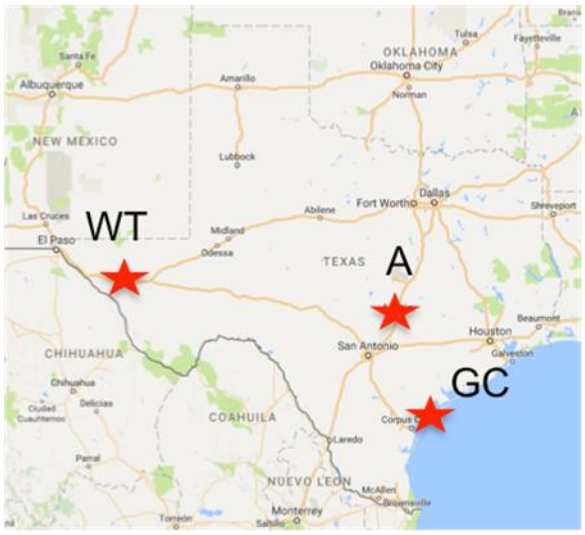

Figure 8.3: Carbonation Exposure Site Locations (A: Austin, GC: Gulf Coast, WT: West Texas)

Very hot and humid summers and mild winters characterize the Austin exposure site. The Gulf Coast exposure site, located in the city of Port Aransas, is subjected to hot and very humid summers and warm winters. Finally, the West Texas exposure site experiences hot and very dry summers, and relatively cold winters compared to the other two exposure sites. A picture of the Austin exposure site is shown in Figure 8.4, and the exposure site on the Gulf Coast can be seen in Figure 8.5. Please note that each exposure site consists of a Stevenson Screen meeting the guidance provisions of the European Committee for Standardization Technical Specification CEN/TS 12390-10. The dimensions of each Stevenson Screen are 1000 x 2000 x 700 mm high (39 x 79 x 28 in.) and they are painted white so as to minimize the radiation effect from the sun. The screens provide "free interchange of atmosphere whilst preventing specimens being exposed directly to precipitation." (CEN/TS 12390-10:2008, 2008)

Table 8.2: Weather Conditions at Each Exposure Site

Exposure Site	High Average Summer Temperature oC (oF)	Low Average Winter Temperature oC (oF)	Average Annual Precipitation mm (in.)
Austin	34.6 (94.3)	6.1 (43.0)	870 (34.3)
Gulf Coast	31.1 (88.0)	11.3 (52.3)	883 (34.8)
West Texas	33.9 (93.0)	-1.1 (30.0)	292 (11.5)

Figure 8.4: Carbonation Exposure Site in Austin, TX

Figure 8.5: Carbonation Exposure Site on the Gulf Coast

8.5.2. Casting, Curing, and Exposure Site Placement Procedure

Six 100 x 100 x 350 mm (4 x 4 x 14 in.) prisms were cast for each mixture (two prisms for each exposure site) and de-molded after 24 hours. For the Austin exposure site, the prisms were taken to the exposure site immediately after de-molding and labeling each specimen. Due to the limited access of the other two exposure sites, the specimens placed at these sites were allowed to dry for three days before they were placed inside of vacuum-sealed bags, to prevent carbonation before exposure at the site. The specimens were then taken to each exposure site at the time of the next exposure site visit. At each exposure site, one prism was placed outside, directly exposed to the elements, and the other prism was placed inside of the Stevenson Screen; the prisms have been denoted as unsheltered and sheltered, respectively.

8.5.3. Carbonation Depth Measurement

A 50-millimeter (2-inch) slice of each prism (sheltered and unsheltered) was obtained by mechanically breaking the prism using a hand-operated beam-breaker. The 50 mm slice was sprayed generously with phenolphthalein solution and the depth of carbonation was measured between 30 and 60 minutes after spraying. The fractured face of the remaining length of broken prism was coated with a very thick paint that does not allow carbon dioxide to penetrate. The paint was allowed to cure for 24 hours before the prism was returned to the exposure site. A schematic detailing the process of the prism-breaking procedure is shown in Figure 8.6.

The depth of carbonation was obtained by measuring the distance from the edge of the prism to the location where the prism changed color to pink/purple at five points for each of the four faces. The depth of carbonation for each prism is the average of the twenty total measurements. A schematic showing the locations where the depths of carbonation measurements were taken for each face can be seen in Figure 8.7.

For the Austin exposure site, carbonation depth measurements were taken for the unsheltered and sheltered prisms every six months for each mixture. For the Gulf Coast exposure site, the carbonation depth measurements were taken as close as possible to the six-month increments, but due to the fact that this exposure site is visited only about three to four times per year, the measurements at the exact dates could not be accommodated. The West Texas exposure site is visited even less frequently, and at the time of writing for this Final Report, no carbonation depth measurements have been taken yet. The first measurements are scheduled for the end of July 2018 after two years of exposure. It is the intent of the research team to continue to monitor these specimens in the long term.

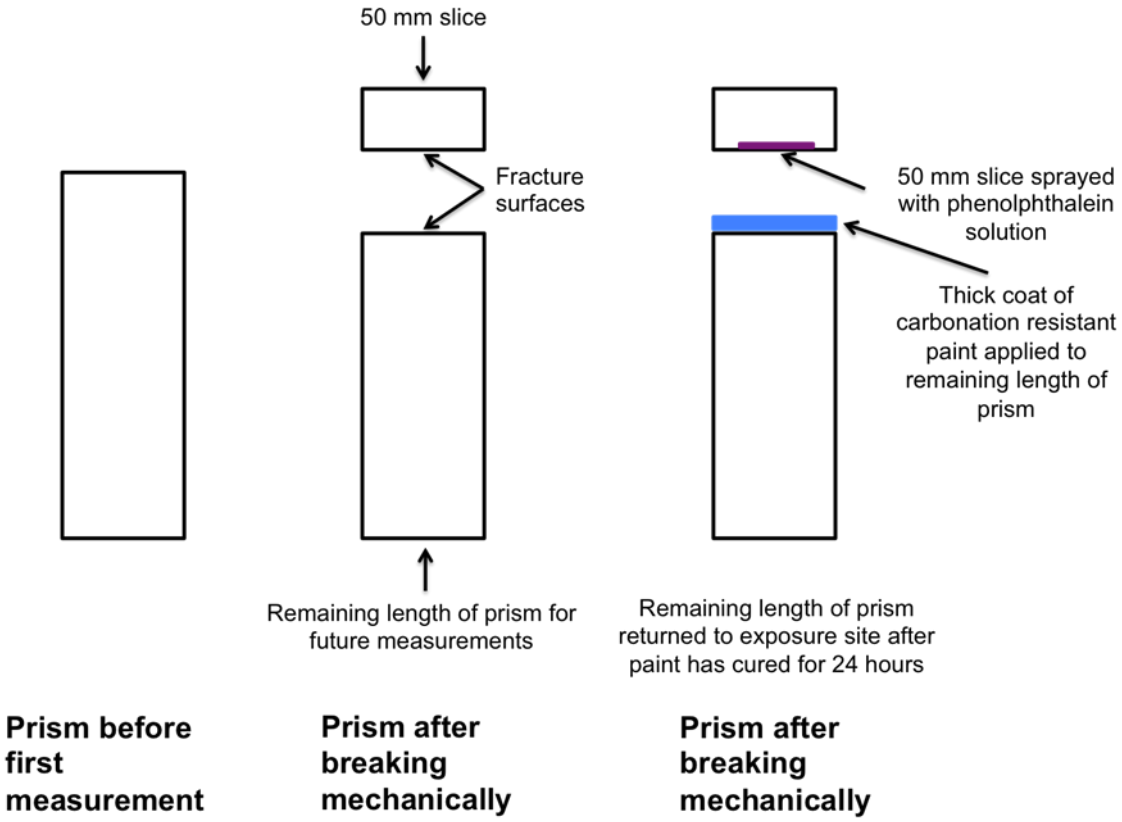

Figure 8.6: Schematic of Prism-Breaking Procedure

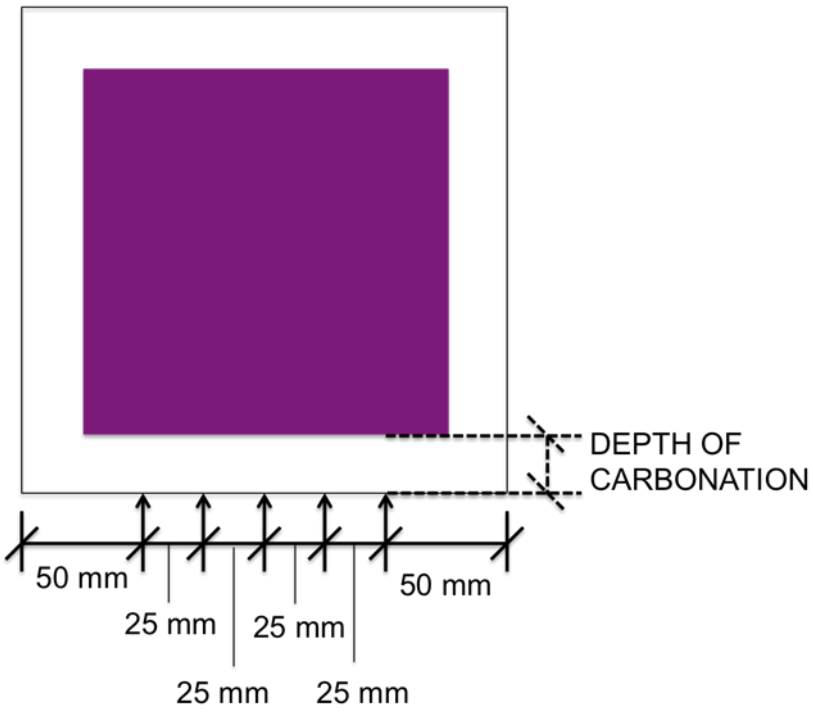

Figure 8.7: Schematic Showing Locations of Carbonation Depth Readings Indicated by Arrows. (Note 25.4 mm = 1 in.)

8.6. Results and Discussion

Sections 8.6.1 through 8.6.3 present the results of this investigation for the mixtures that were placed in the Austin exposure site. Section 8.6.4 presents the results from the specimens in the Gulf Coast exposure site.

8.6.1. Effect of Increasing Limestone

Figure 8.8 shows the depth of carbonation, after two years of outdoor exposure, of the straight cement mixtures made with PLC1 to PLC4 at a constant water-to-cementitious materials ratio of 0.45. The limestone contents for PLC1 through PLC4 are 3.2%, 13.4%, 21.0%, and 30.6%, respectively. As has been reported by a number of researchers, the rate of carbonation, and hence carbonation depth, increase as the limestone content increases, if the w/cm is held constant. Please note that the "unsheltered" specimen, i.e. the specimen outside of the Stevenson Screen carbonates less than the "sheltered" specimen for all mixtures. The fact that the unsheltered specimens carbonate less than their sheltered counterparts is attributed to the fact that the unsheltered specimens have direct access to precipitation. The precipitation increases the relative humidity inside of the specimens, which is known to slow down the carbonation rate (Thomas & Matthews, 1992).

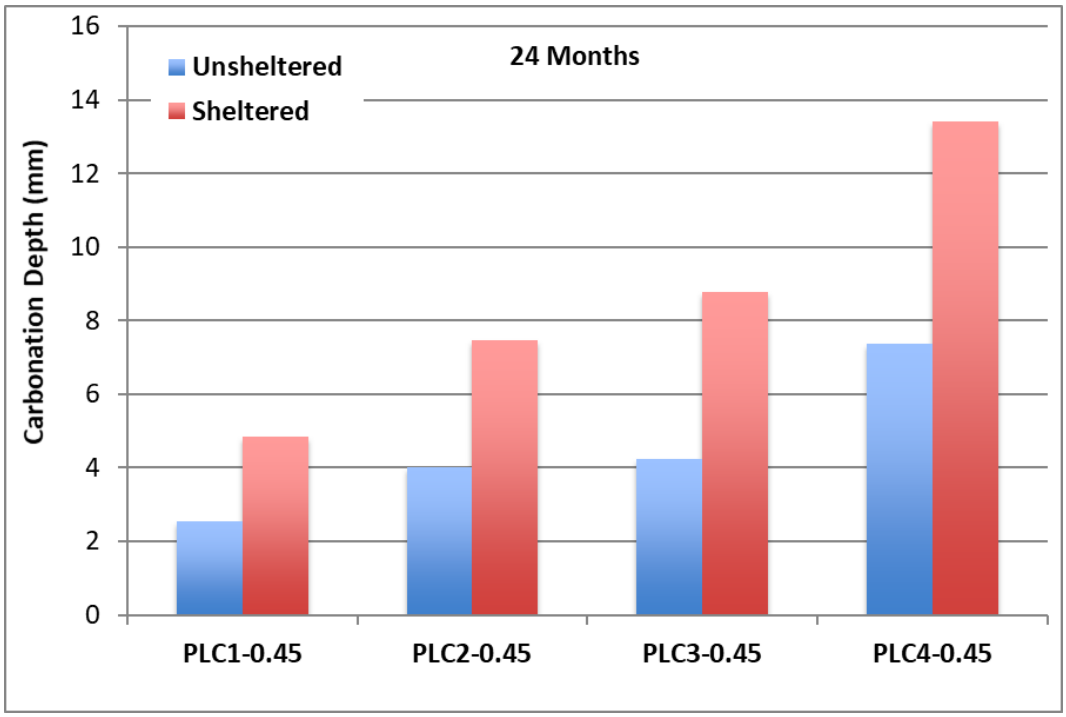

Figure 8.8: Carbonation Depth of Mixtures with PLC1-PLC4 after 24 Months (Note 25.4 mm = 1 in.)

Figure 8.9 shows the carbonation depth for the mixtures that incorporate the cements from Cement Plant 2, PLC5 to PLC7. Interestingly, the carbonation depth measurements for PLC5 and PLC6 were essentially the same after a period of 24 months, even though PLC5 has 4.9% limestone and PLC6 has about 11.6% limestone. PLC7, with a limestone content of 15.5%, carbonated more than PLC5 and PLC6 as expected. It's also worth noting that PLC7 carbonated more than PLC3, even though PLC3 has more limestone than PLC7.

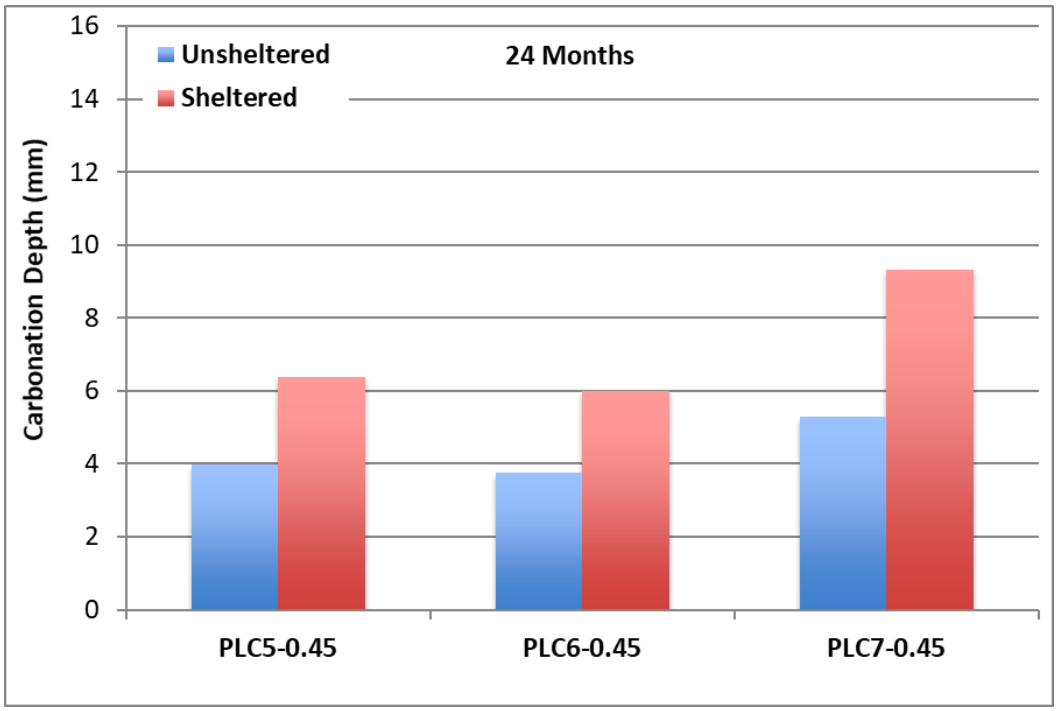

Figure 8.9: Carbonation Depth of Mixtures with PLC5-PLC7 after 24 Months (Note 25.4 mm = 1 in.)

As shown in Figure 8.10, the carbonation depth generally has a negative correlation with the compressive strength for each mixture. In other words, the mixtures that have the highest compressive strength, showed the lowest amount of carbonation. As discussed in Chapter 3, as the limestone content increases, the compressive strength decreases if the water-to-cementitious materials ratio is held constant. The increasing limestone content also results in increased carbonation.

Please note that although PLC1 and PLC2 have the same compressive strength, the PLC2 mixture carbonates faster than PLC1, and the same conclusion can be drawn about PLC7 with respect to PLC5. The results of these particular mixtures are not in agreement with what other researchers have reported in the past regarding equivalent carbonation resistance of mixtures with equivalent compressive strength (Tennis et al., 2011). Further investigation is needed to understand the reason that some mixtures display the carbonation resistance that would be expected based on compressive strength and others do not. One possible explanation is that the cylinders used to obtain the compressive strengths were cast using crushed limestone rock and natural river sand as coarse and fine aggregate, respectively, while the carbonation prisms incorporated crushed limestone rock and manufactured limestone sand as aggregates into the mixture. Another plausible explanation comes from the fact that the mixtures were not cast at the same exact time. Hence, the exposure conditions may not be exactly the same for all the mixtures, since they are placed outdoors in an environment where the temperature and relative humidity are variable. It is likely

that in the future, after a longer exposure time, the effect of variable outdoor exposure conditions is minimized and that a fairer comparison between mixtures can be made.

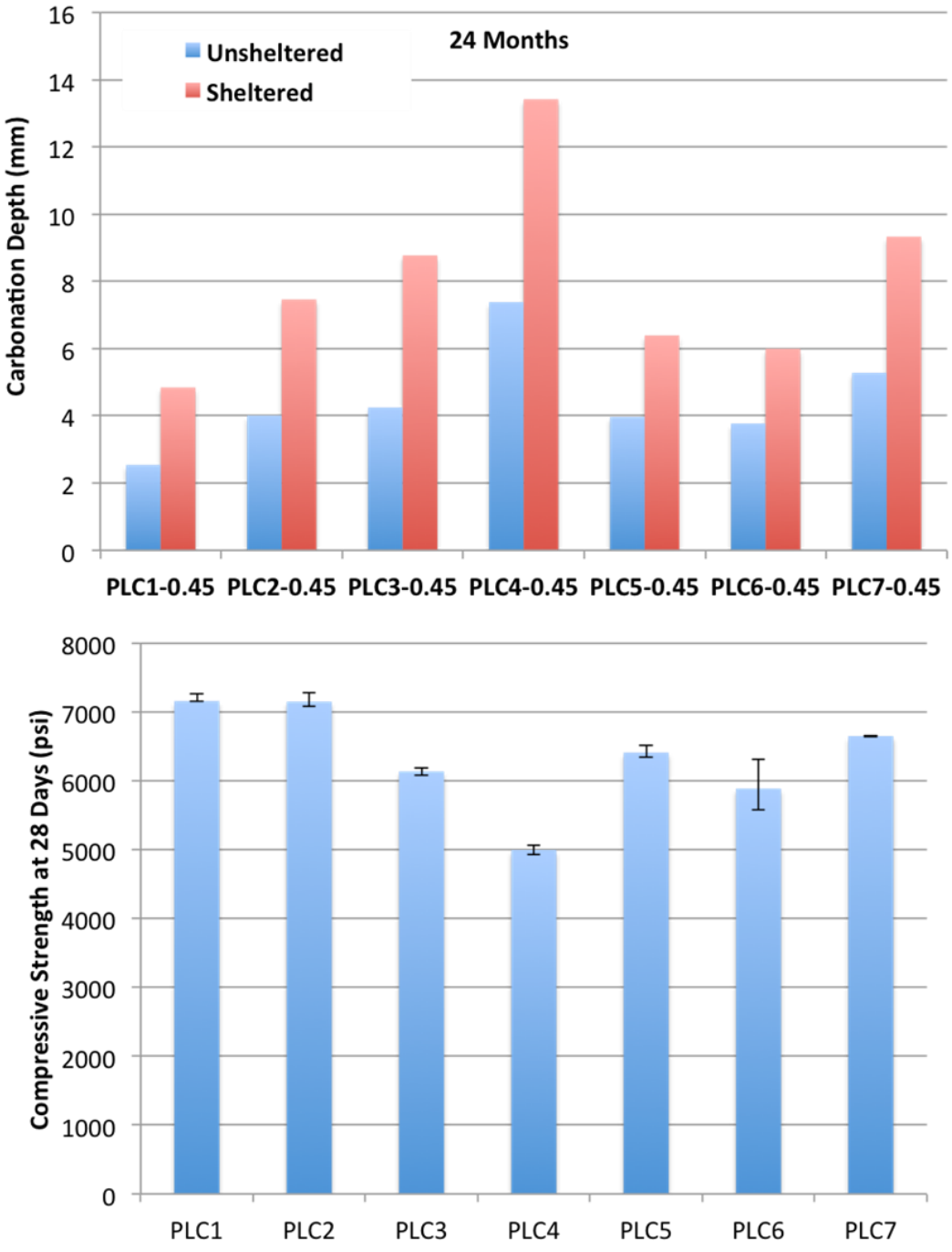

Figure 8.10: Carbonation Depth After 24 Months and 28-Day Compressive Strength of Mixtures with PLC1-PLC7 at w/cm = 0.45 (Note 25.4 mm = 1 in.)

Once the carbonation depth is measured for a given exposure time, the carbonation coefficient, which can be used to predict the depth of carbonation at a given exposure time, can be estimated by using Equation 8.6, which is obtained by manipulating Equation 8.5.

$$k = {}^{x}/_{\sqrt{t}} \qquad \text{(Eq. 8.6)}$$

In theory, the carbonation coefficient k is constant and specific to each concrete mixture. However, Sisomphon and Franke (2007) reported that the value of k decreases with time, although their study focused on accelerated carbonation with specimens exposed to carbon dioxide concentrations much higher than normal. The carbonated coefficients were calculated for each straight cement mixture after 6, 12, 18, and 24 months of exposure to see the effect of increasing limestone on the carbonation coefficients.

Figure 8.11 shows the carbonation coefficients plotted as a function of time for the straight cement mixtures for PLC1 to PLC4 at a water-to-cementitious materials ratio of 0.45. As expected, the carbonation coefficients are higher for the sheltered specimens (shown by the dashed lines) when compared to the unsheltered specimens, which are shown by solid lines. As the limestone content of the cement increases, the carbonation coefficients also increase, which is also expected, as the carbonation coefficient increases as the depth of carbonation increases.

The determination of the carbonation coefficient is possible by measuring the depth of carbonation, which is not an exact science; thus, some variability in the carbonation coefficient should be expected. The carbonation coefficients are fairly consistent for the PLC1 mixture, but there is higher variability in the other mixtures. The coefficients appear to be increasing with time for the PLC2 and PLC4 sheltered specimens. The data is inconclusive as to the effect of increasing limestone content of the cement in regards to the change in carbonation coefficient over time across each mixture.

The same conclusions can be drawn about the straight cement mixtures with PLC5 to PLC7. As shown in Figure 8.12, the calculated carbonation coefficients increase or decrease with time.

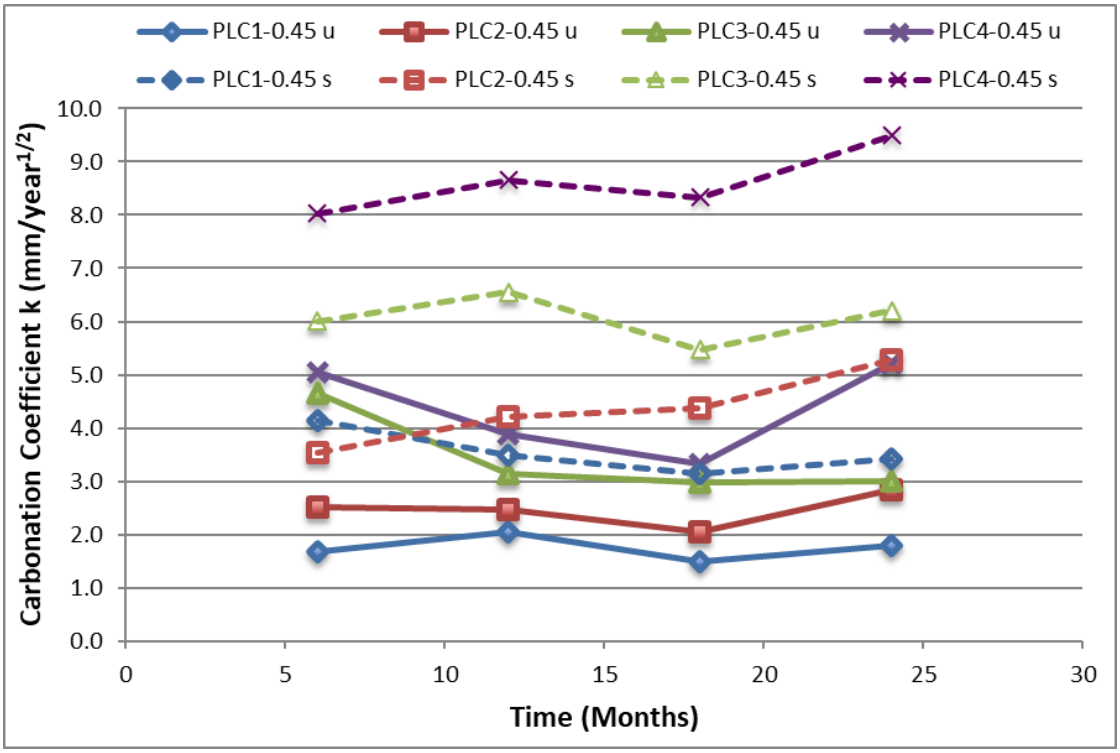

Figure 8.11: Carbonation Coefficients vs. Time for PLC1-PLC4 Mixtures (Notes: "u"= unsheltered specimen and "s" = sheltered specimen; 25.4 mm = 1 in.)

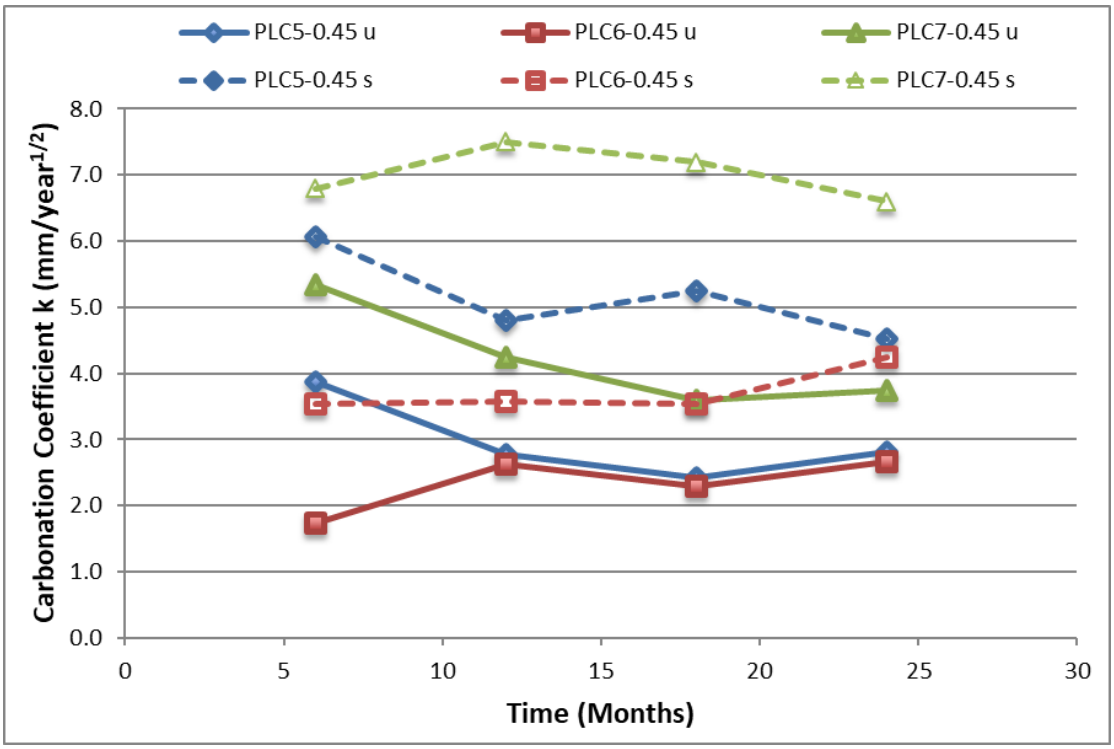

Figure 8.12: Carbonation Coefficients vs. Time for PLC5-PLC7 Mixtures (Notes: "u"= unsheltered specimen and "s" = sheltered specimen; 25.4 mm = 1 in.)

Perhaps the most important benefit of knowing the carbonation coefficient for a given concrete mixture is that it allows the prediction of time that it will take for the carbonation front to reach the steel reinforcement, which is useful for service-life modeling purposes. If Equation 8.6 is manipulated further, the time for the carbonation front to reach the steel reinforcement can be calculated using Equation 8.7.

$$t = (x/k)^2 \qquad \text{(Eq. 8.7)}$$

For the straight cement mixtures, the average k was calculated for each mixture for both the unsheltered and sheltered conditions. Using this average carbonated coefficient, the time for the carbonation depth to be equal to 38.1 mm (1.5 in.) was calculated for all mixtures. The 38.1 mm threshold was chosen because this is a commonly specified steel reinforcement cover for reinforced concrete design (ACI 318, 2014). As discussed in section 8.2.1, once the carbonation depth reaches the steel reinforcement, the protective layer that protects the reinforcement will be destroyed, and the probability of corrosion will increase substantially.

Table 8.3 shows the time, in years, that it would take for the carbonation front to reach the steel reinforcement assuming unsheltered conditions, i.e. a concrete sidewalk with no protection from the rain. Please note that for OPC concrete (PLC1 and PLC5), it could take over 150 years for

carbonation to become a concern. On the other hand, for the mixtures with significant limestone contents in the cement, the time would be closer to 80 years (PLC4 and PLC7).

Table 8.3: Time for Carbonation Front to Reach 38.1 mm (1.5 in.) Under Unsheltered Conditions (Note: 25.4 mm = 1in.)

Mixture ID	Average k (mm/year$^{1/2}$)	Time (years)
PLC1-0.45	1.8	469
PLC2-0.45	2.5	239
PLC3-0.45	3.4	122
PLC4-0.45	4.4	76
PLC5-0.45	3.0	164
PLC6-0.45	2.3	267
PLC7-0.45	4.2	81

Similarly, Table 8.4 shows the time that it would take for the carbonation front to reach the steel reinforcement assuming sheltered conditions, an example of which would be an interior bridge girder, where the bridge deck prevents the girder from being in direct contact with precipitation. In this case, the Type I/II cement mixture (PLC5) would potentially start experiencing corrosion issues in 55 years. For the cement with the highest limestone content, PLC4 (30.6% $CaCO_3$), corrosion could begin in as little as 20 years.

Table 8.4: Time for Carbonation Front to Reach 38.1 mm (1.5 in.) Under Sheltered Conditions (Note: 25.4 mm = 1in.)

Mixture ID	Average k (mm/year$^{1/2}$)	Time (years)
PLC1-0.45	3.6	115
PLC2-0.45	4.3	77
PLC3-0.45	6.1	40
PLC4-0.45	8.6	20
PLC5-0.45	5.2	55
PLC6-0.45	3.7	105
PLC7-0.45	7.0	29

8.6.2. Effect of w/cm

To study the effect of the water-to-cementitious materials ratio on carbonation of PLC concrete systems, PLC1, PLC4, PLC5, and PLC7 were used in mixtures at water-to-cementitious materials ratios of 0.40, 0.45, and 0.50. To date, the mixtures have only been exposed for 17 months, and thus only the six-month and twelve-month results are presented in this section.

Figures 8.13 and 8.14 show the carbonation depth for each of the mixtures after twelve months of exposure in the Austin exposure site under unsheltered and sheltered conditions, respectively. As expected, the depth of carbonation generally increases as the w/cm increases; the exception is the PLC5 mixture, which carbonates slightly more at w/cm equal to 0.45 than at 0.50 under both sheltered and unsheltered conditions. Further investigation is warranted for the PLC5 mixture.

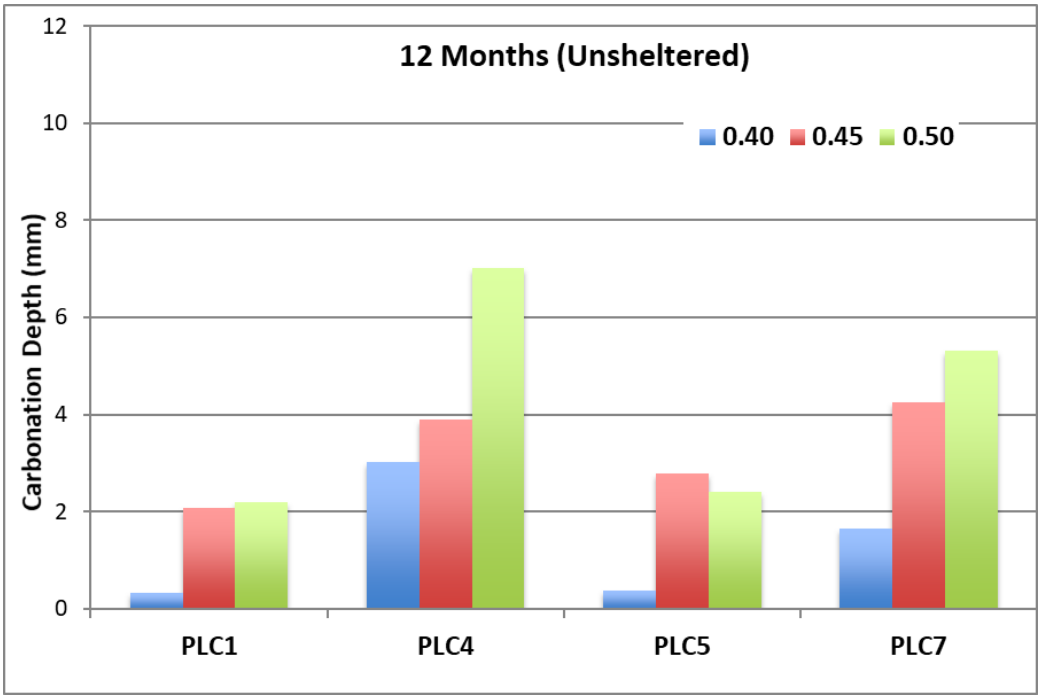

Figure 8.13: Carbonation Depth for Straight Cement Mixtures with Varying w/cm after 12 Months of Exposure under Unsheltered Condition

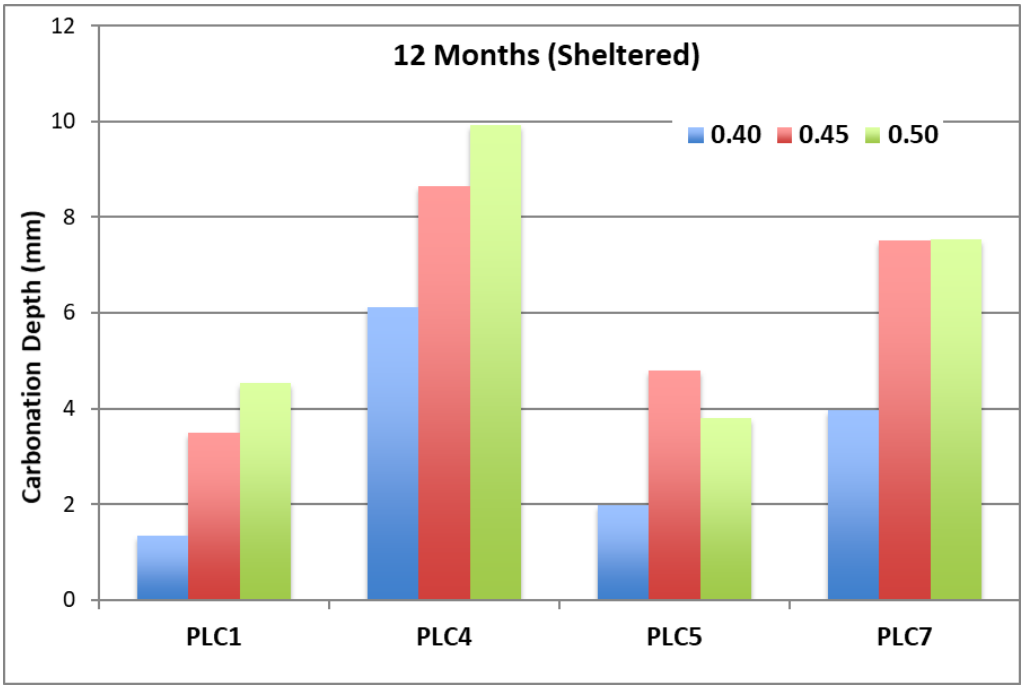

Figure 8.14: Carbonation Depth for Straight Cement Mixtures with Varying w/cm After 12 Months of Exposure under Sheltered Condition

The concept of an effective water-to-cementitious materials ratio was introduced in Chapter 3 and one of the conclusions for Chapter 3 states that the effective w/cm is a better indicator of compressive strength than the actual w/cm. Since carbonation depth is related to compressive strength, and compressive strength is related to the effective w/cm, the carbonation depth was plotted as a function of effective w/cm to verify if a correlation exists. The effective w/cm for these mixtures was calculated using Equation 8.2 and the results for the unsheltered and sheltered conditions are plotted in Figures 8.15 and 8.16.

There is a fairly strong linear relationship between carbonation depth and effective w/cm for both the unsheltered and sheltered conditions, evidenced by the high R^2 values obtained if linear regression trend lines are fitted to the data. It is worth noting that the correlation is stronger after twelve months of exposure than at six months.

The concept of an effective w/cm is evidence that equivalent carbonation resistance can be achieved for mixtures with high limestone content in the cement, provided that the actual w/cm is lowered. While lowering the w/cm may reduce the sustainability benefits of PLCs, the net impact on sustainability should still be positive compared to OPC, especially when considering the lower risk of carbonation-induced corrosion that is provided by lowering the w/cm.

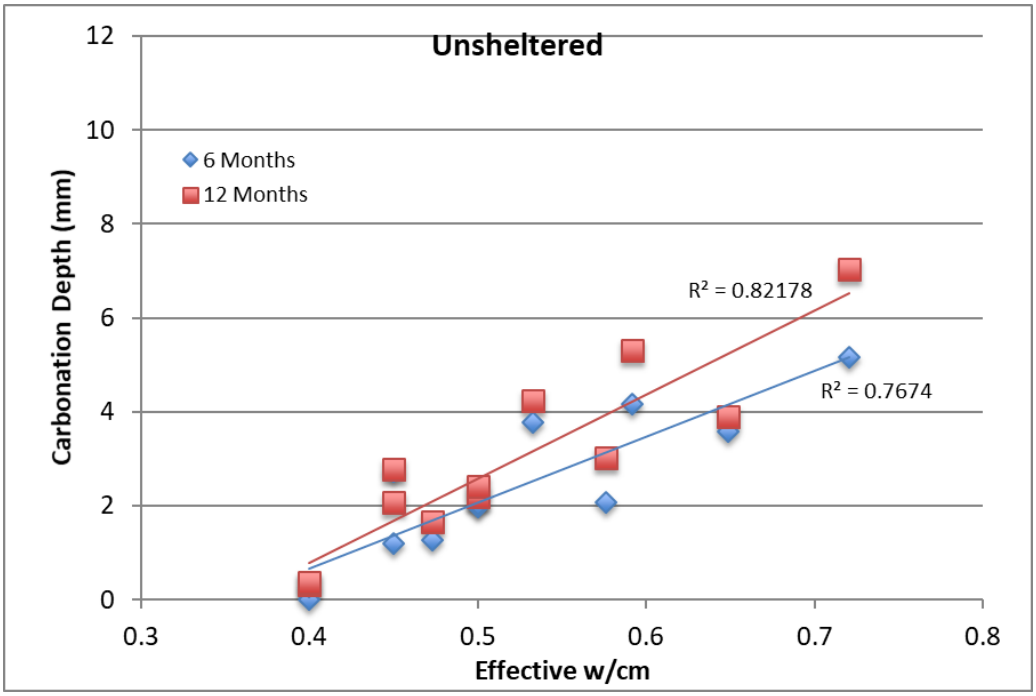

Figure 8.15: Carbonation Depth vs. Effective w/cm After 6 Months and 12 Months under Unsheltered Condition

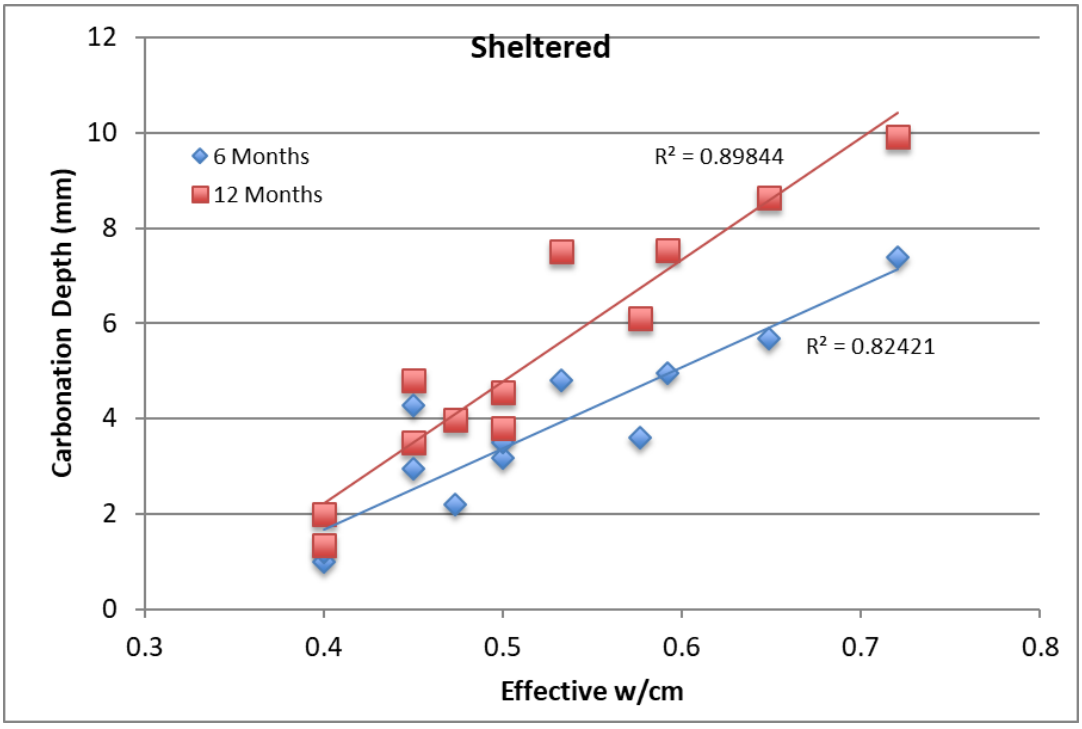

Figure 8.16: Carbonation Depth vs. Effective w/cm After 6 Months and 12 Months under Sheltered Condition

The average carbonation coefficient was calculated for each mixture in this section and the time for the carbonation front to reach 38.1 mm (1.5 in.) was obtained using the calculated carbonation coefficient. Table 8.5 shows the results for the unsheltered condition and Table 8.6 shows the results for the sheltered condition. Lowering the w/cm to 0.40 is very beneficial for all mixtures, but especially for the OPC mixtures (PLC1 and PLC5), in terms of maximizing the time before the carbonation front reaches the threshold value of 38.1 mm (1.5 in). On the other end of the spectrum, if the w/cm is raised to 0.50, the effect is very detrimental, particularly for the high limestone PLC mixtures. For example, the rate of carbonation for PLC4-0.50 is 9.9 mm/year$^{1/2}$, (0.39 in/year$^{1/2}$) resulting in the carbonation front reaching a depth of 38.1 mm in only 15 years.

Table 8.5: Time for Carbonation Front to Reach 38.1 mm (1.5 in.) Under Unsheltered Conditions (Note: 25.4 mm = 1in.)

Mixture ID	Average k (mm/year$^{1/2}$)	Time (years)
PLC1 (0.40)	0.3	14400
PLC1 (0.45)	1.8	469
PLC1 (0.50)	2.2	305
PLC4 (0.40)	3.0	160
PLC4 (0.45)	4.4	76
PLC4 (0.50)	7.0	29
PLC5 (0.40)	0.4	10212
PLC5 (0.45)	3.0	164
PLC5 (0.50)	2.4	252
PLC7 (0.40)	1.6	535
PLC7 (0.45)	4.2	81
PLC7 (0.50)	5.3	51

Table 8.6: Time for Carbonation Front to Reach 38.1 mm (1.5 in.) Under Sheltered Conditions (Note: 25.4 mm = 1in.)

Mixture ID	Average k (mm/year$^{1/2}$)	Time (years)
PLC1 (0.40)	1.3	797
PLC1 (0.45)	3.6	115
PLC1 (0.50)	4.5	70
PLC4 (0.40)	6.1	39
PLC4 (0.45)	8.6	20
PLC4 (0.50)	9.9	15
PLC5 (0.40)	2.0	369
PLC5 (0.45)	5.2	55
PLC5 (0.50)	3.8	100
PLC7 (0.40)	4.0	92
PLC7 (0.45)	7.0	29
PLC7 (0.50)	7.5	26

8.6.3. Effect of SCM Addition to High Limestone Content PLCs

Several concrete mixtures of portland limestone cements, combined with supplementary cementitious materials, were cast to evaluate the interaction of PLCs and SCMs and the effect they have on carbonation of these PLC systems. A constant w/cm of 0.45 was used for all of the mixtures with SCMs.

Figure 8.17 shows the carbonation depth after 12 months for the mixtures with PLC3 and PLC4 combined with different supplementary cementitious materials. It is not surprising that the addition of SCMs increases the rate of carbonation for PLC systems, since it is well established that SCM additions result in increased carbonation for OPC systems due to the pozzolanic reaction (Thomas & Matthews, 1992). Table 8.7 shows the ratio of carbonation depth normalized by the carbonation depth of the control mixture for the subset of mixtures shown in Figure 8.17. For example, the control mixture is PLC3-0.45, which has a carbonation depth of 6.5 mm for the unsheltered condition. PLC3-FAF1(20)-0.45 has a carbonation depth of 10.4 mm, resulting in a ratio of 1.59, which is obtained by dividing 10.4 mm by 6.5 mm. It can be seen that the addition of SCMs is more detrimental for the unsheltered condition than for the sheltered condition, doubling the carbonation rate for the majority of these mixtures under the unsheltered condition.

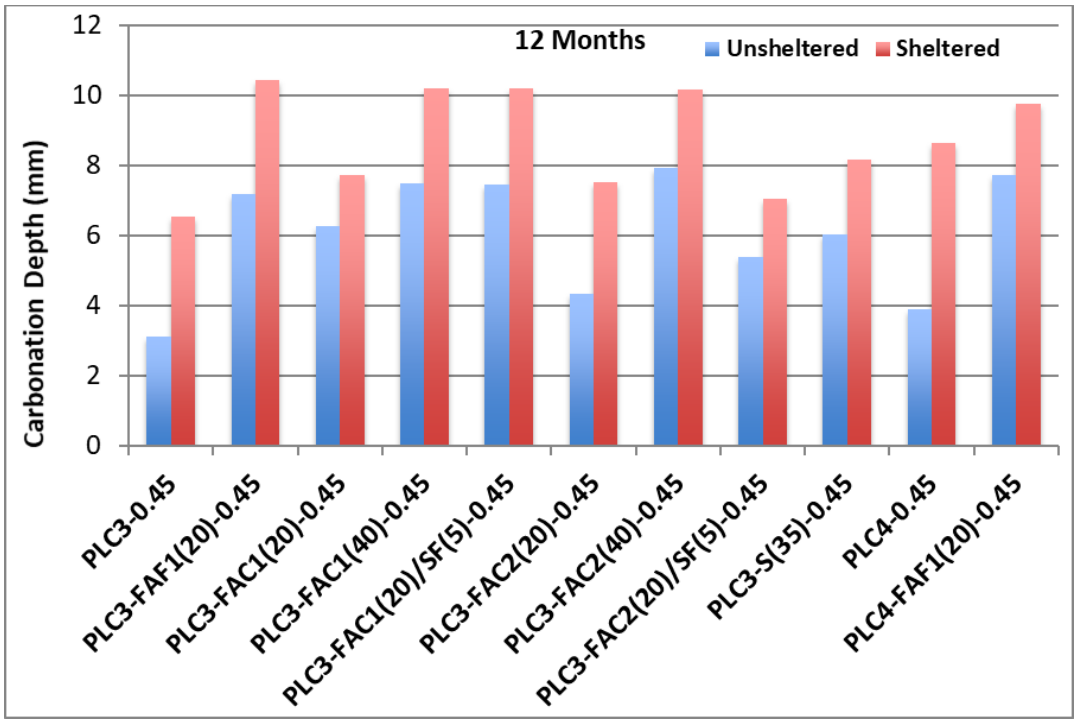

Figure 8.17: Carbonation Depth after 12 Months of Exposure for PLC3 and PLC4 in Combination with Different SCMs (Note 25.4 mm = 1 in.)

Table 8.7: Ratio of Carbonation Depth Normalized by Carbonation Depth of Control Mixture for PLC3 and PLC4 Mixtures

Mixture ID	Unsheltered	Sheltered
PLC3-0.45 (Control)	1.00	1.00
PLC3-FAF1(20)-0.45	2.29	1.59
PLC3-FAC1(20)-0.45	2.00	1.18
PLC3-FAC1(40)-0.45	2.39	1.56
PLC3-FAC1(20)/SF(5)-0.45	2.38	1.56
PLC3-FAC2(20)-0.45	1.38	1.15
PLC3-FAC2(40)-0.45	2.53	1.55
PLC3-FAC2(20)/SF(5)-0.45	1.72	1.08
PLC3-S(35)-0.45	1.92	1.25
PLC4-0.45 (Control)	1.00	1.00
PLC4-FAF1(20)-0.45	1.99	1.13

Figure 8.18 shows the carbonation depth after 12 months for the mixtures with PLC7 combined with different SCMs and Table 8.8 shows the ratio of carbonation depth normalized by the carbonation depth of the control mixture for these same mixtures. Combining SCMs with PLC7 does not have the same effect as combining SCMs with PLC3 or PLC4. While the carbonation depth did increase for some of the mixtures, the increase was not as drastic; the depth of carbonation even decreased for some of the mixtures.

These results are surprising and further investigation is required to determine why adding supplementary cementitious materials increased the carbonation resistance for some PLC7 mixtures, and not for PLC3 and PLC4.

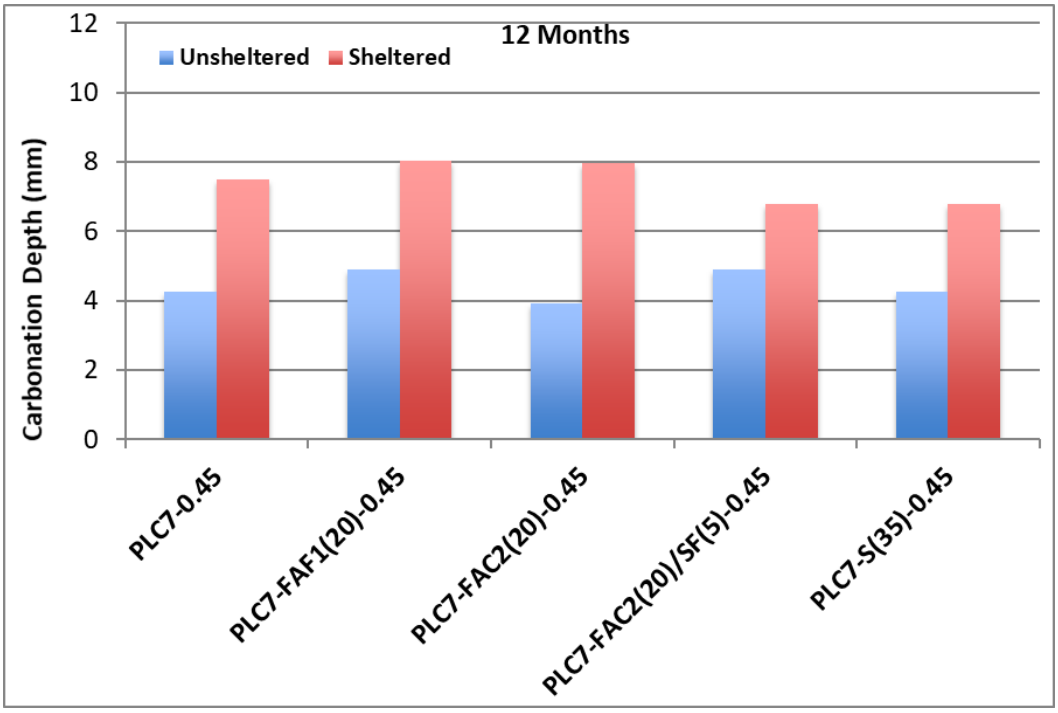

Figure 8.18: Carbonation Depth After 12 Months of Exposure for PLC7 in Combination with Different SCMs (Note 25.4 mm = 1 in.)

Table 8.8: Ratio of Carbonation Depth Normalized by Carbonation Depth of Control Mixture for PLC3 and PLC4 Mixtures

Mixture ID	Unsheltered	Sheltered
PLC7-0.45	1.00	1.00
PLC7-FAF1(20)-0.45	1.15	1.07
PLC7-FAC2(20)-0.45	0.93	1.06
PLC7-FAC2(20)/SF(5)-0.45	1.15	0.90
PLC7-S(35)-0.45	1.00	0.90

Figures 8.19 and 8.20 show the calculated carbonation coefficients plotted as a function of time for the PLC3 mixtures with SCMs under unsheltered and sheltered conditions, respectively. The carbonation coefficients appear to be decreasing and it will be interesting if the trend continues with increased exposure time.

Figure 8.21 shows the calculated carbonation coefficients plotted as a function of time for the PLC4 mixtures with SCMs and Figure 8.22 shows the plots for the PLC7 and SCM combinations.

Although there are a handful of exceptions, both of these figures show the same trend of decreasing carbonation coefficients as time increases.

Additional measurements are needed before concluding that adding SCMs results in the carbonation coefficient decreasing with time. As these specimens continue to be monitored in the future, it will be very interesting to see if the observed trend holds for these mixtures that combine high limestone content cements with supplementary cementitious materials, where the clinker and gypsum fraction of the powder materials is quite low—under 50% in some cases.

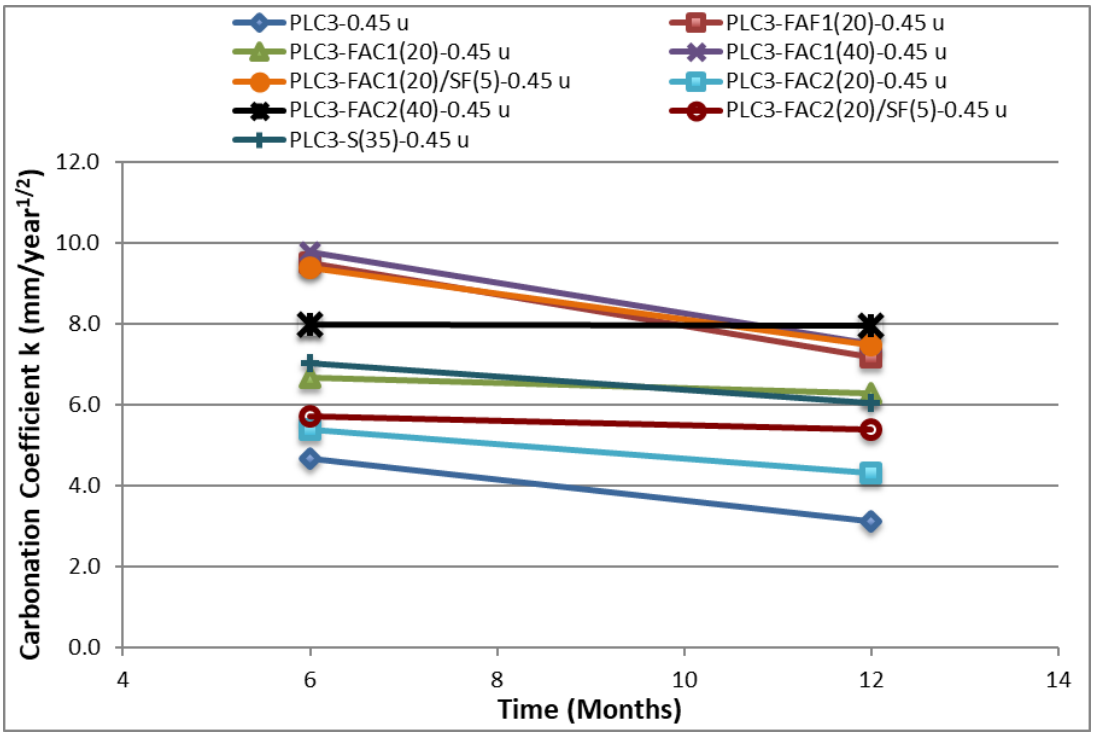

Figure 8.19: Carbonation Coefficients vs. Time for PLC3 Mixtures (Notes: "u"= unsheltered specimen; 25.4 mm = 1 in.)

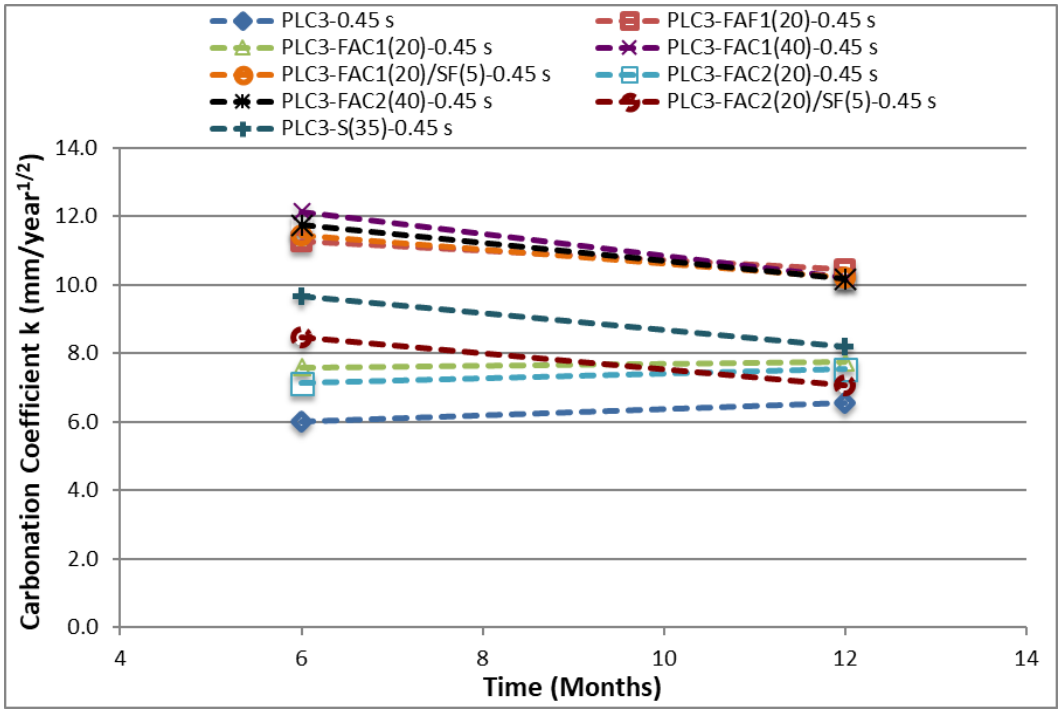

Figure 8.20: Carbonation Coefficients vs. Time for PLC3 Mixtures (Notes: "s" = sheltered specimen; 25.4 mm = 1 in.)

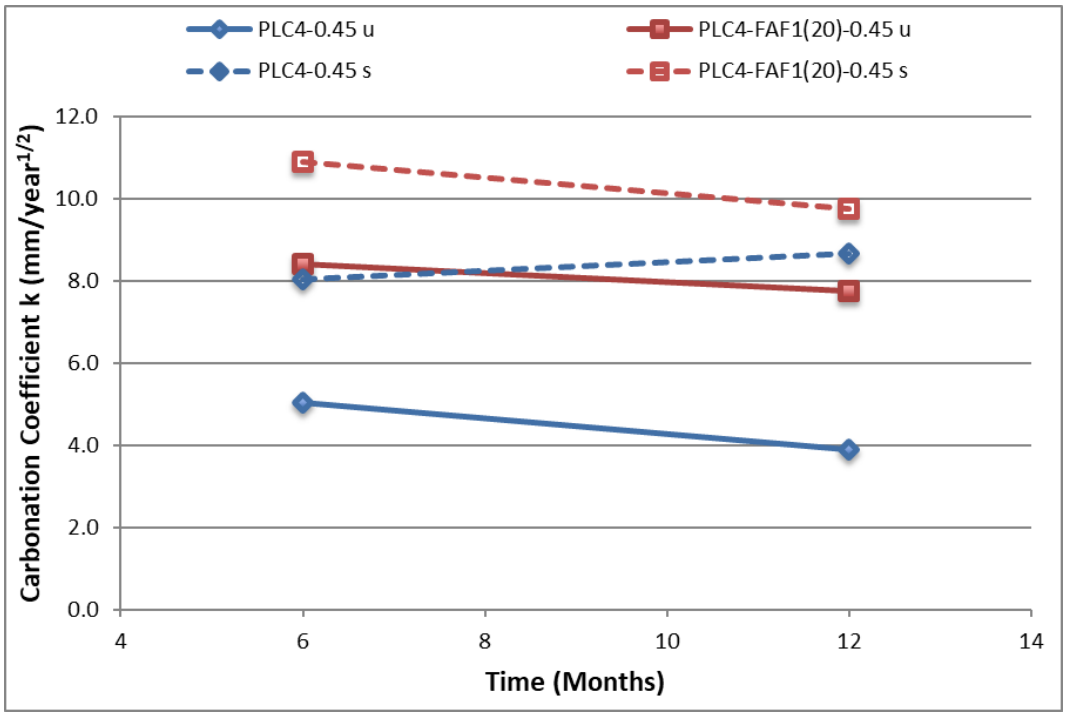

Figure 8.21: Carbonation Coefficients vs. Time for PLC4 Mixtures (Notes: "u"= unsheltered specimen and "s" = sheltered specimen; 25.4 mm = 1 in.)

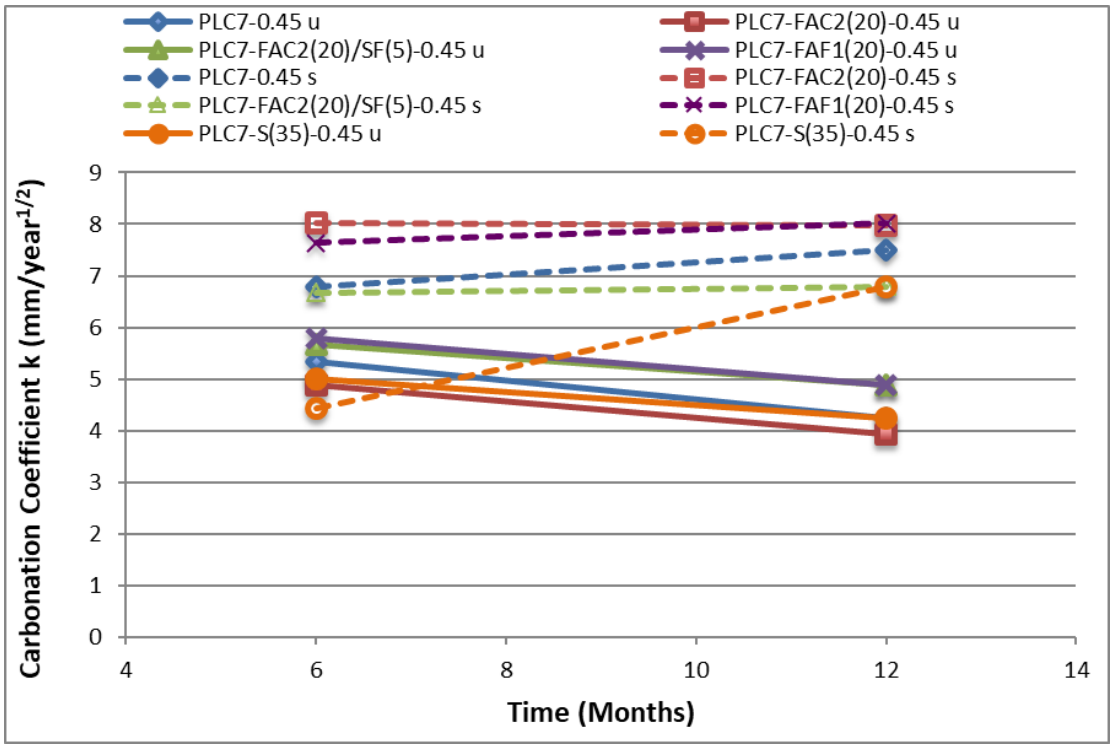

Figure 8.22: Carbonation Coefficients vs. Time for PLC7 Mixtures (Notes: "u"= unsheltered specimen and "s" = sheltered specimen; 25.4 mm = 1 in.)

8.6.4. Additional Exposure Sites

As alluded to earlier in this chapter, the 24-month measurements for the West Texas exposure site will take place after the completion of this Final Report and the results will not be included. For the Gulf Coast exposure site, it is impossible to compare carbonation depths at equivalent exposure times, since access to the exposure site is limited. To complicate things further, in August 2017 Hurricane Harvey caused severe damage to the exposure site and the majority of unsheltered specimens were either lost or unidentifiable. Luckily, the Stevenson Screen and the sheltered specimens weathered the storm and identification was possible. The limited results are presented in this section, and the surviving specimens will continue to be monitored in the future.

Figures 8.23 through 8.30 show the carbonation depth plotted as a function of time for different mixtures with and without SCMs. For each mixture, the measured carbonation depth for the sheltered and unsheltered specimens for the Austin and the Gulf Coast exposure sites are shown on the same plot for comparison. The solid lines represent the specimens from the Austin exposure site, while the dashed lines denote the Gulf Coast exposure site.

Please note that, for every single plot, the trends between the exposure sites are very similar, but the depth of carbonation for the specimens placed in the Gulf Coast is lower, meaning that the rate of carbonation is slower for the Gulf Coast specimens. These results are not unexpected and slower

carbonation rates measured at the Gulf Coast exposure site could be explained by the higher relative humidity that is typical of the region.

There is another plausible explanation for the increased carbonation resistance observed in the gulf coast specimens. When the specimens were placed in vacuum-sealed bags, to prevent carbonation while waiting to deliver the specimens to the exposure site, extended curing may have been provided inadvertently. Carbonation resistance has been reported to increase with extended curing (Thomas & Matthews, 1992).

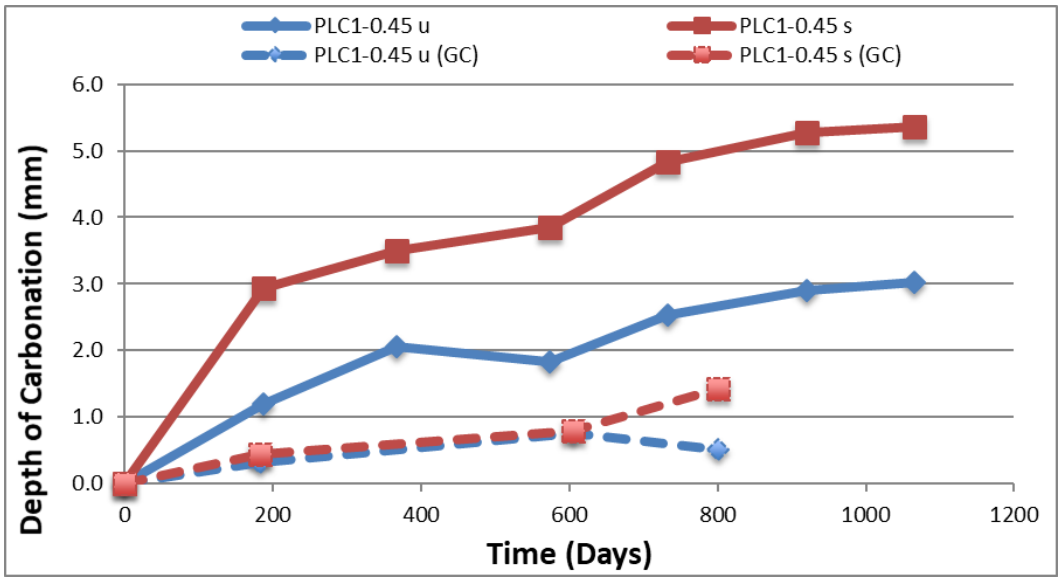

Figure 8.23: Carbonation Depth vs. Time for PLC1—Austin and Gulf Coast Exposure Sites (Note: 25.4 mm = 1 in.)

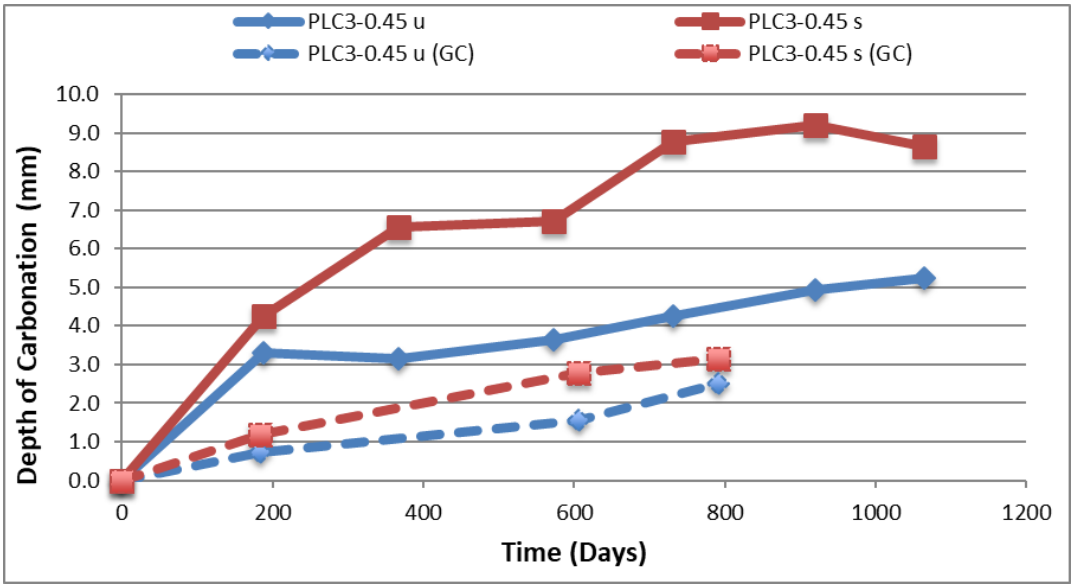

Figure 8.24: Carbonation Depth vs. Time for PLC3—Austin and Gulf Coast Exposure Sites (Note: 25.4 mm = 1 in.)

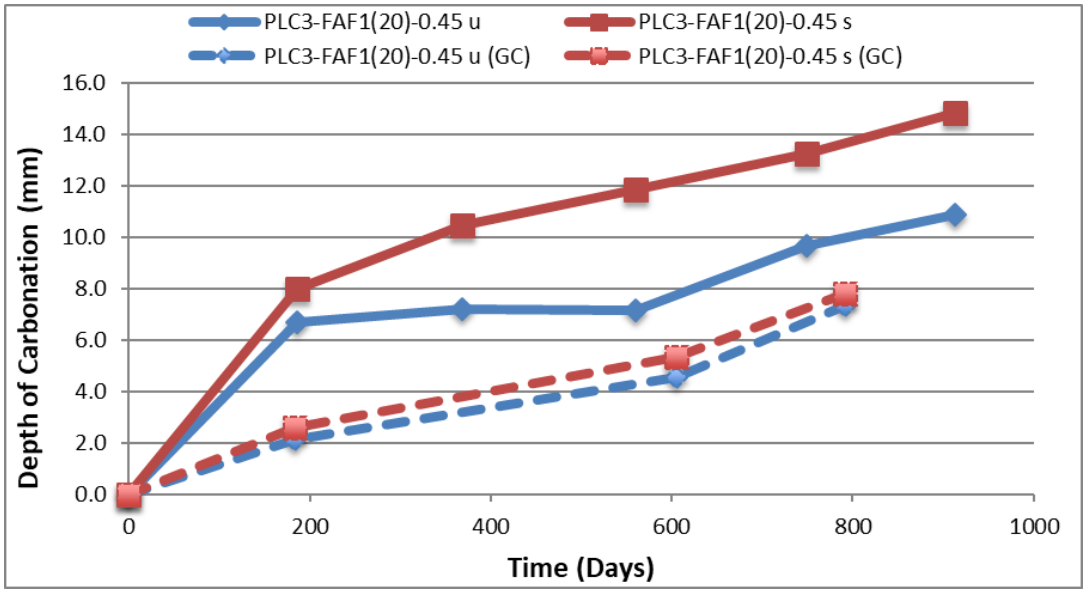

Figure 8.25: Carbonation Depth vs. Time for PLC3-FAF1(20)—Austin and Gulf Coast Exposure Sites (Note: 25.4 mm = 1 in.)

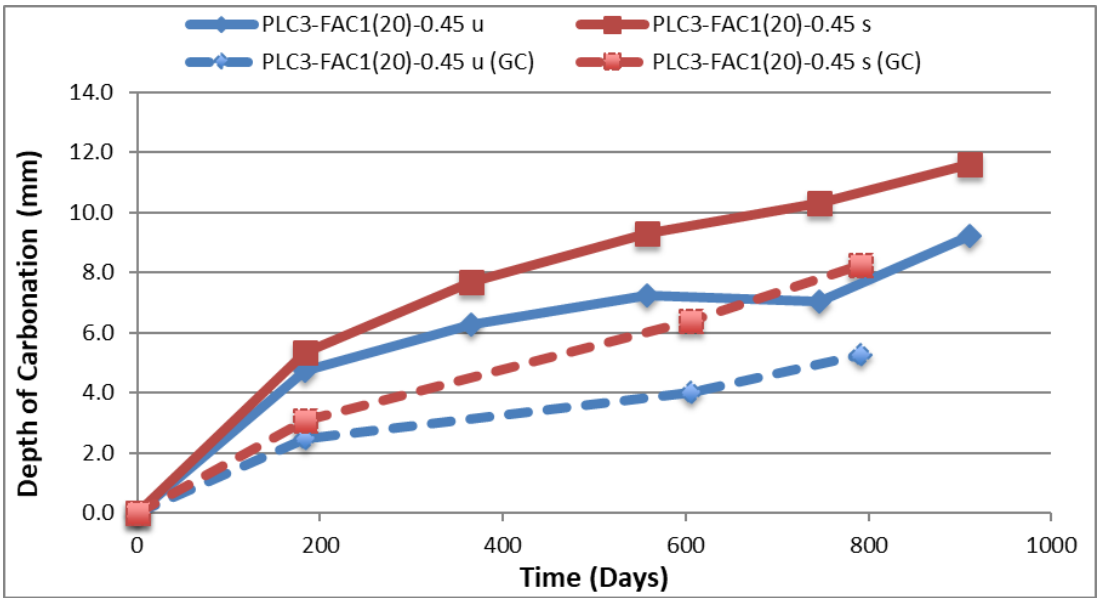

Figure 8.26: Carbonation Depth vs. Time for PLC3-FAC1(20)—Austin and Gulf Coast Exposure Sites (Note: 25.4 mm = 1 in.)

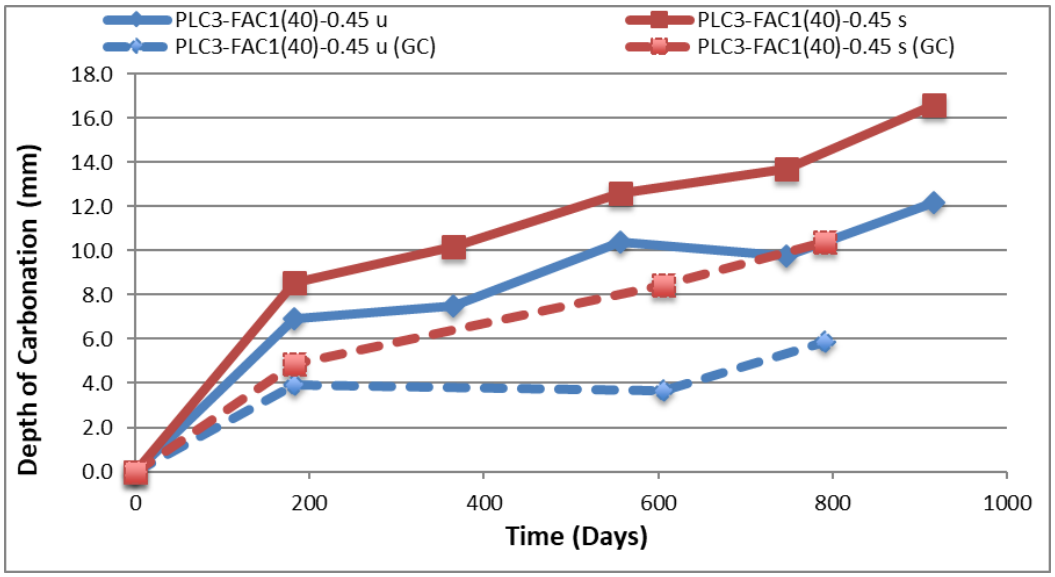

Figure 8.27: Carbonation Depth vs. Time for PLC3-FAC1(40)—Austin and Gulf Coast Exposure Sites (Note: 25.4 mm = 1 in.)

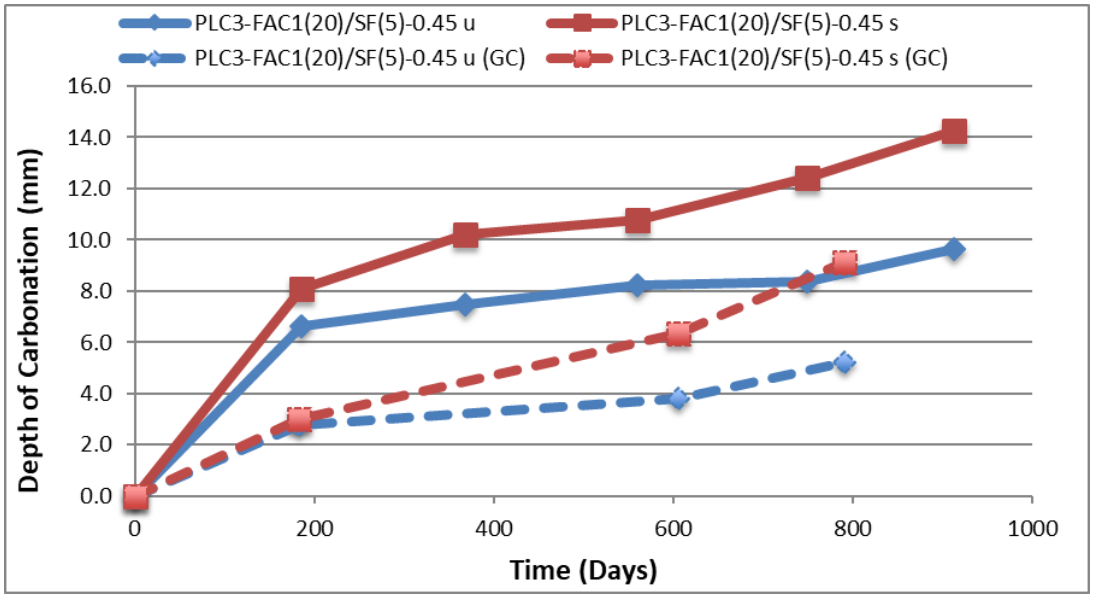

Figure 8.28: Carbonation Depth vs. Time for PLC3-FAC1(20)/SF(5)—Austin and Gulf Coast Exposure Sites (Note: 25.4 mm = 1 in.)

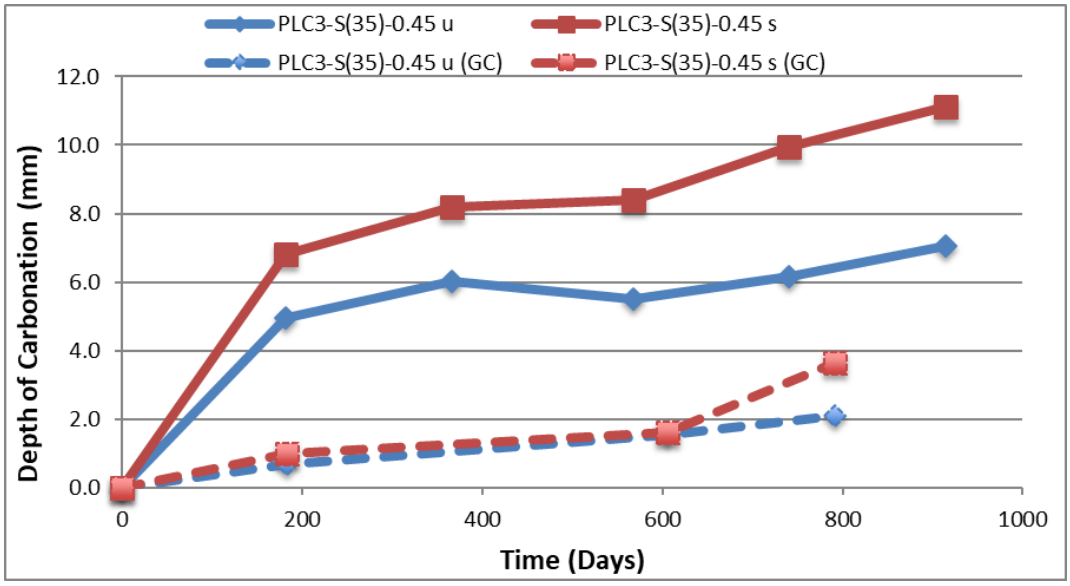

Figure 8.29: Carbonation Depth vs. Time for PLC3-S(35)—Austin and Gulf Coast Exposure Sites (Note: 25.4 mm = 1 in.)

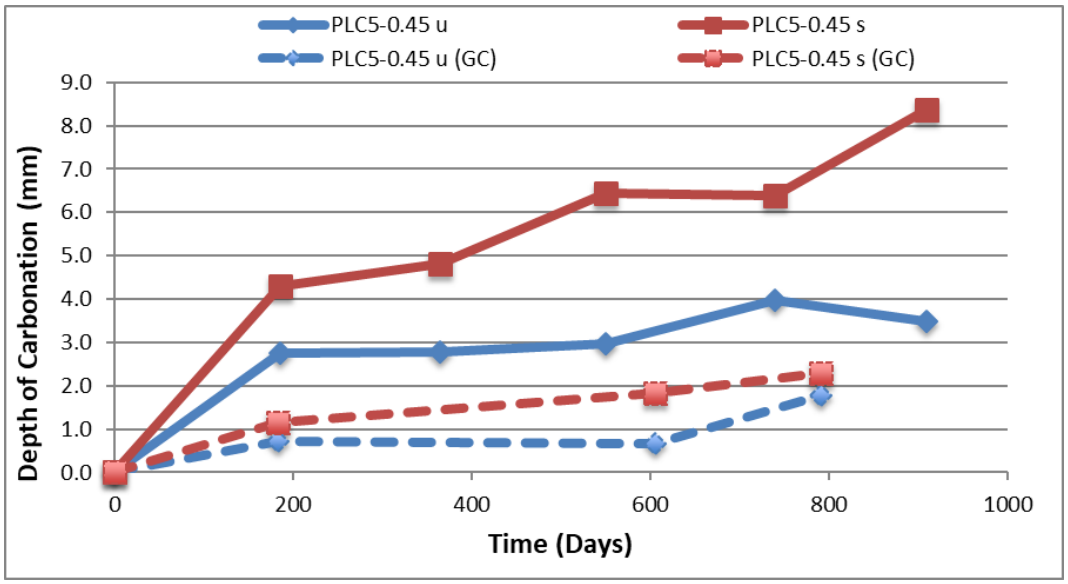

Figure 8.30: Carbonation Depth vs. Time for PLC5—Austin and Gulf Coast Exposure Sites (Note: 25.4 mm = 1 in.)

8.7. Accelerated Carbonation of Portland Limestone Cement Concrete Systems

8.7.1. Development of Accelerated Carbonation Chamber

As detailed in earlier sections of this chapter, natural carbonation testing of concrete can take several years to complete, especially for ordinary portland cement concrete without the incorporation of supplementary cementitious materials. A number of researchers have proposed the standardization an accelerated carbonation testing procedure that would provide results in months, or even weeks, that can be correlated to long-term natural carbonation testing. Calibration of the accelerated testing method would, in theory, be possible by comparing the results of accelerated carbonation to the wealth of data that has been generated on natural carbonation.

Under the guidance of researchers at the University of New Brunswick, an accelerated carbonation chamber was developed at UT Austin. A schematic showing the accelerated carbonation chamber and all of the necessary components can be seen in Figure 8.31 and a picture of the chamber is shown in Figure 8.32. A carbon dioxide concentration of 4%, which is about 100 times higher than the CO_2 concentration in air, was chosen for this investigation based on the recommendation from Dr. Michael Thomas at the University of New Brunswick.

The accelerated carbonation chamber consists of a sealed plastic tank with a removable lid to allow for the placement and removal of test specimens. A carbon dioxide tank supplies the CO_2 gas via plastic tubing. A circulation fan inside of the chamber promotes homogeneous exposure conditions

to all specimens inside of the chamber. The chamber is kept at a temperature of 23 +/- 2 ^{o}C (73 +/- 3 ^{o}F) and a relative humidity of 60 +/- 5% through the use of saturated calcium nitrate solution. A temperature and relative humidity sensor is located inside of the chamber is connected to a computer to log the recorded data. An ADC SB 2000 carbon dioxide chemical analyzer retrieves a sample of air from the chamber every five seconds, determines the carbon dioxide concentration and returns the air to the chamber. The chemical analyzer, which is connected to a computer and to a proportional-integral-derivative (PID) controller, communicates the carbon dioxide concentration to the computer and the PID controller. Based on the CO_2 concentration that was just received, the PID controller then decides how much to open or close a solenoid valve in order to reach and maintain a target concentration of 4%.

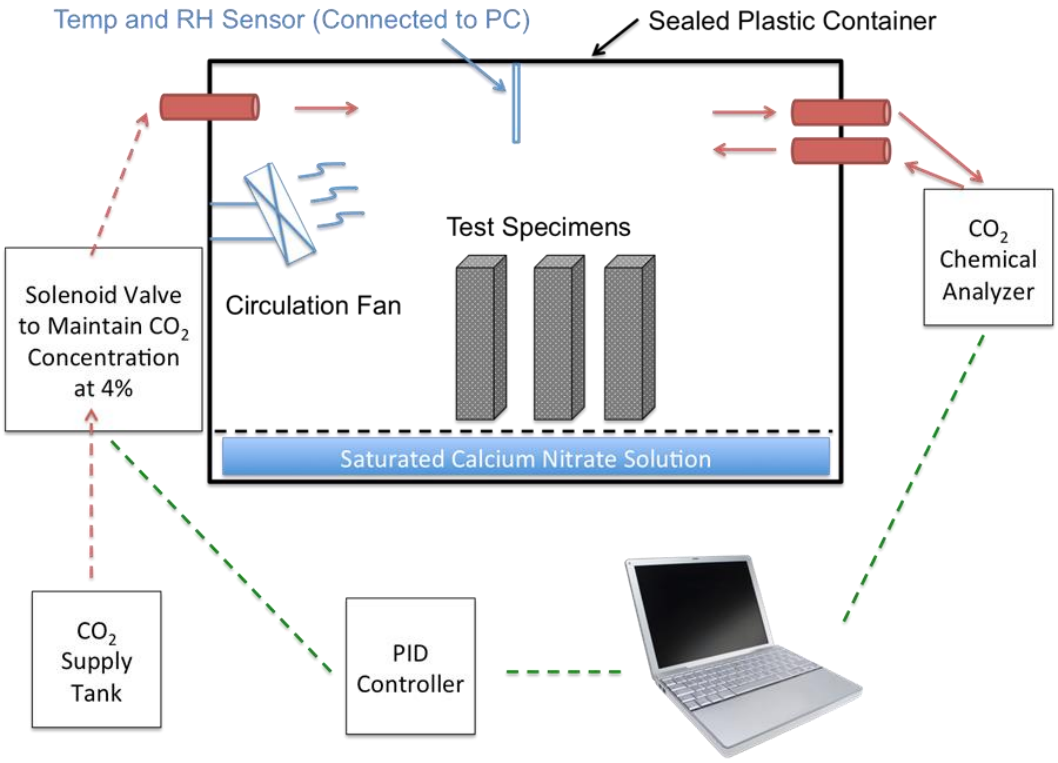

Figure 8.31: Schematic of Accelerated Carbonation Chamber

Figure 8.32: Picture of Accelerated Carbonation Chamber

8.7.2. Research Plan and Preliminary Results

8.7.2.1. Cement Paste Specimens

At the time that the accelerated carbonation chamber was completed, the research plan was to cast relatively small cement paste specimens to minimize the time to completely carbonate the specimens and the time required to obtain results. Eventually, mortar and concrete specimens would also be cast and tested.

Saturated limewater curing of 3, 7, and 28 days for different cement paste mixtures would be followed by a 3-day drying period at 23 ºC and 50% relative humidity before the specimens would be placed inside of the accelerated carbonation chamber. The plan was to conduct the following tests after 0, 7, 14, 28, 42, and 56 days of exposure:

- Compressive strength
- Flexural strength
- pH measurement
- Qualitative XRD analysis
- Carbonation depth

- Scanning electron microscopy (SEM)
- Pore structure analysis using solvent exchange or mercury intrusion porosimetry

Cement paste samples were chosen in an attempt to isolate the additional variability that is associated with aggregates, especially in the case of XRD analysis. The water-to-cementitious materials ratio was initially chosen as 0.45 since the same ratio was used for the natural carbonation specimens. 25 x 25 x 286 mm (1 x 1 x 11.25 in.) bars were cast to determine the flexural strength, measure the carbonation depth, pH, and to obtain XRD and SEM samples. 25 mm (1 in.) cubes were cast to determine the compressive strength of each mixture.

The fresh cement paste with a w/cm equal to 0.45 was very difficult to place and finish in a consistent manner, as an excess amount of water bled to the top of all specimens, especially as the limestone content increased. The addition of limestone has been reported to reduce the water demand in some cases and increase the water demand in other cases (Tennis et al., 2011). The cements used in this investigation all led to a reduction in water demand. The inconsistent placing and finishing resulted in very erratic results. The high w/cm also resulted in very weak paste specimens, where the flexural strength could barely be measured. Flexural strength testing was abandoned at this point.

After several trial mixes, the research team decided to lower the w/cm to 0.35, and the result was very beneficial in terms of placement and finishing of the specimens. Several mixtures were cast and cured for 28 days before the rest of the mixtures in the test matrix were cast and cured for 7 days. After removing the specimens from the limewater solution at the end of the curing period, they were placed in a drying environment for three days before they were tested. When measuring the depth of carbonation at 0 days, to establish a baseline before exposure to the accelerated carbonation chamber, the research team noticed longitudinal and transversal hairline cracks on the specimens. The variability in compressive strength measurements was also quite high.

After 7 and 14 days of exposure to 4% CO_2 in the carbonation chamber, the specimens were taken out of the chamber and it was obvious that the cracks were growing slowly but noticeably. When sprayed with phenolphthalein, he depth of carbonation was much greater around cracks and it was impossible to obtain consistent depth of carbonation measurements even when obtaining different samples from the same bar.

The research team attributed the cracks to drying of the cement paste, which is known to be very unstable volumetrically. Therefore, it was decided to keep measuring the cement paste samples, with the understanding that inconsistent results may be obtained. The results of the limited amount of cement paste specimens that were tested are currently being analyzed and may be published after the completion of this Final Report.

8.7.2.2. Mortar Specimens

Since mortar specimens should be more stable volumetrically, mortar specimens of the same size were cast using graded Ottawa sand. The drying cracks have not been observed for the mortar specimens and testing is currently underway. The accelerated carbonation test matrix of mortar specimens can be seen in Table 8.9. Unfortunately, the results are not available at this time. The results from the accelerated carbonation of mortar specimens will be published at a later date.

Table 8.9: Test Matrix for Accelerated Carbonation of Mortar Specimens

Mixture ID
PLC1-0.45
PLC2-0.45
PLC3-0.45
PLC4-0.45
PLC2-0.40
PLC3-0.36
PLC4-0.32
PLC1-S(35)-0.45
PLC3-S(35)-0.45
PLC4-FAF1(20)-0.45
PLC4-FAC2(20)-0.45
PLC4-FAC2(40)-0.45

8.7.2.3. Concrete Specimens

Although the testing of concrete specimens subjected to accelerated carbonation was planned for a future phase of the project, two mixtures were cast and exposed to natural carbonation and accelerated carbonation as a trial. Using the same mixture proportions presented in Figure 8.33, mixtures PLC1-0.45 and PLC3-0.36 were cast. The w/cm used for PLC3-0.36 was purposefully chosen so that both mixtures would have the same effective w/cm and thus, the carbonation depth would be expected to be similar.

Two 100 x 100 x 350 mm (4 x 4 x 14 in.) specimens for natural outdoor carbonation and two 75 x 75 x 286 mm (1 x 1 11.25 in.) for accelerated carbonation testing were cast from each mixture. The natural carbonation specimens were tested every two months and the accelerated carbonation specimens were measured approximately every two weeks.

The results for the specimens exposed to natural outdoors carbonation is shown in Figure 8.34. Even though the effective water-to-cementitious materials ratios are equal for these two mixtures, the specimens made with PLC3-0.36 carbonate significantly more than PLC1-0.45. Further investigation is required to understand the discrepancy in carbonation resistance.

Figure 8.33 shows the accelerated and natural carbonation depths plotted as function of time for each mixture. The same trend, which is that PLC3-0.36 carbonates more than PLC1-0.45, is observed when the specimens are subjected to the 4% CO_2 concentration. Additionally, Figure 8.34 clearly demonstrates the benefit that accelerated carbonation testing provides. Our findings indicate that it takes PLC1-0.45 three years for the carbonation front to reach 5.5 mm. Under the accelerated carbonation exposure conditions, it only took approximately 45 days for the carbonation front to reach the same 5.5 mm threshold!

The accelerated carbonation test method is currently at the beginning stage and obviously extensive verification and calibration are needed before it can be used reliably to predict long-term carbonation performance. However, based on the preliminary results from the trial mixes, the method shows a lot of promise and significant research efforts should be devoted to its development and standardization.

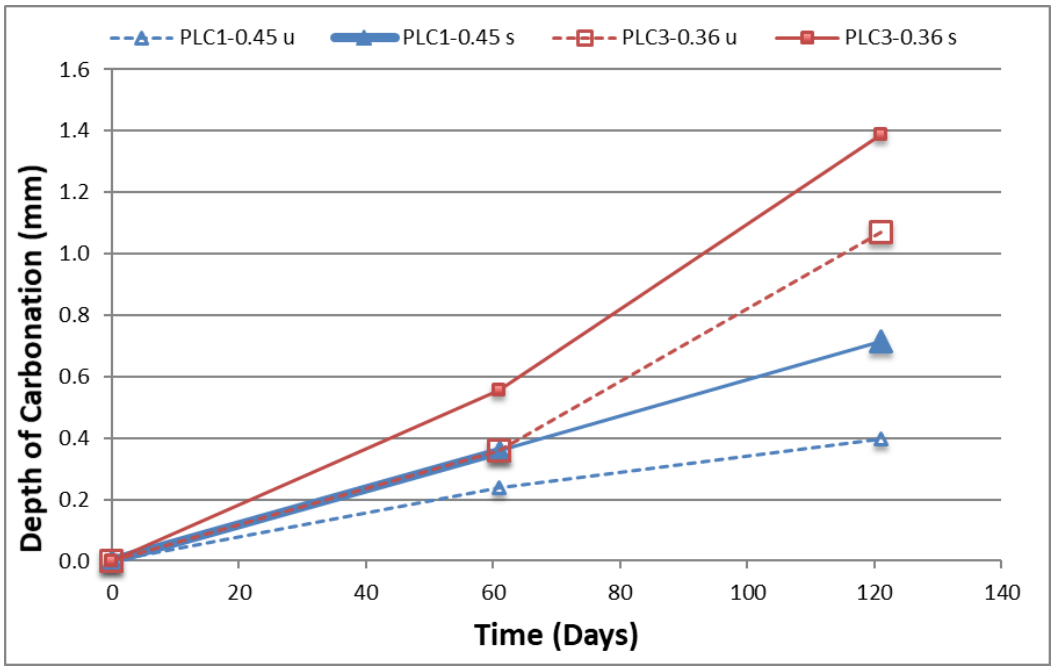

Figure 8.33: Natural Carbonation Depth vs. Time for PLC1-0.45 and PLC3-0.36 (Note: 25.4 mm = 1 in.)

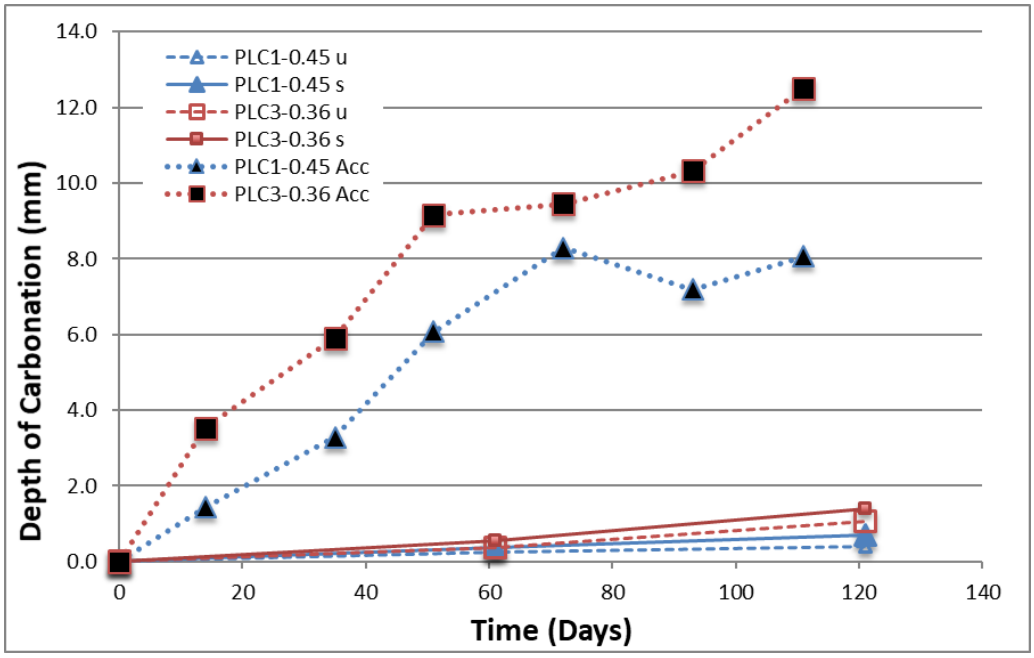

Figure 8.34: Natural Carbonation Depth and Accelerated Carbonation Depth vs. Time for PLC1-0.45 and PLC3-0.36 (Note: 25.4 mm = 1 in.)

8.8. Conclusions and Future Work

The results presented in this chapter are part of an investigation that will continue into the future, as it is not unusual for research on concrete carbonation to last several years. The main objective of this study was to investigate how the carbonation rates of portland limestone cement concrete systems are affected by increasing the limestone content in the cement beyond currently allowed limits, especially when in combination with supplementary cementitious materials, resulting in concrete with extremely low clinker content.

Several PLCs, with a wide range in limestone content, were combined with different SCMs, and the depth of carbonation at several ages was measured for each mixture. The effect of w/cm was also tested by changing the w/cm to 0.40 and 0.50 for a small subset of the evaluated mixtures. The carbonation coefficients and the approximate number of years for the carbonation front to reach an arbitrary value of 38.1 mm (1.5 in.) were also calculated for all mixtures.

The following conclusions are based on the results from the investigation presented in this chapter:

- The depth of carbonation increases as the limestone content increases for straight cement mixtures at constant w/cm.
- The depth of carbonation can increase significantly if SCMs are combined high limestone content PLCs as was observed for PLC3 and PLC4. However, further investigation in this

area is needed, since the combination of SCMs with PLC7 did not have a significant effect in terms of carbonation resistance.

- Effective w/cm can be useful in predicting the carbonation depth of straight cement mixtures with high limestone contents. Further work is needed to extend the concept of effective w/cm to mixes that combine PLCs and SCMs and verify that the concept is still valid.
- It is inconclusive if the carbonation coefficient changes with time for straight cement mixtures and further research is needed.
- It appears that the carbonation coefficient generally decreases with time for PLC systems with SCMs, but the specimens need to continue to be monitored to confirm this is the case.
- The time that it takes for the carbonation front to reach an arbitrary threshold is severely impacted by the following factors:
    - Limestone content of the cement
    - SCM content as a replacement of cement
    - w/cm
    - Exposure conditions (sheltered vs. unsheltered, relative humidity, temperature)
- When compared to the Austin exposure site, the specimens placed in the Gulf Coast exposure site are carbonating at a slower rate, but the same trends are observed.
- The accelerated carbonation chamber shows potential and further research and resources should be dedicated into developing a test method that can predict long-term carbonation performance in a reasonable amount of time.

The specimens will continue to be monitored in the future to validate the preliminary conclusions presented in this section. The depth of carbonation will be measured for the specimens placed in the West Texas exposure site and it will be interesting to see the results, given the extremely low relative humidity that is associated with the region.

Chapter 9. Sulfate Resistance of Portland-Limestone Cement Blended Systems. Part I: Accelerated Mortar Testing

9.1. Introduction

The introduction of limestone as a replacement of portland cement clinker at levels ranging from 5 to 35% has been allowed in many countries for decades [Tennis 2011]. The increased interest in portland limestone cements (PLCs) since their introduction in Europe has been fueled by the need to reduce the environmental impact related to cement production. Although both the use of PLCs and the limestone content in these cements have increased in most regions since the 1990's [WBCSD 2016][CEMBUREAU 2013], their application and validation in North America has been much more limited. Limestone contents up to 5% were initially allowed in ASTM C150 in 2004 [ASTM Standard C150-04] and in CSA A3001 in 2006 [CSA A3000-13]. This maximum amount was subsequently raised to 15% in 2008 in the Canadian standard and in 2012 in ASTM C595 [ASTM Standard C595-12] as extensive research has shown that PLCs containing up to 15% limestone can achieve equivalent performance to ordinary portland cement (OPC) systems when properly optimized [Tennis 2011][Thomas 2010][Hawkins 2003][Cost 2013][Irassar 2009]. This result is explained by the significant impact of the interground limestone on the fresh and hardened properties of the cementitious system, which occurs by both physical and chemical means.

The physical presence of limestone particles has a profound effect on the hydration reactions. On the one hand, the increase in the w/clinker ratio increases the available space for the precipitation of hydration products, which can result in a higher degree of hydration [Scrivener 2015]. In addition, Berodier and Scrivener [Berodier 2014] showed that the presence of finely ground limestone increases the shearing between particles, which increases the number of C-S-H nucleation sites. They demonstrated the critical importance of the interparticle distance, which highlights the need to optimize the particle size distribution (PSD) of the system. Moreover, it was shown that C-S-H tends to nucleate preferentially on the surface of the limestone particles, which further accelerates hydration. The higher efficiency of limestone over other fillers in accelerating the hydration reactions has been reported by other researchers [Oey 2013].

In contrast to limestone-free cements, once gypsum has been depleted, the available alumina reacts with calcite to form hemi and monocarboaluminate instead of monosulfoaluminate. This indirectly stabilizes ettringite, which results in a relative increase in the volume of hydrates [Lothenbach 2008][Matschei 2007][De Weerdt 2011]. Perhaps more important in the context of this work, the stabilization of ettringite and the less-soluble and more thermodynamically stable carbonate-AFm phases increases the stability of the system upon exposure to external sulfates. Properly controlled intergrinding of limestone with portland cement clinker can produce a wider particle size

distribution of the PLC [Tsivilis 1999a], which, in spite of the increased surface area, can lower the water demand [Tsivilis 1999b][Voglis 2005]. At replacement levels up to about 15%, the improved particle packing together with the effects on hydration and the changes in the hydrated phase assemblage and microstructure can lead to a reduced or similar porosity to OPC [Tsivilis 2003][Moon 2017][Elgalhud 2016]. On the other hand, the incorporation of higher limestone contents, which dilutes the clinker fraction and increases the effective water-to-cement ratio, has been shown to lead to higher porosities and decreased strength [Schmidt 2009][Bonavetti 2003][Kumar 2013].

The increase in sulfate resistance obtained by replacing a fraction of portland cement with SCMs is a consequence of many effects, including calcium silicates and aluminates dilution, CH consumption, refinement and depercolation of the pore system, reduction of the pore solution equilibrium pH, and changes in the nature of the hydrates [Thomas 2011][Thomas 2013][Lothenbach 2011]. It has been shown that when alumina-containing SCMs are combined with cements incorporating limestone, synergistic reactions between these two components could result in increased bound water and reduced porosity. Thermodynamic calculations have indicated that the proportion and composition of AFt and AFm phases are a strong function of the SO_3/Al_2O_3 and CO_2/Al_2O_3 molar bulk ratios of the system [Matschei 2007][Matschei 2010]. In addition, the amount of reacted calcite and its dissolution rate are limited by the availability of alumina and by the rate of hemi and monocarbonate formation, respectively [Zajac 2014]. In this context, formation of carboaluminates can be enhanced by the inclusion of additional aluminates to the system, provided that enough calcite is available to react. Accordingly, the effects of limestone are amplified in blends with SCMs containing high amounts of alumina, such as fly ash [De Weerdt 2011a][De Weerdt 2011b], slag [Arora 2016][Menendez 2003], and metakaolin [Antoni 2012][Vance 2013].

A considerable amount of research has been conducted on the sulfate resistance of PLCs. As many detailed reviews have indicated, the incorporation of limestone in amounts greater than about 10-15% will generally worsen the performance of a neat cement, non-sulfate resistant system [Tennis 2011][Irassar 2009]. In addition, upon exposure to sulfate solutions at low temperatures, increasing limestone contents of non-sulfate resistant systems increase the severity of the thaumasite form of sulfate attack (TSA). However, recent testing has shown that when SCMs are incorporated at levels appropriate to mitigate sulfate attack based on standard ASTM C1012 limits, PLC blends with up to 15% limestone perform equivalently to OPC systems [Hooton 2016]. As it was shown that the modified version of ASTM C1012 conducted at 5ºC does not predict accurately the performance of PC-SCM and PLC-SCM concretes, the authors recommended that the standard ASTM C1012 procedure conducted at 23°C be used for determining the sulfate resistance of neat and blended systems. It was finally concluded that a blend designed to mitigate classic sulfate attack using this test method and meeting traditional expansion limits will also mitigate TSA.

The current work evaluates the sulfate resistance of mortars systems incorporating several SCMs in combination with cements with different C_3A levels and interground limestone contents ranging from 3.2% to 30.6%. Based on the reported synergies between limestone and alumina-rich SCMs and the potential for further reducing the carbon footprint associated with cement production and use, this study aims to determine if blends with higher limestone levels can provide acceptable performance in sulfate exposures. Expansion and visual examinations were combined with X-ray diffraction analyses to provide a detailed discussion of the mechanisms responsible for the observed behavior.

9.2. Materials and Methods

In this laboratory study, eight cements were tested. Limestone was interground at one plant with a high-C_3A clinker for the production of four cements, namely PLC1, PLC2, PLC3, and PLC4, which have limestone contents of 3.2%, 13.4%, 21.0%, and 30.6%, respectively. Analogously, other three cements were produced at another plant by intergrinding limestone with a lower-C_3A clinker, and have limestone contents of 4.9%, 11.6%, and 15.5%, namely PLC5, PLC6, and PLC7, respectively. In addition, an ASTM C150 Type V cement from an additional plant was used. Moreover, several supplementary cementing materials (SCMs) were selected as partial replacement of the cements: one Class F and two class C fly ashes, silica fume, and slag. Table 9.1 shows the chemical composition of the cements and SCMs. Figure 9.1 shows the particle size distribution of the PLC1 to PLC7 cements.

Table 9.1: Chemical Composition of the Cements and SCMs

	PLC1	PLC2	PLC3	PLC4	PLC5	PLC6	PLC7	Type V	FA-F	FA-C1	FA-C2	Slag	SF
Chemical analysis [%]													
SiO_2	19.8	18.6	18.1	16.9	19.9	19.0	19.5	20.6	53.2	38.6	32.4	36.1	97.2
Al_2O_3	5.5	5.2	4.7	4.7	4.7	4.6	5.0	3.8	18.0	18.3	17.3	8.0	0.3
Fe_2O_3	2.0	1.8	1.7	1.5	3.3	3.3	3.3	3.7	8.1	5.4	6.1	0.6	0.1
CaO	64.8	66.4	67.1	68.1	64.8	65.7	64.8	62.2	10.8	22.6	27.7	39.8	0.9
MgO	1.1	1.1	1.0	1.2	0.8	0.8	0.8	4.6	2.4	4.8	5.3	10.7	0.3
Na_2O	0.1	0.1	0.1	0.1	0.1	0.1	0.1	0.3	0.3	1.2	1.6	0.3	0.1
K_2O	0.6	0.5	0.6	0.4	0.6	0.7	0.6	0.3	1.1	0.7	0.3	0.5	0.7
SO_3	4.1	4.2	4.6	4.7	3.8	3.8	3.9	3.0	0.5	1.8	2.5	2.6	0.2
LOI	1.4	5.9	9.2	13.4	2.2	5.1	6.8	1.3					
$CaCO_3$	3.2	13.4	21.0	30.6	4.9	11.6	15.5	2.9					
Blaine Fineness (m^2/kg)	375	428	458	516	-	-	-	366					
Cement phase composition (%)—Rietveld analysis													
C_4AF	3.5	3.1	2.0	3.0	7.3	8.1	4.6	8.9					
C_3A	9.2	7.6	6.5	6.0	4.2	2.9	3.8	3.0					
C_3S	47.8	44.9	41.1	34.2	47.9	46.5	35.1	57.9					
C_2S	20.9	16.8	17.8	13.6	22.4	28.7	24.6	13.5					
$CaCO_3$	5.2	13.9	24.8	30.3	1.8	12	14.1	2.8					

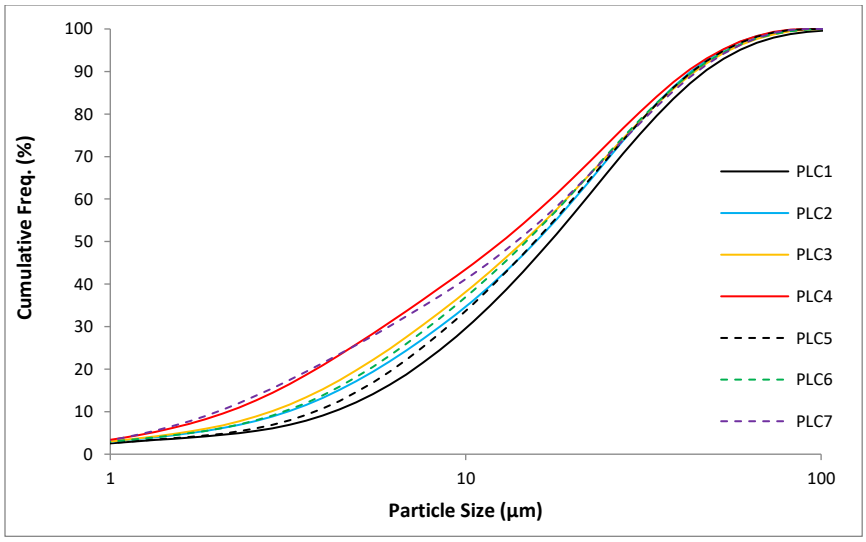

Figure 9.1: Particle Size Distribution of the PLC1 to PLC7 Cements

Mortar bars were cast according to ASTM C1012 using a sand to cementitious material ratio of 2.75 and keeping a constant water to cementitious material ratio (w/cm) of 0.485. For each mix, 6 bars (25 × 25 × 285 mm) and 9-to-12 cubes (50 x 50 mm) were prepared and stored above water in sealed containers at 35°C. After 24 hours, the specimens were demolded and stored in limewater at 23°C until the strength of the companion cubes reached 20 ± 1 MPa. At that time, the bars were measured to record their initial length and mass and stored in the sulfate solution at 23°C. Length and mass changes were calculated as the average of 5 bars after 7, 14, 21, 28, 56, 91, 105, 120, 180 days, and every 3 months thereafter. The sulfate solution was renewed after each measurement. The sixth bar was used to obtain samples for XRD examination at different exposure times. Following the same process, additional mortar bars were exposed to the sulfate solution at 5°C. In this case, after the companion cubes reached 20 ± 1 MPa, the bars were transferred to a refrigerator set at the specified temperature and kept there for a period of 24 hours, after which the bars were measured and stored in the sulfate solution.

At specific exposure times, samples of the bars were obtained and examined with X-ray diffraction (XRD). Samples were collected, finely ground below 105 µm, and analyzed on a Siemens D500 diffractometer with a DacoMP controller operating at 40 kV and 30 mA using a copper target (Cu Kα wavelength = 1.54Å). Scans were run from 5-60° 2θ with a step size of 0.02° and a dwell time of 4 seconds.

Pore size distributions of paste samples were obtained by mercury intrusion porosimetry (MIP). Thin slices (around 2-mm thick) were cut from the paste specimens (w/cm of 0.485) and their hydration was stopped by immersion in isopropanol for 4 days, renewing the solvent periodically. The slices were subsequently stored for 3 days in a desiccator, and cut into 5 pieces of similar size to a total sample weight of approximately 1 g. A Thermo Fisher Pascal 140/440 apparatus was used. The samples were intruded progressively up to a pressure of 100 kPa in the Pascal 140 unit

and then moved to the high-pressure unit, were mercury was pressurized to a maximum value of 400 MPa.

9.3. Results and Discussion

9.3.1. Pore Size Distribution—Influence of Limestone Replacement Level

Figure 9.2 (a) shows the pore size distributions of PLC1, PLC2, PLC3, and PLC4 paste samples obtained after the standard ASTM C1012 curing regime and after 14 days of extra curing in limewater at 23ºC (only for PLC1 and PLC3). The increase in the level of interground limestone in the PLCs increased both the initial total percolated pore volume and critical pore entry size (Figure 9.2 (b)). In this regard, it is interesting to note that, although the total connected pore volume increased almost linearly with the increase in limestone content, the critical pore size of the percolated porosity showed no significant change up to a replacement level of 13.4%. When the PLC1 and PLC3 samples were allowed to hydrate in limewater for 14 additional days, a reduction and refinement of the porosity was observed in both systems. These changes, especially the efficiency in refining the porosity, were significantly more pronounced in the mixture that incorporated the higher limestone content, which may be attributed to the increase in solid volume due to the stabilization of ettringite and the formation of hemi and monocarboaluminate [Lothenbach 2008][De Weerdt 2011a] beyond 1 day, as observed in the XRD analysis presented in Figure 9.3.

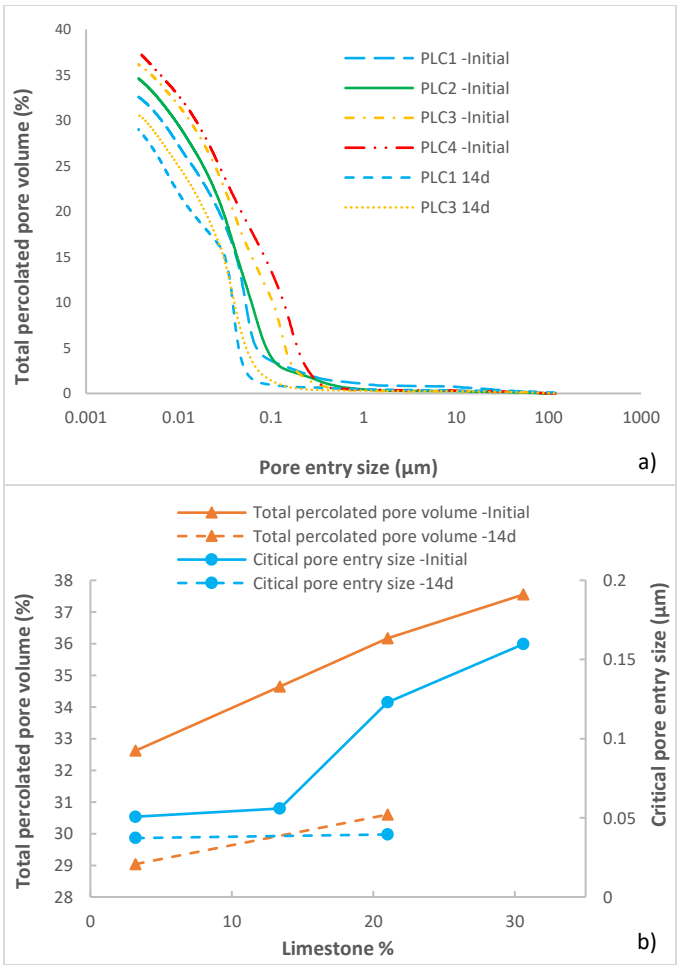

a) Pore size distributions obtained by MIP of PLC1, PLC2, PLC3, and PLC4 paste samples after the standard C1012 curing regime and after 14 days of extra curing in limewater at 23°C (only for PLC1 and PLC3), b) Total percolated pore volume and critical pore entry size as a function of limestone content.

Figure 9.2: Pore Size Distribution and Volume

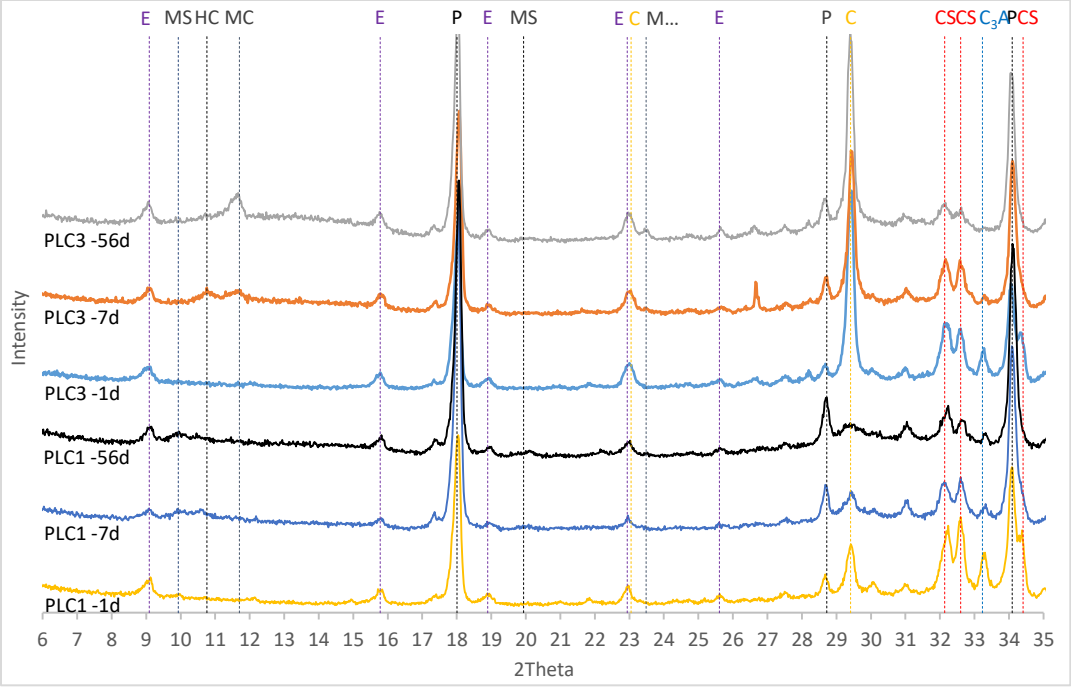

E= Ettringite, T= Thaumasite, MS= Monosulfoaluminate, HC= Hemicarboaluminate, G= Gypsum MC= Monocarboaluminate, P= Portlandite, Q= Quartz, C= Calcite, Ht= Hydrotalcite, CS= Calcium silicate, C_3A= Tricalcium aluminate, F= Ferrite.

Figure 9.3: XRD Patterns for PLC1 and PLC3 Paste Samples after 1, 7, and 56 Days of Hydration at 23°C.

9.3.2. Expansion in 5% Na_2SO_4 Solution

9.3.2.1. Straight Cement Mixtures

Figure 9.4 shows the length change measurements for PLC mortar samples stored in 5% sodium sulfate. The high-C_3A mixtures in all but one case showed an increase in the rate of expansion as the interground limestone level increased. The exception was the PLC2 mixture, which displayed a faster expansion than the PLC1 and PLC3 specimens. This result was surprising considering that the 13.4% limestone mixture showed a compressive strength development similar to the one exhibited by the PLC1 counterpart [Garcia 2018]. However, it highlights the idea that the sulfate resistance of PLC systems cannot be judged only on the basis of the limestone content, as the resistance to sulfate penetration [Irassar 2009][Schmidt 2009] and the chemical and mineralogical composition of the system [Hossack 2015][Irassar 2000] have a significant impact on the performance. In the case of the moderate-C_3A mortars, a significantly faster expansion was observed for the samples with the highest limestone content (PLC7) when compared to the PLC5 and PLC6 systems, both of which expanded at a much slower rate than the rest of the mixtures. In addition, no significant difference in performance was registered between these two systems and the reference Type V specimens.

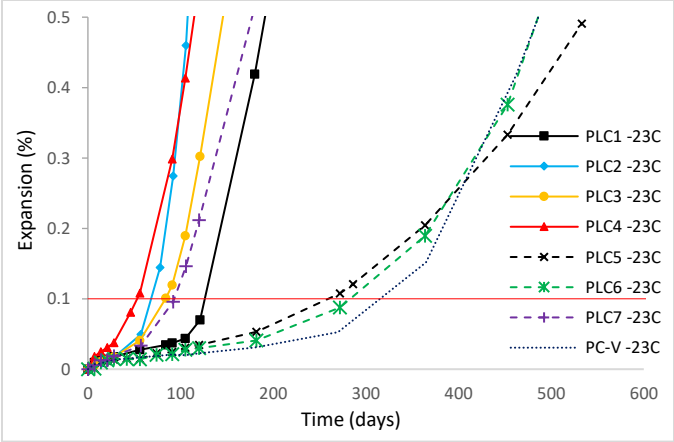

Figure 9.4: Length Change Measurements for PLC Mortar Samples Stored in 5% Sodium Sulfate

Figure 9.5 presents photographs of the high-C_3A mortar bars after different times of exposure to the sulfate solution. Although the first signs of corrosion were analogous to the ones observed in the lower-C_3A specimens (shown in Figure 9.6), the PLC1 and PLC2 mortars displayed a precipitous deterioration that started between 5 and 6 months in the case of the PLC1 mixture and between 4 and 5 months in the PLC2 system. As it is observed in Figure 9.5 (b) and (d), the PLC1 and PLC2 samples were completely disintegrated after 10.5 and 9 months, respectively. The increase in the limestone content, however, changed the damage pattern. Despite the significant expansion after 9 months of exposure, the PLC3 and PLC4 specimens showed moderate cracking at the ends and slight transversal cracks, as seen in Figure 9.5 (e) and (g). After 12 months, both mixtures showed wide cracks growing from severely warped surfaces, which opened up the structure and allowed the sulfate solution to reach the core of the samples. This difference in the rate of deterioration between the low and high-limestone systems, which resulted in a different damage pattern, will also be observed in all the mixtures that incorporated SCMs, which evidences a different mechanism of the attack.


a)
b)
c)
d)
e)
f)

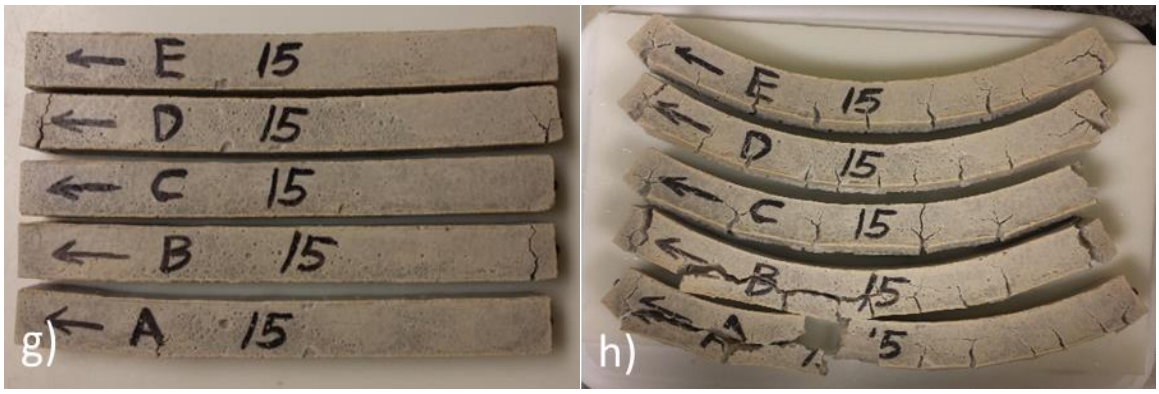

a) PLC1 after 7.5 months, b) PLC1 after 10.5 months, c) PLC2 after 5 months, d) PLC2 after 9 months, e) PLC3 after 9 months, f) PLC3 after 12 months, g) PLC4 after 9 months, h) PLC4 after 12 months.

Figure 9.5: High-C_3A Mortar Bars after Different Times of Exposure to the Sulfate Solution

The moderate-C_3A samples presented in Figure 9.6 exhibited a much less severe deterioration than the high-C_3A systems. After 18 months, the Type I/II cement (PLC5) specimens showed minor cracking localized at the ends of the bars and a slight warping. These damage manifestations were slightly more marked in the PLC6 mortars, which is consistent with the small differences in expansion. The PLC7 samples, however, displayed significantly more warping, which was accompanied by wide cracks along the surface. Nevertheless, even after this severe damage, the bars remained as one piece and no fragmentation was observed.

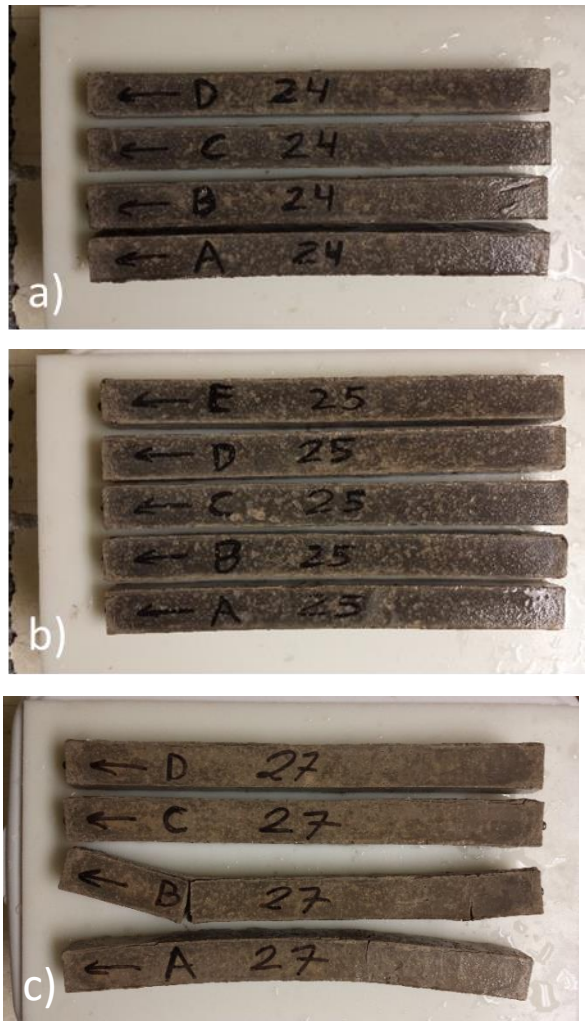

Figure 9.6: Moderate-C_3A Mortar Bars after 18 Months of Exposure to the Sulfate Solution. a) PLC5, b) PLC6, c) PLC7.

9.3.3. Class F Fly Ash Mixtures

The expansion curves for the mixtures that incorporated class F fly ash as cement replacement are presented in Figure 9.7. As expected, all fly ash systems showed an improvement in performance when compared to the control specimens, which agrees with previous laboratory results [Hossack 2015]. The increase in the limestone content changed the shape of the expansion curves to a more linear-like behavior, almost eliminating the induction period before the rapid expansion stage. This is believed to be related to the changes in the pore structure as the effective w/cm increased, which would allow a faster mass transport and decrease the potential for supersaturation and the pressure exerted upon ettringite precipitation [Scherer 1999][Scherer 2004][Flatt 2008]. In the high-C_3A clinker mortars, the reduction in the expansion rate with 20% fly ash incorporation was more pronounced in the two mixtures with the highest limestone content. Consequently, the PLC3 and

PLC4 systems showed a better performance than the lower limestone companion samples. This result may be explained by the well-documented synergy between limestone and alumina-containing SCMs discussed above [De Weerdt 2011a][De Weerdt 2011b]. Furthermore, the increase of the fly ash replacement level to 30% allowed both mixtures to satisfy the 18-month expansion requirement for the most severe exposure class (S3) in ACI 318-14.

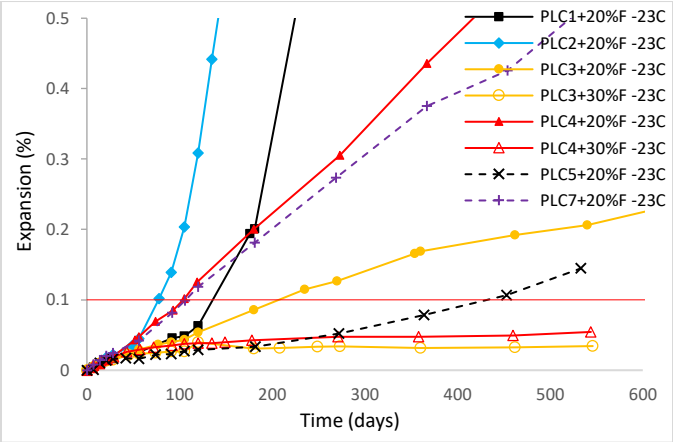

Figure 9.7: Expansion Curves for the Mixtures that incorporated Class F Fly Ash

The XRD plots of the high-C_3A mortar samples exposed to 5% sodium sulfate solution are shown in Figure 9.8. The obtained patterns represent the bulk crystalline assemblage of the whole cross section, as no separation was made between the surface and core regions, unless specified. Regardless of the limestone content, all systems showed ettringite formation starting on the surface region of the bars, as evidenced by the change in the relative intensity of the peaks corresponding to the AFm and AFt phases. In addition, gypsum formation and portlandite dissolution were detected in the outer regions of the mortars. The PLC3 and PLC4 systems with 30% fly ash, which showed negligible expansion after 18 months of testing, exhibited no signs of interaction with external sulfates in the core region of the specimens. These findings are supported by the absence of cracking or spalling at the surface of the bars.

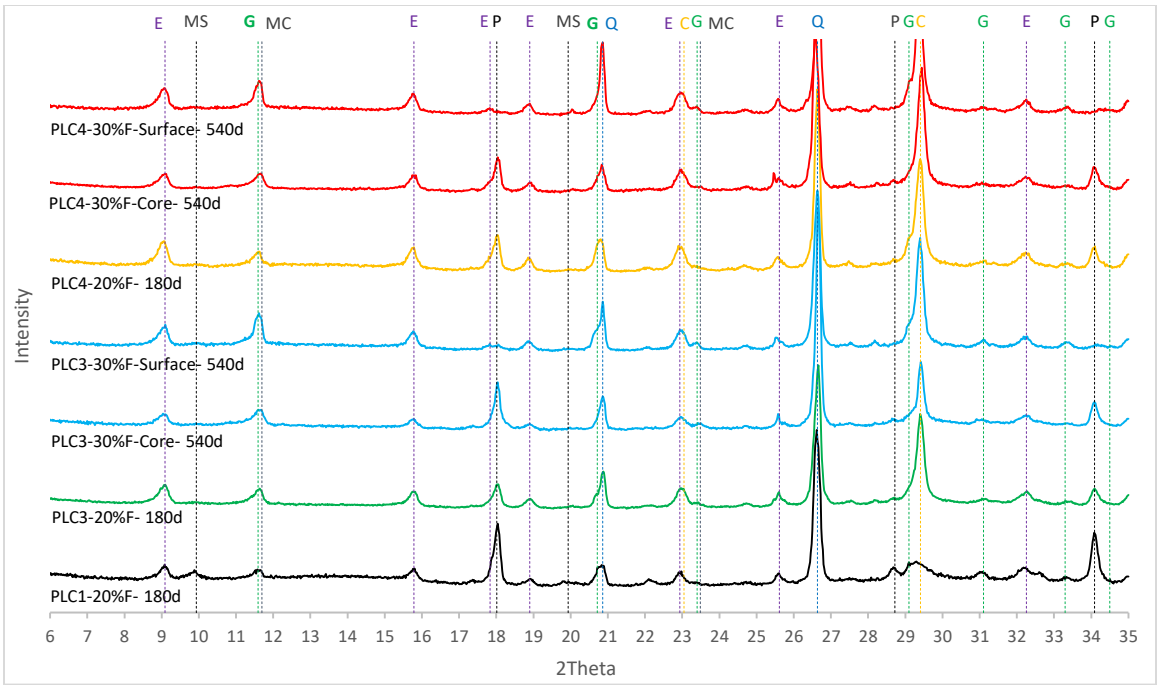

E= Ettringite, T= Thaumasite, MS= Monosulfoaluminate, HC= Hemicarboaluminate, G= Gypsum MC= Monocarboaluminate, P= Portlandite, Q= Quartz, C= Calcite, Ht= Hydrotalcite, CS= Calcium silicate, C_3A= Tricalcium aluminate, F= Ferrite.

Figure 9.8: XRD Patterns for High-C_3A Class F Fly Ash Mortar Samples Exposed to 5% Sodium Sulfate

In contrast, the aforementioned synergy was not observed to the same extent in the moderate-C_3A system. In this case, the PLC7 (15.5% limestone) bars experienced a greater expansion than the PLC5 (4.9% limestone) mixture. The XRD analysis of paste samples hydrated for 56 days at 23°C, which is presented in Figure 9.9, may help explain the obtained results. The increase in the limestone level from 3.2% to 21.0% in the high-C_3A fly ash mixtures significantly increased both the carbonate and sulfate-to-alumina ratios, which resulted in the stabilization of greater amounts of ettringite and the formation of monocarbonate instead of monosulfate and hemicarbonate. The amount of portlandite present at 56 days was reduced and an excess of unreacted calcite was detected in the PLC3 mixture. With further increase in the fly ash replacement level to 30%, the same phase assemblage was detected, although the proportion of monocarboaluminate with respect to ettringite increased, as there was still excess calcite to react with the increased alumina. Moreover, the amount of portlandite further decreased as it was expected due to calcium silicates dilution and pozzolanic reaction. Similar trends were observed in the moderate-C_3A mixtures, although the impact of increasing the limestone content from 4.9% to 15.5% was not as pronounced. The AFt and AFm phases present in the fly ash PLC5 system after 56 days of hydration consisted of ettringite and small amounts of monosulfoaluminate and hemicarboaluminate. This phase assemblage is coherent with the one detected in the analogous PLC1 specimen due to the lower alumina and higher calcium carbonate content in the PLC5 cement. The higher limestone level of PLC7 stabilized the carbonate-containing AFm phases over

monosulfate. However, the reactions seem to have not reached completion after 56 days as evidenced by the coexistence of hemicarbonate and calcite. Based on these results, it is clear that the PLC1 and, to a lesser extent, the PLC5 and PLC7 blends could be further optimized by a slight increase in the sulfate or carbonate contents. Further evidence and a discussion of this outcome will be provided in the following sections.

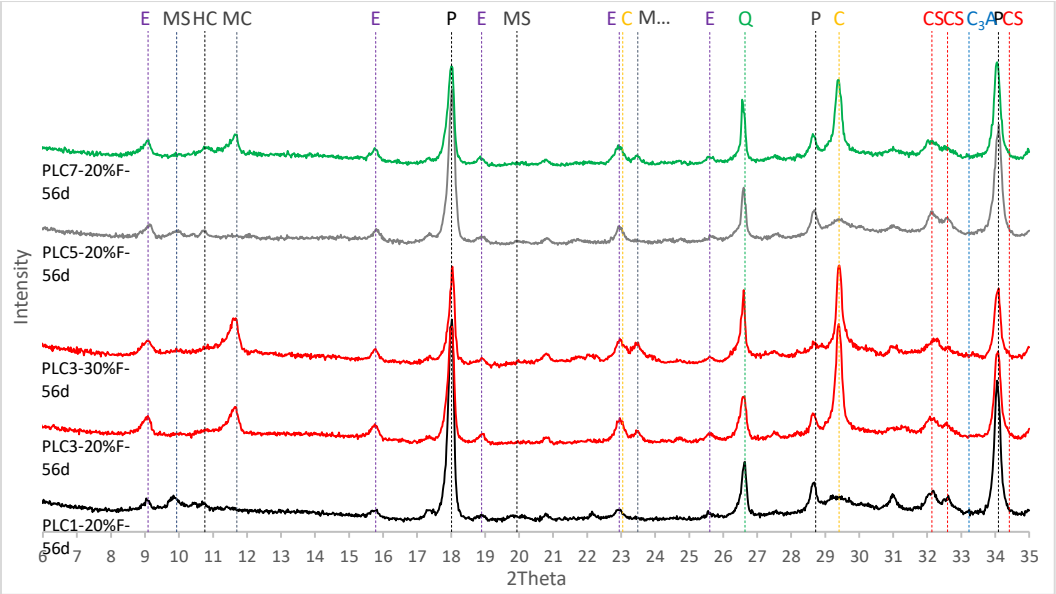

E= Ettringite, T= Thaumasite, MS= Monosulfoaluminate, HC= Hemicarboaluminate, G= Gypsum MC= Monocarboaluminate, P= Portlandite, Q= Quartz, C= Calcite, Ht= Hydrotalcite, CS= Calcium silicate, C3A= Tricalcium aluminate, F= Ferrite.

Figure 9.9: XRD Patterns for Class F fly Ash Paste Samples Hydrated for 56 Days at 23°C

9.3.4. Class C Fly Ash Mixtures

Figure 9.10 shows the expansion curves for the mixtures that incorporated the two class C fly ashes. The replacement of PLC1 with 20% C1 ash (22.6% CaO) resulted in an increase in the rate of expansion compared to the control mixture. On the other hand, when the level of fly ash was increased to 40%, a significant improvement in performance was observed. However, the mixture failed the 12-month expansion limit for Exposure Class S2 in ACI 318-14. Similar results on Type I cement mortar mixtures containing high calcium fly ashes have been observed in previous studies [Drimalas 2007][Dhole 2013][Shashiprakash 2001]. On the contrary, the PLC3 and PLC4 mixtures with 20% C1 ash showed a better performance than the straight cement counterparts. Moreover, the replacement of 40% of the cement with fly ash further reduced the expansion rate and allowed both systems to satisfy the 18-month limit for the S3 Exposure Class. At both C1 replacement levels the higher limestone mixtures performed better than the Type I mortars. Among the former systems, PLC3 showed always the lowest expansion rate.

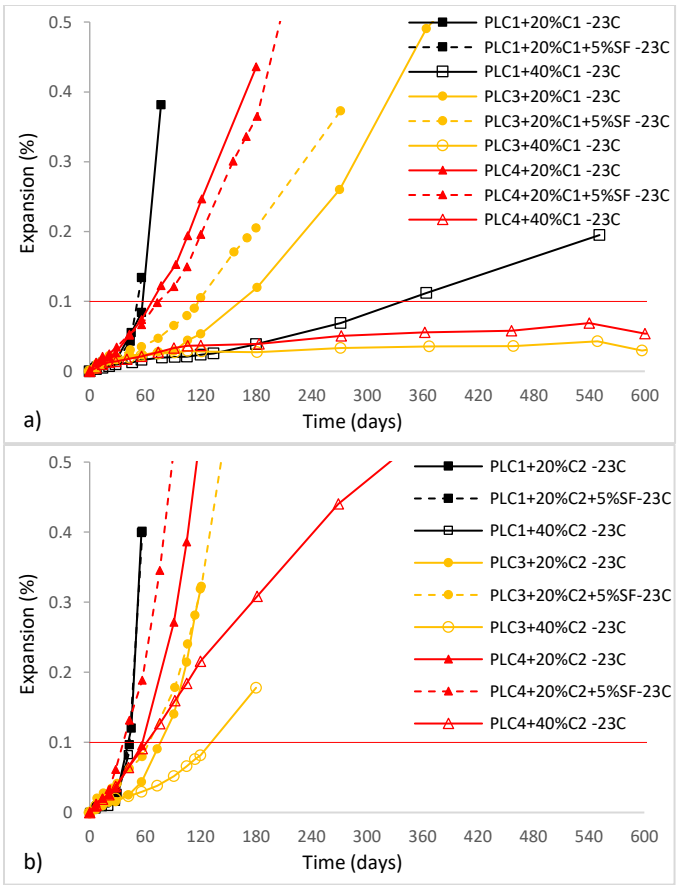

Figure 9.10: Expansion Curves for Mixtures that Incorporated Class C Fly Ash. a) C1 (22.6% CaO), b) C2 (27.7% CaO)

Figure 9.11 shows the XRD patterns for C1 fly ash (22.6% CaO) mixtures exposed to the sodium sulfate solution. The plot presents data at different ages for two sets of mixtures with 20% and 40% C1 fly ash replacement. The PLC1+20% C1 samples showed a rapid formation of ettringite at the expense of monosulfoaluminate, together with gypsum starting at the surface of the specimens. The analogous PLC3 system exhibited the formation of the same secondary sulfate-bearing phases, although to a lesser extent than the Type I mixture. In this high-limestone mortar, ettringite and monocarbonate were stabilized instead of monosulfate. This different phase assemblage is congruent with the higher carbonate and sulfate-to-alumina ratios and may help explain the higher sulfate resistance displayed. As it was suggested by Mehta [Mehta 1986], the performance of a cement-fly ash blend in a sulfate environment is strongly affected by the type of aluminate phases present in the hydrated system. In this regard, the stabilization of ettringite (and monocarbonate) over monosulfate and calcium aluminate hydrates should result in decreased expansions.

The performance improvement of the Type I cement mixture with the increase in C1 ash replacement level cannot be explained by the change in the initial phase assemblage. In fact, the

increased alumina in the system drives the thermodynamic equilibrium towards increased amounts of monosulfoaluminate at the expense of ettringite and carbonate-substituted AFm phases. The reason behind the lower expansion rates is to be found in the widely reported effects of SCMs incorporation, namely dilution of calcium silicates and aluminates from the cement, CH consumption, refinement and depercolation of the pore system, reduction of the pore solution equilibrium pH, and changes in the nature of the hydrates [Thomas 2011][Thomas 2013]. In the PLC3 and PLC4 mixtures, these effects add to the impact of the limestone, itself, as already discussed. As a result, after 18 months of immersion in the sulfate solution, secondary ettringite and gypsum formation and leaching of portlandite were limited to the outer regions of the samples. On the other hand, the core of the specimens exhibited an unaffected crystalline assemblage consisting of ettringite, hemi and monocarbonate, portlandite, and small amounts of calcite.

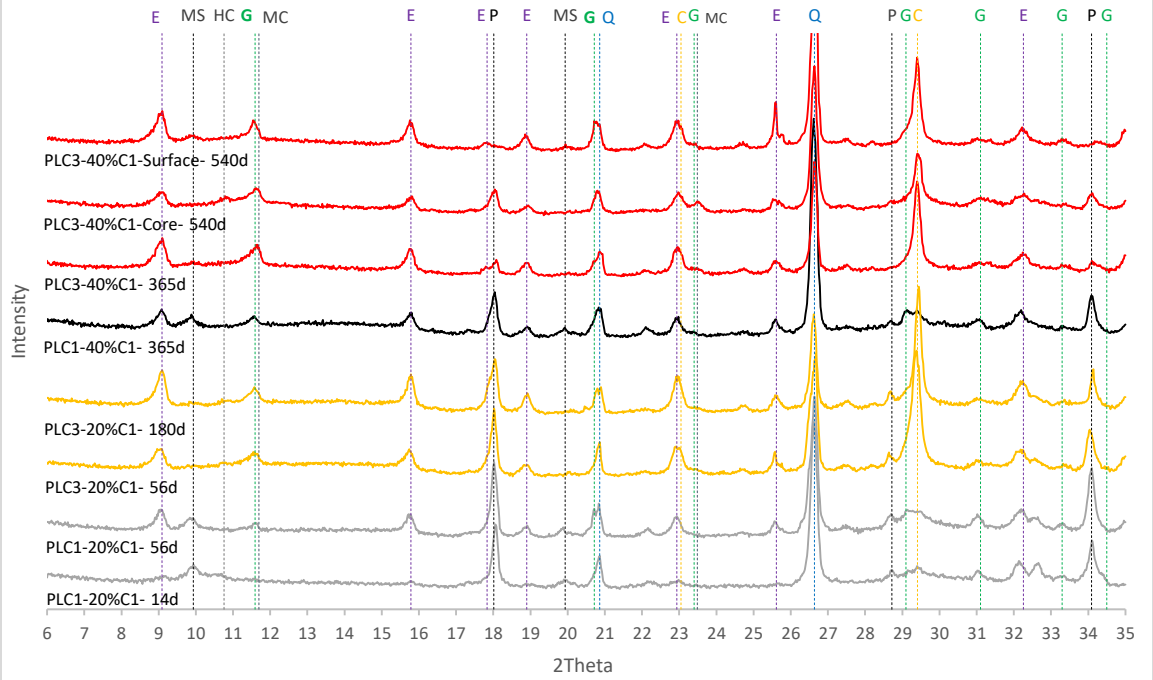

E= Ettringite, T= Thaumasite, MS= Monosulfoaluminate, HC= Hemicarboaluminate, G= Gypsum MC= Monocarboaluminate, P= Portlandite, Q= Quartz, C= Calcite, Ht= Hydrotalcite, CS= Calcium silicate, C_3A= Tricalcium aluminate, F= Ferrite.

Figure 9.11: XRD Patterns for PLC1 and PLC3 Mortar Samples with C1 Fly Ash Exposed to 5% Sodium Sulfate

The mixtures that incorporated the Class C fly ash with the highest CaO content (C2, CaO=27.7%) exhibited a different type of deterioration than the C1 counterparts. The Type I cement with 20% C2 ash specimens expanded at a significantly faster rate than the neat cement mortars. Although this expansion rate seemed to resemble the one of the equivalent C1 system in Figure 9.10, the bars suffered from extensive damage and started to disintegrate after only 8 weeks. On the other hand, the length change of the C1 mortars could be monitored for three more weeks. Figure 9.12 (a) and Figure 9.13 (a) show pictures of the PLC1 mortar bars with 20% C1 and C2 fly ashes,

respectively. As it is depicted, after 15 weeks both systems experienced severe cracking. However, while the C1 mixture displayed transversal cracks that fragmented the samples into five or six pieces, the C2 specimens showed a less localized damage pattern characterized by a bulk disintegration of the mortar.

The mixtures with higher limestone content and 20% C2 ash, contrarily, showed no difference in the expansion rate when compared to the neat PLC3 and PLC4 systems. Nevertheless, the mortar bars lost their integrity more rapidly and were no longer able to be measured after 4 months. Figure 9.12 and Figure 9.13 present pictures of the PLC3 (c) and PLC4 (e) systems with 20% C1 and C2 fly ash after 9 months of exposure, respectively. Both C2 mixtures exhibited a much more severe cracking than the C1 samples. In addition, the PLC4 systems performed worse than the PLC3 counterparts with both fly ashes at 20% replacement level. However, the high limestone bars exhibited a higher sulfate resistance than the Type I mixtures. Finally, the combination of 5% silica fume with 20% fly ash, which has been shown to improve the sulfate resistance of high-calcium fly ash systems [Shashiprakash 2001][Dhole 2011][Thomas 1999], did not enhance the performance of any of the mixtures. This result was surprising, considering the expected decrease in sulfate ions diffusivity, the consumption of portlandite, and the changes in the nature of the hydrates and the pore solution resulting from the incorporation of silica fume [Lothenbach 2011][Muller 2015].

When the C2 fly ash replacement level was increased to 40%, opposite trends were obtained between the Type I and the high limestone systems. The PLC1 mixture showed an extremely fast deterioration and the bars were severely degraded after only 10 weeks, as seen in Figure 9.13 (b). This rate of disintegration was greater than the one observed in the system that incorporated 20% fly ash (Figure 9.13 (a)). Consequently, the mixture failed without showing significant expansion, as it was not possible to measure the mortar bars after 6 weeks of exposure. On the other hand, the PLC3 and PLC4 samples with 40% C2 ash showed a slower rate of expansion with respect to the neat cement and the 20% fly ash mixtures. Similarly to the behavior observed in the Class F fly ash mortars, the expansion became more linear as the clinker content decreased, with the PLC4 + 40% C2 ash as the extreme showing no induction period. In addition, the mode of failure changed substantially in these two low-clinker systems. Transversal cracks grew from the finished surface of the bars and fragmented the PLC3 specimens between 6 and 9 months. However, as opposed to the behavior of the analogous 20% fly ash samples (Figure 9.13 (c)), the individual mortar pieces remained cohesive and minor macroscopic changes were observed between 12 and 18 months, as depicted in Figure 9.13 (d). The PLC4 mixture shown in Figure 9.13 (f) exhibited little damage after 18 months of exposure.

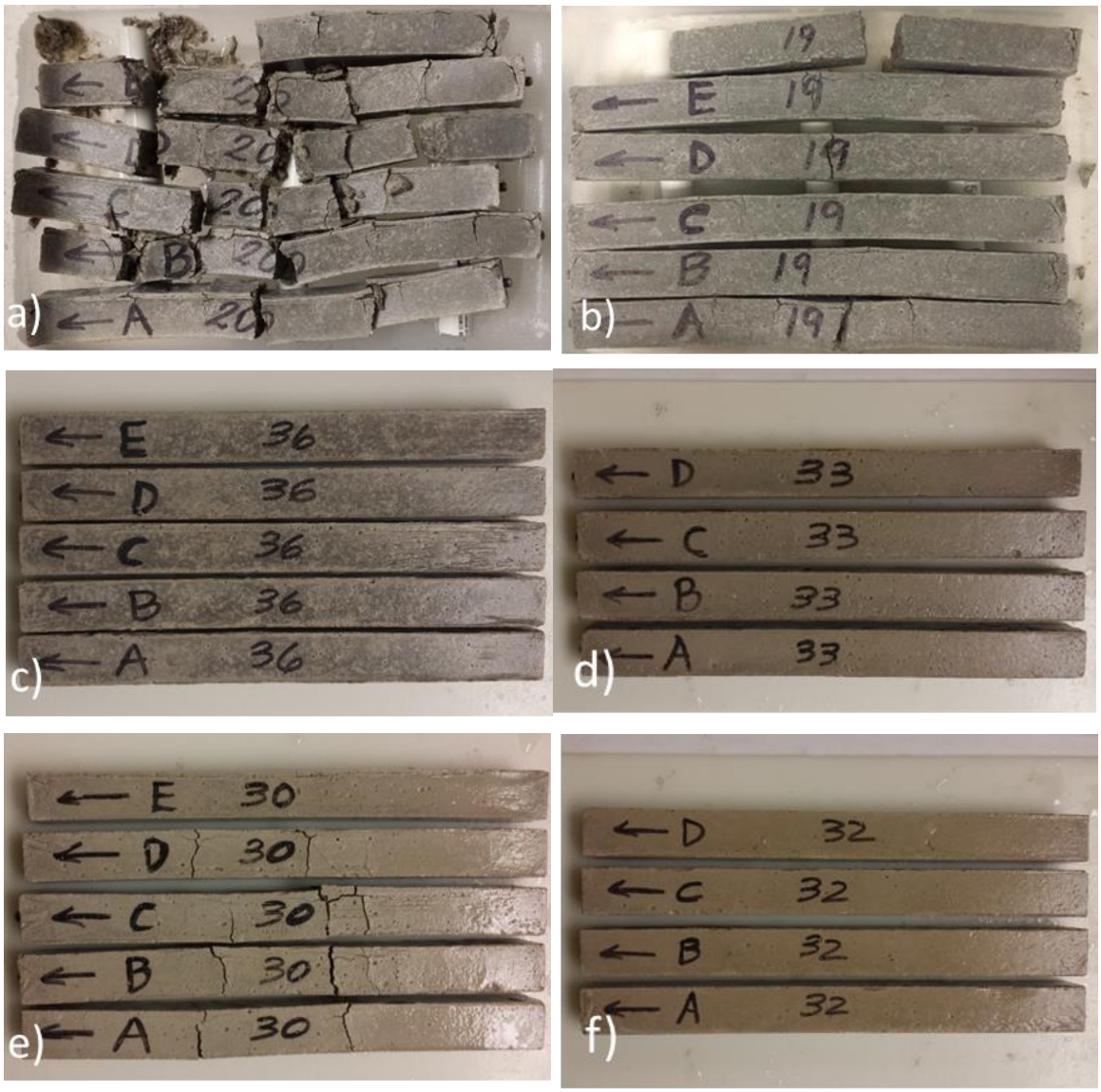

a) PLC1+20% C1 after 15 weeks, b) PLC1+40% C1 after 19 months, c) PLC3+20% C1 after 9 months, d) PLC3+40% C1 after 22 months, e) PLC4+20% C1 after 9 months, f) PLC4+40% C1 after 22 months.

Figure 9.12: C1 Fly Ash Mortar Samples Exposed to the Sulfate Solution

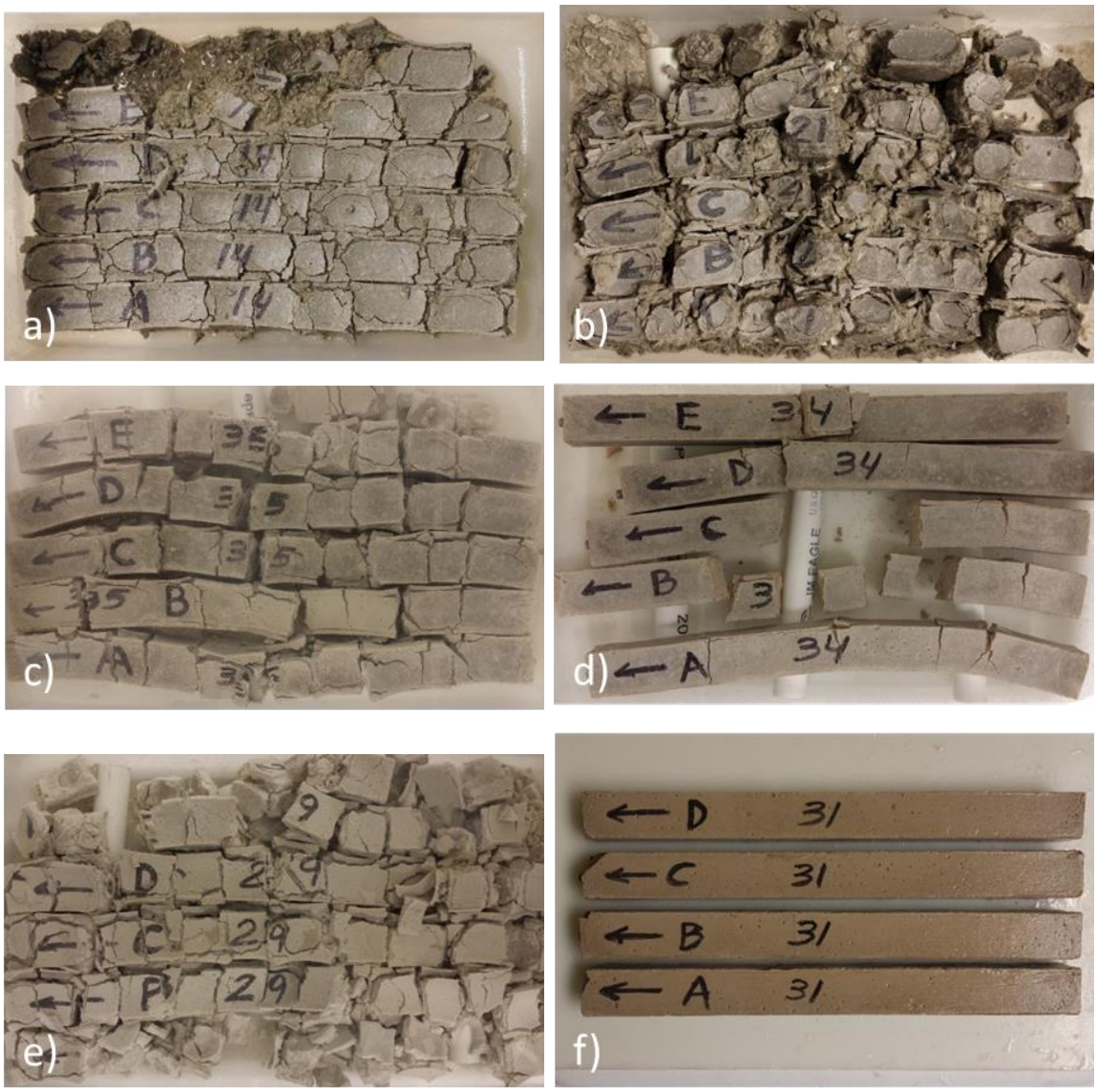

a) PLC1+20% C2 after 15 weeks, b) PLC1+40% C2 after 10 weeks, c) PLC3+20% C2 after 9 months, d) PLC3+40% C2 after 12 months, e) PLC4+20% C2 after 9 months, f) PLC4+40% C2 after 18 months.

Figure 9.13: C2 Fly Ash Mortar Samples Exposed to the Sulfate Solution

Figure 9.14 presents the XRD patterns of the C2 fly ash mixtures at both replacement levels. The plot includes data on cement paste samples hydrated for 56 days in order to depict the phase assemblage under normal hydration in isothermal conditions. In addition, data are presented for each cement system exposed to sodium sulfate. According to the plot, the phases formed as a result of the interaction with the external sulfates were analogous to the ones observed in the C1 ash systems. However, the kinetics were strongly different, as indicated by the macroscopic examinations. Both PLC1 mixtures showed a rapid formation of ettringite at the expense of monosulfoaluminate that resulted in the precipitate disintegration of the mortar bars. In the case of

the PLC3 and PLC4 systems with 20% ash, the formation of ettringite was detected at the expense of monocarbonate.

The increase in the fly ash level decreased the sulfate and carbonate-to-alumina ratios and, therefore, more hemicarbonate was stabilized at the expense of monocarbonate in the PLC3 and PLC4 systems. This is especially evident in the PLC3 mixture due to its lower limestone level. In this case, the relatively low calcite peaks observed are consistent with the decreased monocarbonate stability. On the other hand, the relative intensity of the ettringite peaks showed little change, which is coherent with the absence of monosulfate in both systems hydrated for 56 days. Based on these and the previous observations, it is clear that the dilution of calcium aluminates and silicates from the cement and the stabilization of ettringite and monocarboaluminate are deciding factors in the performance exhibited by the systems with high C2 ash replacement. In this regard, the high limestone content of the PLC4 mixture accomplishes both objectives and may help explain its improved performance.

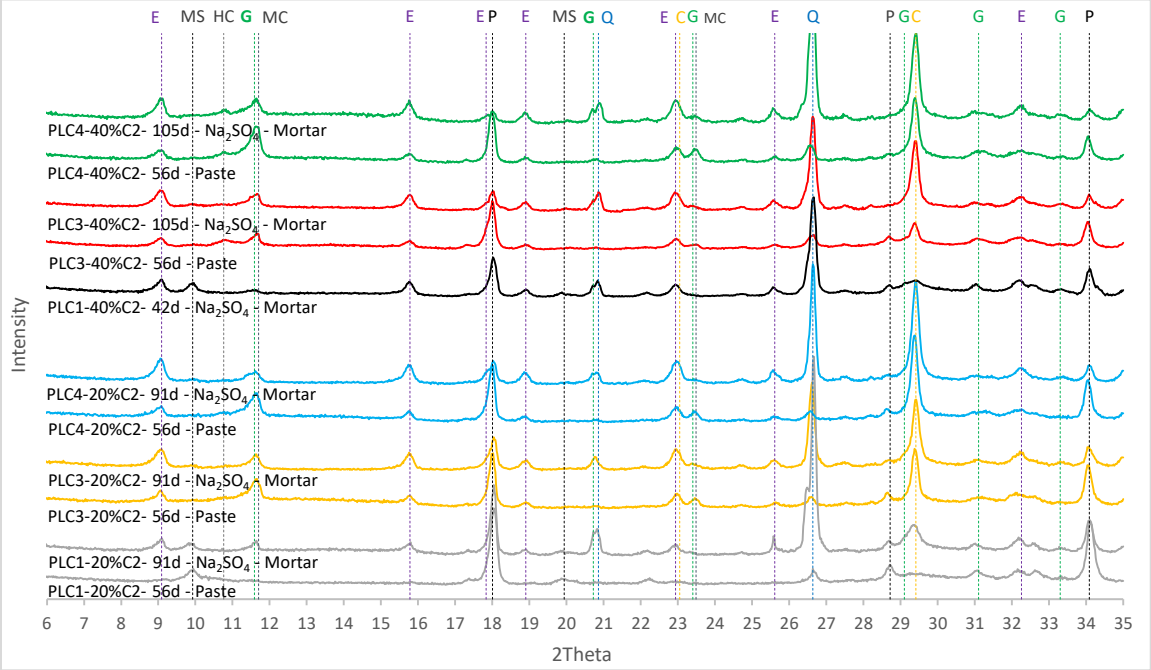

E= Ettringite, T= Thaumasite, MS= Monosulfoaluminate, HC= Hemicarboaluminate, G= Gypsum MC= Monocarboaluminate, P= Portlandite, Q= Quartz, C= Calcite, Ht= Hydrotalcite, CS= Calcium silicate, C_3A= Tricalcium aluminate, F= Ferrite.

Figure 9.14: XRD Patterns for C2 Fly Ash Paste Samples Hydrated for 56 Days and Companion ASTM C1012 Mortar Samples Exposed To 5% Sodium Sulfate

The differences in the composition of the fly ashes used and in the phase assemblages resulting from the hydration reactions further support the obtained results. Several studies on the sulfate resistance of high and low-calcium fly ash systems have shown that both the chemical and, perhaps more importantly, the mineralogical composition of the ash determine the performance in a sulfate

environment [Dhole 2013][Dhole 2011]. Class F fly ashes, which have widely been shown to improve the sulfate resistance of blended systems [Drimalas 2007][Thomas 1999][Dhole 2010], are composed of nonreactive crystalline phases, namely quartz, mullite, magnetite, and hematite. In addition, the amorphous material is aluminosilicate in nature, which is considered non-reactive with sulfates. On the other hand, Class C fly ashes contain reactive crystalline phases, such as anhydrite, periclase, gehlenite, C_3A, merwinite, and dicalcium silicate. Moreover, in these high-calcium ashes, the amorphous material is high in alumina and calcium but low in silica, which makes it reactive with sulfates [Dhole 2013]. Figure 9.15 shows the crystalline composition of the three fly ashes used in this study. The class F fly ash presents the nonreactive crystalline phases often found in low-CaO fly ashes, as discussed above. On the other extreme, the highest-CaO fly ash (C2) contains significant amounts of reactive crystalline phases. The C1 fly ash (CaO= 22.6%), which imparted an improved sulfate resistance to the blended systems when the level of replacement was increased from 20% to 40%, exhibited not only the same crystalline phases as the F fly ash, but also extremely similar amounts of them. The only 1% difference in the amorphous content between these two SCMs was due to the presence of that similar amount of anhydrite in the C1 fly ash. These results agree with previous studies [Drimalas 2007][Dhole 2013] and reinforce the need of evaluating the mineralogy of the fly ash in order to select a combination of materials that offers the required performance.

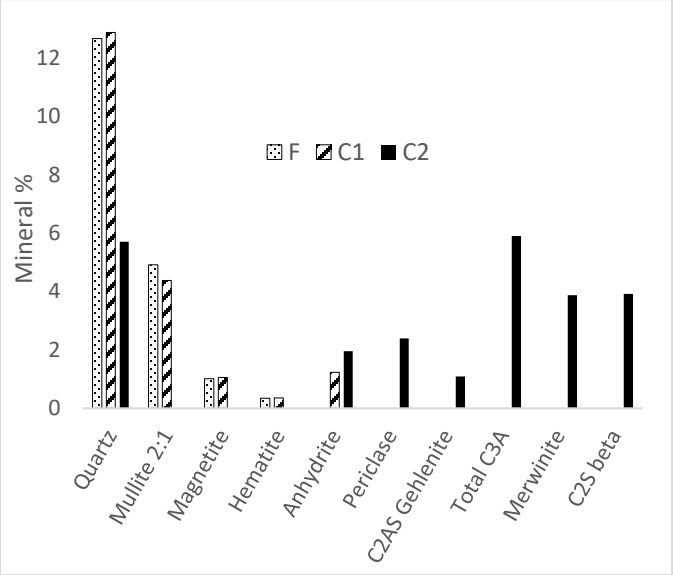

Figure 9.15: Crystalline Composition of the Three Fly Ashes

9.3.5. Slag-cement Mixtures

The expansion curves for the mixtures that incorporated 35% slag are shown in Figure 9.16. All the systems exhibited very small expansions after 18 months and satisfied the requirement for the most severe exposure class (S3) in ACI 318-14. These results are in line with those reported in

earlier studies [Hossack 2015][Ramezanianpour 2012] where limestone contents up to 22% were used. Although the effect of temperature on the rate and mechanism of attack was discussed in Chapter 1, the expansion curves of companion slag blends exposed to sodium sulfate at 5ºC are presented in Figure 9.17 (b). As the relative differences between the blends' expansions were more noticeable at this low testing temperature, data are shown here to better highlight the effect of cement type on the resistance to sulfates when combined with slag. As it was shown in Chapter 1, the mechanism leading to the expansion of mortars at the lower temperature in a highly concentrated sodium sulfate solution is analogous to the one observed at 23ºC. Pronounced differences are found, however, in the kinetics and in the manifestation of the secondary reactions at each exposure condition, especially in non-sulfate-resistant systems. In the systems incorporating limestone, thaumasite formation at low temperatures resulted in superficial damage. Nevertheless, this process does not seem to influence the initiation of the rapid expansion in sulfate-resisting systems, as thaumasite was detected always after the induction period in the surface region of the mortars. With this in mind, the comparison of the length changes of the slag blends stored at 5ºC seems appropriate. In addition, the expansion curves of the neat cement mixtures are shown in Figure 9.17 (a) to serve as reference.

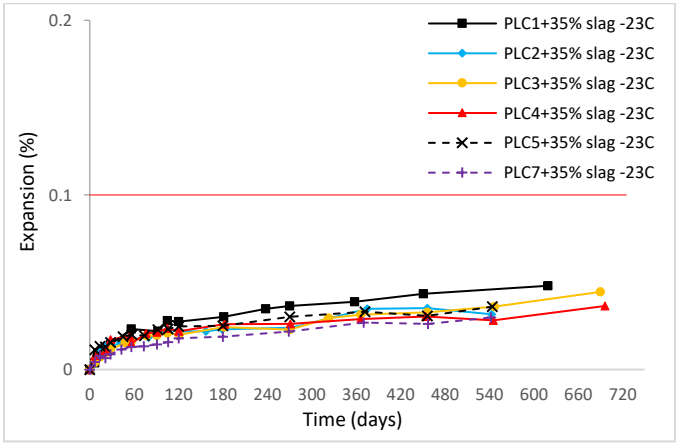

Figure 9.16: Expansion Curves for the Mixtures that Incorporated 35% Slag

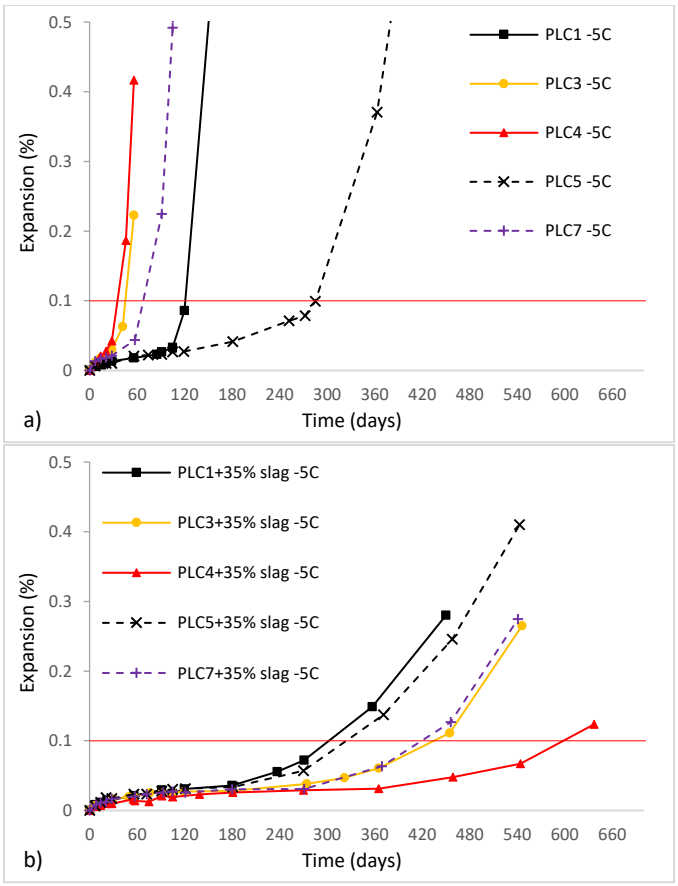

Figure 9.17: Expansion Curves. a) neat cement and b) blends with 35% slag mortars exposed to 5% sodium sulfate at 5°C

As is shown in Figure 9.17 (a), the increase in the limestone percentage accelerated the expansion of both the low and high-C_3A neat cement mixtures. This relative behavior is analogous to the one obtained at 23°C presented in Figure 9.4. When 35% slag was incorporated in the mortar systems, the opposite behavior was observed; the rate of expansion was decreased as the limestone content of the cement increased. This trend was observed before between the PLC1 and PLC3 blends with all the SCMs. However, the expansion rates of the PLC4 + SCM systems, while still lower than the Type I analogous, were greater than the ones of the PLC3 counterparts in the three fly ash cases discussed before. Similarly, the PLC7-slag blend performed better than the PLC5 equivalent, whereas the opposite behavior was observed in the Class F fly ash systems. These results indicate that a different mechanism may be responsible for the enhanced sulfate resistance of the higher limestone mixes when slag is used. In this regard, several points can be discussed to better understand and compare this performance with those of the SCM systems presented before.

Berodier and Scrivener [Berodier 2015] showed that cement-slag blends are more efficient in refining the porosity than neat cement and fly ash-blended systems. They observed that cement paste specimens with 40% slag exhibited a similar or slightly smaller critical pore radius than that

of a plain cement paste after 3 and 4 weeks, even though the total porosity in the blended system was higher. Their results also showed that the ability of the slag blend to refine the porosity is less affected by an increase in the water/solids ratio, as compared to both a plain cement and a 40% fly ash system. These effects have been observed to be amplified in the presence of limestone [Arora 2016][Menendez 2003].

Although the incorporation of slag will increase the bulk alumina content of the blend, better performances are generally obtained with higher slag fractions, which contrasts with the observations of some high-CaO fly ash systems. This has been attributed to the decrease of the available alumina due to the higher proportion of unreacted slag expected at high replacement levels, and to the increase in the amount bound to the C-S-H and hydrotalcite-like phases [Gollop 1996]. The alumina content of the slag used in this study, which significantly affects the sulfate resistance of the system [Gollop 1996][Osborne 1999][Whittaker 2016], is considerably lower than the three fly ashes tested. This should result in lower amounts of AFt and AFm phases in the hydrated system. Moreover, the presence of higher amounts of magnesium in the slag blend should promote the stabilization of greater levels of hydrotalcite-like phases [Lothenbach 2011][Whittaker 2014]. Consequently, the thermodynamic stability of the system upon exposure to sulfates should increase, as these alumina-bearing solids are more stable in a sulfate environment than monosulfate and other aluminate hydrates [Whittaker 2016][Feng 2015][Yu 2015]. This bound alumina adds to the aluminum incorporated in the C-S-H, which, similarly, is not available to participate in secondary ettringite formation [Whittaker 2016][Yu 2015][Gollop 1996]. Furthermore, the alumina present in the unreacted slag grains may not contribute to the formation of ettringite upon exposure to sulfates. Mass balance calculations for systems with low and high-alumina slags have shown that C-A-S-H and hydrotalcite formation would consume most of the alumina and CaO released by a full dissolution of the SCM [Whittaker 2016]. These effects, which are complemented by calcium leaching, may limit the formation of secondary ettringite and, therefore, the potential for significant damage. Nevertheless, monosulfate and ettringite have been reported to form inside slag rims, which would indicate the reaction of the anhydrous slag with the external sulfates [Yu 2015].

Yu et al. [Yu 2015] reported that the mechanism of deterioration of high-alumina slag mortar systems exposed to sodium sulfate solutions is governed by the loss of material at the surface rather than by macroscopic expansion. The samples were shown to experience progressive superficial damage until the affected area overcame the restraint of the sound core, after which the slag blends expanded substantially. In another study, Whittaker et al. [Whittaker 2016] showed that the incorporation of slag significantly improved the performance of paste samples immersed in a Na_2SO_4 solution of low concentration. Although expansion was not monitored, high-alumina slag mixtures exhibited slight cracking, which was attributed to the increased porosity and loss of strength associated with portlandite leaching and C-A-S-H decalcification. In the experiments performed at 23^{o}C in this study, minor cracking localized at the ends of the PLC1 and PLC5 mortar bars constituted the only signs of damage detected. No deterioration of the higher limestone

mixtures was observed after 18 months of testing. On the other hand, the mortar bars stored at 5°C displayed more pronounced signs of the attack. As Figure 9.18 indicates, the damage pattern of the mortars after 27 months corresponded to the one typically associated with expansion due to ettringite formation. Thaumasite formation was detected in this exposure condition, but only in the surface region of the bars where cracks facilitated the interaction with the sulfate solution, which is not believed to have contributed to the measured expansion. In agreement with the trend in length change, the level of deterioration of the high-C_3A mixtures decreased with the increase in the limestone content. The difference between PLC5 and PLC7, however, was not as evident.

Figure 9.18: Slag Mortar Bars after 27 Months of Exposure to the Sulfate Solution at 5°C. a) PLC1, b) PLC3, c) PLC4, d) PLC5, e) PLC7

Data reported previously using ASTM C1012 [Hossack 2015][Ramezanianpour 2012] have also shown small differences between PLC-slag blends with limestone contents up to 22% when tested at the standard temperature. However, no improvement or, when tested at 5ºC, a decline in performance was exhibited by the higher limestone blends with respect to CSA A3001 GU cement (equivalent to ASTM C150 Type I) equivalents when slag contents were equal to 30% [Ramezanianpour 2012] and equal or lower than 40% [Hossack 2015]. Only when the slag levels were increased to 50% [Ramezanianpour 2012] and 60% [Hossack 2015] did the high-limestone blends show equivalent or marginally better performance than the GU counterparts. In this regard, not only has the present work shown that previously published results can be extended to systems with higher limestone contents, but it has also demonstrated that the performance of commercially-available PC-SCM blends can be significantly enhanced by adjusting the SO_3/Al_2O_3 and CO_2/Al_2O_3 molar bulk ratios through proper selection of limestone, sulfate, and lower-than-thought SCM levels. Accordingly, some considerations must be made.

Figure 9.19 presents the XRD patterns of cement-slag paste specimens after 56 days of hydration at 23ºC. The PLC1 blend showed the presence of portlandite, monosulfate, and small amounts of ettringite and hemicarbonate. The formation of hydrotalcite was evident by the presence of a broad peak between the ones corresponding to hemi and monocarboaluminate, which is expected due to its relative lower crystallinity. The increased limestone content in the PLC2, PLC3, and PLC4 blends stabilized greater amounts of ettringite and suppressed the formation of monosulfate. As with the three fly ashes discussed before, the carbonate-AFm phases formed instead. In addition, the relative intensity of the portlandite peaks decreased. In these PLC systems, the formation of hydrotalcite-like phases was less easily identifiable due to the overlapping with the monocarboaluminate peak. Nevertheless, in comparison to neat cement patterns (the PLC3 control mixture has been included here as reference), a broad "hump" between 11º and 11.75º (2Theta) was observed, which would support the assumption of its presence made on the basis of the system's chemistry. Similar trends were observed in the moderate-C_3A mixtures, although the relative differences between the lowest and highest-limestone blends were not as pronounced. The PLC5-slag system showed no monosulfate; the AFt and AFm phases present consisted of ettringite and hemicarboaluminate. This phase assemblage is consistent again when compared to the PLC1 system due to the higher carbonate and sulfate-to-alumina ratios of the PLC5 blend. In addition, the presence of hemicarboaluminate in all the systems with added limestone may indicate that the reactions have not reached completion after 56 days, as this phase is not thermodynamically stable when excess carbonate is available.

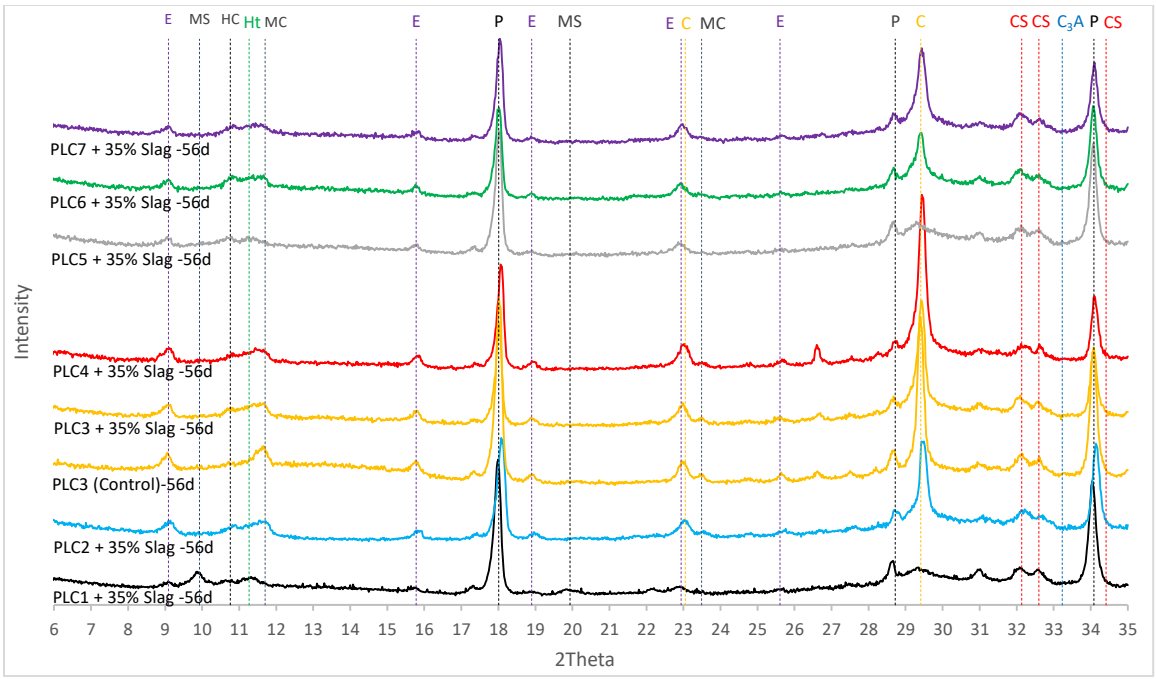

E= Ettringite, T= Thaumasite, MS= Monosulfoaluminate, HC= Hemicarboaluminate, G= Gypsum MC= Monocarboaluminate, P= Portlandite, Q= Quartz, C= Calcite, Ht= Hydrotalcite, CS= Calcium silicate, C_3A= Tricalcium aluminate, F= Ferrite.

Figure 9.19: XRD Patterns for 35% Slag Paste Samples Hydrated for 56 Days

Based on these results, and in close analogy to the fly ash observations, it is evident that the Type I and, to a lesser extent, the Type I/II blends could be further optimized by increasing their sulfate or carbonate contents. This combined strategy has been shown to increase the sulfate resistance of blended systems [Gollop 1996][Ogawa 2012][Higgins 2003a][Higgins 2003b] by lowering the Al_2O_3/CO_2 and Al_2O_3/SO_3 ratios of the blend and stabilizing ettringite and monocarbonate over monosulfate and less-stable calcium-aluminate hydrates. This would consequently increase the stability of the system upon interaction with external sulfates and increase the volume of solids. A similar approach seems applicable to the PLC7 blends, in which case the optimized phase assemblage would further help compensate the dilution of the clinker. In this work, the increase in the limestone content from 3.2% in PLC1 to 30.6% in PLC4 followed this idea and was accompanied by an increase in the SO_3%. This allowed the high-limestone systems to maintain a more stable phase assemblage even when high percentages of alumina-rich SCMs were introduced. In the particular case of the slag blends, the benefits derived from the SCM incorporation may have been amplified by its higher efficiency in refining the porosity and its lower sensitivity to the increase in the effective w/cm ratio. Accordingly, the highest limestone blends showed the best performance. On the other hand, the dilution of clinker by limestone may have had a relatively greater influence in the fly ash systems, which may explain the higher resistance exhibited by the PLC3 blends over the PLC4 counterparts. All the discussed points emphasize the main differences between the present work and the cited previous studies and help explain the better performance

of the higher-limestone blends, particularly the PLC3 and PLC4 systems, with respect to the Type I counterparts.

9.4. Conclusions

The sulfate resistance of PLC systems cannot be judged only on the basis of the limestone content. The clinker composition, the limestone and sulfate contents, the type and replacement level of SCMs, the w/cm ratio, and the curing history will define the resistance to sulfate penetration, the extent of leaching, and the phase assemblage of the hydrated system, consequently determining the performance in a specific exposure. The current work evaluated the sulfate resistance of mortars systems incorporating several SCMs in combination with eight cements with different C_3A levels and interground limestone contents ranging from 3.2% to 30.6%. Expansion and visual examinations were combined with X-ray diffraction analyses and a detailed discussion of the mechanisms responsible for the observed behavior was provided. A summary and the conclusions of this study are presented below.

- The performance of the PLC-SCM blends was shown to be strongly affected by the type of aluminate phases present in the hydrated system. In this regard, the stabilization of ettringite and carbonate-AFm phases over monosulfate and less stable calcium aluminate hydrates significantly increased the stability of the mixtures upon exposure to the external sulfates. In this work, the increase in the limestone content from 3.2% in PLC1 to 30.6% in PLC4 was accompanied by an increase in the SO_3%. This allowed the high-limestone systems to maintain a more stable phase assemblage even when high percentages of alumina-rich SCMs were introduced. In the particular case of the slag blends, the benefits derived from the SCM incorporation may have been amplified by its higher efficiency in refining the porosity and its lower sensitivity to the increase in the effective w/cm ratio, which add to the lower levels of available alumina. Accordingly, the highest limestone blends showed the best performance. On the other hand, the dilution of clinker by limestone may have had a relatively greater influence in the fly ash systems, which may explain the higher resistance exhibited by the PLC3 blends over the PLC4 counterparts. All the discussed points emphasize the main differences between the present work and the cited previous studies and help explain the better performance of the higher-limestone blends, particularly the PLC3 and PLC4 systems, with respect to the Type I counterparts.

- All the combinations of high-C_3A clinker systems with 21.0% and 30.6% interground limestone and SCMs showed a better performance than the analogous Type I cement-SCM mixtures. Moreover, the partial replacement of both PLCs with 30% Class F fly ash, 40% Class C fly ash (CaO= 22.6%), and 35% slag allowed the low-clinker systems to satisfy the 18-month expansion requirement for the most severe exposure class (S3) in ACI 318-14. Furthermore, the differences in the rate of deterioration between the low and high-limestone systems, which resulted in a different damage pattern in the neat cement

mixtures, were also observed in all the blended mortars. These effects were particularly pronounced in the systems that incorporated both Class C fly ashes.

- The incorporation of limestone contents greater than 15% in neat cement mixtures decreased the time to failure according to standard expansion limits. The intergrinding of lower limestone amounts, however, produced varied results. While high-C_3A specimens with 13.4% limestone showed the worse performance among all mixtures, no significant difference in expansion was observed with the incorporation of up to 11.6% limestone in moderate-C_3A mortars, which exhibited an expansion rate similar to the reference Type V system.

    - The failure mode of the neat cement mortars was strongly dependent on the chemical composition of the system. The high-C_3A specimens with up to 13.4% limestone displayed a precipitous deterioration after an initial period characterized by slow expansion and minimal macroscopic signs of damage. The systems with limestone contents equal or greater than 21.0%, which have lower C_3A contents, reached higher levels of expansion accompanied by extensive cracking and warping. However, this process was less abrupt and did not cause the complete disintegration of the samples as it occurred in the lower-limestone counterparts. The moderate-C_3A samples exhibited a much less severe deterioration than the high-C_3A systems. In agreement with the expansion behavior, the performance worsened with the increase in the limestone content up to 15.5%. Nevertheless, even after severe damage, the bars remained as one piece and no fragmentation was observed.

Not only has the present work shown that previously published results can be extended to systems with higher limestone contents, but it has also demonstrated that the performance of commercially available PC-SCM blends can be significantly enhanced by adjusting the SO_3/Al_2O_3 and CO_2/Al_2O_3 molar bulk ratios through proper selection of limestone, sulfate, and lower-than-thought SCM levels.

Chapter 10. Sulfate Resistance of Portland-Limestone Cement Blended Systems. Part II: Concrete Investigation

10.1. Introduction

This chapter is the last of a series of three manuscripts that comprehensively evaluate the performance and mechanisms of deterioration of portland-limestone cement (PLC) blended systems in different sulfate exposures. The first study systematically investigated the impact of exposure temperature on the rate and mechanism of deterioration of mortar specimens [Tiburzi 2018], which has constituted one of the most critical issues regarding the validation of PLC systems for use in sulfate environments. The second manuscript explored the mechanisms of sulfate resistance of mortars systems incorporating several SCMs in combination with eight cements with different C_3A levels and interground limestone contents ranging from 3.2% to 30.6% [Tiburzi 2018].

The results of the referred studies have indicated that a similar progression of the reactions leading to the expansion of mortar systems occurs at low (5ºC) and moderate/warm (23ºC) temperatures. However, the kinetics and the manifestations at each exposure condition are not the same. In addition, it was indicated that increased surface deterioration due to leaching and thaumasite formation can facilitate sulfate ingress and exacerbate expansion of non-sulfate resistant mixtures, which was shown to be affected by the C_3A and limestone contents of the system. Moreover, it was demonstrated that when exposure solutions of lower sulfate concentration are used severe corrosion and mass loss resulting from thaumasite formation can occur without or well before any measurable expansion.

The nature of the attack was found to be the same in all of the samples exposed to the same temperature, regardless of the curing regime. A more mature microstructure achieved by extended curing, however, delayed the onset of both the rapidly expansion stage and the surface deterioration. This effect was shown to be particularly significant in the mixes that incorporated fly ash, owing to their high sensitivity to curing temperature. Nonetheless, a faster expansion rate independent of the initial maturity was observed in the 5ºC vs. the 23ºC experiments. These effects evidenced an influence of the exposure temperature on the expansion rate that goes beyond the changes in microstructural development.

The performance of the PLC-SCM blends was shown to be strongly affected by the type of aluminate phases present in the hydrated system. In this regard, the stabilization of ettringite and carbonate-AFm phases over monosulfate and less stable calcium aluminate hydrates significantly increased the stability of the mixtures upon exposure to the external sulfates. In the three studies comprising the present work, the increase in the limestone content from 3.2% in PLC1 to 30.6%

in PLC4 was accompanied by an increase in the SO_3%. This allowed the high-limestone systems to maintain a more stable phase assemblage even when high percentages of alumina-rich SCMs were introduced. Subsequently, all the combinations of high-C_3A clinker systems with 21.0% and 30.6% interground limestone and SCMs investigated showed a better performance than the analogous Type I cement-SCM mixtures. Moreover, the partial replacement of both PLCs with 30% Class F fly ash, 40% Class C fly ash (CaO= 22.6%), and 35% slag allowed the low-clinker systems to satisfy the 18-month expansion requirement for the most severe exposure class (S3) in ACI 318-14.

The work presented in this paper comprises an extensive testing program on the resistance of PLC concrete systems to external sulfate attack. The results of this investigation are critical to validate the new and valuable insights into the mechanisms of deterioration in sulfate exposures provided by the accelerated testing presented in the previous chapters. Several mixture parameters, namely interground limestone content, C_3A content, and SCM type and replacement level, were evaluated in a series of experimental conditions designed to link, replicate, and predict laboratory and field performances. The methodology adopted will be crucial to evaluate/develop an accelerated testing procedure that provides a better correlation with actual field performance of concrete structures.

10.2. Materials and Methods

In this laboratory study, eight cements were tested. Limestone was interground at one plant with a high-C_3A clinker for the production of four cements, namely PLC1, PLC2, PLC3, and PLC4, which have limestone contents of 3.2%, 13.4%, 21.0%, and 30.6%, respectively. Analogously, other three cements were produced at another plant by intergrinding limestone with a lower-C_3A clinker, and have limestone contents of 4.9%, 11.6%, and 15.5%, namely PLC5, PLC6, and PLC7, respectively. In addition, an ASTM C150 Type V cement from an additional plant was used. Moreover, several supplementary cementing materials (SCMs) were selected as partial replacement of the cements: one Class F and two class C fly ashes, silica fume, and slag. Table 10.1 shows the chemical composition of the cements and SCMs. Figure 10.1 shows the particle size distribution of the PLC1 to PLC7 cements.

Table 10.1: Chemical Composition of the Cements and SCMs

	PLC1	PLC2	PLC3	PLC4	PLC5	PLC6	PLC7	Type V	FA-F	FA-C1	FA-C2	Slag	SF
Chemical analysis [%]													
SiO_2	19.8	18.6	18.1	16.9	19.9	19.0	19.5	20.6	53.2	38.6	32.4	36.1	97.2
Al_2O_3	5.5	5.2	4.7	4.7	4.7	4.6	5.0	3.8	18.0	18.3	17.3	8.0	0.3
Fe_2O_3	2.0	1.8	1.7	1.5	3.3	3.3	3.3	3.7	8.1	5.4	6.1	0.6	0.1
CaO	64.8	66.4	67.1	68.1	64.8	65.7	64.8	62.2	10.8	22.6	27.7	39.8	0.9
MgO	1.1	1.1	1.0	1.2	0.8	0.8	0.8	4.6	2.4	4.8	5.3	10.7	0.3
Na_2O	0.1	0.1	0.1	0.1	0.1	0.1	0.1	0.3	0.3	1.2	1.6	0.3	0.1
K_2O	0.6	0.5	0.6	0.4	0.6	0.7	0.6	0.3	1.1	0.7	0.3	0.5	0.7
SO_3	4.1	4.2	4.6	4.7	3.8	3.8	3.9	3.0	0.5	1.8	2.5	2.6	0.2
LOI	1.4	5.9	9.2	13.4	2.2	5.1	6.8	1.3					
$CaCO_3$	3.2	13.4	21.0	30.6	4.9	11.6	15.5	2.9					
Blaine Fineness (m^2/kg)	375	428	458	516	-	-	-	366					
Cement phase composition (%)—Rietveld analysis													
C_4AF	3.5	3.1	2.0	3.0	7.3	8.1	4.6	8.9					
C_3A	9.2	7.6	6.5	6.0	4.2	2.9	3.8	3.0					
C_3S	47.8	44.9	41.1	34.2	47.9	46.5	35.1	57.9					
C_2S	20.9	16.8	17.8	13.6	22.4	28.7	24.6	13.5					
$CaCO_3$	5.2	13.9	24.8	30.3	1.8	12	14.1	2.8					

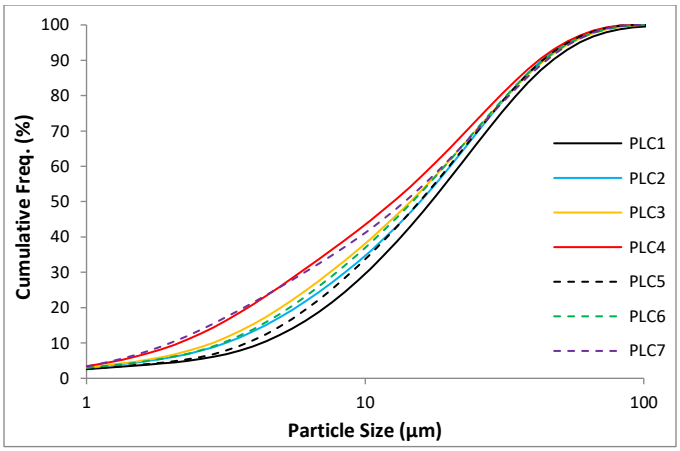

Figure 10.1: Particle Size Distribution of the PLC1 to PLC7 Cements

A crushed limestone coarse aggregate and a manufactured limestone sand from Texas sources were selected for use in all concrete mixtures. This aggregate source was selected due to their non-reactivity with regard to alkali-silica reaction (ASR). All concrete mixtures had a constant w/cm ratio equal to 0.45, a total cementitious content of 362 kg/m^3, a coarse aggregate content of 1045 kg/m3, and a fine aggregate content equal to 668 kg/m3. SCMs were incorporated as partial replacement of the cement. The replacement levels evaluated are indicated in the following section.

Concrete prisms (75 × 75 × 285 mm) were cast and stored in a temperature-controlled room at 23 +/- 3 °C until the age of 24 hours. Subsequently, the specimens were demolded and stored in a fog room at RH of 100% and 23°C. After 28 days of curing, initial length and mass measurements were taken and the prisms were moved to the respective exposure setting.

Several laboratory and field exposure conditions were evaluated in the present work. Three concrete prisms were stored indoors in a 5% Na_2SO_4 solution at 23ºC, replicating standard ASTM C1012 testing conditions. In addition, three companion prisms were also stored indoors in a 5% Na_2SO_4 solution at 5ºC. The last set of prisms stored in laboratory conditions consisted of three specimens immersed in a saturated Ca_2SO_4 solution at 23ºC. In this last case, the calcium sulfate solution was prepared to match the sulfate ion concentration of the 5% sodium sulfate solution. However, due to the limited solubility of calcium sulfate in water in relation to that of the sodium salt, large amounts of gypsum remained as solid accumulated at the bottom of the storage container. In order to prevent contact with this material, the prisms were placed on top of spacers.

The rest of the specimens of the same mixture were stored outdoors in two different locations. The first exposure site is located in Austin, TX. It consists of several 0.9 x 0.6 x 3.0 m galvanized feed troughs partially filled with soil typically used as fill material in residential construction. Two different exposure solutions were used in the current work. A 5% Na_2SO_4 solution was prepared and added to half of the troughs until a height of approximately 95 mm above the soil line was reached. This setup allowed to achieve a water-soluble sulfate content greater than 2.0% by mass

of soil, which corresponds to the most severe exposure class (S3) in ACI 318. Similarly, a calcium sulfate solution prepared to match the sulfate ion concentration of the 5% sodium sulfate solution was added to the other half of the troughs. Analogously to the indoor situation, large amounts of gypsum remained out of solution, but were added anyway and mixed thoroughly. The solutions were allowed to evaporate until they reached the soil line and were subsequently re-filled with water up to the original level. This outdoor setup is analogous to the one employed previously by Drimalas [Drimalas 2007].

Five concrete specimens per mixture were stored in the sodium sulfate troughs. Three prisms were placed vertically partially submerging 1/3 of their length in the soil. The middle 1/3 of the samples was initially submerged in the sodium sulfate solution, and the top 1/3 exposed to the air, as it is depicted in Figure 10.2. Two additional prisms were stored completely submerged below the soil line. On the other hand, three specimens were stored in the calcium sulfate troughs. These samples were placed below the soil level.

Figure 10.2: Partially Submerged Concrete Prisms in Na_2SO_4 Outdoor Exposure Site

After the initial measurement, successive length and mass change determinations were performed every month until the age of 6 months and every 3 months thereafter. In the case of the indoor specimens, the sulfate solution was renewed after each measurement.

A limited number of specimens were exposed to real field conditions in gypsiferous soils at two different exposure sites near the city of Van Horn, TX (Figure 10.3), where sulfate contents in the soil as high as 0.91% SO_4 were measured (Exposure class S3 in ACI 318) [Drimalas 2007]. A detailed description of these sites can be found in the dissertation of Drimalas [Drimalas 2007]. In analogy to the outdoor site in Austin, TX, partially and fully submerged specimens were evaluated.

Figure 10.3: Exposure Sites near Van Horn, TX in Areas of Calcium Sulfate Soil

Mortar bars were cast according to ASTM C1012 using a sand to cementitious material ratio of 2.75 and keeping a constant water to cementitious material ratio (w/cm) of 0.485. For each mix, 6 bars (25 × 25 × 285 mm) and 9-to-12 cubes (50 x 50 mm) were prepared and stored above water in sealed containers at 35°C. After 24 hours, the specimens were demolded and stored in limewater at 23°C until the strength of the companion cubes reached 20 ± 1 MPa. At that time, the bars were

measured to record their initial length and mass and stored in the sulfate solution at 23°C. Length and mass changes were calculated as the average of 5 bars after 7, 14, 21, 28, 56, 91, 105, 120, 180 days, and every 3 months thereafter. The sulfate solution was renewed after each measurement. The 6th bar was used to obtain samples for XRD examination at different exposure times. Following the same process, additional mortar bars were exposed to the sulfate solution at 5°C. In this case, after the companion cubes reached 20 ± 1 MPa, the bars were transferred to a refrigerator set at the specified temperature and kept there for a period of 24 hours, after which the bars were measured and stored in the sulfate solution.

At specific exposure times, samples of the bars were obtained and examined with X-ray diffraction (XRD). Samples were collected, finely ground below 105 μm, and analyzed on a Siemens D500 diffractometer with a DacoMP controller operating at 40 kV and 30 mA using a copper target (Cu Kα wavelength = 1.54Å). Scans were run from 5-60° 2θ with a step size of 0.02° and a dwell time of 4 seconds.

Pore size distributions of paste samples were obtained by mercury intrusion porosimetry (MIP). Thin slices (around 2mm thick) were cut from the paste specimens (w/cm of 0.485) and their hydration was stopped by immersion in isopropanol for 4 days, renewing the solvent periodically. The slices were subsequently stored for 3 days in a desiccator, and cut into 5 pieces of similar size to a total sample weight of approximately 1g. A Thermo Fisher Pascal 140/440 apparatus was used. The samples were intruded progressively up to a pressure of 100 kPa in the Pascal 140 unit and then moved to the high-pressure unit, were mercury was pressurized to a maximum value of 400 MPa.

10.3. Results and Discussion

This section presents the results of the testing conducted on concrete specimens under laboratory and field conditions. The performance of concrete prisms stored indoors in a 5% sodium sulfate solution at 23°C is compared to that of their counterparts stored at 5°C and to the samples submerged in the outdoor sulfate trenches. In addition, the concrete results are compared to the performance of mortar bars exposed to the same conditions. The final set of tests in sodium sulfate exposures includes the evaluation of the performance of prisms partially submerged in the outdoor sulfate-bearing soil. Finally, the results of concrete exposed to calcium sulfate under laboratory and field conditions are discussed.

10.3.1. Sodium Sulfate

10.3.1.1. Control Mixtures

Figure 10.4 shows the expansion curves of the control mixtures stored at 23°C. The high-C_3A mixtures showed an increase in the initial rate of expansion as the interground limestone level

increased. In good agreement with the mortar tests, the PLC2 mixture displayed a faster expansion than the PLC1 and PLC3 specimens. This result was surprising considering that the 13.4% limestone mixture showed a compressive strength development similar to the one exhibited by the PLC1 system [Garcia 2018]. The PLC4 samples displayed the highest initial rate of expansion. However, as opposed to the behavior observed in the lower-limestone counterparts, this expansion rate did not increase afterwards, and the length change of the specimens exhibited a linear-like behavior. This result was also observed in the mortar experiments. In this regard, the slow expansion displayed up to 200 days by the concrete prisms, which was not observed in the mortar tests, it is likely a consequence of the size difference between both specimens. In the case of the low-C_3A samples, a significantly faster expansion was exhibited by the mixture with the highest limestone content (PLC7) when compared to the PLC5 and PLC6 concretes, which expanded at a much slower rate than the rest of the mixtures. Finally, the Type V specimens showed negligible expansion after 2 years.

A good correlation between mortar and concrete testing was observed in all the PLC neat cement mixtures. The same trends in expansion were obtained by both procedures. However, the results of the Type V mortars reveal some of the inconsistencies widely acknowledged with regard to the ASTM C1012 test method. Although the Type V system met the expansion requirement at 6 months indicated in ASTM C595 to be qualified as highly sulfate resistant (HS), it subsequently exceeded the 12-month limit. In addition, it showed a greater expansion than the Type I/II counterpart after 400 days of exposure. On the other hand, the concrete specimens displayed negligible expansion after 2 years of immersion in a sodium sulfate solution of the same concentration and at the same temperature. The slower rate of expansion of the concrete specimens may be attributed to several factors, including the greater specimen size, the longer curing time before exposure to the aggressive solution, the slightly lower w/cm ratio, the wider aggregate gradation, and the lower paste/aggregate ratio.

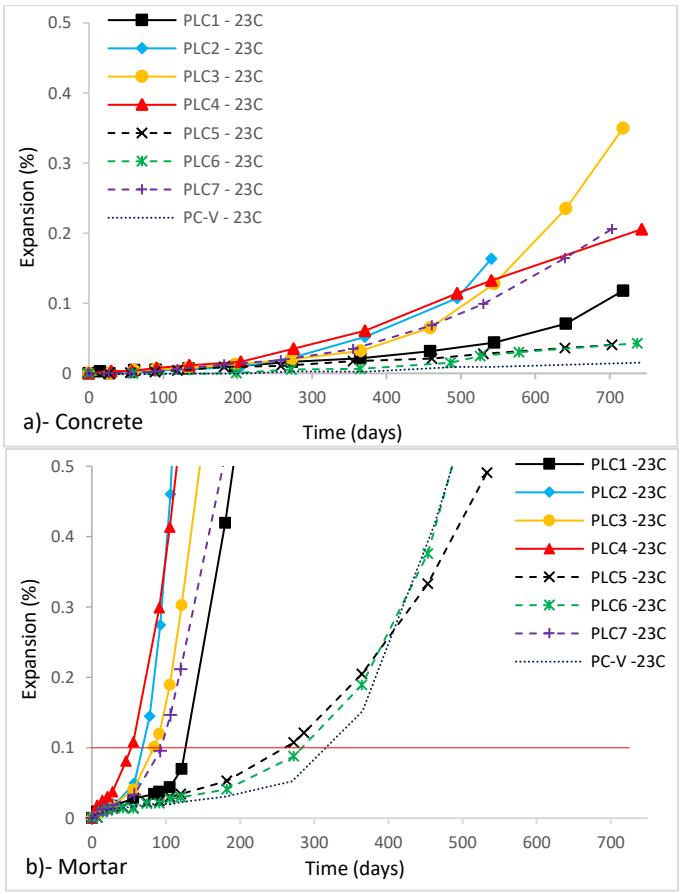

Figure 10.4: Expansion Curves of the Control Mixtures Stored at 23ºC in 5% Sodium Sulfate Solution. a) Concrete prisms and b) Mortar bars

The expansion of the samples stored at 5ºC is displayed in Figure 10.5. The high-C_3A specimens showed the same relative trends as their 23ºC analogous, i.e. the rate of initial expansion increased as the interground limestone level increased with the exception of the PLC2 mixture, which exhibited a faster length change than the PLC3 equivalent. In the case of the lower-C_3A systems, the PLC5 displayed negligible expansion after almost 2 years of exposure, outperforming all the other PLC mixtures in this testing condition as well. Interestingly, the PLC6 counterpart showed a precipitous increase in the expansion rate after 18 months. On the other hand, the PLC7 system exhibited a gradual increase of the rate of expansion and no abrupt acceleration was observed after almost two years of testing. While no difference in expansion was observed between the PLC5 and PLC6 mixtures at 23ºC, exposure at the low temperature significantly accelerated the rapid expansion of the mixture with 11.6% limestone. In this case, the prisms started showing a progressive surface deterioration between 6 and 9 months (Figure 10.8). At this time, samples of the loose material were examined by XRD and showed the presence of thaumasite, ettringite, and gypsum, and the complete depletion of portlandite. Since the surface degradation increased in severity from this time until after the onset of the rapid expansion at 18 months, it could be assumed

that it may have affected the sulfate ingress and contributed to the expansion phenomenon. Similarly, the PLC6 mortars, which showed an almost equivalent rate of expansion to the PLC5 counterparts when tested at 23°C, exhibited an earlier and more severe surface degradation than the PLC5 system and rapidly increased the expansion rate. The shift of the stage of fast expansion to earlier times may have been influenced by the greater extent of superficial damage observed, which at later times took the form of severe loss of cohesion corresponding to the formation of thaumasite. However, in the mortar case thaumasite was not detected until after the bars exhibited a significant acceleration of the expansion. This could be related to the difference in the time at which the macroscopic changes take place due to the size difference with respect to the concrete specimens.

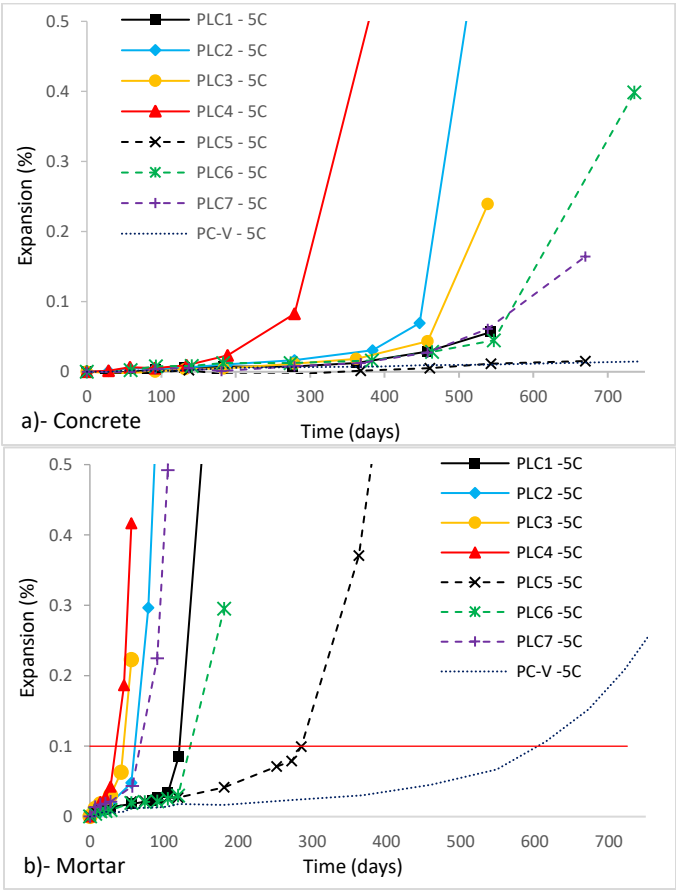

Figure 10.5: Expansion Curves of the Control Mixtures Stored at 5°C in 5% Sodium Sulfate Solution. a) Concrete prisms and b) Mortar bars.

The mass change monitoring of the concrete mixtures is presented in Figure 10.6. The specimens stored at 23°C experienced an increase in mass with time until 2 years of testing except for the PLC1 and PLC2 systems. In those two cases, the prisms exhibited loss of material associated with cracking and spalling. On the other hand, at the low testing temperature the PLC specimens displayed a faster deterioration characterized by an initial increase and a subsequent reduction in

mass. This mass drop was initially related to a progressive loss of material from the surface of the samples, which was accompanied by cracking and spalling as damage progressed. Contrastingly, the Type V samples showed a continuous mass gain with time.

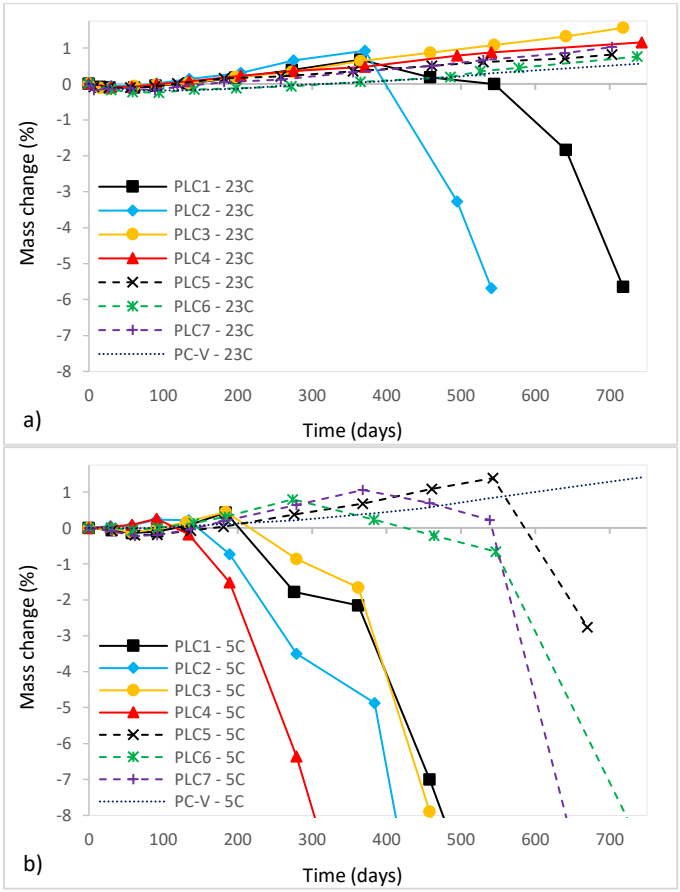

Figure 10.6: Mass Change of the Neat Cement Concrete Mixtures Stored in 5% Sodium Sulfate Solution at a) 23°C and b) 5°C.

The deterioration mechanism of the prisms stored at 23°C was considerably different to that observed at 5°C. Figure 10.7 and Figure 10.8 present pictures of the neat cement concrete mixtures exposed to the 23°C and 5°C sodium sulfate solutions, respectively. The PLC1 and PLC2 samples showed considerable loss of material due to cracking and spalling at both ends of the prism. The PLC2 system exhibited the worse damage and, after 18 months of testing, one of the specimens was fragmented in several pieces. On the other hand, the rest of the control mixtures showed minimal signs of damage after 2 years of exposure at 23°C. These results agree with mortar experiments [Tiburzi 2018b], where the PLC1 and PLC2 systems displayed the worst deterioration among all control mixtures.


Mix S1
C
Mix S1
B
Na
Mix S1
A
Na
a)
S-10
C
Na
indoor
S-10
B
Na
indoor
A
Na
indoor
b)
6858 MIX S2 06/30/15
C
Na
6858 MIX S2 06/30/15
B
Na
6858 MIX S2 06/30/15
A
Na
c)
C
S-11
Na
indoor
B
S-11
Na
A
S-11
Na
indoor
d)
MIX S-8 A
PLC5 STRAIGHT
MIX S-8 B
PLC5 STRAIGHT
e)
C
6858 S-13
Na
Indoor
6/7/16
B
6858 S-13
Indoor
Na
6/7/16
A
6858 S-13
Na
Indoor
f)

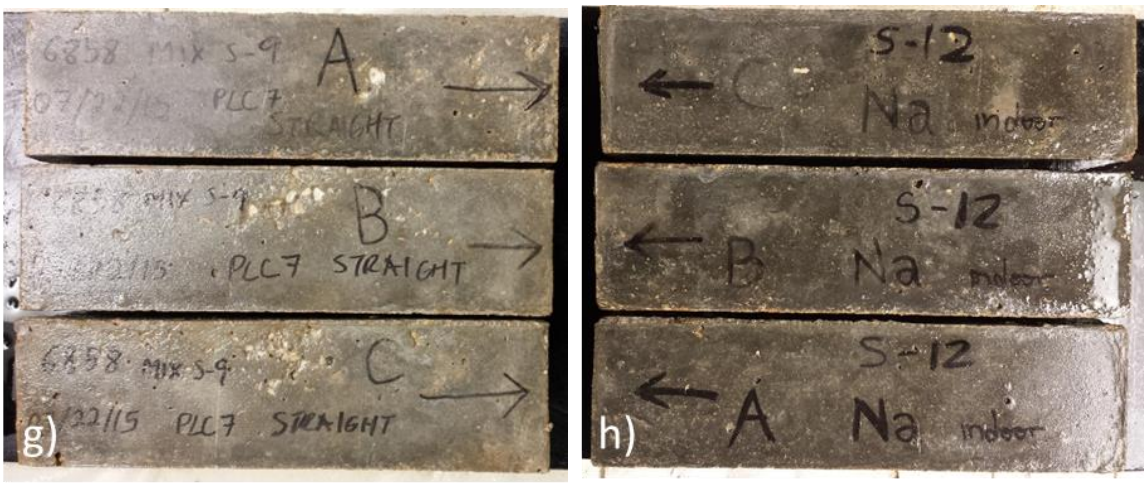

a) PLC1 after 24 months, b) PLC2 after 18 months, c) *PLC3 after 24 months, d) PLC4 after 24 months, e) PLC5 after 24 months, f) PLC6 after 24 months, g) PLC7 after 24 months, h) Type V after 24 months.*

Figure 10.7: Neat Cement Concrete Mixtures Stored in 5% Sodium Sulfate Solution at 23°C

At 5°C, a much faster degradation of the PLC samples was observed. The high-C_3A systems exhibited severe loss of cohesion and material from the surface of the specimens. This phenomenon was initially observed between 3 and 4 months in the PLC2 and PLC4 systems and between 5 and 6 months in the PLC1 and PLC3 counterparts and progressed in increasing severity as the degraded structure allowed a greater interaction with the sulfate solution. A white and soft material composed of thaumasite, ettringite, and calcite formed at the surface of the concrete. This substance formed initially at the finished surface of the specimens, but was found in higher amounts underneath a relatively harder, thin paste layer on the sides of the prisms, where it was protected from direct exposure to the sulfate solution. As time progressed, the samples cracked into several pieces and exhibited a severely degraded surface. In addition, significant amounts of the material accumulated at the bottom of the container transformed into a non-cohesive mush. The described phenomenon was much more pronounced in the mixtures with higher interground limestone content. On the other hand, the lower-C_3A mixtures displayed a delayed and less extensive damage, which is consistent with the differences observed in the mass change. The Type V specimens showed the highest resistance, and no loss of cohesion was detected.


a)
b)
c)
S-2
B
S-2
d)
e)
S-8
B
S-8
A
f)
6/7/16
B
A

a) PLC1 after 22 months, b) PLC2 after 18 months, c) PLC3 after 22 months, d) PLC4 after 18 months, e) PLC5 after 22 months, f) PLC6 after 24 months, g) PLC7 after 22 months, h) Type V after 24 months

Figure 10.8: Neat Cement Concrete Mixtures Stored in 5% Sodium Sulfate Solution at 5°C

The expansion and mass change data for the neat cement concrete mixtures fully submerged in the sulfate-bearing soil are presented in Figure 10.10 (a) and (b), respectively. The outdoor samples exhibited a faster expansion than that of the specimens stored continuously at both 5°C and 23°C in laboratory conditions. The disparities observed are influenced by the differences in the temperature history (Figure 10.9) and the constant changes in the concentration of the sulfate solution as evaporation proceeds. In these conditions, the prisms are likely to experience a combined form of attack, chemical and physical in nature. The only exception to this result was the PLC4 mixture, which expanded at a faster rate when stored continuously at 5°C. Nevertheless, the comparison of expansion rates does not seem appropriate to evaluate relative performances, as the degradation mechanism at each exposure condition was different. This was demonstrated in Chapter 2 for mortar systems exposed to diverse sulfate solutions at different temperatures [Tiburzi 2018a].

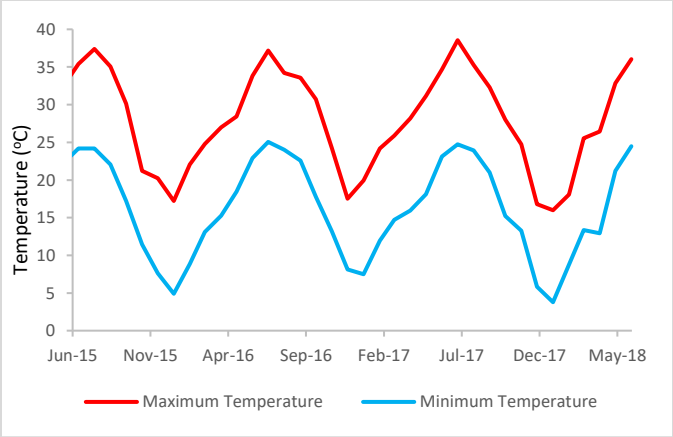

Figure 10.9: Monthly Average Maximum and Minimum Temperatures in Austin, TX throughout the Duration of the Outdoor Testing Program

Although the outdoor exposure differed significantly from the isothermal storage at 23°C, the relative trends in expansion were analogous in these two conditions. The Type V mixture exhibited the best performance among all neat cement systems. However, it reached an expansion greater than 0.07% after 24 months of testing, which does not indicate a high level of sulfate resistance. Similarly, the PLC5 and PLC6 systems showed no difference in the expansion rate until 18 months, after which the PLC6 specimens started expanding more rapidly. On the other hand, a significantly faster expansion was observed for the samples with the highest limestone content (PLC7). This relative behavior between the moderate-C_3A concrete mixtures resembles exactly the results in mortar stored at 23°C shown in Figure 10.4 (b).

The results of the outdoor high-C_3A specimens, likewise, presented a good correlation with the 23°C concrete and mortar experiments. The PLC2 mixture displayed the fastest deterioration, followed by the PLC1 counterpart. As it was shown before, these two systems exhibited extensive cracking and loss of material and, in this particular exposure condition, were completely disintegrated in less than 18 months. This is clearly observed in Figure 10.10 (b), which depicts the severe mass loss that accompanied the precipitous increase in the expansion rate. The increase in the limestone content significantly changed the expansion behavior, progressively reducing the abruptness of the expansion. This result was also observed in the indoor concrete experiments and in the evaluation of plain and blended mortar systems, which is discussed in detail in Chapter 3 [Tiburzi 2018b]. In the outdoor study however, the effect on the expansion rate of the highest limestone mixture was especially pronounced, allowing the PLC4 mixture to expand at a constant rate and reach a similar expansion level to the Type I/II concrete after 2 years.

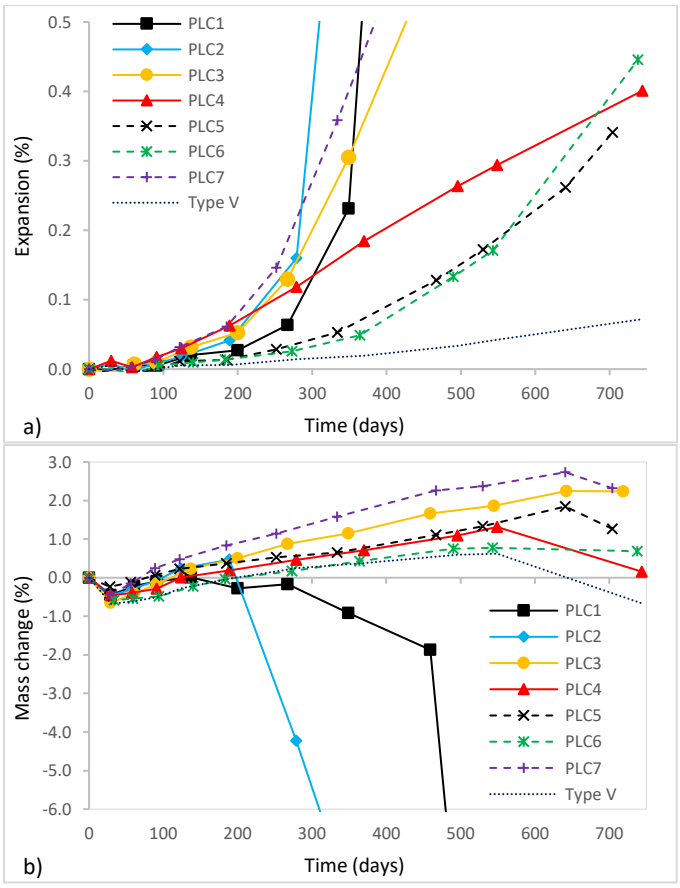

Figure 10.10: Mass Loss. a) Expansion and b) mass change data for the outdoor neat cement concrete mixtures fully submerged in the sodium sulfate trough.

Figure 10.11 present pictures of the neat cement outdoor concrete mixtures. The PLC1 and PLC2 samples showed clear signs of a precipitous deterioration. Both mixtures exhibited significant cracking and spalling and lost their integrity in less than 18 months, which is associated with the fast expansion experienced. On the other hand, the rest of the control mixtures displayed a more gradual damage process. After 2 years of exposure, the PLC3, PLC5, PLC6, and PLC7 prisms showed rounded edges and slight-to-moderate cracking at both ends. This degradation caused the slight mass loss observed in Figure 10.10 (b). Distinctively, the PLC4 and Type V mixtures, which showed no sudden change in the expansion rate after 2 years of testing, exhibited marginal cracking. Instead, the prisms displayed a generalized scaling of the surface that caused a relatively greater mass loss.

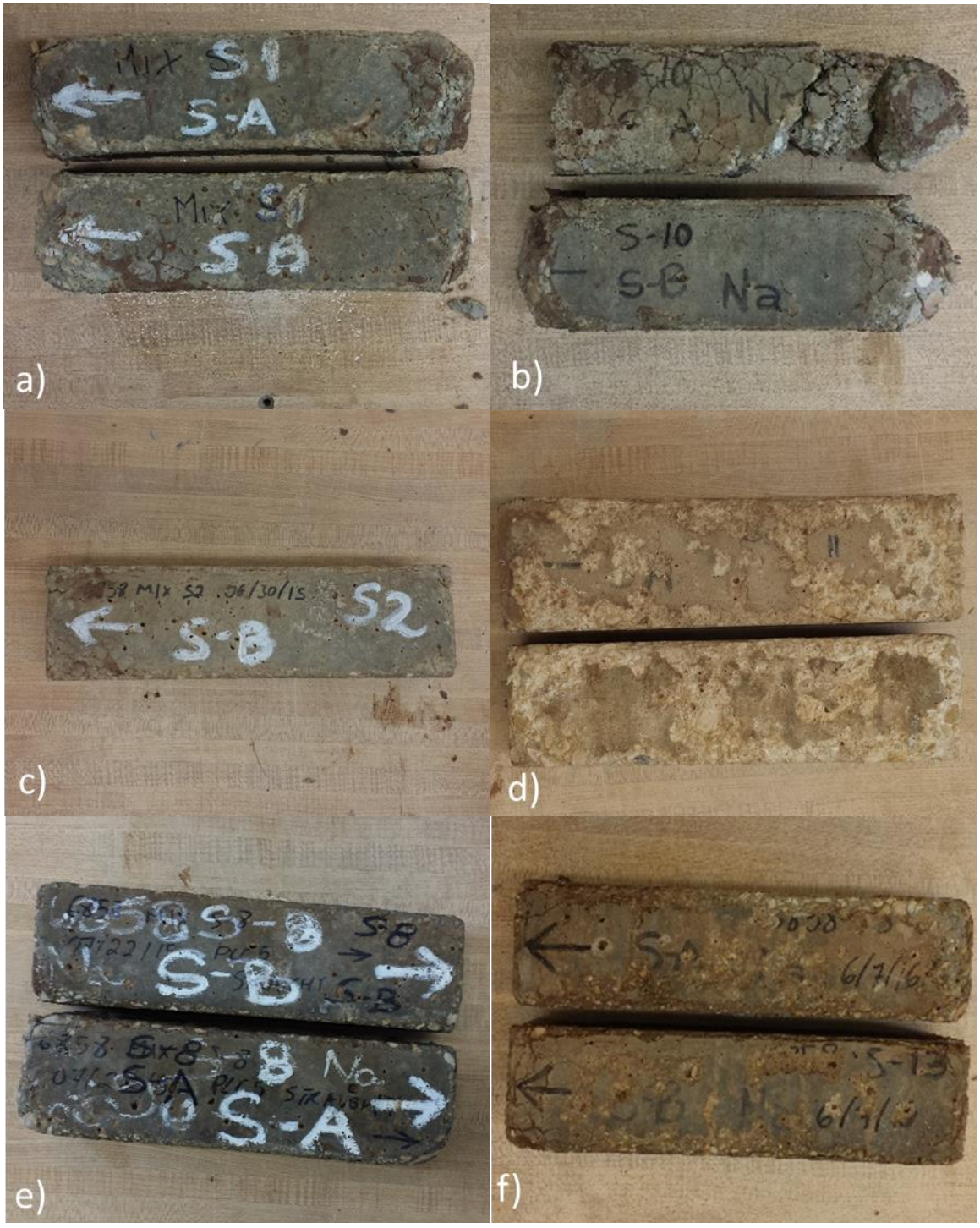
Mix S1
S-A
Mix S1
S-B
a)
S-10
S-B Na
b)
S2
S-B
c)
d)
S-B
S-B
e)
S-A
f)

a) PLC1 after 15 months, b) PLC2 after 16 months, c) PLC3 after 24 months, d) PLC4 after 24 months, e) PLC5 after 24 months, f) PLC6 after 24 months, g) PLC7 after 24 months, h) Type V after 24 months.

Figure 10.11:. Neat Cement Concrete Mixtures Fully Submerged in the Outdoor Sodium Sulfate Trough

10.3.2. Class F Fly Ash Mixtures

Figure 10.12 (a) presents the expansion data of the concrete prisms that incorporated 20% Class F fly ash stored in laboratory conditions at 5ºC and 23ºC. As expected, the three SCM mixtures showed a decrease in expansion with respect to the neat cement specimens when stored in the sulfate solution at 23ºC. This result was also observed in the mortar experiments shown in Figure 10.12 (b). However, the relative behavior between the three concrete mixtures was not the same as the one obtained in the mortar tests. Although the PLC3 mortar blend outperformed the PLC4 and PLC7 counterparts, the concrete samples showed a greater strain than the PLC4 system, which expanded at the lowest rate. In this regard, the extended 28-day curing of the concrete specimens may have played a particularly significant role in enhancing the resistance of the lowest-clinker blend, which is expected to exhibit a limited microstructural development before exposure to sulfates under the ASTM C1012 curing regime. The three 5ºC mixtures showed a faster degradation and a sudden increase in the expansion after 9 months in the case of the PLC4 mixture and after 12 months in the case of the PLC3 and PLC7 systems. The accelerated deterioration of the prisms exposed to the 5ºC solution as compared to the companion samples stored indoors at 23ºC and outdoors was more marked in these SCM specimens. This may be explained by the higher sensitivity of SCM systems to the curing temperature [De Weerdt 2012][Deschner 2013]. This effect was also observed in the mortar tests and is discussed in detail in Chapter 9 [Tiburzi 2018a].

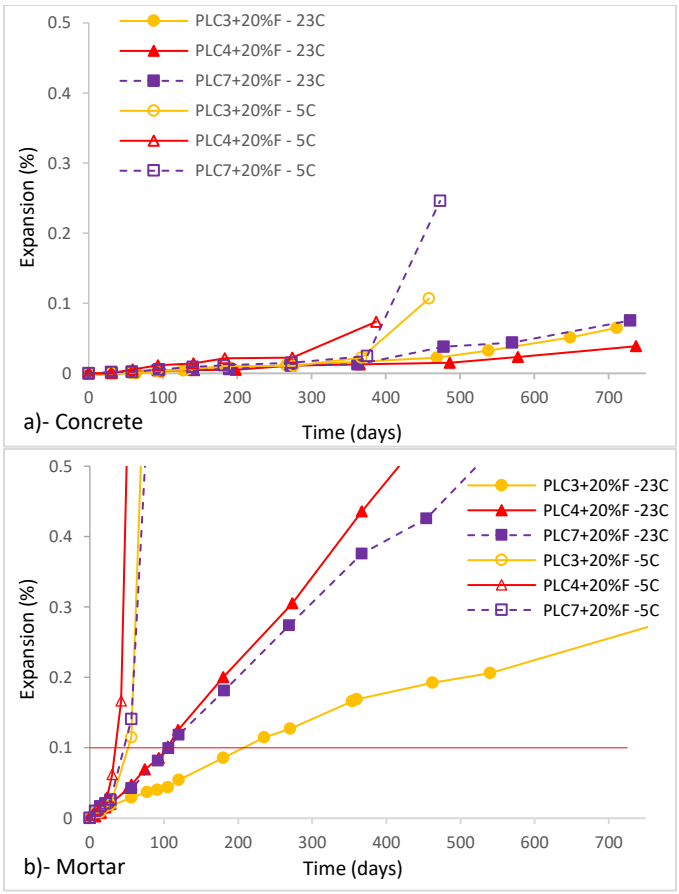

Figure 10.12: Expansion Data of Systems with 20% Class F Fly Ash Stored in Laboratory Conditions at 5ºC and 23ºC. a) Concrete prisms, b) Mortar bars.

The mass change plots presented in Figure 10.13 show analogous results to the control mixtures. The three 23ºC mixtures exhibited a relatively linear mass increase with time. On the other hand, the 5ºC samples displayed a rapid mass drop resulting from the progressive loss of material from the surface, which at later times was complemented by cracking and spalling. This phenomenon started considerably before the onset of expansion and was more pronounced in the two mixtures with the highest limestone content. In agreement with this evaluation, the damage pattern of the fly ash systems resembled the one exhibited by the neat cement concretes, as it is observed in Figure 10.14.

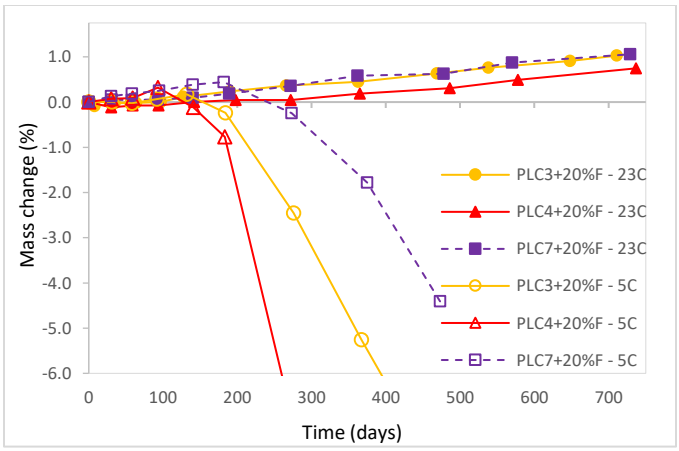

Figure 10.13: Mass Change Data of Concrete Systems with 20% Class F Fly Ash Stored in Laboratory Conditions at 5°C and 23°C

a) PLC3 at 23°C, b) PLC3 at 5°C, c) PLC4 at 23°C, d) PLC4 at 5°C, e) PLC7 at 23°C, f) PLC7 at 5°C.

Figure 10.14: Concrete Specimens with 20% Class F Fly Ash Stored in Laboratory Conditions after 18 Months of Exposure

Finally, as it occurred in the evaluation of the neat cement systems, the outdoor fly ash mixtures fully submerged displayed a faster expansion than the counterparts stored indoors at 23ºC. In addition, the same relative trends between mixtures were obtained, as it is shown in Figure 10.15 (a). In this case, however, the outdoor samples expanded at a slower rate than the 5ºC specimens. The mass change plots presented in Figure 10.15 (b) clearly depict the slight mass loss due to scaling at the edges of the prisms observed in Figure 10.16. This effect was again more pronounced in the PLC4 blend, which showed the lowest expansion after 2 years of exposure.

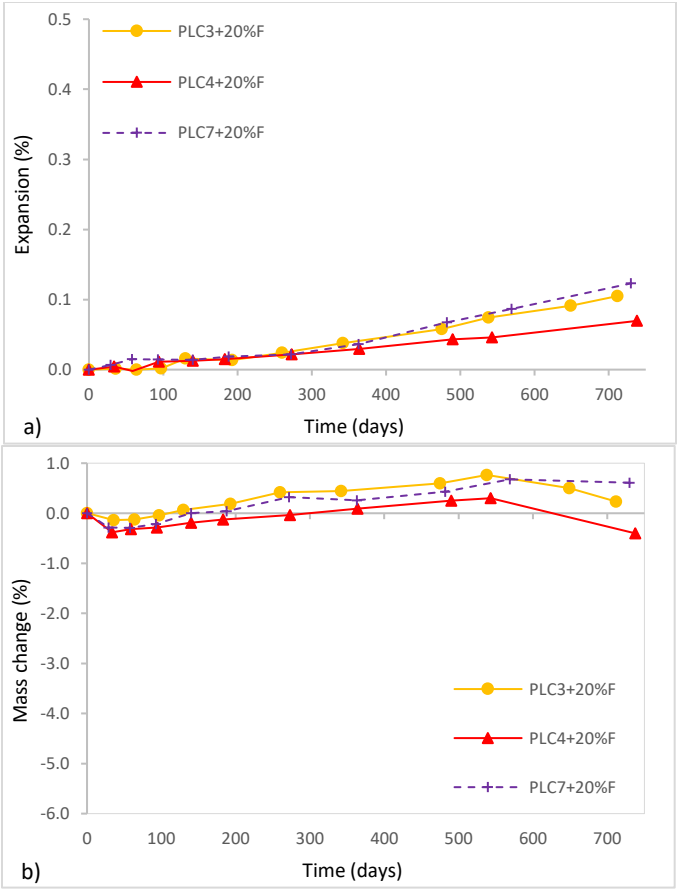

Figure 10.15 Mass Change Plots. a) Expansion and b) mass change data of concrete systems with 20% Class F fly ash fully submerged in the outdoor sodium sulfate trough.

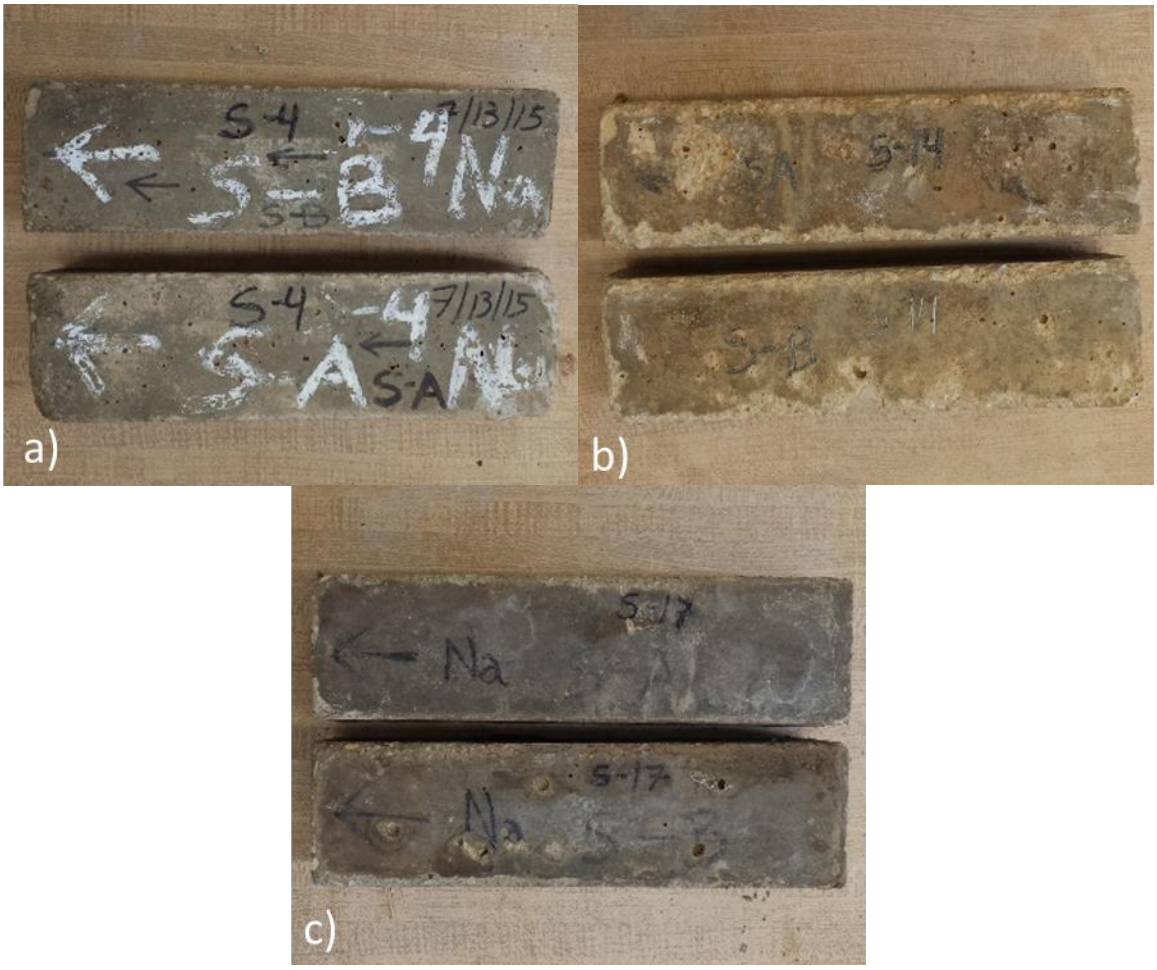

Figure 10.16: Class F Fly Ash Concrete Mixtures Fully Submerged in the Outdoor Sodium Sulfate Trough after 24 Months of Exposure. a) PLC3, b) PLC4, c) PLC7.

10.3.3. Class C Fly Ash Mixtures

The length change curves for the systems with the two Class C fly ashes stored at 23ºC are presented in Figure 10.17. The incorporation of 20% of any of these two SCMs accelerated the expansion of the control mixture. This effect was more pronounced with the incorporation of the C2 fly ash, which has the highest calcium content and a mineralogy significantly different from that of the C1 fly ash [Tiburzi 2018b]. These results differ from the observations in mortar samples, which showed no difference in expansion with respect to neat PLC3 mixture with the incorporation of 20% C2 fly ash and an enhanced performance with the use of 20% C1 fly ash. On the other hand, the combination of 5% silica fume with 20% of any of the two fly ashes significantly improved the performance of the concrete systems. Although this effect has been previously reported [Shashiprakash 2001][Dhole 2011][Thomas 1999], it was not observed in the mortar experiments presented in this work. Contrarily, the addition of 5% silica fume slightly accelerated the expansion of both 20% Class C fly ash mortar systems. In this case, the disparity between the

mortar and concrete results may be explained by the greater influence of the silica fume incorporation on the densification of the interfacial transition zone (ITZ) in concrete, which is expected to be more pronounced due to the presence of the coarse aggregate. In addition, the extended curing regime of the concrete prisms may have contributed to the further reduction of the ionic diffusivity due to hydration and pozzolanic reactions. Finally, the replacement of 40% of the cement with fly ash reduced the expansion rate of both SCM systems. This performance enhancement was more significant in the case of the lower-calcium Class C fly ash, which agrees with the trend observed in the mortar tests.

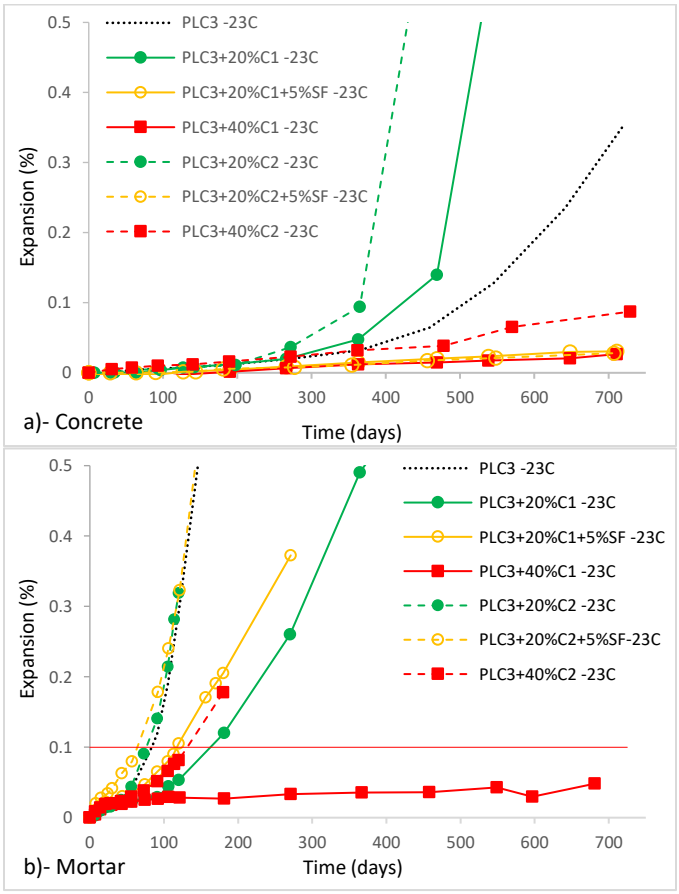

Figure 10.17: Expansion Curves of the Class C Fly Ash Mixtures Stored at 23ºC in 5% Sodium Sulfate Solution. a) Concrete prisms and b) Mortar bars.

The exposure to the sulfate solution at 5ºC significantly accelerated the deterioration of all the concrete and mortar specimens, as it is shown in Figure 10.18. The mixtures that exhibited minimal expansion in the 23ºC experiments outperformed the control system in this condition as well. However, they displayed a marked acceleration of the expansion between 15 and 18 months. On the other hand, both mixtures with 20% Class C fly ash and the system with 40% C2 showed a much earlier onset of the rapid expansion. The relative differences between the mortar samples were evident in a considerably shorter time span, as all the mixtures expanded significantly before

56 days. In any case, the SCM mortars performed worse than the control mixture. In addition, in contrast to the 23ºC counterparts, the increase in the fly ash content from 20% to 40% did not change the expansion or even accelerated it.

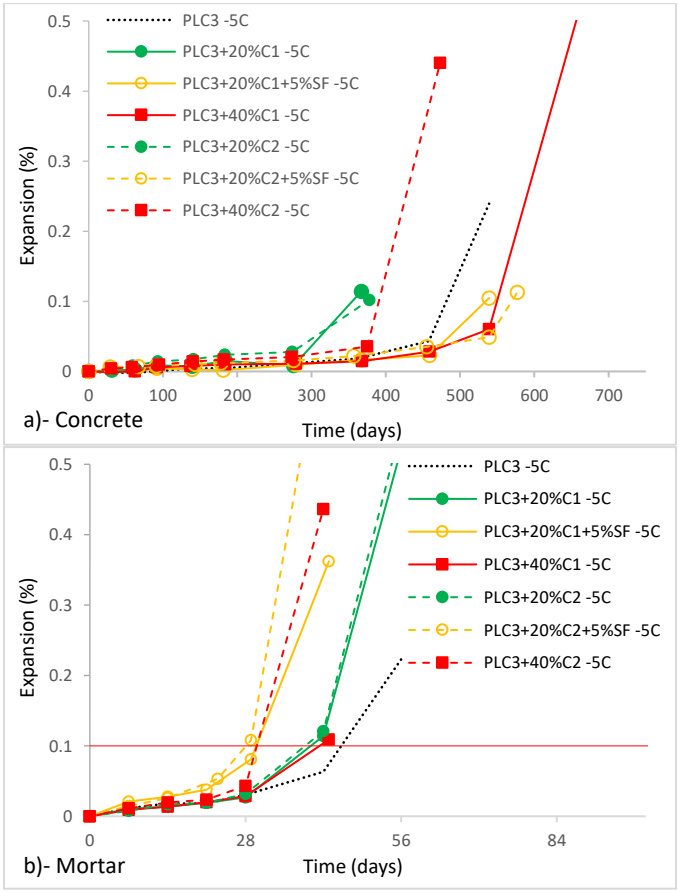

Figure 10.18: Expansion Curves of the Class C fly Ash Mixtures Stored at 5ºC in 5% Sodium Sulfate Solution. a) Concrete prisms and b) Mortar bars.

Figure 10.19 (a) and (b) present the mass change data for the concrete mixtures exposed at 23ºC and 5ºC, respectively. The 23ºC specimens with 20% fly ash were the only ones that showed a decrease in mass, which was a consequence of the severe cracking and spalling that accompanied the abrupt expansions, as observed in Figure 10.20. The rest of the mixtures experienced an increase in mass with time and only minor signs of damage. In line with the previous results, the 5ºC prisms displayed a significant mass loss due to a gradual surface degradation that was complemented by cracking and spalling as the samples increased their expansion rate (Figure 10.21). Accordingly, the samples with 5% silica fume and the mixture with 40% C1 fly ash exhibited the less severe deterioration. Interestingly, the 40% C1 system experienced a more gradual mass drop despite showing an initially greater rate than the silica fume specimens.

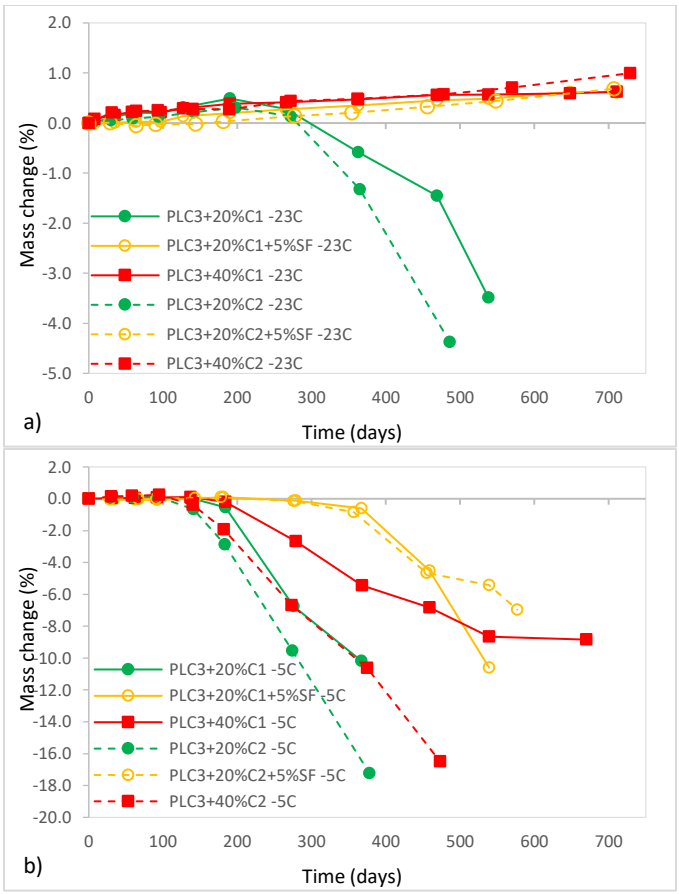

Figure 10.19: Mass Change of the Class C Fly Ash Concrete Mixtures Stored in 5% Sodium Sulfate Solution. a) 23°C, and b) 5°C.

a) PLC3+20%C1 after 24 months, b) PLC3+20%C2 after 15 months, c) PLC3+20%C1+5%SF after 24 months, d) PLC3+20%C2+5%SF after 24 months, e) PLC3+40%C1 after 24 months, f) PLC3+40%C2 after 24 months.

Figure 10.20: Class C Fly Ash Concrete Mixtures Stored in 5% Sodium Sulfate Solution at 23°C.

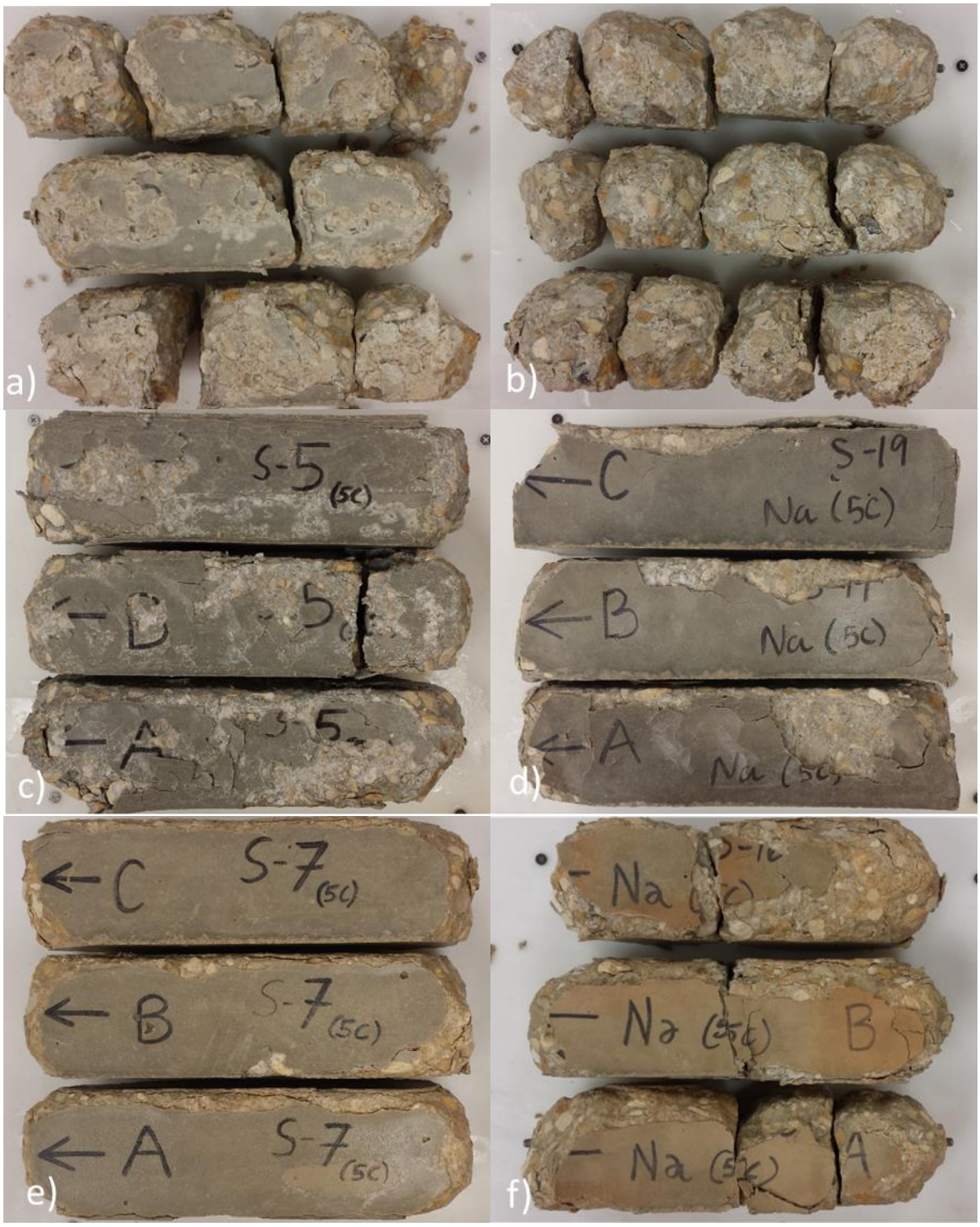

a) PLC3+20%C1 after 15 months, b) PLC3+20%C2 after 18 months, c) PLC3+20%C1+5%SF after 18 months, d) PLC3+20%C2+5%SF after 18 months, e) PLC3+40%C1 after 18 months f) PLC3+40%C2 after 18 months.

Figure 10.21: Class C Fly Ash Concrete Mixtures Stored in 5% Sodium Sulfate Solution at 5°C.

Consistently with the results already discussed, the outdoor samples fully submerged exhibited analogous trends to the companion specimens stored indoors at 23ºC. The expansion data, mass change, and pictures of the concrete mixtures are presented in Figure 10.22 (a), Figure 10.22 (b), and Figure 10.23, respectively.

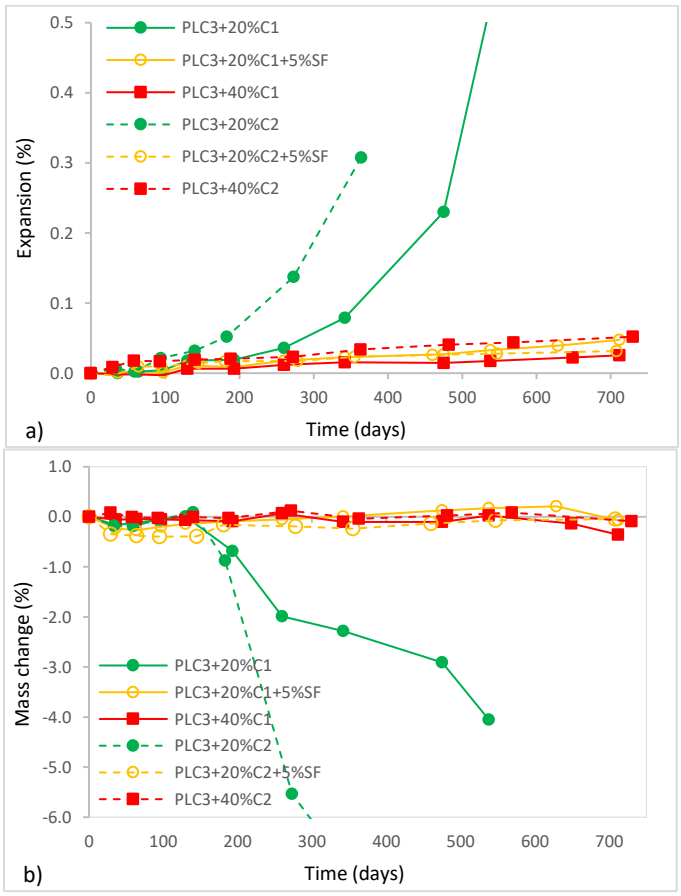

Figure 10.22: Expansion and Mass Data. a) Expansion and, b) mass change data of concrete systems with Class C fly ash fully submerged in the outdoor sodium sulfate trough.

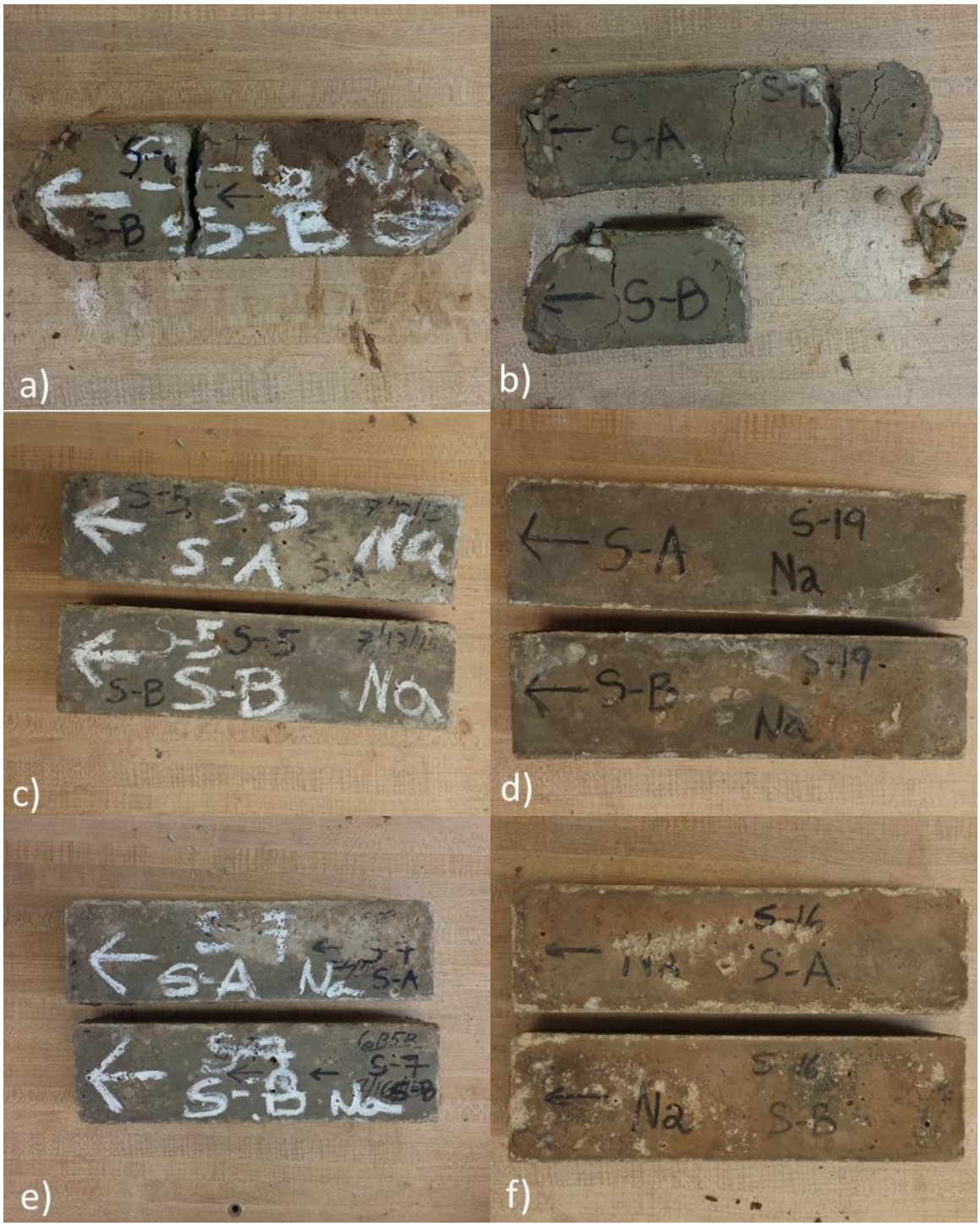

a) PLC3+20%C1 after 21 months, b) PLC3+20%C2 after 16 months, c) PLC3+20%C1+5%SF after 24 months, d) PLC3+20%C2+5%SF after 24 months, e) PLC3+40%C1 after 24 months f) PLC3+40%C2 after 24 months.

Figure 10.23: Class C Fly Ash Concrete Mixtures Fully Submerged in the Outdoor Sodium Sulfate Trough

10.3.4. Slag Mixtures

The length change of the concrete slag mixtures store indoors at 5°C and 23°C, and outdoors is shown in Figure 10.24 (a). In comparison with the rest of the neat cement and blended systems, the resistance of the 35% slag blends was significantly superior. No difference was observed between the concrete specimens stored indoors at 5°C and 23°C, all of which experienced negligible expansions after 2 years of exposure (note that the scale of the vertical axis in Figure 10.24 (a) has been changed). Similarly, the outdoor prisms showed a good performance relative to the other SCM systems. The mortar specimens stored at 23°C displayed analogous results. However, the expansion of the low-temperature samples did not match that of the standard mortars.

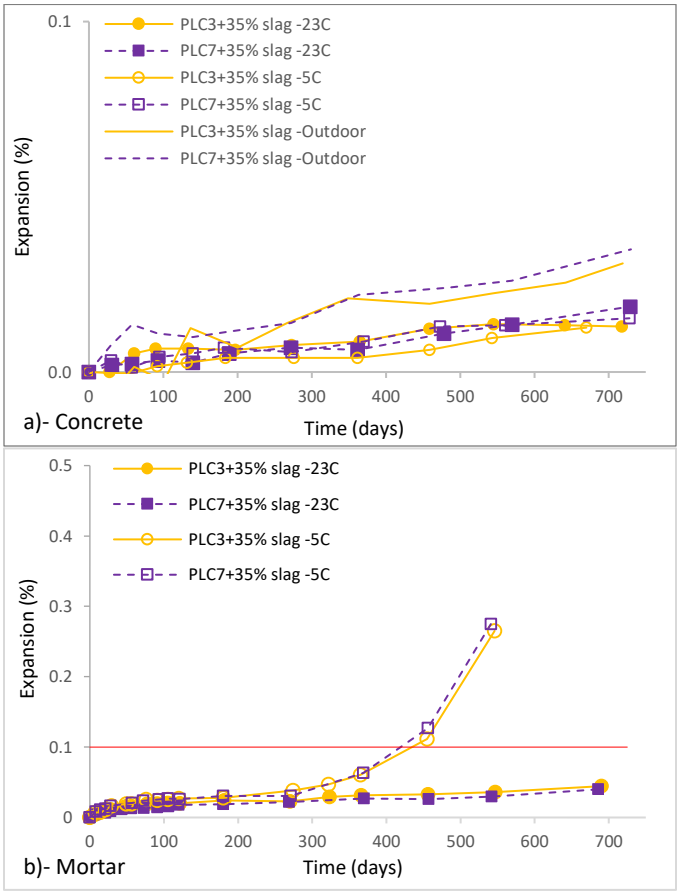

Figure 10.24: Length Change of the Systems with 35% Slag Stored Indoors in 5% Sodium Sulfate at 5°C and 23°C and Fully Submerged in the Outdoor Sodium Sulfate Trough. a) Concrete prisms and b) Mortar bars.

The mass change data of the slag concrete mixtures are shown in Figure 10.25. In contrast to all of the systems presented before with the exception of the Type V mixture, the indoor slag blends showed an increase in mass at both temperatures, which agrees with the good condition of the prisms shown in Figure 10.26. Slight cracking localized at the corners of the specimens constituted

the only signs of damage detected. On the other hand, the outdoor samples fully submerged exhibited moderate scaling that resulted in the mass loss observed after 18 months.

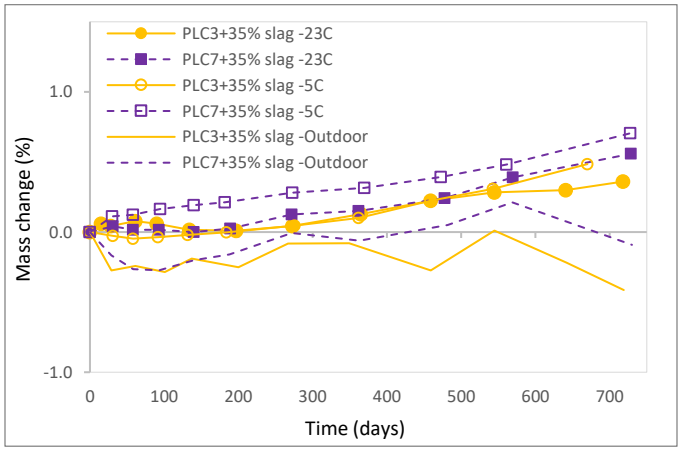

Figure 10.25: Mass Change of the Concrete Systems with 35% Slag Stored Indoors in 5% Sodium Sulfate at 5°C and 23°C and Fully Submerged in the Outdoor Sodium Sulfate Trough

a) PLC3 at 23°C after 24 months, b) PLC7 at 23°C after 24 months, c) PLC3 at 5°C after 22 months, d) PLC7 at 5°C after 24 months, e) Outdoor PLC3 after 24 months, f) Outdoor PLC7 after 24 months.

Figure 10.26: Concrete Mixtures with 35% Slag

10.3.5. Partially Submerged Specimens

The expansion and mass change plots of the specimens partially submerged in the outdoor sulfate-bearing soil are presented in Figure 10.27 (a) and (b), respectively. With the exception of the PLC1 and PLC7 neat cement mixtures, the prisms subjected to this condition displayed an expansion slightly slower than that of the submerged ones. This result was expected, as a smaller fraction of the specimens was directly exposed to the sulfate solution. Regarding the PLC1 and PLC7 cases mentioned, although no difference was observed in the expansion behavior, the submerged and partially-submerged prisms exhibited a significantly different damage mechanism, as it is shown in Figure 10.28.

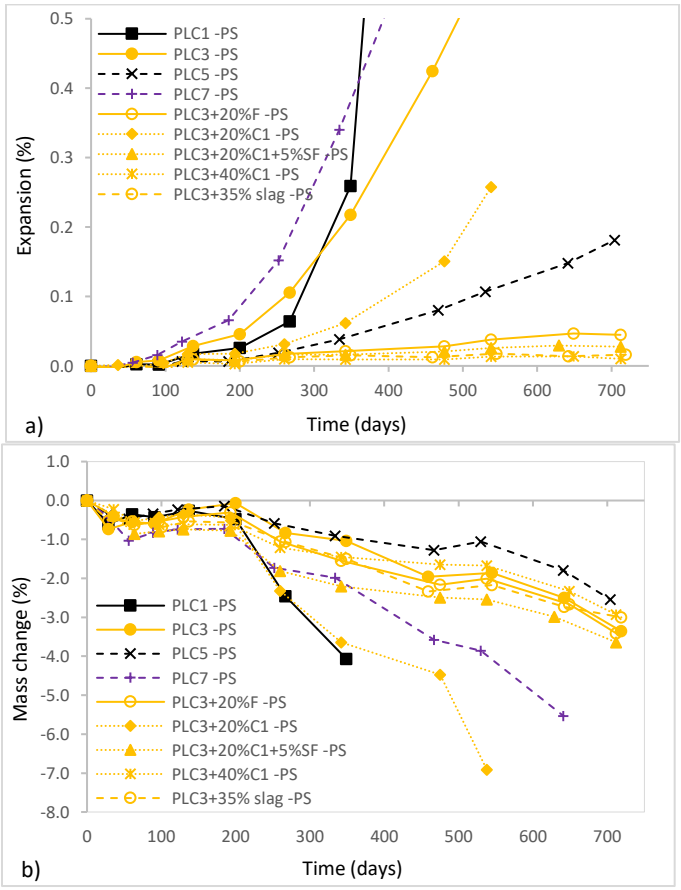

Figure 10.27:Expansion and Mass Change Plots. a) Expansion and b) mass change plots of the concrete specimens partially submerged in the outdoor sulfate-bearing soil.


a)
b)
c)
d)
e)
f)

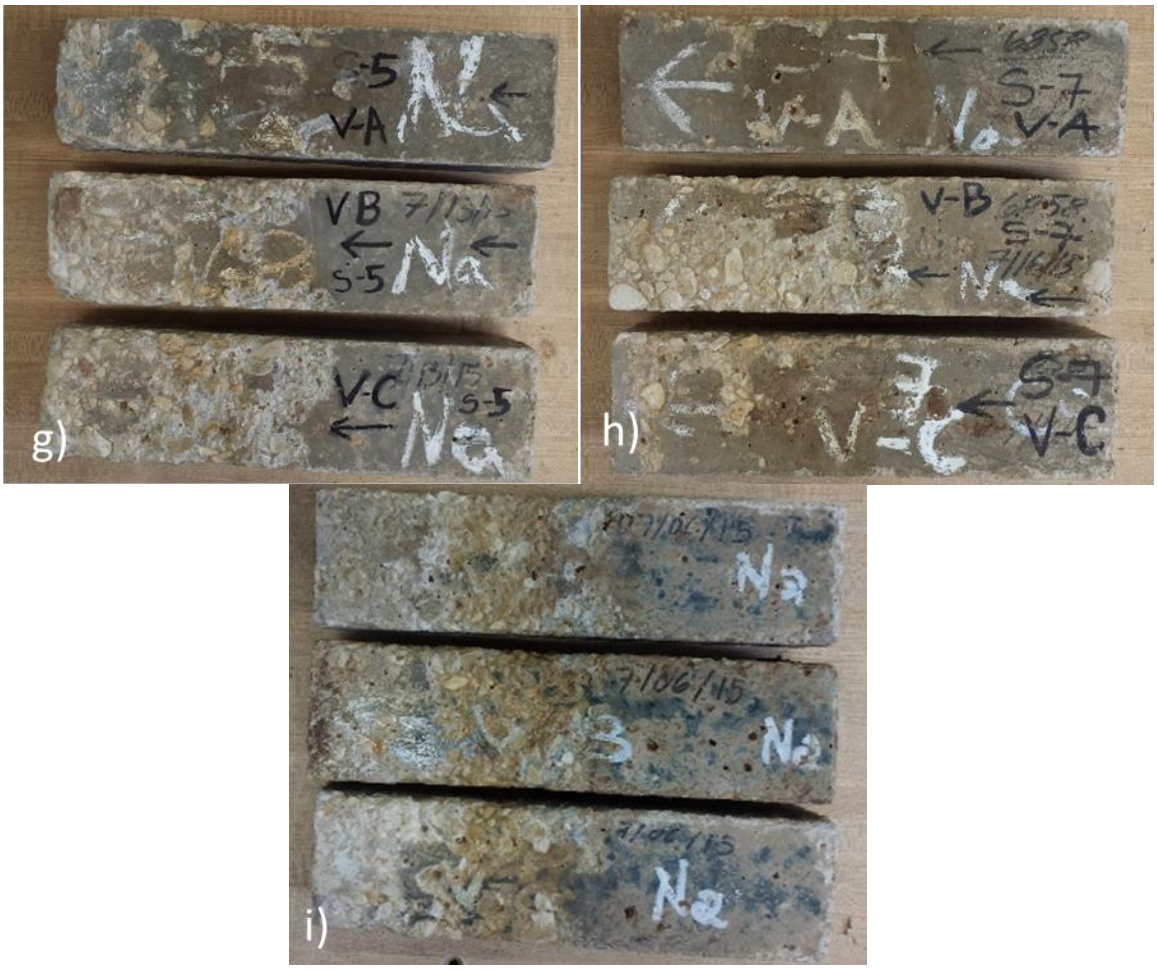

a) PLC1 after 15 months, b) PLC3 after 24 months, c) PLC5 after 24 months, d) PLC7 after 24 months, e) PLC3+20%F after 24 months, f) PLC3+20%C1 after 21 months, g) PLC3+20%C1+5%SF after 24 months, h) PLC3+40%C1 after 24 months, i) PLC3+35% Slag after 24 months.

Figure 10.28: Concrete Mixtures Partially Submerged in the Outdoor Sodium Sulfate Trough.

Damage due to physical salt attack is attributed to crystallization pressure due to the growth of crystals from a supersaturated solution in confined spaces. As it has been demonstrated by Scherer and Flatt [Scherer 1999][Scherer 2004][Flatt 2008], it is the degree of supersaturation and the characteristics of the sites (shape/size) at which the salts precipitate what dictate the pressure developed. In this study, the portion of the prisms above the soil level experienced a progressive scaling that increased in severity as the distance from the soil line increased. This damage gradient can be explained by the differences in the location at which the sodium sulfate crystals grow and the changes in the concentration of the rising solution as a function of the height, as explained by Scherer [Scherer 2004] and illustrated in Figure 10.29. The solution rises into the concrete specimen at a rate that decreases with height, while evaporation from the surface occurs at a nearly constant rate. Near the soil/solution level, the rate of capillary rise is greater than the rate of evaporation. Consequently, a liquid film forms on the concrete surface. Although evaporation

raises the concentration of the solution near the surface, at this low height the diffusion of salt back toward the source may prevent the solution from becoming supersaturated. As the distance from the soil increases, the relative weight of capillary rise respect to evaporation decreases, which reduces the thickness of the liquid film. At this greater height, the increase in the salt concentration can cause the solution to become supersaturated and crystals may precipitate in the liquid film on the concrete surface, which is known as efflorescence. Finally, above a certain height, the rate of evaporation exceeds the rate of capillary rise, which causes the liquid-vapor interface to retreat inside the material. When crystals precipitate at this location, which is known as subflorescence, damage will occur if the crystallization pressure exceeds the tensile strength of the concrete.

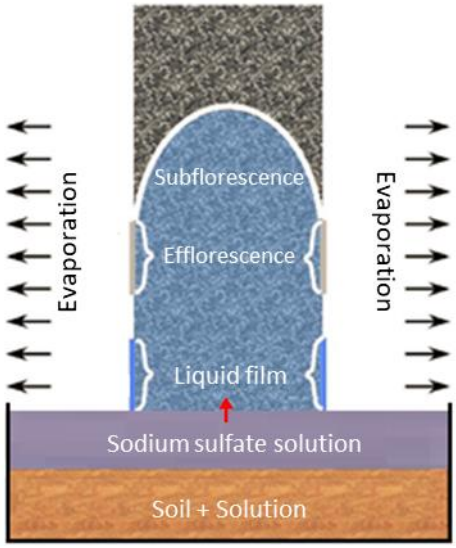

Figure 10.29: Schematic of Capillary Rise and Evaporation from a Concrete Sample Partially Submerged in a Sodium Sulfate Solution. Adapted from [11].

Concurrently with the mechanism involving capillary rise and evaporation, damage may also be caused by phase changes induced by variations in temperature and relative humidity [Folliard 1994][Skalny 2002]. In the particular case of sodium sulfate, severe damage has been reported to occur due to phase changes between its anhydrous form thenardite (Na_2SO_4) and the decahydrate form mirabilite ($Na_2SO_4 \cdot 10H_2O$), and due to rapid crystallization of mirabilite from a supersaturated solution induced by rapid cooling, without transition to thenardite [Folliard 1994][Haynes 1996][Haynes 2008]. The cyclic volumetric changes associated with these phenomena can subsequently damage the cement paste matrix and contribute to the deterioration pattern described.

The evaluation of the attack based solely on mass loss can lead to wrong interpretations in the cases where cracking and spalling due to ettringite formation are significant. In this regard, the different deterioration patterns observed in the portions below and above the soil level clearly revealed the two different mechanisms of damage. While the nature of the damage above the soil

is primarily “physical”, chemical and physical effects act simultaneously in the submerged portions of the specimen. This condition was clearly evident in the PLC1 (Figure 10.28 (a)) and PLC3+20%C1 (Figure 10.28 (f)) systems, which exhibited the greatest mass drop due to severe cracking and loss of material in the submerged part of the prisms. The PLC7 mixture showed the worst degradation in the evaporation zone. However, minor damage was observed in the submerged portion, which is reflected in the more gradual mass loss as a function of exposure time. This same effect was detected in the rest of the mixtures, although the damage due to salt crystallization in the evaporation area (and consequently the loss of mass) was less severe.

As it is shown in Figure 10.28, the PLC7 mixture suffered from the most severe damage above the soil line, followed by the PLC3+20%C1 and PLC1 systems. The PLC3, PLC5, and PLC3+20%F specimens exhibited a slightly higher resistance. Finally, the PLC3+35% slag, PLC3+20%C1+5%SF, and PLC3+40%C1 systems showed the least severe damage, although with moderate differences to the other mixtures. These results are not intuitive, as several studies have shown increased degrees of deterioration due to physical salt attack in systems with high SCM replacement levels [Irassar 1996][Stark 1989]. Nevertheless, improvements in performance have also been reported, particularly in low w/cm SCM blends [Folliard 1994][Zhutovsky 2016][Bassuoni 2016].

The increased degradation in systems incorporating SCMs has been widely attributed to the increase in capillary sorption due to the refinement of the percolated pore volume. In these conditions, capillary rise and the total volume of solution absorbed would be exacerbated in systems with high sorptivity values. In addition, salt crystallization in more confined spaces would cause higher stresses. Moreover, early exposure of mixtures incorporating slowly-reactive SCMs [Nehdi 2014] and the increased susceptibility to carbonation of SCM systems [Yoshida 2010] have been proposed as additional factors that can accelerate the deterioration of the surface in the evaporation zone. On the other hand, the reduction in the average pore size and the depercolation of the pore structure of hydrated SCM systems have similarly been suggested as the deciding parameters in the cases where an enhanced performance has been observed.

The incorporation of limestone has a profound impact on the microstructure of the hardened system. This effect is the result of several processes of both chemical and physical nature. In this work, although the total volume of the percolated porosity increased, a decrease in the average pore size with respect to the Type I system was obtained with the incorporation of 21.0% limestone, as it is shown in Figure 10.30 for cement paste samples hydrated for 14 days at 23ºC. This effect has been observed in PLC systems with lower limestone contents, and its impact on the resistance to physical salt attack has been shown to depend on the w/cm ratio of the system [Nadelman 2016]. While high w/cm (0.6) PLC mixtures exhibited an inferior resistance to PSA due to the increased crystallization pressure that can develop in pores of an average smaller size, no detriment to the performance was observed for companion mixtures of 0.4 w/cm. As opposed to the higher w/cm systems, the 0.4 w/cm PLC mixtures showed secondary sorptivity values lower

than the control counterpart. Consequently, it was suggested that greater driving forces for salt crystallization might be required in low w/cm limestone-containing systems, attributed to the difficulty in penetrating the refined pore structure, which would increase the resistance to the attack. This result could help explain the better resistance of the PLC3+40%C1, PLC3+20%C1+5%SF, and PLC3+35% slag over the neat cement and the two mixtures with 20% fly ash observed in this work. Similarly, the severe degradation of the PLC7 mixture may have been exacerbated by the high fineness of the cement, which would be expected to increase capillary sorption and the crystallization stress generated. However, more research is needed to confirm this hypothesis. In this regard, sorptivity and accelerated PSA [Folliard 1994] testing of concrete samples of high maturity is ongoing and results will be included in the final publication.

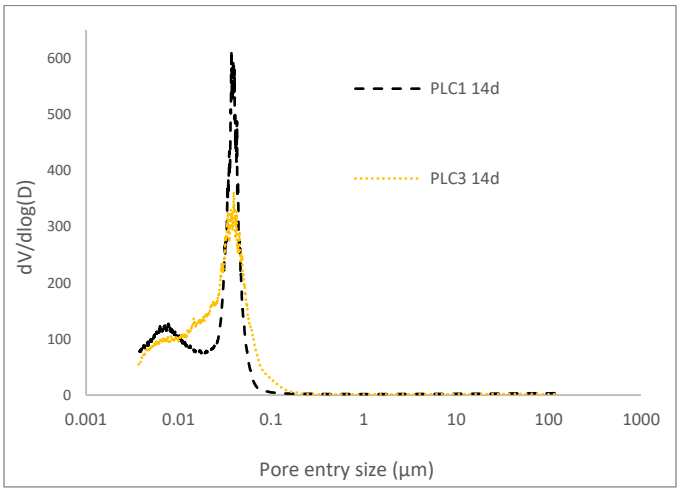

Figure 10.30: First Derivative of the MIP Pore Volumes as a Function of Pore Diameter for PLC1 and PLC3 Neat Cement Pastes with w/cm= 0.485 after 14 Days of Hydration at 23°C

10.3.6. Calcium Sulfate

All the indoor mixtures exposed to the calcium sulfate solution at 23oC, the outdoor samples in the exposure site in Austin, TX, and the field samples at both exposure sites near Van Horn, TX have shown expansions lower than 0.0375% after 2 years of testing. However, some mixtures have exhibited signs of damage constituted by cracking and spalling at the corners and edges of the prisms. The most severe damage was observed in the PLC2 neat cement specimens, followed by the PLC1 samples and the two PLC3 mixtures with 20% Class C ash (PLC3+20%C2 and PLC3+20%C1). These effects were only observed in the specimens stored indoors. The expansion plots of all the mixtures stored in laboratory conditions are shown in Figure 10.31. It must be noted that the scale of the vertical axis has been modified in these two graphs in order to appreciate the small differences between mixtures. As it is observed, it seems that the PLC2 and PLC4 neat cement mixtures, and both PLC3 systems with 20% Class C fly ash have started to expand at a slightly faster rate between 21 and 24 months. Similar results obtained by Drimalas [Drimalas 2007] and Aguayo [Aguayo 2016] have also indicated a slower rate of deterioration in calcium

sulfate exposures in both laboratory and field conditions, which has been attributed to the limited solubility of this salt. Nevertheless, based on the superficial damage observed and the initiation of expansion in some systems after comparable long exposure times, both referred studies have emphasized that the potential for damage to concrete structures should not be neglected. The results of this work agree with those previous findings.

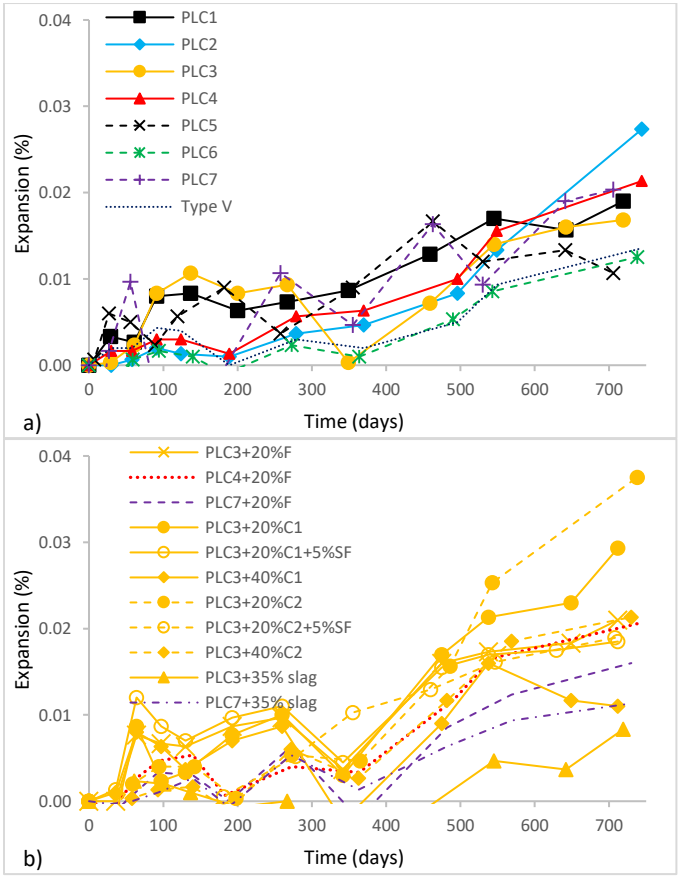

Figure 10.31: Expansion of the Concrete Specimens Stored Indoors in a Saturated Calcium Sulfate Solution at 23°C. a) Neat cement mixtures, b) SCM mixtures.

10.4. Conclusions

An extensive testing program on the resistance of PLC concrete systems to external sulfate attack has been completed. Several mixture parameters, namely interground limestone content, C_3A content, and SCM type and replacement level, were evaluated in a series of experimental conditions designed to link, replicate, and predict laboratory and field performances. The results of this investigation are critical to validate the new and valuable insights into the mechanisms of deterioration due to sulfate attack provided by the accelerated testing presented in the previous chapters. The conclusions of the present work are presented below.

- The results of the present work have highlighted the role that the experimental conditions play in the degradation process, which were shown to be particularly pronounced in systems of low sulfate resistance with high limestone contents, owing to their high propensity for thaumasite formation. Accordingly, it was demonstrated that the results obtained under specific testing conditions are not, in many cases, applicable to other exposures. In addition, it was established that the trends in expansion do not always reflect the type, rate, and severity of the deterioration. This result was observed in mortar specimens subjected to different exposure conditions and confirmed by the investigation of laboratory and field concrete samples. In this context, the adoption of testing protocols conducted at 23ºC to validate or predict the sulfate resistance of a system that will be exposed to lower temperatures seems questionable. This statement is founded on the severe degradation observed in most of the mortar and concrete specimens exposed to sulfate solutions at 5ºC, some of which showed negligible expansion and no signs of macroscopic deterioration when tested according to standard procedures at 23ºC. In this regard, testing at 23ºC seems definitely suitable to classify non-sulfate resistant systems, but, in its current form and according to standard expansion limits, it cannot guarantee the high sulfate resistance of a system in a low temperature exposure.

- Mortar and concrete tests of all the neat cement mixtures showed a good correlation. However, a less consistent parallelism was obtained with the incorporation of SCMs. This effect was observed with all the SCM types and can be attributed to the differences in the initial maturity before exposure to the sulfate solution, which is of particular importance in SCM systems, in addition to the specimen size, w/cm ratio, aggregate gradation, and paste/aggregate ratio. These factors combined are responsible for the slower rates of deterioration of the concrete specimens, which in turn reduce their sensitivity to the variations in the experimental parameters. Nevertheless, the results in concrete samples suggest that the use of ASTM C1012 to evaluate the performance of concrete of w/cm equal or lower than 0.45 that will be exposed to temperatures similar to the one at which the test was conducted is conservative.

- Most 5ºC concrete samples displayed a rapid degradation involving the progressive loss of material from the surface, which was complemented by cracking and spalling as the deteriorated structure allowed a greater interaction with the sulfate solution. The accelerated deterioration in comparison to that of the samples stored indoors at 23ºC and outdoors was more marked in the SCM systems, which may be explained by the higher sensitivity of the SCM blends to the curing temperature. The superficial corrosion increased gradually and, at later times, resulted in severe loss of cohesion associated with the formation of significant amounts of thaumasite. In the concrete specimens, this phenomenon started considerably before the onset of expansion and was much more pronounced in the high-C_3A mixtures with the highest limestone content. The increased

surface deterioration can facilitate sulfate ingress and exacerbate expansion of non-sulfate resistant mixtures, which was shown to be affected by the C_3A and limestone contents of the system. However, a severe degradation does not necessarily imply a faster expansion. This was clearly observed in most of the outdoor neat cement mixtures, which exhibited a faster expansion than that of the specimens stored indoors at both 5ºC and 23ºC, although with very different deterioration patterns. In the mortar case, however, thaumasite was not detected until after the bars exhibited a significant acceleration of the expansion. This could be related to the difference in the time at which the macroscopic changes take place due to the size difference with respect to the concrete specimens.

- The increase in the limestone content significantly changed the length change behavior, progressively reducing the abruptness of the expansion. This effect was observed in plain and blended mortar systems and in the indoor and outdoor concrete experiments. In contrast to the low-limestone systems, no transition from a slow to a fast-expansion stage was observed and the length change of the lowest-clinker mixtures exhibited an almost linear relationship with exposure time. This is believed to be related to the changes in the pore structure as the effective w/cm increased, which would allow a faster mass transport and decrease the potential for supersaturation and the pressure exerted upon ettringite precipitation.

- Although the outdoor exposure conditions differed significantly from the laboratory storage at 23ºC, the relative trends in expansion of concrete samples exposed to sodium sulfate solutions were analogous in these two environments. The outdoor samples, however, exhibited a faster expansion than that of the specimens stored continuously at 23ºC in laboratory setups. The disparities observed are influenced by the differences in the temperature history and the constant changes in the concentration of the sulfate solution as evaporation proceeds in the outdoor site. In these conditions, the outdoor prisms are likely to experience a combined form of attack, chemical and physical in nature.

- Concrete prisms partially submerged in sodium sulfate-bearing soil displayed an expansion equal or slower than that of companion specimens fully submerged. Both types of samples, however, exhibited a significantly different damage mechanism. The portion of the prisms above the soil level experienced a progressive scaling due to salt crystallization that increased in severity as the distance from the soil line increased. While the nature of this damage above the soil was primarily “physical”, chemical and physical effects acted simultaneously in the submerged portions of the specimens, which showed cracking and spalling associated with ettringite formation. Although these effects are widely acknowledged, in the present work the least severe degradation was observed in the mixtures that exhibited the highest resistance to “chemical sulfate attack” at similar temperatures. The high resistance of these systems, which incorporated relatively high amounts of SCMs in combination with 21.0% limestone, contradicts the established

assumption about the low resistance to physical salt attack of systems with high SCM replacement levels. It is hypothesized that the decrease in the average pore size of the hydrated system obtained with the incorporation of 21.0% limestone may have contributed to limit the mass transport, thus increasing the resistance to the attack.

- The rate of deterioration of concrete specimens exposed to calcium sulfate solutions and gypsiferous soils in both laboratory and field conditions has been considerably slower than that of companion samples in sodium sulfate exposures. This result is believed to be related to the lower solubility of this salt. Nevertheless, the same mixtures that exhibited the worst performance in sodium sulfate environments have shown cracking and spalling at the corners and edges of the prisms stored in the indoor calcium sulfate solution. In addition, indications of the onset of a faster expansion stage were evident in the damaged samples after 21 to 24 months of testing. Although further monitoring of the specimens is needed, these findings suggest that the potential for damage to concrete structures in similar exposure conditions should not be neglected.

Chapter 11. Alkali Silica Reaction and Delayed Ettringite Formation in Portland Limestone Cement Systems

11.1. ASR

11.1.1. Introduction

Alkali–silica reaction (ASR) is a deleterious reaction between the alkaline pore solution of concrete and various reactive forms of silica present in many aggregates. The silica structure is attacked by OH^- ions, which leads to the formation of an alkali-silica gel composed predominantly of Na, K, Si, and minor amounts of Ca. Swelling of this gel leads to stress development and eventually, cracking of concrete. ASR is one of the most recognized durability problems of concrete structures and pavements in the United States. It is widely acknowledged that four main prerequisites are needed in order to trigger ASR:

- A source of metastable silica

  The reactivity of silica increases as the level of microstructural disorder increases. The less stable forms of silica exhibit amorphous or poorly crystalline structures or crystalline structures containing many lattice defects, residual strains, or internal microcracks [Rajabipour 2015].

- High alkali concentration in the pore solution

  The apparent solubility of metastable silica increases significantly at high pH values. The main source of alkalis in concrete is the portland cement. However, supplementary cementing materials (SCMs), chemical admixtures, aggregates, and external sources such as de-icing chemicals can contribute to the total alkali in concrete.

- A source of soluble Ca

  It is acknowledged today that considerable expansion of concrete only occurs when an sufficient supply of soluble calcium is available [Rajabipour 2015]. The role of calcium in ASR is not fully understood, but it has been attributed to two main phenomena. First, calcium can replace alkalis in the reaction gel, thus "recycling" alkalis in the pore solution, which are subsequently available for further reaction [Thomas 2001]. Secondly, calcium affects the composition and the potential for expansion of the reaction gel. Several mechanisms have been proposed to explain the impact of calcium on the properties of the

reaction product. However, its exact role remains unclear. The reader is referenced to [Thomas1998] for a more detailed discussion.

- Sufficient moisture

  Swelling of the reaction gel depends strongly on the availability of moisture. ASR is not expected to develop to a significant extent in a dry environment (RH< 60%) [Fournier, 2010.].

11.1.1.1. Alkali–silica Reaction in PLC Systems

There is a very limited amount of research conducted on the propensity of PLC systems to alkali–silica reaction. Thomas et al. [Thomas, 2010] showed that no consistent difference between the expansion of ordinary portland cement mixtures and that of systems incorporating 12% limestone was found according to standard accelerated test methods, namely ASTM C1260, ASTM C1293, and a modified version of ASTM C1293 in which the specimens are stored at 140°F. Rajbhandari [Rajbhandari, 2010] presented results of ASTM C1260 tests of three cements with limestone contents of 3.5%, 15%, and 22% in combination with 25% Class F fly ash and 40% slag. Slight differences between the low and high-limestone systems were obtained. In each case, the system with the highest limestone content showed the best performance. Based on these results, the author concluded that the level of limestone does not seem to have a significant impact on the expansion due to alkali-silica reaction and on the efficacy of SCMs to mitigate it.

11.1.2. Materials and Methods

Standard accelerated laboratory tests, including ASTM C1293 (concrete prism test, CPT) and ASTM C1260 (accelerated mortar bar test, AMBT), were used to evaluate the ASR susceptibility of several systems. In addition, large scale exposure blocks were cast to provide more realistic information on the behavior of these systems in field applications.

In this laboratory study, five cements were tested. Limestone was interground at one plant with a high-C_3A clinker for the production of three cements—PLC1, PLC3, and PLC4—which have limestone contents of 3.2%, 21.0%, and 30.6%, respectively. Analogously, two other cements were produced at another plant by intergrinding limestone with a lower-C_3A clinker, and have limestone contents of 4.9% and 15.5%, namely PLC5 and PLC7, respectively. Moreover, several supplementary cementing materials (SCMs) were selected as partial replacement of the cements: one Class F fly ash, one class C fly ash, and slag. Table 11.1 shows the chemical composition of the cements and SCMs. Figure 11.1 shows the particle size distribution of the PLC1 to PLC7 cements.

Table 11.1: Chemical Composition of the Cements and SCMs

	Material							
	PLC1	PLC3	PLC4	PLC5	PLC7	FA-F	FA-C2	Slag
Chemical analysis [%]								
SiO_2	19.8	18.1	16.9	19.9	19.5	53.2	32.4	36.1
Al_2O_3	5.5	4.7	4.7	4.7	5.0	18.0	17.3	8.0
Fe_2O_3	2.0	1.7	1.5	3.3	3.3	8.1	6.1	0.6
CaO	64.8	67.1	68.1	64.8	64.8	10.8	27.7	39.8
MgO	1.1	1.0	1.2	0.8	0.8	2.4	5.3	10.7
Na_2O	0.1	0.1	0.1	0.1	0.1	0.3	1.6	0.3
K_2O	0.6	0.6	0.4	0.6	0.6	1.1	0.3	0.5
SO_3	4.1	4.6	4.7	3.8	3.9	0.5	2.5	2.6
LOI	1.4	9.2	13.4	2.2	6.8			
$CaCO_3$	3.2	21.0	30.6	4.9	15.5			
Na_2O_{eq}	0.52	0.47	0.34	0.50	0.54			
Calculated phase composition (%) Rietveld analysis								
C_4AF	3.5	2.0	3.0	7.3	4.6			
C_3A	9.2	6.5	6.0	4.2	3.8			
C_3S	47.8	41.1	34.2	47.9	35.1			
C_2S	20.9	17.8	13.6	22.4	24.6			
$CaCO_3$	5.2	24.8	30.3	1.8	14.1			

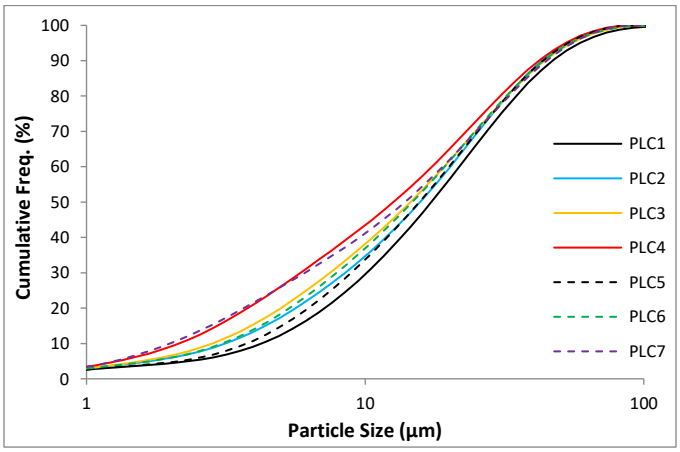

Figure 11.1: Particle Size Distribution of the PLC1 to PLC7 Cements

Two aggregate sources of known reactivity with regard to ASR from Texas were selected in this study to evaluate the performance of each cementitious system. The fine aggregate was a natural, highly reactive siliceous sand containing quartz (64.0 %), chert (17.1 %), and feldspar (11.5 %) from El Paso, TX. The reactive coarse aggregate was a natural siliceous river gravel from El Indio, TX. In the concrete mixtures, each of these two aggregates was used in combination with a non-reactive coarse/fine aggregate consisting in dolomitic limestone from Texas.

For use in concrete, the coarse aggregate was sieved using a fractionator machine into three equal parts of the three gradation sizes: 1/2 in, 3/8 in, and 1/5 in (or No.4) and proportioned according to ASTM C1293. For use in the mortar mixtures, the reactive coarse aggregate was crushed and sieved to meet the gradation limits stated in ASTM C1260. In this case, the reactive fine aggregate was only sieved. All concrete mixtures had a constant w/cm ratio equal to 0.45 and a total cementitious content of 708 lb/yd^3. The mixtures incorporating the El Indio aggregate had a coarse aggregate content of 1950 lb/yd^3, and a fine aggregate content equal to 836 lb/yd^3. The mixtures incorporating the El Paso aggregate had a coarse aggregate content of 1790 lb/yd^3, and a fine aggregate content equal to 985 lb/yd^3. SCMs were incorporated as partial replacement of the cement. The replacement levels evaluated are indicated in the following section. As indicated in ASTM C1293, all the concrete mixtures were boosted by dissolving NaOH in the mixing water in order to reach an alkali content of the concrete, expressed as Na_2O_e = % Na_2O + 0.6583 % K_2O, of 1.25 % by mass of cement.

Three mortar bars with dimensions of 1.0 x 1.0 x 11.25 in were cast for each system following ASTM C1260. After casting, the mortar bars were covered with plastic and placed inside a fog room at 23ºC for 24 hours. Subsequently, the bars were demolded and placed in water at 80 °C for 24 hours. After this conditioning, initial length measurements were taken and the bars were placed in 1 M NaOH solution and at 80 °C. Length measurements were recorded four times between 1 and 14 days. In addition, 21- and 28-day measurement were taken. The expansion limit of 0.10% at 14 days was selected as the criteria to compare the different systems.

Three concrete prisms were cast according to ASTM C1293 for each of the mixtures indicated in Table 11.2 and Table 11.3. The dimensions of the prisms are 3 x 3 x 11.25 in. Stainless steel gauge studs were embedded at each end of the prisms to provide an effective length of 10 in. After casting, the prisms were covered with wet burlap and plastic and stored in a temperature-controlled room at 23ºC for 24 hours and then demolded. Once demolded, initial length measurements were taken and the specimens were placed in a 5-gallon bucket according to ASTM C1293. The samples were separated from the bottom using a perforated rack and water was added to a height of 1 in from the bottom of the container. A layer of felt fabric was placed in contact with the interior (lateral) surface of the bucket in order to facilitate wicking of the water from the bottom and create a high RH environment. The buckets were then placed in temperature-controlled chamber at 100°F until the time of each measurement. Expansion measurements were obtained as indicated in ASTM C1293.

For each concrete mixture, two large-scale exposure blocks were cast. The exposure blocks were chosen to have a cubic shape and a volume of 2 ft3. Wood formworks were built and a protective layer of polyurethane was applied to the sides facing the concrete. Concrete was mixed in a steel concrete mixer in a temperature-controlled room at 23°C and then poured into the formwork. A single batch was prepared to cast the 2 ft^3 exposure blocks and the ASTM C1293 specimens. Each block was instrumented with 12 cast-in-place 3/8 in stainless steel bolts. Each bolt was screwed

into wood inserts located at each side of the formwork. The end of each bolt was machined using a drill press to imprint a hole that allows for monitoring of length changes using a comparator. After casting, the specimens were stored in the same temperature-controlled room covered with wet burlap and plastic film to prevent evaporation until the age of 24 hours. At that age, the blocks were striped and covered with wet burlap and plastic for six additional days. After this curing period, initial measurements were taken and one block was moved to the exposure site in Austin, TX. The other block was kept indoors at 23ºC (uncovered) until it could be transported to other exposure site located in Port Aransas, TX. Eight expansion measurements were taken and averaged at each exposure time when the outside temperature was approximately 73 °F, in concurrence with the ASTM C1293 measurements. Figure 11.2 shows photographs of both field exposure sites.

Figure 11.2: Field Exposure Sites. a) Austin, TX, b) Port Aransas, TX

Table 11.2: Concrete Mixtures Evaluated with Both Reactive Aggregates

SCM	Cement	Mixture
Control	PLC1	PLC1
	PLC4	PLC4
	PLC5	PLC5
	PLC7	PLC7
FA-F	PLC1	PLC1 + 20% F
	PLC4	PLC4 + 20% F
	PLC5	PLC5 + 20% F
	PLC7	PLC7 + 20% F
FA-C2	PLC1	PLC1 + 40% C2
	PLC4	PLC4 + 40% C2
	PLC5	PLC5 + 40% C2
	PLC7	PLC7 + 40% C2
Slag	PLC1	PLC1 + 35% Slag
	PLC4	PLC4 + 35% Slag
	PLC5	PLC5 + 35% Slag
	PLC7	PLC7 + 35% Slag

Table 11.3: Additional Concrete Mixtures Evaluated

Aggregate	Cement	Mixture
El Indio	PLC5	PLC5 + 40% C2 (Unboosted)
	PLC7	PLC7 + 40% C2 (Unboosted)
Jobe	PLC1	PLC1 (Unboosted)
	PLC4	PLC4 (Unboosted)
	PLC5	PLC5 + 40% C1
	PLC7	PLC7 + 40% C1

11.1.3. Results

11.1.3.1. ASTM C1260 (Accelerated Mortar Bar Test, AMBT)

11.1.3.1.1. Control Mixtures

Figure 11.3 shows the expansion curves for the neat cement mortar samples cast with the two reactive aggregate sources. As expected, all straight cement systems failed the expansion criteria. Although no difference between the five cements tested was observed in the El Indio mixtures, the samples incorporating the highly reactive sand from El Paso exhibited a slightly lower expansion at 28 days with the increase in the limestone level.

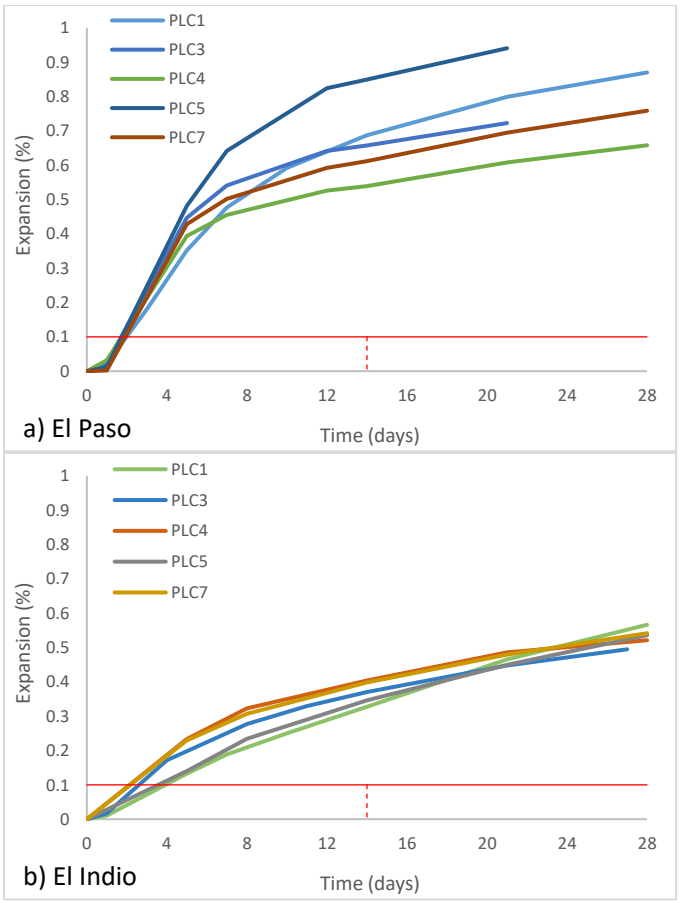

Figure 11.3: Expansion Curves for the Neat Cement Mortar Samples with the Two Reactive Aggregate Sources. a) El Paso, b) El Indio

11.1.3.1.2. Class F Fly Ash Mixtures

The incorporation of SCMs as a partial replacement of cement is expected to mitigate the expansion due to ASR. This effect is the result of several mechanisms:

1) Dilution of the alkalis and calcium silicates from the portland cement,

2) Reduction of the equilibrium pH of the pore solution by OH^- ions consumption and alkali binding,

3) Consumption of portlandite,

4) Reduction of the permeability and mass transport (moisture and external alkali sources are important),

5) In the case of alumina-rich SCMs: the presence of alumina in the SCM is believed to contribute to prevent the long-term release of alkalis back into the pore solution [Thomas 2011].

The mixtures that incorporated 20% Class F fly ash are shown in Figure 11.4. The expansion of all the systems, as expected, decreased in relationship to the control systems. With both aggregate sources, the PLC4 blends showed the best performance. In the case of the El Indio mixtures, the highest-limestone blend satisfied the expansion limit at 14 days. Contrarily, due to the high reactivity of the El Paso aggregate, all mortars exhibited a greater expansion and failed the test.

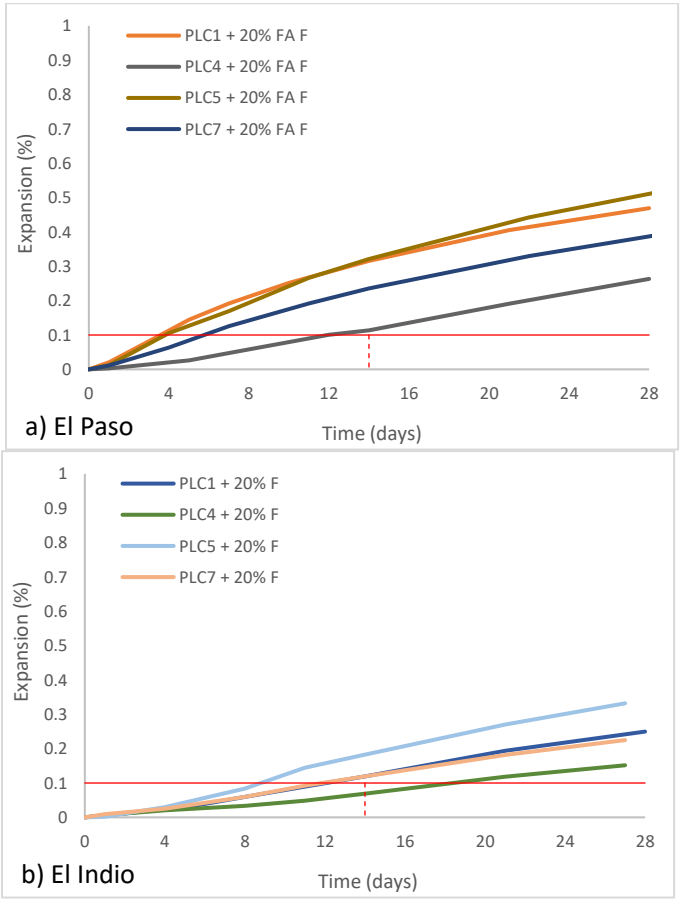

Figure 11.4: Expansion Curves for Class F Fly Ash Mixtures with the Two Reactive Aggregate Sources. a) El Paso, b) El Indio

11.1.3.1.3. Class C Fly Ash Mixtures

Figure 11.5 shows the expansion curves for the mortar samples that incorporated 40% Class C fly ash (C2, CaO% = 27.7%) as cement replacement. Similar results to the Class F systems were obtained with this class C fly ash. However, this combination allowed all mixtures with the reactive

aggregate from El Indio to pass the expansion test. The mortars with the fine aggregate from El Paso showed greater expansion values and only the PLC4 blend was able to pass the test.

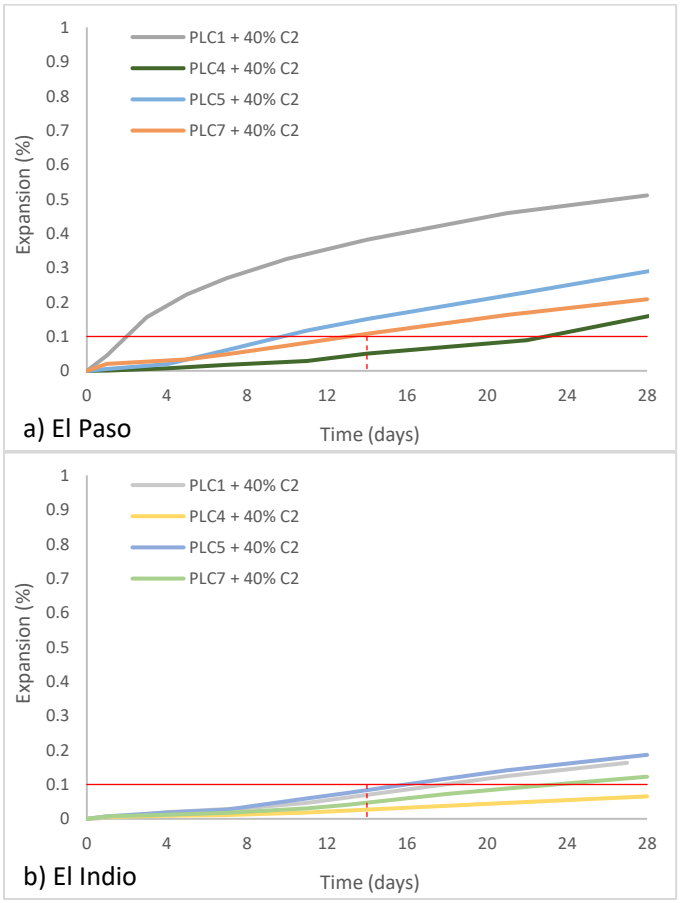

Figure 11.5: Expansion Curves for Class C Fly Ash (C2, CaO% = 27.7%) Mixtures with the Two Reactive Aggregate Sources. a) El Paso, b) El Indio

11.1.3.1.4. Slag-cement Mixtures

The mixtures that incorporated 35% slag are shown in Figure 11.6. Analogous results to the fly ash systems were obtained with the incorporation of 35% slag. The efficiency in mitigating the expansion, however, was slightly less pronounced, which could be attributed to the lower alumina level in this SCM relative to both fly ashes.

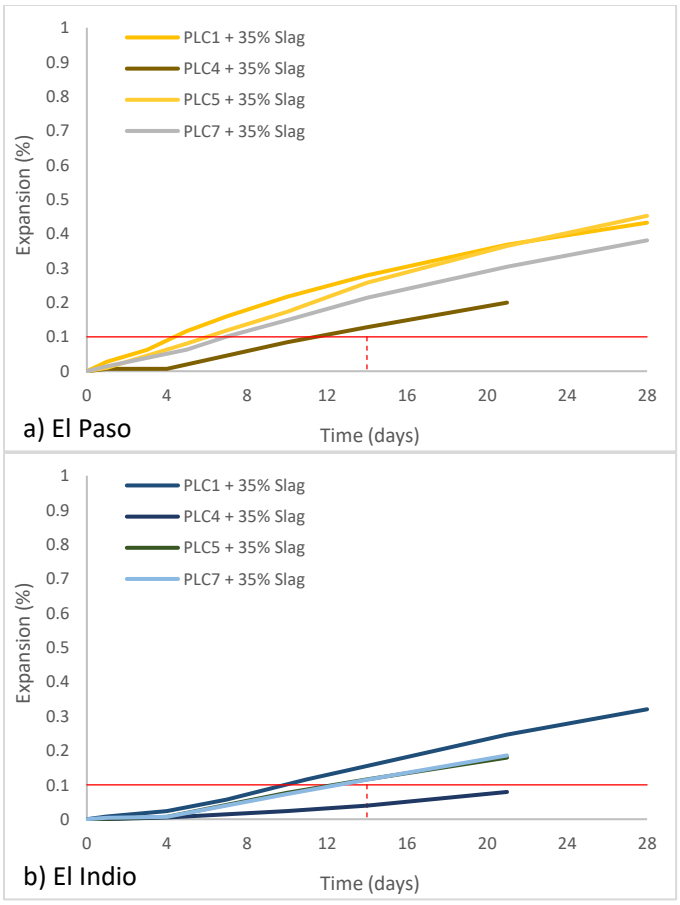

Figure 11.6: Expansion Curves for Slag-Cement Mixtures with the Two Reactive Aggregate Sources. a) El Paso, b) El Indio

11.1.3.2. ASTM C1293 (Concrete Prism Test, CPT)

11.1.3.2.1. Control Mixtures

Figure 11.7 shows the expansion curves for the neat cement concrete samples cast with the two reactive aggregate sources. As expected, all the straight cement systems failed the expansion criteria (0.04% at 2 years). The expansion was considerably greater for the systems that incorporated the reactive sand from El Paso. On the other hand, the two unboosted systems (PLC1 and PLC4) showed negligible expansion after more than 850 days.

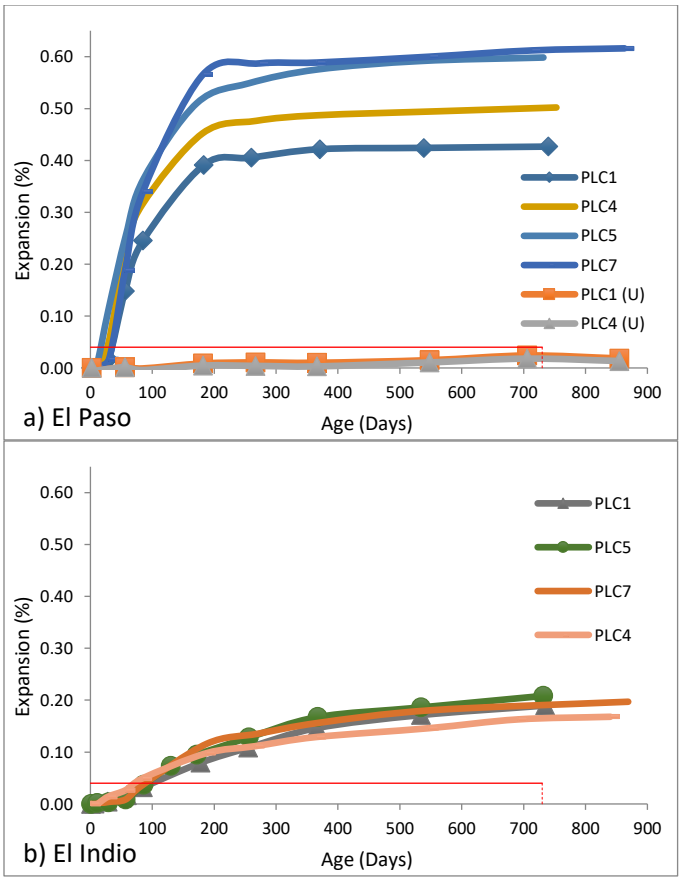

Figure 11.7: Expansion Curves for the neat Cement Concrete Mixtures with the Two Reactive Aggregate Sources. a) El Paso, b) El Indio

11.1.3.2.2. SCM Mixtures

The expansion of all the SCM systems, as expected, decreased in relationship to the straight cement control systems. The plots for the Class F fly ash, Class C fly ash, and slag mixtures are shown in Figure 11.8, Figure 11.9, and Figure 11.10, respectively. In all but two cases, the cement-SCM blends passed the expansion criteria at 2 years. The exceptions were the Type I (PLC1) and Type I/II (PLC5) blends with 40% Class C fly ash (C2, CaO%= 27.7%) shown in Figure 11.9. In the rest of the mixtures no significant impact of the limestone content on the measured expansion was observed in the concrete tests.

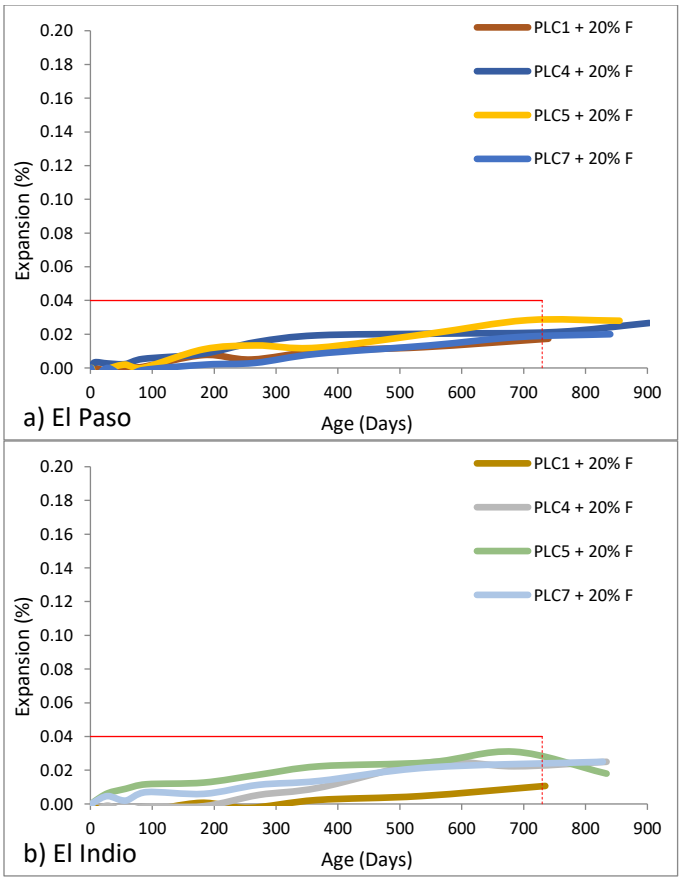

Figure 11.8: Expansion Curves for Class F Fly Ash Concrete Mixtures with the two Reactive Aggregate Sources. a) El Paso, b) El Indio

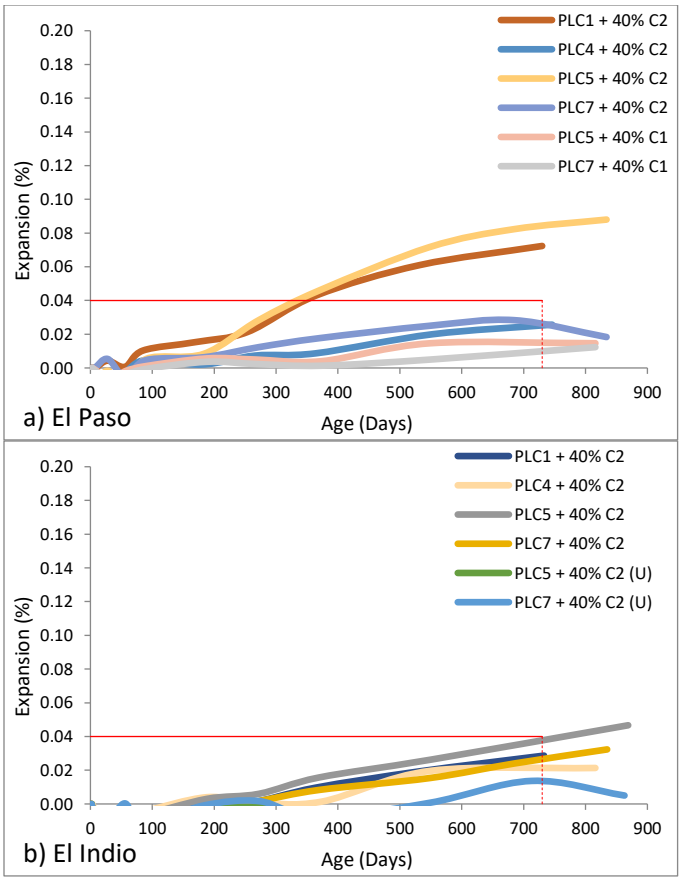

Figure 11.9: Expansion Curves for Class C Fly Ash Concrete Mixtures with the Two Reactive Aggregate Sources. a) El Paso, b) El Indio

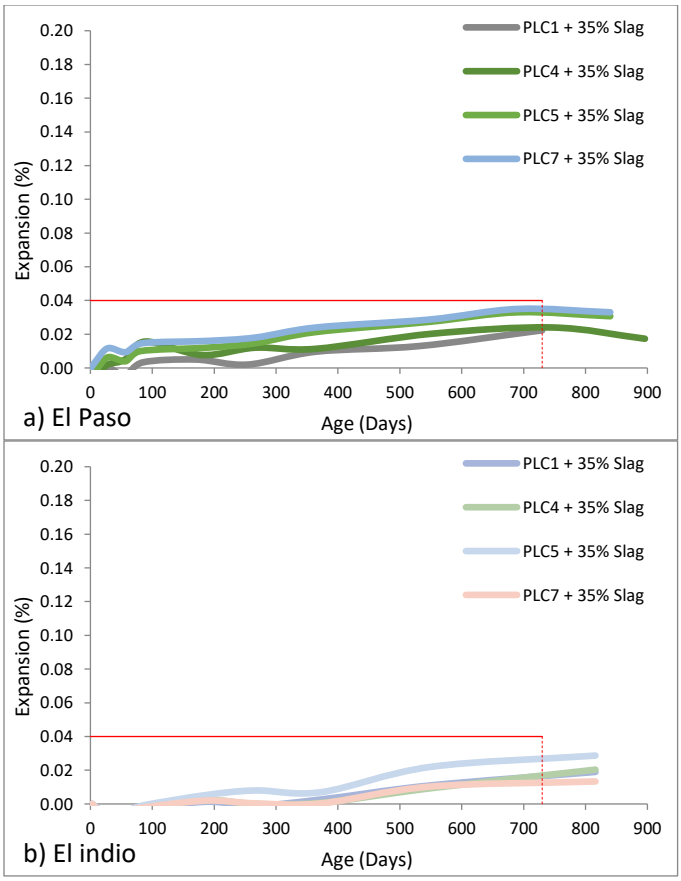

Figure 11.10: Expansion Curves for Slag-Cement Concrete Mixtures with the Two Reactive Aggregate Sources. a) El Paso, b) El Indio

11.1.3.3. Exposure Blocks

The expansion plots for the exposure blocks are shown in Figure 11.11. The mixtures with the reactive aggregate from El Paso stored at Austin's exposure site showed similar trends to the concrete prisms tested according to ASTM C1293. The two unboosted blocks (PLC1 and PLC4) have shown no expansion after 18 months of testing. All the neat cement mixtures expanded rapidly and exceeded the 0.04% expansion value in less than 4 months of testing. The Type I and Type I/II blocks started expanding before their counterpart specimens with higher limestone content (PLC4 and PLC7, respectively). The incorporation of SCMs greatly reduced the expansion of all mixtures. The blends with 30.6% limestone have exhibited a lower expansion rate than that of the equivalent blends with the Type I cement.

In the case of the exposure blocks stored in Port Aransas, TX, similar results were obtained regarding the straight cement mixtures. However, no difference in the onset of expansion was observed between the OPC and the PLC counterparts. The incorporation of SCMs, similarly, was more efficient in controlling the expansion of all the systems with high limestone content (PLC4).

The blend with Type I cement and 40% class C fly ash was the only SCM system that showed significant expansion.

The blocks stored in Austin, TX that incorporated the reactive aggregate from El Indio followed again the trends observed before. In this case, only slight differences were observed between the straight cement mixtures, which expanded rapidly regardless of the cement type. The expansion rates, however, were significantly lower than those of the counterparts with the aggregate from El Paso. Likewise, the SCM systems showed a similar rate of expansion, almost independent of the cement type (PLC1, PLC5, and PLC7). The four blends tested have exceeded the 0.04% value after 18 months of exposure. Finally, the two unboosted blocks (PLC5 + 40% C2 and PLC7 + 40% C2) have shown no expansion after 18 months of testing.

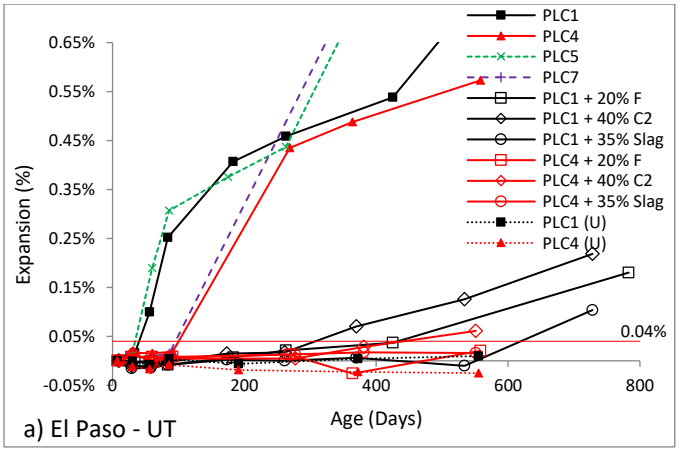

(a) Expansion curves for concrete blocks with the reactive aggregate from El Paso stored at UT Austin's exposure site in Austin, TX.

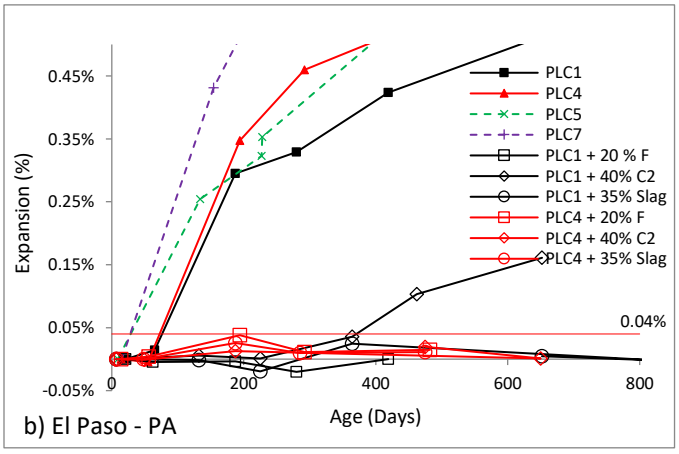

(b) Expansion curves for concrete blocks with the reactive aggregate from El Paso stored at UT Austin's exposure site in Port Aransas, TX.

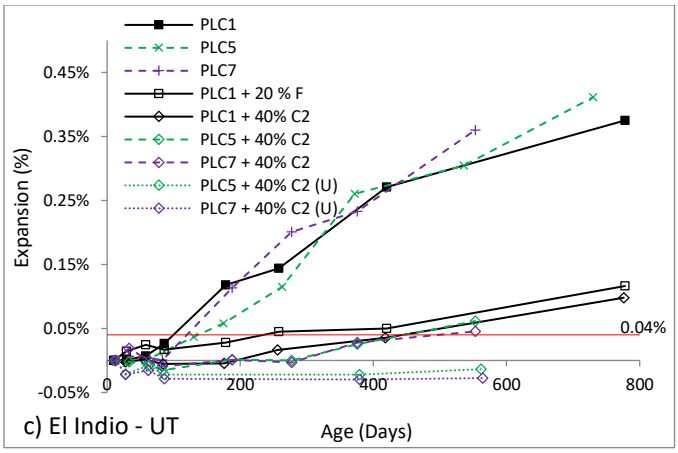

(c) Expansion curves for concrete blocks with the reactive aggregate from El Indio stored at UT Austin's exposure site in Austin, TX.

Figure 11.11: Expansion Curves

11.2. Delayed Ettringite Formation

11.2.1. Introduction

The formation of ettringite after concrete has hardened is known as delayed ettringite formation (DEF). This phenomenon typically occurs in concrete that has reached a temperature above 70 °C for a substantial period of time during curing. Curing at elevated temperatures can cause the incongruent dissolution of ettringite, releasing alumina and sulfate that are encapsulated in the rapidly-forming C-S-H. Later on, as the concrete is exposed to moisture and ambient temperatures, ettringite becomes stable and can be formed as the alumina and sulfate are released from the inner C-S-H and react with monosulfoaluminate and calcium aluminate hydrates. This process is typically triggered by ASR in field structures as the reduction in the pore solution pH caused by ASR promotes the stability of ettringite. The manifestations typically include severe expansion and cracking of the hardened structure.

It is widely known that delayed ettringite formation can be prevented with the partial replacement of portland cement by SCMs. However, there is no consensus regarding the effect of the incorporation of limestone on the potential for DEF. Silva et al. (Silva 2010) showed that the addition of limestone at any replacement level (10%, 15%, 20%, and 30%) increased the expansion of concrete cylinders heat-cured to simulate the temperature cycle of a massive cast-in-place structure. The samples reached a maximum temperature of 80ºC after 15 hours and were maintained at temperatures above 70ºC during 3 days. After this heat curing, the concrete specimens were subjected to two drying and humidification cycles. After these cycles, the specimens were immersed in tap water for long-term storage at 20ºC. Contrastingly, the use of fly ash, metakaolin, slag, and silica fume decreased the expansion upon storage in water. The authors attributed the differences in the ability to control the expansion to the differences in the efficiency

of the SCM to consume portlandite. On the other hand, Kurdowski and Duszak (Kurdowski 2002) showed that limestone presented the same efficiency as fly ash to reduce expansion of mortar samples stored in water at 15% and 30% replacement levels. The mortars were cured for 4 hours in a moist atmosphere and then heat treated at 90°C in saturated steam for 6 hours. Aqel and Panesar (Aqel 2017) showed that the incorporation of 15% limestone slightly reduced the expansion of Type I concrete samples steam-cured at 82°C [180°F]. They attributed this result to the reduction in concrete permeability with the addition of limestone and to the reduction of the cement content.

11.2.2. Materials and Methods

In this laboratory study, four cements were tested. Limestone was interground at one plant with a high-C3A clinker for the production of two cements—PLC1 and PLC3—which have limestone contents of 3.2%, and 21.0%, respectively. Analogously, other two cements were produced at another plant by intergrinding limestone with a lower-C3A clinker, and have limestone contents of 4.9% and 15.5%, namely PLC5 and PLC7, respectively. Moreover, several supplementary cementing materials (SCMs) were selected as partial replacement of the cements: one Class F fly ash, one class C fly ash, slag, and silica fume. Table 11.4 shows the chemical composition of the cements and SCMs. Figure 11.12 shows the particle size distribution of the PLC1 to PLC7 cements.

Table 11.4: Chemical Composition of the Cements and SCMs

Material	PLC1	PLC3	PLC5	PLC7	FA-F	FA-C2	Slag	SF
Chemical analysis [%]								
SiO2	19.8	18.1	19.9	19.5	53.2	32.4	36.1	97.2
Al2O3	5.5	4.7	4.7	5.0	18.0	17.3	8.0	0.3
Fe2O3	2.0	1.7	3.3	3.3	8.1	6.1	0.6	0.1
CaO	64.8	67.1	64.8	64.8	10.8	27.7	39.8	0.9
MgO	1.1	1.0	0.8	0.8	2.4	5.3	10.7	0.3
Na2O	0.1	0.1	0.1	0.1	0.3	1.6	0.3	0.1
K2O	0.6	0.6	0.6	0.6	1.1	0.3	0.5	0.7
SO3	4.1	4.6	3.8	3.9	0.5	2.5	2.6	0.2
LOI	1.4	9.2	2.2	6.8	-	-	-	-
CaCO3	3.2	21.0	4.9	15.5	-	-	-	-
Calculated phase composition (%) Rietveld analysis								
C4AF	3.5	2.0	7.3	4.6	-	-	-	-
C3A	9.2	6.5	4.2	3.8	-	-	-	-
C3S	47.8	41.1	47.9	35.1	-	-	-	-
C2S	20.9	17.8	22.4	24.6	-	-	-	-
CaCO3	5.2	24.8	1.8	14.1	-	-	-	-

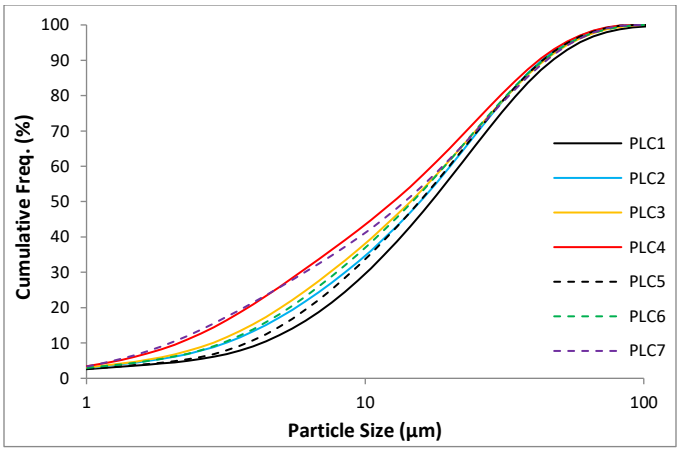

Figure 11.12: Particle Size Distribution of the PLC1 to PLC7 Cements

The fine aggregate used was a reactive, natural siliceous sand containing quartz (64.0 %) chert (17.1 %), and feldspar (11.5 %) from Texas. Three mortar bars of w/cm ratio equal to 0.45 and dimensions of 1.0 x 1.0 x 11.25 in were cast for each system following proportions specified in ASTM C1260.

Immediately after casting, the molds with the mortar specimens were placed above water in sealed containers and moved to an environmental chamber. The curing regime selected is presented in Figure 11.13. After the heat curing, the samples were demolded, measured, and stored in limewater at 23ºC. Periodic length change measurements were taken every month.

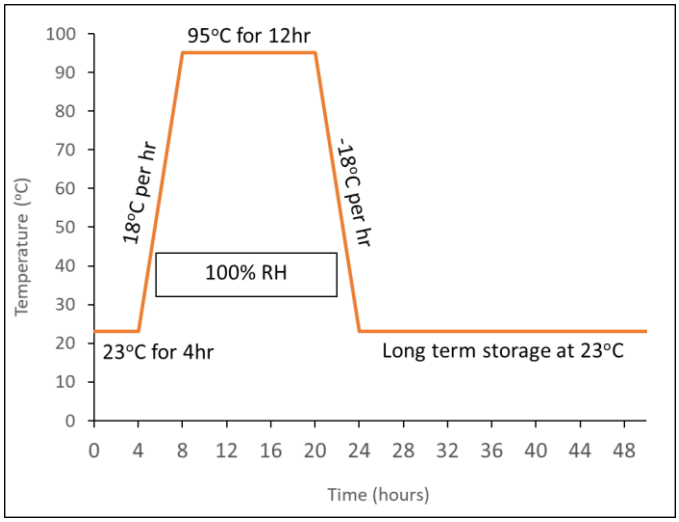

Figure 11.13: Heat-curing Regime of Mortar Samples

11.2.3. Results

The expansion data of the mortar samples stored in limewater after the heat curing are shown in Figure 11.14. All the mixtures that incorporated SCMs have not expanded after 14 months of

storage. On the other hand, the straight cement mixtures showed conflicting trends. In the case of the high-C3A systems, the PLC3 mortars expanded significantly before the Type I counterpart. On the other hand, the PLC7 has shown no expansion, whereas the Type I/II equivalent exhibited a great expansion that started after 2 months of storage. These results do not allow to draw definite conclusions. The mixtures will continue to be monitored and this section will be updated once more trends are noticeable.

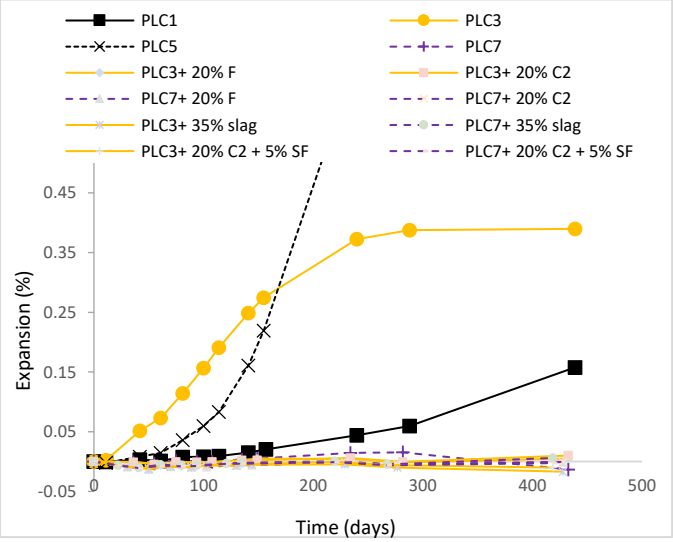

Figure 11.14: Expansion of Mortar Samples Stored in Limewater after Heat Curing

11.3. Conclusions

Based on the results of this section, the following conclusions can be drawn:

- All straight cement systems failed the ASR expansion criteria in both mortar and concrete tests, regardless of limestone content.
- The expansion due to ASR of all the SCM systems, as expected, decreased in relationship to the straight cement control systems.
- With both aggregate sources, the PLC4-SCM blends showed a better performance than the Type I-SCM counterparts, in both mortar and concrete. Less pronounced differences were observed between the PLC5 and PLC7 blends.
- Further research is needed to understand the role of limestone on the expansion of concrete due to ASR, especially in unboosted specimens.
- These results of the DEF tests did not allow to draw definite conclusions. The mixtures will continue to be monitored and this section will be updated once more trends are noticeable.

Chapter 12. Conclusions and Future Research Needs

This report summarized the results of a comprehensive study of the properties of mortar and concrete containing various PLCs, some with a limestone content as high as 30 percent. The key findings are briefly highlighted, and potential areas for future research are identified.

12.1. Conclusions

Based on the overall results from this study, the following conclusions can be presented:

- The addition of limestone promotes the hydration of carboaluminates including:
  - Monocarboaluminate
  - Hemicarboaluminate
  - Carbonated hemicarboaluminate
- Similar compressive strengths to OPC concrete are possible at limestone contents higher than 15%, provided that the cement is ground finer. Lowering the w/cm ratio and/or the use of water reducing admixtures may be necessary, depending on the actual limestone content. These options may reduce the environmental benefits, but the net environmental benefit is still positive.
- Good quality, low permeability concrete can be obtained by combining supplementary cementitious materials with high limestone PLCs. Depending on the severity of the environment and the exact application, additional measures may be required such as increasing the concrete cover of steel reinforcement.
- The addition of limestone results in concrete that is more volumetrically stable than OPC due to the following reasons:
  - Stabilization of ettringite and subsequent formation of carboaluminates, instead of formation of monosulfoaluminate.
  - Decreased drying shrinkage due to lower volume of hydrated cement paste.
- The corrosion potential of concrete seems to increase as the limestone content increases. Special attention should be paid to applications where severe exposure to chlorides is typical. The incorporation of SCMs should be strongly considered.
- PLC concrete has much lower carbonation resistance when compared to OPC concrete at an equivalent w/cm ratio. For applications where carbonation-induced corrosion is a

concern, lowering the w/cm ratio and increasing curing time should be done to minimize the permeability of the concrete. The addition of SCMs will only exacerbate carbonation and special care must be exercised.

- The performance of the PLC-SCM blends was shown to be strongly affected by the type of aluminate phases present in the hydrated system. In this regard, the stabilization of ettringite and carbonate-AFm phases over monosulfate and less stable calcium aluminate hydrates significantly increased the stability of the mixtures upon exposure to the external sulfates.

- All the combinations of high-C3A clinker systems with 21.0% and 30.6% interground limestone and SCMs showed a better performance than the analogous Type I cement-SCM mixtures. Moreover, the partial replacement of both PLCs with 30% Class F fly ash, 40% Class C fly ash (CaO= 22.6%), and 35% slag allowed the low-clinker systems to satisfy the 18-month expansion requirement for the most severe exposure class (S3) in ACI 318-14. Furthermore, the differences in the rate of deterioration between the low and high-limestone systems, which resulted in a different damage pattern in the neat cement mixtures, were also observed in all the blended mortars. These effects were particularly pronounced in the systems that incorporated both Class C fly ashes.

- The incorporation of limestone contents greater than 15% in neat cement mixtures decreased the time to failure according to standard expansion limits. The intergrinding of lower limestone amounts, however, produced varied results. While high-C3A specimens with 13.4% limestone showed the worse performance among all mixtures, no significant difference in expansion was observed with the incorporation of up to 11.6% limestone in moderate-C3A mortars, which exhibited an expansion rate similar to the reference Type V system.

- Not only has the present work shown that previously published results can be extended to systems with higher limestone contents, but it has also demonstrated that the performance of commercially available PC-SCM blends can be significantly enhanced by adjusting the SO3/Al2O3 and CO2/Al2O3 molar bulk ratios through proper selection of limestone, sulfate, and lower-than-thought SCM levels.

- The results of the present work have highlighted the role that the experimental conditions play in the degradation process, which were shown to be particularly pronounced in systems of low sulfate resistance with high limestone contents, owing to their high propensity for thaumasite formation. Accordingly, it was demonstrated that the results obtained under specific testing conditions are not, in many cases, applicable to other exposures. In addition, it was established that the trends in expansion do not always reflect the type, rate, and severity of the deterioration. This result was observed in mortar

specimens subjected to different exposure conditions and confirmed by the investigation of laboratory and field concrete samples. In this context, the adoption of testing protocols conducted at 23 ºC to validate or predict the sulfate resistance of a system that will be exposed to lower temperatures seems questionable. This statement is founded on the severe degradation observed in most of the mortar and concrete specimens exposed to sulfate solutions at 5 ºC, some of which showed negligible expansion and no signs of macroscopic deterioration when tested according to standard procedures at 23 ºC. In this regard, testing at 23 ºC seems definitely suitable to classify non-sulfate resistant systems, but, in its current form and according to standard expansion limits, it cannot guarantee the high sulfate resistance of a system in a low temperature exposure.

- Mortar and concrete tests of all the neat cement mixtures showed a good correlation. However, a less consistent parallelism was obtained with the incorporation of SCMs. This effect was observed with all the SCM types and can be attributed to the differences in the initial maturity before exposure to the sulfate solution, which is of particular importance in SCM systems, in addition to the specimen size, w/cm ratio, aggregate gradation, and paste/aggregate ratio.

- Most 5 °C concrete samples displayed a rapid degradation involving the progressive loss of material from the surface, which was complemented by cracking and spalling as the deteriorated structure allowed a greater interaction with the sulfate solution. The accelerated deterioration in comparison to that of the samples stored indoors at 23oC and outdoors was more marked in the SCM systems, which may be explained by the higher sensitivity of the SCM blends to the curing temperature. The superficial corrosion increased gradually and, at later times, resulted in severe loss of cohesion associated with the formation of significant amounts of thaumasite. In the concrete specimens, this phenomenon started considerably before the onset of expansion and was much more pronounced in the high-C_3A mixtures with the highest limestone content. The increased surface deterioration can facilitate sulfate ingress and exacerbate expansion of non-sulfate resistant mixtures, which was shown to be affected by the C_3A and limestone contents of the system. However, a severe degradation does not necessarily imply a faster expansion. This was clearly observed in most of the outdoor neat cement mixtures, which exhibited a faster expansion than that of the specimens stored indoors at both 5 °C and 23 °C, although with very different deterioration patterns. In the mortar case, however, thaumasite was not detected until after the bars exhibited a significant acceleration of the expansion. This could be related to the difference in the time at which the macroscopic changes take place due to the size difference with respect to the concrete specimens.

- The increase in the limestone content significantly changed the length change behavior, progressively reducing the abruptness of the expansion. This is believed to be related to the changes in the pore structure as the effective w/cm increased, which would allow a

faster mass transport and decrease the potential for supersaturation and the pressure exerted upon ettringite precipitation.

- Although the outdoor exposure conditions differed significantly from the laboratory storage at 23 °C, the relative trends in expansion of concrete samples exposed to sodium sulfate solutions were analogous in these two environments. The outdoor samples, however, exhibited a faster expansion than that of the specimens stored continuously at 23 °C in laboratory setups. The disparities observed are influenced by the differences in the temperature history and the constant changes in the concentration of the sulfate solution as evaporation proceeds in the outdoor site. In these conditions, the outdoor prisms are likely to experience a combined form of attack, chemical and physical in nature.

- Concrete prisms partially submerged in sodium sulfate-bearing soil displayed an expansion equal or slower than that of companion specimens fully submerged. Both types of samples, however, exhibited a significantly different damage mechanism. The portion of the prisms above the soil level experienced a progressive scaling due to salt crystallization that increased in severity as the distance from the soil line increased. While the nature of this damage above the soil was primarily "physical", chemical and physical effects acted simultaneously in the submerged portions of the specimens, which showed cracking and spalling associated with ettringite formation. Although these effects are widely acknowledged, in the present work the least severe degradation was observed in the mixtures that exhibited the highest resistance to "chemical sulfate attack" at similar temperatures. The high resistance of these systems, which incorporated relatively high amounts of SCMs in combination with 21.0% limestone, contradicts the established assumption about the low resistance to physical salt attack of systems with high SCM replacement levels. It is hypothesized that the decrease in the average pore size of the hydrated system obtained with the incorporation of 21.0% limestone may have contributed to limit the mass transport, thus increasing the resistance to the attack.

- The rate of deterioration of concrete specimens exposed to calcium sulfate solutions and gypsiferous soils in both laboratory and field conditions has been considerably slower than that of companion samples in sodium sulfate exposures. This result is believed to be related to the lower solubility of this salt. Nevertheless, the same mixtures that exhibited the worst performance in sodium sulfate environments have shown cracking and spalling at the corners and edges of the prisms stored in the indoor calcium sulfate solution. In addition, indications of the onset of a faster expansion stage were evident in the damaged samples after 21 to 24 months of testing. Although further monitoring of the specimens is needed, these findings suggest that the potential for damage to concrete structures in similar exposure conditions should not be neglected.

- There was no significant effect of limestone content on expansion due to alkali-silica reaction. However, it should be mentioned that the accelerated tests relied on "boosted" alkalies in the concrete prism test and immersion in a high temperature, highly alkaline soak solution in the accelerated mortar bar test.

- Due to the long-term nature of DEF, it is not yet possible to determine the effects of PLCs on the potential for DEF-induced expansion.

12.2. Future Research Needs

Based on the key findings from this study, coupled with a review of published literature, the following are some areas that deserve future emphasis in laboratory and field studies:

- Long-term monitoring of concrete containing PLCs is needed, especially for concrete samples stored at outdoor exposure sites. This is especially needed to benchmark the results of accelerated durability tests (e.g., sulfate resistance, corrosion, carbonation, etc.)

- More work is needed to evaluate the impact of carbonation of PLC concrete on the actual corrosion resistance of reinforced concrete.

- Research should continue on the optimization of sulfate resistance of PLC mixtures, especially given the better than expected performance of PLCs with high limestone contents. More work on better understanding the inter-relation between C_3A content of the clinker, the amount of gypsum added, and the type and dosage of SCMs.

- Full-scale implementation projects using PLCs with limestone contents greater than 15 percent should be initiated, especially for concrete pavements. Such trials should be well-monitored for a long duration to best correlate the laboratory findings with actual field performance. It will be of particular interest to evaluate the impact of PLCs on abrasion and skid resistance of pavements and/or bridge decks, given the high contents of relatively soft limestone particles.

- The potential use of PLCs in mass concrete should be evaluated, especially when using lower clinker contents in combination with SCMs.

- Work is needed to optimize the overall performance of PLCs, including not only equivalent strength, but equivalent (or better) durability.

References

ACI Committee 318-14, Building Code Requirements for Structural Concrete: (ACI 318-14); and Commentary (ACI 318R-14). (2014). Farmington Hills, MI: American Concrete Institute.

Adams, L. D., & Race, R. M. (1990). Effect of limestone additions upon drying shrinkage of Portland cement mortar. In Carbonate additions to cement. ASTM International.

Aqel, M.A., D.K. Panesar, Delayed Ettringite Formation in Concrete Containing Limestone Filler, 10th ACI/RILEM International Conference on Cementitious Materials and Alternative Binders for Sustainable Concrete, SP-320—43, 43.1–43.12 (2017).

ASTM C33 (2016), Standard Specification for Concrete Aggregates

ASTM C39 (2015), Standard Test Method for Compressive Strength of Cylindrical Concrete Specimens

ASTM C150 (2016), Standard Specification for Portland Cement

ASTM C157 (2014), Standard Test Method for Length Change of Hardened Hydraulic-Cement Mortar and Concrete

ASTM C192 (2016), Practice for Making and Curing Concrete Test Specimens in the Laboratory

ASTM C469 (2014), Standard Test Method for Static Modulus of Elasticity and Poisson's Ratio of Concrete in Compression

ASTM C496 (2011), Standard Test Method for Splitting Tensile Strength of Cylindrical Concrete Specimens

ASTM C595 (2016), Standard Specification for Blended Cements

ASTM C618 (2017a), Standard Specification for Coal Fly Ash and Raw or Calcined Natural Pozzolan for Use in Concrete

ASTM C876 (2015), Standard Test Method for Corrosion Potentials of Uncoated Reinforcing Steel in Concrete

ASTM C989 (2018), Standard Specification for Slag Cement for Use in Concrete and Mortars

ASTM C1202 (2010), Standard Test Method for Electrical Indication of Concrete's Ability to Resist Chloride Ion Penetration

ASTM C1240 (2015), Standard Specification for Silica Fume Used in Cementitious Mixtures

ASTM C1556 (2016), Standard Test Method for Determining the Apparent Chloride Diffusion Coefficient of Cementitious Mixtures by Bulk Diffusion

Alunno-Rosetti, V., and Curcio, F., "A Contribution to the Knowledge of the Properties of Portland-Limestone Cement Concretes, with Respect to the Requirements of European and Italian Design Code," Proceedings of the 10th International Congress on the

Chemistry of Cement, Gothenburg, Sweden, June 2-6, 1997, Ed. H. Justnes, pages 3v026 to 3V032.

Antoni, M., J. Rossen, F. Martirena, K. Scrivener, Cement substitution by a combination of metakaolin and limestone, Cem. Concr. Res. 42 (2012) 1579-1589.

Arora, A., G. Sant, N. Neithalath, Ternary blends containing slag and interground/blended limestone: Hydration, strength, and pore structure, Constr. Build. Mater. 102 (2016) 113–124.

Barcelo, L., M. Moranville, B. Clavaud, Autogenous shrinkage of concrete: a balance between autogenous swelling and self-desiccation, Cement and Concrete Research 35 177–183, (2005).

Bassuoni, M.T., M.M. Rahman, Response of concrete to accelerated physical salt attack exposure, Cem. Concr. Res. 79 (2016) 395–408.

Bazant, Z. P., & Baweja, S. (2000). Creep and shrinkage prediction model for analysis and design of concrete structures: Model B3. ACI Special Publications, 194, 1-84.

Bensted, J., & Barnes, P. (2002). Structure and Performance of Cements (2nd ed.). London: Taylor & Francis.

Bentz, DP, Sato T, De la Varga I, Weiss WJ. Fine limestone additions to regulate setting in high volume fly ash mixtures. Cem. Concr. Compos. 34 (2012) 11–17.

Berodier, E., K.L. Scrivener, Understanding the filler effect on the nucleation and growth of C–S–H, J. Am. Ceram. Soc. 97 (2014) 3764–3773

Berodier, E., K. Scrivener, Evolution of pore structure in blended systems, Cem Concr. Res. 73 (2015) 25–35.

Bishnoi, S., Automated Chemical Shrinkage Test and Shrinkage Suite Software. Lausanne, (2009).

Boden, T.A., G. Marland, and R.J. Andres. (2017). Global, Regional, and National Fossil-Fuel CO2 Emissions. Carbon Dioxide Information Analysis Center, Oak Ridge National Laboratory, U.S. Department of Energy, Oak Ridge, Tenn., U.S.A. doi 10.3334/CDIAC/00001_V2017.

Bohan, R. (2004). Innovations in Portland cement manufacturing (Vol. 2004). J. I. Bhatty, F. M. Miller, & S. H. Kosmatka (Eds.). Skokie, Ill, USA: Portland Cement Association.

Bonavetti, V., H. Donza, G. Menendez, O. Cabrera, E. Irassar, Limestone filler cement in low w/c concrete: A rational use of energy. Cem. Concr. Res. 33 (2003) 865-871

Bucher, B.; Radlinska, A.; and Weiss, J., Preliminary Comments on Shrinkage and Shrinkage Cracking Behavior of Cement Systems that Contain Limestone, SN3051, Portland Cement Association, Skokie, Illinois, USA, 2008, 9 pages. Reprinted from Concrete Technology Forum, National Ready Mixed Concrete Association, Silver Spring, Maryland, USA, 2008.

Cam, H. T., & Neithalath, N. (2010). Moisture and ionic transport in concretes containing coarse limestone powder. Cement and Concrete Composites, 32(7), 486-496.

CEN/TS 12390-10:2008 (2008). Testing Hardened Concrete–Part 10: Determination of the Relative Carbonation Resistance of concrete

Cost, V., Howard, I., & Shannon, J. (2013). Improving concrete sustainability and performance with use of portland-limestone cement synergies. Transportation Research Record: Journal of the Transportation Research Board, (2342), 26-34.

CSA A3001 (2013), Cementitious Materials for Use in Concrete

De Weerdt, K., Haha, M. B., Le Saout, G., Kjellsen, K. O., Justnes, H., & Lothenbach, B. (2011). Hydration mechanisms of ternary Portland cements containing limestone powder and fly ash. Cement and Concrete Research, 41(3), 279-291.

De Weerdt, K., Haha, M. B., Le Saout, G., Kjellsen, K. O., Justnes, H., & Lothenbach, B. (2012). The effect of temperature on the hydration of composite cements containing limestone powder and fly ash. Materials and structures, 45(7), 1101-1114.

De Weerdt,K., K.O. Kjellsen, E. Sellevold, H. Justnes, Synergy between fly ash and limestone powder in ternary cements, Cem. Concr. Compos. 33 (2011) 30-38.

Deschner, F., Lothenbach, B., Winnefeld, F., & Neubauer, J. (2013). Effect of temperature on the hydration of Portland cement blended with siliceous fly ash. Cement and concrete research, 52, 169-181.

Dhir, R. K., Limbachiya, M. C., McCarthy, M. J., & Chaipanich, A. (2007). Evaluation of Portland limestone cements for use in concrete construction. Materials and Structures, 40(5), 459.

Dhole, R., Sulfate Resistance of High Calcium Fly Ash Concrete, PhD Thesis, University of New Brunswick, Fredericton, NB, Canada (2010).

Dhole, R., M.D.A. Thomas, K.J. Folliard, T. Drimalas, Sulfate Resistance of Mortar Mixtures of High-Calcium Fly Ashes and Other Pozzolans, ACI Materials Journal 108 (2011) 645-654.

Drimalas, T., Laboratory and Field Evaluations of External Sulfate Attack, PhD Dissertation, The University of Texas at Austin (2007).

Elgalhud, A.A.,R.K. Dhir, G. Ghataora, Limestone addition effects on concrete porosity, Cem. Concr. Compos. 72 (2016) 222-234.

Feng, P.,E. J. Garboczi, C. Miao, J. W. Bullard, Microstructural origins of cement paste degradation by external sulfate attack, Constr. Build. Mater. 96 (2015) 391–403.

Flatt, R.J., G.W. Scherer, Thermodynamics of crystallization stresses in DEF, Cem. Concr. Res. 38 (2008) 325–336.

Folliard, K.J., P. Sandberg, Mechanisms of Concrete Deterioration by Sodium Sulfate Crystallization, Proceedings of the Third International ACI/CANMET Conference on Concrete Durability, Nice, France, (1994) 933-945.

Fournier, B., Marc-André Bérubé, Kevin J. Folliard, Michael Thomas, Report on the Diagnosis, Prognosis, and Mitigation of Alkali-Silica Reaction (ASR) in Transportation Structures, Federal Highway Administration, Report FHWA-HIF-09-004, 2010.

Galan, I., Andrade, C., Mora, P., & Sanjuan, M. A. (2010). Sequestration of CO2 by concrete carbonation. Environmental science & technology, 44(8), 3181-3186.

Garcia, J.E., Durability of Concrete using Portland Limestone Cements Containing Greater than 15% Limestone with a Special Focus on Carbonation, PhD Dissertation, The University of Texas at Austin, (2018).

Gollop, R.S., H.F.W. Taylor, Microstructural and microanalytical studies of sulfate attack. IV. Reactions of a slag cement paste with sodium and magnesium sulfate solutions, Cem. Concr. Res. 26 (1996) 1013-1028.

Gollop, R.S., H.F.W. Taylor, Microstructural and microanalytical studies of sulfate attack. V. Comparison of Different Slag Blends, Cem. Concr. Res. 26 (1996)1029–1044.

Hawkins, P., Tennis, P. D., & Detwiler, R. J. (2003). The use of limestone in Portland cement: a state-of-the-art review. Portland Cement Association.

Haynes, H., R. O'Neill, P.K. Mehta, Concrete Deterioration from Physical Attack by Salts, Concrete International 18 (1996) 63-68.

Heiyantuduwa, R., Alexander, M. G., & Mackechnie, J. R. (2006). Performance of a penetrating corrosion inhibitor in concrete affected by carbonation-induced corrosion. Journal of materials in civil engineering, 18(6), 842-850.

Higgins, D.D., Increased sulfate resistance of ggbs concrete in the presence of carbonate, Cem. Concr. Compos. 25 (2003) 913–919.

Higgins, D.D., N.J. Crammond, Resistance of concrete containing ggbs to the thaumasite form of sulfate attack, Cem. Concr. Compos. 25 (2003) 921–929.

Hooton, R. D. (1990). Effects of carbonate additions on heat of hydration and sulfate resistance of Portland cements. In Carbonate additions to cement. ASTM International.

Hooton, R. D., Nokken, M., & Thomas, M. D. A. (2007). Portland-limestone cement: state-of-the-art report and gap analysis for CSA A 3000. Cement Association of Canada. University of Toronto.

Hooton, D., Ramezanianpour, A., & Schutz, U. (2010). Decreasing the clinker component in cementing materials: performance of Portland-limestone cements in concrete in combination with SCMs. In Concrete Sustainability Conference, National Ready Mixed Concrete Association, Tempe, Ariz.

Hooton, R.D., M.D.A. Thomas, Sulfate Resistance of Mortar and Concrete Produced with Portland-Limestone Cement and Supplementary Cementing Materials: Recommendation

for ASTM C595/AASHTO M 240, PCA R&D SN3285a, Portland Cement Association (2016).

Hossack, A.M., M.D.A. Thomas, Varying fly ash and slag contents in Portland limestone cement mortars exposed to external sulfates, Constr. Build. Mater. 78 (2015) 333–341.

Innis, A. (2014). Portland Limestone Cements. Lecture presented at Technology Transfer Concrete Consortium (TTCC) and National Concrete Consortium (NCC), Jacksonville. Retrieved May 4, 2018, from http://www.cptechcenter.org/ncc/TTCC-NCC-documents/Sp2014/SP14-16-Innis-Limestone-sec.pdf

IPCC. (2013). Climate Change 2013: The Physical Science Basis. Contribution of Working Group I to the Fifth Assessment Report of the Intergovernmental Panel on Climate Change [Stocker, T.F., D. Qin, G.-K. Plattner, M. Tignor, S.K. Allen, J. Boschung, A. Nauels, Y. Xia, V. Bex and P.M. Midgley (eds.)]. Cambridge University Press, Cambridge, United Kingdom and New York, NY, USA, 1535 pp, doi:10.1017/CBO9781107415324.

Irassar, E. F., Bonavetti, V. L., Menendez, G., Donza, H., & Cabrera, O. (2001). Mechanical properties and durability of concrete made with portland limestone cement. ACI SPECIAL PUBLICATIONS, 202, 431-450.

Irassar, E.F., M.A. Gonzalez, V.F. Rahhal, Sulphate resistance of type V cements with limestone filler and natural pozzolana, Cem. Concr. Compos. 22 (2000) 361–368

Irassar, E.F., Sulfate attack on cementitious materials containing limestone filler — a review, Cem. Concr. Res. 39 (2009) 241–254.

Irassar, E.F., A. Di Maio, O.R. Batic, Sulfate attack on concrete with mineral admixtures, Cem. Concr. Res. 26 (1996) 113–123.

Jensen,O.M., P.F. Hansen, Autogenous deformation and RH-change in perspective, Cement and Concrete Research 31, 1859– 1865, (2001)

Kumar, A., T. Oey, S. Kim, D. Thomas, S. Badran, J. Li, F. Fernandes, N. Neithalath, G. Sant, Simple Methods to Estimate the Influence of Limestone Fillers on Reaction and Property Evolution in Cementitious Materials, Cem. Concr. Comp. 42 (2013) 20-29.

Kurdowski W., Duszak S., Can addition of limestone eliminate the expansion of the mortars due to DEF?, International RILEM TC 186-ISA Workshop on Internal Sulfate Attack and Delayed Ettringite Formation, 4-6 September 2002, Villars, Switzerland, 229-235.

Kwan, A. K., McKinley, M., & Chen, J. J. (2013). Adding limestone fines as cement paste replacement to reduce shrinkage of concrete. Magazine of Concrete Research, 65(15), 942-950.

Lollini, F., Redaelli, E., & Bertolini, L. (2014). Effects of portland cement replacement with limestone on the properties of hardened concrete. Cement and Concrete Composites, 46, 32-40.

Lothenbach, B., Le Saout, G., Gallucci, E., & Scrivener, K. (2008). Influence of limestone on the hydration of Portland cements. Cement and Concrete Research, 38(6), 848-860.

Lura, P., O. M. Jensen, K. van Breugel, Autogenous shrinkage in high-performance cement paste: An evaluation of basic mechanisms, Cement and Concrete Research 33, 223–232, (2003)

Lute, R. D. (2016). DURABILITY OF CALCIUM-ALUMINATE BASED BINDERS FOR RAPID REPAIR APPLICATIONS (Doctoral dissertation, The University of Texas at Austin, 2016) (p. 72). Austin, TX: The University of Texas at Austin.

Marceau, M., Nisbet, M. A., & Van Geem, M. G. (2006). Life cycle inventory of portland cement manufacture (No. PCA R&D Serial No. 2095b). IL: Portland Cement Association.

Matschei, T., B. Lothenbach, F.P. Glasser, The AFm phase in Portland cement, Cem. Concr. Res. 37 (2007) 118–130.

Matschei, T., B. Lothenbach, F.P. Glasser, The role of calcium carbonate in cement hydration, Cem. Concr. Res. 37 (2007) 551–558.

Matschei, T., Lothenbach, B., & Glasser, F. P. (2007). The role of calcium carbonate in cement hydration. Cement and Concrete Research, 37(4), 551-558.

Matschei, T., F.P. Glasser, Temperature dependence, 0 to 40 °C, of the mineralogy of Portland cement paste in the presence of calcium carbonate, Cem. Concr. Res. 40 (2010) 763–777.

Mehta, P. K., & Monteiro, P. J. (2006). Concrete: Microstructure, properties, and materials (3rd ed.). New York: McGraw-Hill Education.

Menendez, G., V. Bonavetti, E.F. Irassar, Strength development of ternary blended cement with limestone filler and blast-furnace slag, Cem. Concr. Compos. 25 (2003) 61-67.

Mindess, S., Young, J. F., & Darwin, D. (2003). Concrete (2nd ed.). Upper Saddle River (New Jersey), NJ: Prentice Hall.

Moon, G.D., S. Oh, S.H. Jung, Y.C. Choi, Effects of the fineness of limestone powder and cement on the hydration and strength development of PLC concrete, Constr. Build. Mater. 135 (2017) 129–136.

Muller, A.C.A., K. Scrivener, J. Skibsted , A.M. Gajewicz , P.J. McDonald, Influence of silica fume on the microstructure of cement pastes: New insights from 1H NMR relaxometry, Cem. Concr. Res. 74 (2015) 116–125.

Nadelman, E.I., Hydration and Microstructural Development of Portland Limestone Cement-Based Materials, PhD Dissertation, Georgia Institute of Technology (2016).

Nehdi, M.L., A.R. Suleiman, A.M. Soliman, Investigation of concrete exposed to dual sulfate attack, Cem. Concr. Res. 64 (2014) 42–53.

Ng, T. S., Foster, S., Castel, A., Sanjayan, J., & Berndt, M. L. (2015). State of Practice: High Volume Applications of Fly Ash and Barriers to Commercialisation(Rep. No. RP1004-II). CRC for Low Carbon Living.

National Ready Mixed Concrete Association. (2008). Concrete CO2 Fact Sheet. NRMCA Publication, (2PCO2), 13.

Oey, T, A. Kumar, J.W. Bullard, N. Neithalath, G. Sant, The Filler Effect: The Influence of Filler Content and Surface Area on Cementitious Reaction Rates. Journal of the American Ceramic Society 96 (2013) 1978-1990.

Ogawa, S., T. Nozaki, K. Yamada, H. Hirao, R.D. Hooton, Improvement on sulfate resistance of blended cement with high alumina slag, Cem. Concr. Res. 42 (2012) 244–251.

Osborne, G.J., Durability of Portland blast-furnace slag cement concrete, Cem. Concr. Compos. 21 (1999) 11–21.

Pesek, P., Riding, K., Schindler, A. K., Folliard, K. J., Drimalas, T., & Byard B. E. (2017). Development of Predictive Model for Bridge Deck Cracking and Strength Development (No. FHWA/TX-130/0-6332-2).

Peter, M. A., Muntean, A., Meier, S. A., & Böhm, M. (2008). Competition of several carbonation reactions in concrete: a parametric study. Cement and Concrete Research, 38(12), 1385-1393.

Poole, J.L, K.A. Riding, K.J. Folliard, M.C.G. Juenger, A.K. Schindler, Methods for Calculating Activation Energy for Portland Cement, ACI Materials Journal 104 (2007), 303-311.

Rajabipour, F., E. Giannini, C. Dunant, J.H. Ideker, M. D.A. Thomas, Alkali–silica reaction: Current understanding of the reaction mechanisms and the knowledge gaps, Cem. Concr. Res. 76 (2015) 130–146.

Rajbhandari N., Determining the Effect of Intergrinding Limestone with Portland Cement on the Durability of Concrete with and without SCM, Master Thesis, The University of New Brunswick, 2010

Ramezanianpour, A. M., & Hooton, R. D. (2013). Thaumasite sulfate attack in Portland and Portland-limestone cement mortars exposed to sulfate solution. Construction and Building Materials, 40, 162-173.

Ramezanianpour, A. M., & Hooton, R. D. (2014). A study on hydration, compressive strength, and porosity of Portland-limestone cement mixes containing SCMs. Cement and Concrete Composites, 51, 1-13.

Ramezanianpour, A. A., Ghiasvand, E., Nickseresht, I., Mahdikhani, M., & Moodi, F. (2009). Influence of various amounts of limestone powder on performance of Portland limestone cement concretes. Cement and Concrete Composites, 31(10), 715-720.

Ramezanianpour, A.M., Sulfate Resistance and Properties of Portland-Limestone Cements, PhD Thesis, University of Toronto, (2012).

Runčevski, T., Dinnebier, R. E., Magdysyuk, O. V., & Pöllmann, H. (2012). Crystal structures of calcium hemicarboaluminate and carbonated calcium hemicarboaluminate from synchrotron powder diffraction data. Acta Crystallographica Section B: Structural Science, 68(5), 493-500.

Scherer, G.W., Crystallization in pores, Cem. Concr. Res. 29 (1999) 1347–1358.

Scherer, G.W., Stress from crystallization of salt, Cem. Concr. Res. 34 (2004) 1613–1624.

Schmidt, M. (1992). Cement with interground additives--capabilities and environmental relief: I. ZKG International, Edition B, 45(2), 64-9.

Schmidt, T., B. Lothenbach, M. Romer, J. Neuenschwander, K. Scrivener, Physical and microstructural aspects of sulfate attack on ordinary and limestone blended Portland cements, Cem. Concr. Res. 39 (2009) 1111–1121.

Scrivener, K.L., P. Juilland, P.J.M. Monteiro, Advances in understanding hydration of Portland cement, Cem. Concr. Res. 78 (2015) 38–56

Silva, A.S., D. Soares, L. Matos, M. Salta, L. Divet, A. Pavoine, A. Candeias, J. Mirão, Influence of Mineral Additions in the Inhibition of Delayed Ettringite Formation in Cement based Materials – A Microstructural Characterization, Materials Science Forum Vols. 636-637 (2010) pp 1272-1279.

Shashiprakash, S.G., M.D.A. Thomas, Sulfate Resistance of Mortars Containing High Calcium Fly Ashes and Combinations of Highly Reactive Pozzolans and Fly ash, Seventh CANMET/ACI International Conference on Fly Ash, Silica Fume, Slag, and Natural Pozzolans in Concrete, American Concrete Institute SP 199-13. 221-237, (2001).

Sisomphon, K., & Franke, L. (2007). Carbonation rates of concretes containing high volume of pozzolanic materials. Cement and Concrete Research, 37(12), 1647-1653.

Skalny, J., J. Marchand, I. Odler, Sulfate Attack on Concrete, Spon Press, London and New York (2002).

Stark, D., Durability of Concrete in Sulfate-Rich Soils, Research and Development Bulletin RD 097. Portland Cement Association. Skokie IL. (1989)

Tennis, P. D., Thomas, M. D. A., & Weiss, W. J. (2011). State-of-the-Art Report on Use of Limestone in Cements at Levels of up to 15%. Portland Cement Association: Skokie, IL, USA.

Thomas, M. D. A., & Matthews, J. D. (1992). Carbonation of fly ash concrete. Magazine of Concrete Research, 44(160), 217-228.

Thomas, M. (1996). Chloride thresholds in marine concrete. Cement and concrete research, 26(4), 513-519.

Thomas, M.D.A., The role of calcium in alkali–silica reaction, in: M. Cohen, S. Mindess, J.P. Skalny (Eds.), Materials Science of Concrete — The Sidney Diamond Symposium, American Ceramic Society, Westerville, OH 1998, pp. 325–331.

Thomas,M.D.A., M.H. Shehata, S.G. Shashiprakash, D.S. Hopkins, K. Cail, Use of ternary cementitious systems containing silica fume and fly ash in concrete, Cem. Concr. Res. 29 (1999) 1207–1214.

Thomas, M.D.A., The role of calcium hydroxide in alkali recycling in concrete, in: J. Skalny, J. Gebauer, I. Odler (Eds.), Materials Science of Concrete Special Volume on Calcium Hydroxide in Concrete, American Ceramic Society, 269–280, 2010.

Thomas,M.D.A., The effect of supplementary cementing materials on alkali-silica reaction: A review, Cem. Concr. Res. 41 (2011) 1224–1231.

Thomas, M.D.A, Delagrave, A., Blair, B., & Barcelo, L. (2013). Equivalent durability performance of portland limestone cement. Concrete international, 35(12), 39-45.

Thomas, M.D.A., The effect of supplementary cementing materials on alkali-silica reaction: A review, Cem. Concr. Res. 41 (2011) 1224–1231.

Thomas, M. D. A.; Cail, K.; Blair, B.; Delagrave, A.; and Barcelo, L., "Equivalent Performance with Half the Clinker Content using PLC and SCM," 2010 Concrete Sustainability Conference, National Ready Mixed Concrete Association, April 13 to 15, 2010b, Tempe, Arizona.

Thomas, M. D. A., Cail, K., Blair, B., Delagrave, A., Masson, P., & Kazanis, K. (2010). Use of low-CO2 Portland limestone cement for pavement construction in Canada. International Journal of Pavement Research and Technology, 3(5), 228-233.

Thomas, M. D., & Matthews, J. D. (1992). Carbonation of fly ash concrete. Magazine of Concrete Research, 44(160), 217-28.

Thomas, M.D.A., R. D. Hooton. The Durability of Concrete Produced with Portland-Limestone Cement: Canadian Studies, Portland Cement Association, Skokie, IL, (2010).

Thomas, M.D.A., Supplementary Cementing Materials in Concrete, 1st Ed. CRC Press, Taylor & Francis Group (2013) (ISBN 978-1-4665-7298-0).

Tiburzi, N. B. (2018). MECHANISMS OF DETERIORATION OF PORTLAND-LIMESTONE CEMENT BLENDED SYSTEMS IN LABORATORY AND FIELD SULFATE EXPOSURE (Doctoral dissertation, The University of Texas at Austin, 2018). Austin, TX: The University of Texas at Austin.

Tiburzi, N.B., J. Garcia, T. Drimalas, K.J. Folliard, K. Scrivener, Temperature Effects on the Rate and Mechanism of Deterioration due to Sulfate Attack. To be submitted to Cement and Concrete Research (2018).

Tiburzi, N.B., J. Garcia, T. Drimalas, K.J. Folliard, Sulfate Resistance of Portland-Limestone Cement Blended Systems. Part I: Accelerated Mortar Testing. To be submitted to Cement and Concrete Composites (2018).

Tsivilis, S., Batis, G., Chaniotakis, E., Grigoriadis, G., & Theodossis, D. (2000). Properties and behavior of limestone cement concrete and mortar. Cement and Concrete Research, 30(10), 1679-1683.

Tsivilis, S., N. Voglis, J. Photou, A study of the intergrinding of clinker and limestone, Minerals Engineering, Vol. 12, No. 7 (1999) 837-840.

Tsivilis, S.,J. Tsantilas, G. Kakali, E. Chaniotakis, A. Sakellariou, The permeability of Portland limestone cement concrete, Cem. Concr. Res. 33 (2003) 1465-1471.

Tsivilis, S., E. Chaniotakis, E. Badogiannis, G. Pahoulas, A. Ilias, A study on the parameters affecting the properties of Portland limestone cements. Cem. Concr. Comp. 21 (1999) 107-116.

Valcuende, M., & Parra, C. (2010). Natural carbonation of self-compacting concretes. Construction and Building Materials, 24(5), 848-853.

Vance, K., M. Aguayo, T. Oey, G. Sant, N. Neithalath, Hydration and strength development in ternary portland cement blends containing limestone and fly ash or metakaolin, Cem. Concr. Compos. 39 (2013) 93-103

Voglis, N., Kakali, G., Chaniotakis, E., & Tsivilis, S. (2005). Portland-limestone cements. Their properties and hydration compared to those of other composite cements. Cement and Concrete Composites, 27(2), 191-196.

Whittaker, M., M. Zajac, M. Ben Haha, L. Black, The impact of alumina availability on sulfate resistance of slag composite cements, Constr. Build. Mater. 119 (2016) 356-369.

Whittaker, M., M. Zajac, M. Ben Haha, F. Bullergahn, L. Black, The role of the alumina content of slag, plus the presence of additional sulfate on the hydration and microstructure of Portland cement-slag blends, Cem. Concr. Res. 66 (2014) 91–101.

Wight, J. K. (2016). Reinforced Concrete: Mechanics and Design (7th ed.). Upper Saddle River, NJ: Pearson

Yoshida N., Y. Matsunami, M. Nagayama, E. Sakai, Salt weathering in residential concrete foundations exposed to sulfate-bearing ground, J. Adv. Concr. Technol. 8 (2010) 121–134.

Yu, C., W. Sun, K. Scrivener, Degradation mechanism of slag blended mortars immersed in sodium sulfate solution, Cem. Concr. Res. 72 (2015) 37–47

Zajac, M., Rossberg, A., Le Saout, G., & Lothenbach, B. (2014). Influence of limestone and anhydrite on the hydration of Portland cements. Cement and Concrete Composites, 46, 99-108.

Zhou, Y., Gencturk, B., Willam, K., & Attar, A. (2014). Carbonation-induced and chloride-induced corrosion in reinforced concrete structures. Journal of Materials in Civil Engineering, 27(9), 04014245.

Zhutovsky, S., D. Hooton, Effect of supplementary cementitious materials on the resistance of mortar to physical sulfate salt attack, Proceedings 5th Int. Mater. Spec. Conf., CSCE 2016, London, Ontario, Canada, (2016) 742-1–742-11.